

Consideration of Aircraft Noise Annoyance during Conceptual Aircraft Design

**Berücksichtigung der subjektiven Flugzeuglärmbelästigung während des
Flugzeugvorentwurfs**

Von der Fakultät für Maschinenwesen der Rheinisch-Westfälischen Technischen
Hochschule Aachen zur Erlangung des akademischen Grades eines Doktors der
Ingenieurwissenschaften genehmigte Dissertation

vorgelegt von

Abhishek Kumar Sahai

Berichter: Univ.-Prof. Dr.-Ing. Eike Stumpf
Prof. Dr. Dick G. Simons

Tag der mündlichen Prüfung: 24 Juni, 2016

Diese Dissertation ist auf den Internetseiten der Universitätsbibliothek online verfügbar.

Abstract

This dissertation focuses on the ‘annoyance’ aspect of aircraft noise and how it could be minimized during early aircraft design. The annoyance in this case corresponds to the acoustic annoyance, which is directly related to the quality of an aircraft sound. A new approach is followed rather than the current common practice of assessing aircraft noise solely via A-weighted level (dBA) or Effective Perceived Noise Level (EPNL) values during aircraft design optimization. Use is made of the advanced current knowledge on psychoacoustics to optimize aircraft designs for optimal sound quality.

To consider aircraft noise impact during conceptual aircraft design, a detailed parametric aircraft noise simulation and assessment software INSTANT was developed during the course of this dissertation’s research. To determine the annoyance aspect, INSTANT was appended with a capability to assess aircraft noise in the psychoacoustics based sound quality metrics of loudness, tonality and sharpness. These metrics capture several characteristics of aircraft noise such as the intensity of overall noise and individual noise components, ratio of high frequency to low frequency content and the perceived unmasked prominence of tonal components.

Design sensitivity studies were performed for a representative short-range commercial aircraft by integrating INSTANT into the aircraft design environment MICADO. It was observed that a larger wing can increase the loudness of aircraft noise and at the same time reduce the tonality, by reducing tonal prominence and increasing masking effects. It was also seen that a larger engine can be significantly quieter than a smaller engine, although with a much higher tonality. To explore the optimization possibilities, optimized designs for the EPNL, loudness and tonality metrics were produced. It was found that the minimal EPNL and minimal loudness designs captured the loudness aspect of aircraft noise, via a larger engine and a smaller wing, but didn’t sufficiently capture the tonal content. The minimal tonality design minimized the tonality very effectively by reducing the engine size and increasing the wing size.

A conversion to synthesized audio of the simulated aircraft noise of the optimized aircraft designs showed that reductions in tonal intensity could be perceived audibly. The fundamental fan tone for the minimal tonality design was observed to have a reduced intensity in excess of 10 dB in the spectrograms, created at a sample ground location during a standard approach procedure. The results indicate that it is possible to modify the sounds of current aircraft towards less annoying or more acceptable sounds, by knowing beforehand which design parameter can change the aircraft sound quality in which way and form.

Zusammenfassung

Die vorliegende Arbeit konzentriert sich auf den subjektiven ‚Belästigung‘ (annoyance, im Englischen) Aspekt des Flugzeuglärums und wie dieser während des Flugzeugvorentwurfs minimiert werden kann. Die Belästigung entspricht hierbei der akustischen Belästigung, die direkt mit der Qualität des Flugzeugklangs zusammenhängt. Ein neuer Ansatz für die Bewertung von Flugzeuglärm während des Flugzeugvorentwurfs und dessen Optimierung wird verwendet, anstatt der gängigen Praxis einer Bewertung in A-bewerteter Pegel (dBA) oder Effektiver empfundener Schallpegel (Effective Perceived Noise Level, EPNL). Die fortgeschrittene heutige Kenntnis von Psychoakustik wird verwendet um Flugzeugentwürfe für optimale Klangqualität zu optimieren.

Um die Auswirkung von Flugzeuglärm während des Flugzeugvorentwurfs zu berücksichtigen, wurde im Rahmen dieser Arbeit eine detaillierte parametrische Flugzeuglärm Simulationssoftware „INSTANT“ entwickelt. Um den Belästigungsaspekt zu berücksichtigen, wurde INSTANT mit der Fähigkeit zur Bewertung in ‚Sound Quality‘ Metriken von Lautheit, Tonalität und Schärfe erweitert. Diese Metriken erfassen unterschiedliche Eigenschaften des Flugzeuglärums, wie die Gesamtstärke des Schalls oder die Stärke der einzelnen Komponenten, das Verhältnis von Hochfrequenz- zu Tieffrequenzlärmen und die wahrgenommene unmaskierte Ausgeprägtheit der tonalen Komponenten.

Sensitivitätsstudien wurden für ein repräsentatives Kurzstreckenflugzeug mittels einer Integration von INSTANT in einer Flugzeugentwurfsumgebung MICADO durchgeführt. Als Ergebnis dieser Studien wurde beobachtet, dass ein größerer Flügel die Lautheit des Flugzeuglärums erhöht. Gleichzeitig wird die entsprechende Tonalität auf Grund reduzierter tonaler Ausgeprägtheit und verstärkter Abdeckungseffekte verringert. Es wurde ebenfalls bemerkt, dass ein größeres Triebwerk maßgeblich leiser ist als ein kleineres Triebwerk, allerdings mit einer wesentlich höheren Tonalität. Um die Optimierungsmöglichkeiten zu untersuchen, wurden optimierte Flugzeugentwürfe für die EPNL, Lautheit und Tonalität Metriken erzeugt. Die Ergebnisse zeigten, dass die EPNL- und Lautheit-optimierten Entwürfe den Lautheitsaspekt mittels eines größeren Triebwerks und eines kleineren Flügels erfassten aber den tonalen Anteil des Flugzeuglärums nicht hinreichend erfassten. Der Tonalität-optimierte Entwurf minimierte sehr effektiv die Tonalität des Flugzeuglärums durch eine Wahl eines kleineren Triebwerks und eines größeren Flügels.

Eine Umsetzung des simulierten Flugzeuglärums in eine synthetisierte Audioaufnahme zeigte, dass die Reduzierung der tonalen Stärke des Tonalität-optimierten Flugzeugentwurfs hörbar wahrgenommen werden konnte. Die Intensität des fundamentalen Tons des Fans, welche an einem repräsentativen Ort am Boden für ein Standard Anflugverfahren erzeugt wurde, verringerte sich mit mehr als 10 dB in den Spektrogrammen. Die Resultate zeigen, dass es möglich ist den Klang der heutigen Flugzeuge in Richtung weniger Belästigung beziehungsweise höherer Akzeptanz hinsichtlich der Vorkenntnis welcher Parameter in welcher Art und Weise die Flugzeugklangqualität beeinflusst, zu modifizieren.

Acknowledgements

Writing a dissertation is a mammoth and often unpleasant task. The fun part i.e. making new as yet never before seen results is over and now one must write a long (or short, if you can manage it) piece of paper saying why you did it, how you did it, what exactly you did and for whom you did it. Experience, both your own and of those who preceded you, shows that many days and nights spread over many months result in a preliminary version of a monster called a PhD dissertation, which often has to be transformed into a coherent, somewhat understandable entity in subsequent versions. What a task to join a club of members who refer to themselves as ‘Doctors’, although who are actually academics, scientists and often simply engineers. Yet I decided to try to join this club in any case, fully aware of the tough yet fun road ahead of discovering new and never before seen things and trying to prove that that’s how things really were. I started it happily and ended it happily. In between were a large spectrum of emotions, which are inevitable when you’re trying to do something over four to five years of your life.

Luckily, there are several people who help you along the way to becoming a Doctor in Engineering Sciences (the German title makes more sense than the international Doctor of Philosophy – I didn’t study philosophy and I don’t intend to philosophize about aircraft noise or aircraft design... at least for now). These kind people are the ones you thank and acknowledge – your guides, your peers, your friends and family, as well as your critics.

I first and foremost thank Prof. Dr. Eike Stumpf, who allowed me to work at the ILR for the four years and agreed to be my promotor. Staying in Aachen, I would like to thank all my colleagues at the ILR for accepting me as one of their own and appreciating my research as the ‘noise guy’. I thank Fabian for the three years of being my office mate and for the countless meaningful as well as pointless yet hilarious conversations. Rainer for being one of the few people who spoke to me in English when my German wasn’t great in the beginning and showing me the life in Aachen. I also thank Kathi, Christine, Sebastian, Florian, Yaolong and everyone else at ILR for the many lunches, dinners and drinks together. I thank Dr. Ralf Hoernschemeyer for seeing potential in my profile and forwarding my job application to the then head Prof. Henke, whom I thank for offering me the job and opportunity to come to Aachen and work at the ILR.

I thank further very much Prof. Dr. Dick Simons for agreeing to be the second reviewer of my dissertation and for offering me the chance to continue my career at the Aircraft Noise and Climate Effects Research Group of TU Delft. I also thank the VASTCON community and Dr. Steve Rizzi for the idea and initiative that we form such a community. I also thank him for letting me visit NASA Langley, which was a very memorable experience of my PhD.

I thank my family and particularly my parents. It’s a comforting thought to know that I have their unconditional support although they are in another continent. I can’t imagine having been successful without their love, help and support.

I thank lastly the remaining colleagues at RWTH Aachen and my new colleagues in Delft. May the future hold great heights for everyone who helped me along the way to achieving this first goal in a scientific career. There will certainly be many challenges ahead but with everyone's help and support, I hope to continue progressing, learning and being inspired. Thank you, danke schön, bedankt and shukriya to all.

Contents

1 Introduction	1
2 Motivation for alternate assessment of aircraft noise	4
2.1 Currently used metrics in the aerospace industry.....	6
2.1.1 Loudness based weighted Sound Pressure Level metrics	6
2.1.2 Annoyance based Perceived Noise Level metrics	8
2.1.3 Multiple event average level metrics	14
2.2 Deficiencies in currently used metrics and scope for improvements	15
3 Current state of the art	19
3.1 State of the art in aircraft noise perception.....	19
3.2 State of the art in low annoyance aircraft design	23
4 Noise modeling for aircraft design and optimization.....	27
4.1 The physics behind aircraft noise generation	27
4.2 Aircraft source noise modeling using parametric models	32
4.2.1 Fan noise	34
4.2.2 Combustor noise	42
4.2.3 Turbine noise	44
4.2.4 Jet noise.....	46
4.2.5 Engine noise validation at source	50
4.2.6 Airframe noise	54
4.2.7 Noise validation on the ground	60
5 Development of an aircraft noise prediction and assessment environment.....	64
5.1 The aircraft design environment MICADO	64
5.1.1 Aircraft design and assessment methodology.....	65
5.1.2 Aircraft design and analysis modules	67
5.2 The aircraft noise prediction and assessment environment INSTANT	74

5.2.1	Propagation of source noise to the observer on the ground.....	77
5.2.2	Assessment of aircraft noise	86
6	Annoyance assessment using sound quality metrics	100
6.1	Implementation of the sound quality metrics	100
6.2	Community noise assessment in sound quality metrics	114
7	Design parameter sensitivity analysis.....	121
7.1	Uncoupled parametric variation studies	122
7.1.1	Noise impact analysis at certification points	122
7.1.2	Community noise impact analysis	128
7.2	Coupled parametric variation studies	133
7.2.1	Wing-loading variation	134
7.2.2	Thrust-to-weight ratio variation.....	138
8	Optimization possibilities for low annoyance aircraft design	142
8.1	Comparison of optimized aircraft designs	142
8.1.1	Correlation of optimized designs with sound	156
8.1.2	Comparison with current aircraft having acoustic liner technology.....	159
9	Conclusions and outlook.....	162
9.1	Conclusions.....	162
9.2	Outlook	165
References		167
Appendix A: Noise relevant engine geometry parameter estimation		174
Appendix B: Annoyance assessment of noise abatement flight procedures		179
1.	SR aircraft Continuous Descent Approach (CDA).....	179
2.	LR aircraft Continuous Descent Approach (CDA).....	180

List of Figures

Figure 2.1: Variation of fan and jet perceived noise with bypass ratio reproduced from [23].....	5
Figure 2.2: Equal loudness contours for pure tones of different levels and frequency (left), approximation of 40 phon loudness curve with A-weighting used for the dBA metric (right).....	7
Figure 2.3: Equal noisiness curves used for PNL calculation	10
Figure 2.4: Duration correction for final EPNL calculation [6]	13
Figure 3.1: Correlation of aircraft interior noise annoyance of listeners in test environments to the loudness (left) and tonality (right) of the sounds from [48]. Tonality is defined from 0 – 1 tonality units (t.u.)	21
Figure 4.1: Major aircraft noise sources as modeled using ANOPP based source noise models*	33
Figure 4.2: Mode propagation for sample case of fan with 4 rotors and 3 stators (left) and 5 stators (right) [6]. Blue arrow denotes fan rotational direction and red arrow denotes mode spin direction. Fundamental tone is attenuated on the right.....	36
Figure 4.3: Primary noise sources originating from the fan (Fan configuration from [6])	40
Figure 4.4: Noise suppression due to acoustic liner technology for two sample engines – CF6-80C2 (top) and V2527-A5 (bottom).....	41
Figure 4.5: Jet mixing noise and the various mixing regions near the nozzle exit	47
Figure 4.6: Comparison of implemented models with NASA’s ANOPP from [90] in forward arc, $\theta = 50^\circ$ – reference spectra (top); simulated spectra with ref. values (middle); simulated spectra with Gasturb values (bottom).....	52
Figure 4.7: Comparison of implemented models with NASA’s ANOPP from [90] in aft arc, $\theta = 150^\circ$ – reference spectra (top); simulated spectra with ref. values (middle); simulated spectra with Gasturb values (bottom)	53
Figure 4.8: Comparison of implemented models with measured values from [90] – forward arc, $\theta = 50^\circ$ (top); aft arc, $\theta = 150^\circ$ (bottom).....	54

Figure 4.9: Clean trailing edge noise generation due to convection of turbulent flow over trailing edge [98]	55
Figure 4.10: Sample spectra of airframe source noise for departure settings (top) and approach settings (bottom) at $\theta = 40^\circ$ and $\psi = 0^\circ$	60
Figure 4.11: Comparison of simulated spectra on ground with DC-10 measured spectra from [99] for departure settings – $\theta = 50^\circ$ (top); $\theta = 90^\circ$ (middle); $\theta = 150^\circ$ (bottom)	61
Figure 4.12: Comparison of simulated spectra on ground with DC-10 measured spectra from [99] for approach settings – $\theta = 50^\circ$ (top); $\theta = 90^\circ$ (middle); $\theta = 150^\circ$ (bottom)	62
Figure 5.1: Aircraft design and assessment methodology of the MICADO environment [100].....	67
Figure 5.2: Geared turbofan unmixed model and thermodynamic station numbers as used in Gasturb [92]	69
Figure 5.3: Parametric variation of T/W and W/S to analyze impact on block fuel over a study mission [100].....	73
Figure 5.4: VR simulation achieved for the interdisciplinary VATSS project.....	74
Figure 5.5: The ILR Noise Simulation and Assessment module INSTANT	76
Figure 5.6: The global coordinate system with the aircraft and observer vectors as implemented in INSTANT.....	78
Figure 5.7: Calculation of atmospheric absorption by division of aircraft-observer distance into segments	80
Figure 5.8: Variation of atmospheric absorption with relative humidity.....	81
Figure 5.9: Geometry for ground reflection and attenuation calculation	82
Figure 5.10: Aircraft noise spectra displaying propagation effects of spreading, atmospheric absorption and ground reflection	84
Figure 5.11: Propagated aircraft noise spectrum for a snowy ground surface	84
Figure 5.12: ICAO specified aircraft noise certification points	89

List of Figures

Figure 5.13: PNLT vs. polar directivity variation at the sideline and flyover points for a short-range aircraft.....	91
Figure 5.14: PNLT vs. polar directivity variation at the approach point for a short- range aircraft.....	91
Figure 5.15: Time-dependent community noise assessment for a short-range aircraft standard departure flight path	93
Figure 5.16: Time-dependent community noise assessment for a short-range aircraft standard approach flight path	94
Figure 5.17: Sample time-dependent noise contours made using INSTANT – (1).....	95
Figure 5.18: Maximum value noise contours made using INSTANT for a standard short-range aircraft departure procedure in the dBA metric (top) and EPNL metric (bottom)	98
Figure 5.19: Maximum value noise contours made using INSTANT for a standard short-range aircraft approach procedure in the dBA metric (top) and EPNL metric (bottom)	99
Figure 6.1: Masking of a 2 kHz test tone due to narrowband noise centered at 1 kHz (left) and due to white noise (right) [139]	102
Figure 6.2: Effect of critical bandwidth on the loudness perception of band-pass noise [140].....	103
Figure 6.3: Critical bandwidth as a function of frequency [139].....	103
Figure 6.4: Sample spectra for sharp and less sharp sounds used for loudness and sharpness validation [56]	106
Figure 6.5: Variation of relative tonality with frequency in Bark (left) and bandwidth in Bark (right) for pure sine tones \circ , band-pass noise with bandwidth of 30 Hz \diamond , bandwidth of 1 kHz ∇ and high-pass noise with lower cut-off frequency of 2 kHz \blacktriangle from Aures' original paper [49]	109
Figure 6.6: Sample spectrogram of an aircraft departure from [65]	111
Figure 6.7: Sample spectrograms for the SR aircraft: standard departure (left) and standard approach (right)	113
Figure 6.8: Sample spectrograms for the LR aircraft: standard departure (left) and standard approach (right)	113

Figure 6.9: Sound quality contours for the SR aircraft standard departure: maximum loudness values in phon (top); maximum sharpness values in acum (middle); maximum tonality values in t.u. (bottom)....	115
Figure 6.10: Sound quality contours for the SR aircraft standard approach: maximum loudness values in phon (top); maximum sharpness values in acum (middle); maximum tonality values in t.u. (bottom)....	116
Figure 6.11: Sound quality contours for the LR aircraft standard departure: maximum loudness values in phon (top); maximum sharpness values in acum (middle); maximum tonality values in t.u. (bottom)....	119
Figure 6.12: Sound quality contours for the LR aircraft standard approach: maximum loudness values in phon (top); maximum sharpness values in acum (middle); maximum tonality values in t.u. (bottom)....	120
Figure 7.1: Engine geometry parameter variation results on noise impact at the flyover certification point	124
Figure 7.2: Time-dependent component level noise variation at the flyover certification point for reference fan inlet area (left) and for a larger fan inlet area (right)	125
Figure 7.3: Engine geometry parameter variation results on noise impact at the approach certification point	127
Figure 7.4: Engine geometry parameter variation results on community noise impact for a standard SR departure in sound quality metrics.....	129
Figure 7.5: Engine geometry parameter variation results on community noise impact for a standard SR departure in the dBA and EPNL metrics.....	130
Figure 7.6: Engine geometry parameter variation results on community noise impact for a standard SR approach in sound quality metrics	132
Figure 7.7: Engine geometry parameter variation results on community noise impact for a standard SR approach in the dBA and EPNL metrics	133
Figure 7.8: W/S variation results for noise impact of the SR aircraft at flyover and approach certification points.....	135
Figure 7.9: Flight path comparison of the SR departure for low and high wing-loading values – initial departure phase (left) and later departure phase (right)	136

List of Figures

Figure 7.10: Wing-loading variation results for community noise impact of the SR aircraft for departure and approach flight paths in sound quality metrics	137
Figure 7.11: W/S variation results for community noise impact of the SR aircraft departure and approach flight paths in dBA and EPNL metrics	138
Figure 7.12: T/W variation results for community noise impact of the SR aircraft in sound quality metrics	140
Figure 7.13: Thrust to weight ratio variation results for community noise impact of the SR aircraft for departure and approach flight paths dBA and EPNL metrics	141
Figure 8.1: Departure noise contours of the SR-Ref and min. EPNL variants for – a) EPNL SR-Ref, b) EPNL min. EPNL, c) Loudness SR-Ref, d) Loudness min. EPNL, e) Tonality SR-Ref and f) Tonality min. EPNL	146
Figure 8.2: Approach noise contours of the SR-Ref and min. EPNL variants for – a) EPNL SR-Ref and b) EPNL min. EPNL - 1).....	147
Figure 8.3: Standard departure tonality contours for the reference SR aircraft (top) and minimal tonality SR aircraft design variant (bottom)	155
Figure 8.4: Standard approach tonality contours for the reference SR aircraft (top) and minimal tonality SR aircraft design variant (bottom)	155
Figure 8.5: Spectrograms of synthetic audio created at $(X,Y) = (-25 \text{ km}, 0 \text{ km})$ for a standard approach procedure – a) reference SR aircraft, b) minimum tonality variant, c) minimum EPNL variant and d) minimum loudness variant	157
Figure 8.6: Spectrograms of synthetic audio created at $(X,Y) = (12.5 \text{ km}, 0 \text{ km})$ for a standard departure procedure - reference SR aircraft (left) and minimum loudness variant (right)	158
Figure A.1: Best-fit curve and corresponding empirical equation for estimating the fan inlet area based on the engine's SLST	174
Figure A.2: Best-fit curve and corresponding empirical equation for estimating the fan rotor blade number based on the engine's SLST	175
Figure A.3: Best-fit curve and corresponding empirical equation for estimating the fan rotor tip design Mach number based on the engine's SLST.....	175

Figure A.4: Best-fit curve and corresponding empirical equation for estimating the combustor entrance area based on the engine's SLST	176
Figure A.5: Best-fit curve and corresponding empirical equation for estimating the LP turbine entrance area based on the engine's SLST	176
Figure A.6: Best-fit curve and corresponding empirical equation for estimating the LP turbine rotor blade number based on the engine's SLST	177
Figure A.7: Best-fit curve and corresponding empirical equation for estimating the primary jet area based on the engine's SLST	177
Figure A.8: Best-fit curve and corresponding empirical equation for estimating the secondary jet area based on the engine's SLST	178
Figure B.1: Flight parameter variation and noise contours in the conventional metrics of dBA and EPNL for the SR aircraft CDA with 4° glideslope	179
Figure B.2: Noise contours in the sound quality metrics of loudness (top), sharpness (middle) and tonality (bottom) for the SR aircraft CDA with 4° glideslope	180
Figure B.3: Flight parameter variation and noise contours in the conventional metrics of dBA and EPNL for the LR aircraft CDA with 4° glideslope	181
Figure B.4: Noise contours in the sound quality metrics of loudness (top), sharpness (middle) and tonality (bottom) for the LR aircraft CDA with 4° glideslope	182

List of Tables

Table 2.1: A- and C-weighting for 1/3 octave frequency bands.....	7
Table 2.2: Tone correction factors, C depending on frequency and protrusion level, F	12
Table 4.1: Summary of geometric and operational parameters required for parametric fan noise prediction	41
Table 4.2: Summary of geometric and operational parameters required for parametric combustor noise prediction	44
Table 4.3: Summary of geometric and operational parameters required for parametric turbine noise prediction	45
Table 4.4: Summary of geometric and operational parameters required for parametric jet noise prediction	50
Table 4.5: Summary of geometric and operational parameters required for parametric airframe noise prediction	58
Table 5.1: Comparison of key Gasturb simulated and reference values for the V2527-A5 engine (TO represents takeoff thrust setting).....	71
Table 5.2: Comparison of key Gasturb simulated and reference values for the GE90-85B engine (TO represents takeoff thrust setting).....	71
Table 5.3: Relevant geometric and atmospheric data used for propagation in Fig. 5.10	85
Table 5.4: Simulated and reference EPNL values for the A320-200 aircraft with V2527-A5 engine model	90
Table 6.1: Comparison of reference [56], [142] and INSTANT simulated OSPL, loudness and sharpness values for sample spectra from Fig. 6.4	106
Table 6.2: Comparison of tonality exceeded 10% of the time (K_{10}) for various aircraft and procedures between the SQA software for synthesized audio and ILR's INSTANT for predicted spectra.....	112
Table 7.1: SR aircraft reference engine geometry values	123
Table 7.2: SR aircraft reference noise metric values at the flyover certification point.....	123
Table 7.3: SR aircraft reference noise metric values at the approach certification point.....	127

Table 7.4: SR aircraft reference community noise impacted area for a standard takeoff flight path.....	128
Table 7.5: SR aircraft reference community noise impacted area for a standard approach flight path	131
Table 7.6: SR aircraft reference W/S , T/W , SLST and airframe geometry values	134
Table 7.7: SR aircraft engine geometry values for two T/W values	139
Table 8.1: Comparison of reference SR aircraft and minimal EPNL optimized designs.....	143
Table 8.2: Community noise impact comparison of reference SR aircraft and minimum EPNL optimized design	144
Table 8.3: Certification noise impact comparison of reference SR aircraft and minimum EPNL optimized design	145
Table 8.4: Comparison of reference SR aircraft and minimal loudness optimized designs.....	151
Table 8.5: Certification noise impact comparison of reference SR aircraft and minimum loudness optimized design.....	152
Table 8.6: Community noise impact comparison of reference SR aircraft and minimum loudness optimized design.....	152
Table 8.7: Comparison of reference SR aircraft and minimal tonality optimized designs	153
Table 8.8: Certification noise impact comparison of reference SR aircraft and minimum tonality optimized design.....	154
Table 8.9: Community noise impact comparison of reference SR aircraft and minimum tonality optimized design	154
Table 8.10: SR aircraft reference with liner and minimum tonality optimized designs comparison.....	161
Table 8.11: SR aircraft reference with liner and minimum tonality optimized designs comparison.....	161

List of Symbols

Acronyms

ICAO	International Civil Aviation Organization
UHB	Ultra-High Bypass ratio
EPNL	Effective Perceived Noise Level
dBA	A-weighted decibel
CROR	Counter Rotating Open Rotor
GE	General Electric Company
IAE	International Aero Engines consortium
ILR	Institute of Aerospace Systems
VATSS	Virtual Air Traffic System Simulation
SPL	Sound Pressure Level
SEL	Sound Exposure Level
PNL	Perceived Noise Level
LP	Low Pressure
US	United States
FAA	Federal Aviation Authority of the US
OSPL	Overall SPL
PNLT	Tone-corrected PNL
PNLTM	Maximum tone-corrected PNL
DNL	Day-night average level

USEPA	United States Environmental Protection Agency
NNI	Noise and Number Index
UK	United Kingdom
NEF	Noise Exposure Forecast
BPF	Blade Passage Frequency
PA	Psychoacoustic Annoyance
NASA	National Aeronautics and Space Administration
NLR	Dutch Aerospace Laboratory
HWB	Hybrid Wing Body
DEP	Distributed Electric Propulsion
CDA	Continuous Descent Approach
EC	European Commission
SEFA	Sound Engineering For Aircraft
COSMA	Community Orientated Solutions to Minimize Aircraft Noise Annoyance
SSM	Sound Synthesis Machine
ATC	Air Traffic Control
CFD	Computational Fluid Dynamics
CAA	Computational Aeroacoustics
LES	Large Eddy Simulation
FWH	Ffowcs-Williams and Hawking
ANOPP	Aircraft Noise Prediction Program
BPF	Blade Passage Frequency

List of Symbols

IGV	Inlet Guide Vane
IFD	Inlet Flow Distortion
EEE (also E^3)	Energy Efficient Engine
SLST	Sea-level Static Thrust
IAE	International Aero Engines
ACARE	Advisory Council for Aviation Research and Innovation in Europe
HP	High Pressure
NG	Nose Gear
MG	Main Gear
DLR	German Aerospace Center
MICADO	Multidisciplinary Integrated Conceptual Aircraft Design and Optimization environment
INSTANT	ILR Noise Simulation and Assessment module
XML	Extensible Markup Language
MTOW	Maximum Takeoff Weight
TLAR	Top-Level Aircraft Requirement
MDO	Multidisciplinary Design Optimization
TSFC	Thrust Specific Fuel Consumption
EASA	European Aviation Safety Agency
EI	Emission Index
UHC	Unburned Hydrocarbon
CSV	Comma Separated Value

EGT	Exhaust Gas Temperature
BPR	Bypass Ratio
FPR	Fan Pressure Ratio
OPR	Overall Pressure Ratio
CAS	Calibrated Airspeed
NOMAD	Nonsmooth Optimization by Mesh Adaptive Direct Search software
ITA	Institute of Technical Acoustics
VRG	Virtual Reality Group
FFP	Fast Field Program
PE	Parabolic Equation
ISA	International Standard Atmosphere
INM	Integrated Noise Model
TOW	Takeoff Weight
LW	Landing Weight
FFT	Fast Fourier Transform
LR	Long Range
SR	Short Range
ICA	Initial Cruise Altitude
TOFL	Takeoff Field Length
LDN	Landing Distance

List of Symbols

Symbols

η_p	[-]	Propulsive efficiency
V	[m/s]	Aircraft airspeed
v_j	[m/s]	Jet (exhaust) velocity
Π	[W]	Acoustic power
K	[-]	Acoustic power coefficient
ρ	[kg/m ³]	Density of air
c	[m/s]	Speed of sound
d_j	[m]	Jet diameter
N	[noy]	Overall noy value of a spectrum
n	[noy]	noy value at band frequency
L_A	[dBA]	A-weighted decibel
L_{AE}	[dBA]	Sound Exposure Level
T_1	[s]	1 second normalizing time-constant
C	[dB]	Tone correction value
s	[-]	Slope of 1/3 octave SPL values
\bar{s}	[-]	Average slope of 3 adjacent 1/3 octave SPL values
F	[dB]	Difference between original and adjusted background SPL values
D	[dB]	Duration correction
$L_{Aeq,T}$	[dBA]	Average or equivalent A-weighted level
T	[hr]	Day or night specific time Period
L_D	[dBA]	Average A-weighted day-time level

L_N	[dBA]	Average A-weighted night-time level
L_{DN}	[dBA]	Day-night average A-weighted level
L_E	[dBA]	Average A-weighted evening-time level
L_{DEN}	[dBA]	Day-evening-night average A-weighted level
PA	[-]	Psychoacoustic Annoyance
N_5	[sone]	Loudness value exceeded 5% of the time
w_s	[-]	Sharpness weightage term
S	[acum]	Sharpness
w_{FR}	[-]	Roughness and fluctuation strength weightage term
F	[vacil]	Fluctuation strength
R	[asper]	Roughness
PA_{mod}	[-]	Modified Psychoacoustic Annoyance
ρ	[kg/m ³]	Fluid density
\mathbf{v}	[-]	Fluid velocity vector
\mathbf{P}	[-]	Stress tensor of fluid
\mathbf{f}	[-]	External force field acting on volume element
p	[N/m ²]	Fluid pressure
\mathbf{I}	[-]	Identity tensor
δ_{ij}	[-]	Kronecker delta
$\boldsymbol{\sigma}$	[-]	Viscous stress tensor
c_0	[m/s]	Speed of sound of unperturbed fluid
\mathbf{T}	[-]	Lighthill's turbulence stress tensor

List of Symbols

p'	[N/m ²]	Fluid pressure perturbation from unperturbed value p_0
ρ'	[N/m ²]	Fluid density perturbation from unperturbed value ρ_0
\mathbf{x}	[-]	Vector for receiver/observer position
\mathbf{y}	[-]	Vector for aircraft/source position
V	[kg/m ³]	Volume of source region
r	[m]	Distance between source and receiver
t_e	[s]	Emission time
t	[s]	Retarded/reception time
δ	[-]	Dirac delta function
u_{jet}	[m/s]	Mean jet velocity
f_c	[Hz]	Characteristic frequency of turbulence
l	[m]	Characteristic length of turbulence
u_c	[m/s]	Convection speed of eddy
t_c	[s]	Time needed to convect a turbulent eddy over characteristic dimension l with convection speed u_c
I	[W/m ²]	Acoustic intensity
F	[N]	Instantaneous force exerted by compact object on surrounding fluid
\mathbf{n}	[-]	Vector normal to compact object surface
v_n	[m/s]	Velocity of compact object (= $\mathbf{v} \cdot \mathbf{n}$)
D	[m]	Largest dimension of compact object
U	[m/s]	Flow speed
M	[-]	Flow Mach number

θ	[°]	Polar directivity angle
ψ	[°]	Azimuthal directivity angle
S	[-]	Spectral weighting function
η	[-]	Frequency parameter of spectral weighting function
D	[-]	Directional weighting function
f	[Hz]	Frequency
NI	[s ⁻¹]	Fan or low-pressure spool speed
B	[-]	Fan rotor blade number
K'	[-]	Fan component acoustic power constant
G	[-]	IGV and tone cut-off matrix
δ	[-]	Tone cut-off factor
M_t	[-]	Fan rotor tip Mach number
V	[-]	Stator vane number
d	[m]	Diameter
n	[-]	Harmonic number
s	[m]	Rotor-stator spacing
C	[m]	Mean chord of fan rotor blade
a	[-]	Rotor-stator spacing exponent
M_m	[-]	Design point Mach number index
b	[-]	Mach number index exponent
$M_{t,d}$	[-]	Fan rotor tip design Mach number
M_r	[-]	Relative rotor tip Mach number

List of Symbols

M_x	[$-$]	Axial flow Mach number
\dot{m}	[kg/s]	Mass flow
A_e	[m 2]	Engine reference area
ΔT	[K]	Temperature rise across fan
T	[K]	Temperature
p_{ref}	[N/m 2]	Reference acoustic pressure at threshold of hearing
T_t	[K]	Total temperature
p_t	[N/m 2]	Total pressure
ΔT_{des}	[K]	Design point temperature extraction from turbine
ρ_j	[kg/m 3]	Jet density
A_j	[m 2]	Jet area
ω_0	[$-$]	Primary jet density exponent
D_m	[$-$]	Directivity function for mixing noise
F_m	[$-$]	Spectral function for mixing noise
H_m	[$-$]	Forward flight effects function for mixing noise
G_c	[$-$]	Coaxial nozzle configuration factor for mixing noise pressure
G_p	[$-$]	Plug nozzle configuration factor for mixing noise pressure
S_m	[$-$]	Strouhal number for mixing noise
δ'	[$^\circ$]	Angle between engine axis and flight vector
θ'	[$^\circ$]	Modified polar directivity angle
g_c	[$-$]	Coaxial nozzle configuration factor for Strouhal number
g_p	[$-$]	Plug nozzle configuration factor for Strouhal number

T_j	[K]	Jet temperature
f_s	[-]	Frequency shift parameter
R_d	[-]	Ratio of hydraulic diameter to equivalent diameter
d_p	[m]	Plug diameter
d_h	[m]	Plug nozzle hydraulic diameter
$\omega - \omega_0$	[-]	Density exponent for forward flight effects factor
L	[m]	Characteristic dimension of airframe noise component
K	[-]	Empirical constant for airframe component acoustic power
G	[-]	Geometry function for airframe component acoustic power
b	[m]	Span
δ_w	[m]	Turbulent boundary layer thickness
μ	[kg/ms]	Dynamic viscosity
δ_f	[°]	Flap deflection angle
n	[-]	Number of landing gear wheels
l	[m]	Gear strut length
T/W	[-]	Aircraft thrust to weight ratio
W/S	[kg/m ²]	Aircraft wing-loading
T	[N]	Aircraft thrust
D	[N]	Aircraft drag
g	[m/s ²]	Gravitational acceleration constant
m	[kg]	Mass
h	[m]	Aircraft altitude

List of Symbols

r_s	[m]	Source radius
r_o	[m]	Observer radius
α	[dB/m]	Atmospheric absorption coefficient
h	[% mol fraction]	Absolute humidity
h_r	[%]	Relative humidity
p_{sat}	[kPa]	Saturation vapor pressure of air
p_{ref}	[kPa]	Atmospheric pressure at ISA mean sea-level
T_{ref}	[kPa]	Atmospheric temperature at ISA mean sea-level
T_{0I}	[K]	Triple point isotherm temperature
f_r	[Hz]	Relaxation frequency of molecules
δL_t	[dB]	Overall atmospheric absorption
γ	[°]	Elevation angle
r_1	[m]	Direct path distance between source and observer ($= r$)
r_2	[m]	Reflected path distance between source and observer
Δr	[m]	Path length difference
θ	[°]	Incidence angle
h	[m]	Observer height
G	[-]	Ground effects factor
R	[-]	Magnitude of complex spherical-wave reflection coefficient
α	[-]	Argument of complex spherical-wave reflection coefficient
a	[-]	Incoherence constant
Γ	[-]	Complex plane-wave reflection coefficient

v	[-]	Complex specific ground admittance
z	[-]	Complex specific ground impedance
σ	[kPa/m ² s]	Surface effective flow resistivity
η	[-]	Dimensionless frequency parameter for specific admittance
l	[m]	Horizontal distance from aircraft on the ground
G	[dB]	Lateral attenuation factor
t_r	[s]	Reception time (also t)
t_d	[s]	Time delay
$t_{e,ret}$	[s]	Retarded emission time
L_N	[phon]	Loudness level
z	[Bark]	Critical band rate/number
f_c	[Hz]	Band center frequency
N	[sone]	Loudness
N'	[sone/Bark]	Specific loudness
L_E	[dB]	Excitation level per critical band
L_{EHS}	[dB]	Excitation level at threshold in quiet
$g(z)$	[-]	Sharpness weighting function
ΔL	[dB]	Excess SPL value of tonal component
L	[dB]	SPL value of tonal component
L_{EK}	[dB]	Secondary excitation level at frequency f_k due to i th tonal component
s	[dB/Bark]	Steepness of slope of excitation level-critical band rate pattern
E_{Gr}	[dB]	Masking intensity of noise in critical band surrounding tone

List of Symbols

E_{HS}	[dB]	Intensity at threshold of hearing
Δz	[%]	Bandwidth as percentage of CBW
w_1	[-]	Bandwidth weighting function
w_2	[-]	Frequency weighting function
w_3	[-]	Prominence weighting function
w_T	[-]	Tonal weighting function
w_{Gr}	[-]	Loudness weighting function
N_{Gr}	[sone]	Loudness of spectrum without tones
c	[-]	Calibration constant for tonality
K	[t.u.]	Tonality
V_{app}	[m/s]	Aircraft approach speed

Indices

∞	Freestream condition
0	Observer/sea-level condition
o	Unperturbed flow condition
$j,1$	Primary jet parameter
$j,2$	Secondary jet parameter
w	Wing parameter
f	Flap parameter
NG	Nose gear parameter
MG	Main gear parameter

h Horizontal tail parameter

v Vertical tail parameter

s Source condition

1 Introduction

Aircraft noise is a very relevant modern problem, with residents being exposed to a much more frequent exposure than what was observed at the beginning of the commercial aviation age. Not just the frequency of air-traffic but also the spread of air-traffic has reached wider parts of the world due to the continuously increasing air-traffic demand and the resulting increase in air traffic volume. New avenues of growth in aviation are continuously being found by the aircraft manufacturers and airlines, with growth markets currently being seen in Asia [1] and the demand is seen to continue to increase at roughly five percent per year by both Airbus and Boeing [2]. Meeting this demand is going to require the construction of several new airports, both large and small, and also an expansion of the current air transport infrastructure. With the construction of new airports and construction of more runways on existing airports [3], [4], [5], more and more people are beginning to be affected by the problem of aircraft noise than was the case in the previous decades. This has led to aircraft and engine manufacturers to come up with quieter designs and noise reduction technologies to increase the acceptance of new aircraft by reducing their noise impact on the residents. The aircraft have over the past decades indeed become quieter [6] and the relevant governing bodies such as the International Civil Aviation Organization (ICAO) also continue to enforce increasingly stringent noise certification requirements [7].

A point however is close to being reached now, where it becomes physically difficult to achieve increasingly quieter engines that can still be practically integrated onto conventional tube and wing aircraft designs, as Ultra-High Bypass ratio (UHB) engines that may yield large noise reductions [8] will have exceedingly large diameters and geared turbofan engines presently entering the aerospace market can also only yield noise reductions to a certain physical limit. This physical and practical limitation to achieving endlessly quieter engines and also the residents' expectations for aircraft that disturb or 'annoy' them as less as possible has led to a need to not just reduce the overall noise level, but to reduce aircraft noise components that might individually be contributing to the experienced annoyance. The latter reduction may not necessarily lead to aircraft that are quieter, but rather aircraft that sound less disturbing and more acceptable to the residents, involving an improvement in the 'quality of the sound'.

Conventional metrics that are used today for aircraft noise certification and community noise assessment are the Effective Perceived Noise Level (EPNL) and the A-weighted decibel (dBA) respectively. The dBA metric has already been seen to be a poor indicator of actual subjective annoyance experienced by residents [9], [10], [11] and the EPNL metric, although a comprehensive metric taking into account a number of factors such as noise level, tonal penalty and effect of duration, still assumes a simplistic frequency division for allotting tonal penalties, only bases the magnitude of tonal penalty on the strongest protruding tone and lacks in providing information on the tonal content if is of low intensity although the tones may still be audible. Different engines having different bypass ratios can have significantly different composition and magnitudes of broadband and tonal content. Larger engines such as the General Electric (GE)-90 will sound noticeably different to a smaller International Aero Engines (IAE) V2500 engine. The deficiencies of the current metrics will be further magnified for future unconventional aircraft and engines such as Counter Rotating Open Rotor (CROR) engines, which not only have tones of much stronger prominence at much lower frequencies, but also a significantly higher number of tones [12], [13]. This understanding leads to the need for alternate new metrics that better capture differences in spectral

content of aircraft noise, which in turn can lead to a better prediction of annoyance as experienced by residents.

Although some amount of research has been carried out on what characteristics of aircraft noise contribute to the annoyance experienced by residents via psychoacoustic surveys [14], [15], [16], [17], hardly any research currently exists that correlates the annoyance causing noise characteristics with aircraft and engine design parameters that actually produce the noise at the source. The goal of this dissertation is to provide a means with which noise reduction can be approached in an alternate way such that not just an intensity reduction is achieved but rather an improvement in the quality of the sound produced by aircraft and their engines, so that they cause lower annoyance to the residents. This involves detailed knowledge of the spectral characteristics of aircraft noise, how aircraft noise is generated and by what primary components, as well as what interplay exists between the major broadband and tonal components. This interplay between the broadband components such as jet and airframe noise plus the tonal components such as fan inlet and exhaust tones is analyzed in this work to understand how each design parameter affects both the overall level as well as sound quality. Furthermore, it is investigated how the aircraft and engine design parameters can lead to a redistribution of the spectral energy of the produced aircraft noise, with the goal of improving aircraft noise sound quality and hence of reducing annoyance at an early design stage, preventing costly noise reduction measures at a later stage.

Designing aircraft that produce favorable sounds will improve the acceptance of aircraft noise and thus allow lower resistance from the residents to the construction of new airports and expansion of air-traffic. Furthermore, by identifying any negative sound effects at an early stage, the need for expensive noise reduction technologies such as fan acoustic liners at a later stage can be reduced. An attempt has been made in the current research work to assess aircraft designs for the annoyance they produce at an early conceptual design phase and to see if current civil aircraft could be optimized at an early stage to produce minimal annoyance to the residents. In order to this, the use of psychoacoustic sound quality metrics has been made to assess aircraft noise for annoyance and preliminary optimizations of aircraft designs for minimal community noise impact in standard and sound quality metrics will be shown in this dissertation, after a description of the noise modeling, assessment and aircraft design methodologies. To keep a check on realistic application of annoyance optimizing design changes, the effect on aircraft performance by following aircraft weight and fuel changes as well as changes to certain top level requirements such as takeoff and landing distance for each design has also been considered.

The assessment of aircraft noise in the various metrics firstly requires tools with which noise can be modeled for each aircraft and engine component at the source. This in turn requires models for the engine geometry and thermodynamics as well as aircraft design information and the aircraft flight paths. The noise thus modeled at the source must then be propagated through the atmosphere before it reaches the resident on the ground and can be assessed. The work in this dissertation has been divided into firstly an explanation of the motivation for alternate assessment of aircraft noise in Chapter 2, followed by the current state of the art in annoyance assessment and its consideration during conceptual aircraft design in Chapter 3. Chapter 4 gives a description of the source noise models used in the current work for each relevant aircraft and engine noise component as well as a brief description of the physical theory behind the source noise generation. Chapter 5 describes the integration of the source noise models in a complete simulation and assessment toolchain for simulating noise impact from the source to the ground, and also

the toolchain's integration in an aircraft design environment for performing preliminary aircraft design parametric variations and optimizations. The sound quality metrics and their implementation in the noise simulation and assessment toolchain are explained in Chapter 6, as well as some sample results for the annoyance impact of current short range and long range aircraft. Chapter 7 shows design parameter sensitivity study results for individual aircraft and engine geometry parameters used in the source noise models and how they affect the noise produced on the ground as well as overall aircraft design variations of the aircraft thrust to weight ratio and wing-loading. Chapter 8 shows optimizations for conventional and sound quality metrics and a comparison of their changes from reference design values, parallel to performance considerations. Chapter 8 also shows how the metric optimized designs correlate with sound via synthetic sounds of each aircraft and also compares the noise reductions of the optimized designs with the reductions produced by the use of modern acoustic liner technology. Chapter 9 provides the conclusions of the current work and outlook for future applications.

The research work in this dissertation has been performed at the Institute of Aerospace Systems (ILR) of RWTH Aachen University and was partly sponsored by the Exploratory Research Space Boost fund of RWTH Aachen's excellence initiative via the interdisciplinary project VATSS – Virtual Air Traffic System Simulation [18], [19].

2 Motivation for alternate assessment of aircraft noise

The first sound of the jet engine came with the advent of the jet age, which was and still is recognized as one of the loudest sounds known to man. The extremely high levels of noise produced by these aircraft, flying over populated areas which were not used to such sounds, led to research specializing in the understanding and abatement of the noise produced. The field of aeroacoustics was developed [20], [21] to understand the physics behind the noise generation and operational constraints were placed on air operations to alleviate the noise impact on communities in airport vicinities [22]. The first jet engines that flew were considerably fuel inefficient and extremely loud with their noise signatures being dominated by the broadband jet mixing noise due to the very high jet exhaust velocities they produced. The high jet velocities were produced due to the early engines being pure turbojet engines. Eventual research into improving the fuel efficiency of the jet engines led to the discovery that lowering the jet velocity v_j closer to the aircraft velocity V would yield considerable improvement in the engine's propulsive efficiency (cf. Eq. 2.1), which is proportional to the engine's fuel efficiency. This led to the development of engines with bypass ratios, that allowed a part of the air mass flow to 'bypass' the primary engine core, lowering the jet velocity as well as improving the propulsive efficiency and with it, the fuel efficiency. A useful side effect of introducing bypass or secondary flow was that with the reduction in jet velocity, the jet noise was also reduced.

$$\eta_p = \frac{2}{1 + \frac{v_j}{V}} \quad (2.1)$$

$$\Pi = \frac{K \rho_\infty v_j^8 d_j^2}{c_\infty^5} \quad (2.2)$$

Jet noise acoustic power varies theoretically with the eighth power of jet velocity for subsonic jets according to Lighthill's acoustic power law from [20], shown in Eq. 2.2. The relation is seen to hold true for cold jets with a temperature ratio (T_j/T_∞) of close to unity, with a relation between sixth to eighth power of jet velocity observed for actual jets, which are hotter in practical situations [6], [23]. In Eq. 2.2, Π is the acoustic power, K is the acoustic power coefficient, c_∞ is the speed of sound and d_j is the jet diameter, which indicates that an increase in the jet diameter or jet area would also increase the jet noise intensity produced. Much of the focus till the 1960s was put on the reduction of jet noise produced by low bypass ratio turbofan engines of that time, which dominated the other noise sources. Many of the other aircraft noise components such as fan and turbine tones, combustor noise as well as noise from the airframe such as slats, flap trailing edge and landing gear were seen to be of secondary importance, due to their lower prominence in the observed aircraft noise spectra of that time. It was only when the bypass ratio was continuously increased and jet noise brought down to lower levels that the other components started gaining audible prominence. The increase in prominence of fan noise with reduction in jet noise is for instance shown in Fig. 2.1, reproduced from [23].

The high to very high bypass ratio engines of today produce relatively low jet noise, particularly during the approach phase where the fan and airframe are now typically the dominating noise sources. Jet noise still remains dominant during takeoff for most aircraft and engines, although the larger high bypass ratio engines such as GE90 variants can produce more dominant fan noise also during takeoff [24]. The noise

signatures of current aircraft and engines are therefore very different from their counterparts of fifty years ago, with components such as fan rotor-stator interaction tones, buzzsaw noise and fan broadband noise, low-pressure turbine tones, combustor noise as well as airframe noise being clearly identifiable depending on the aircraft engine thrust setting and flight phase. This change in the noise signature has led to a need for a more focused approach to noise reduction rather than just of overall levels.

For larger engines with dominant fan noise, a continual increase in bypass ratio is therefore not the ideal solution. Other technologies such as acoustic liners have thus become increasingly essential on modern high bypass ratio engines, which absorb or favorably reflect individual frequencies, with most effective reductions of 6-10 dB typically in the range of 1000-3500 Hz. The use of acoustic liner material however increases the costs and also adds additional weight to the engines, which in turn partly reduces the aircraft level fuel reduction obtained by using a high bypass ratio engine.

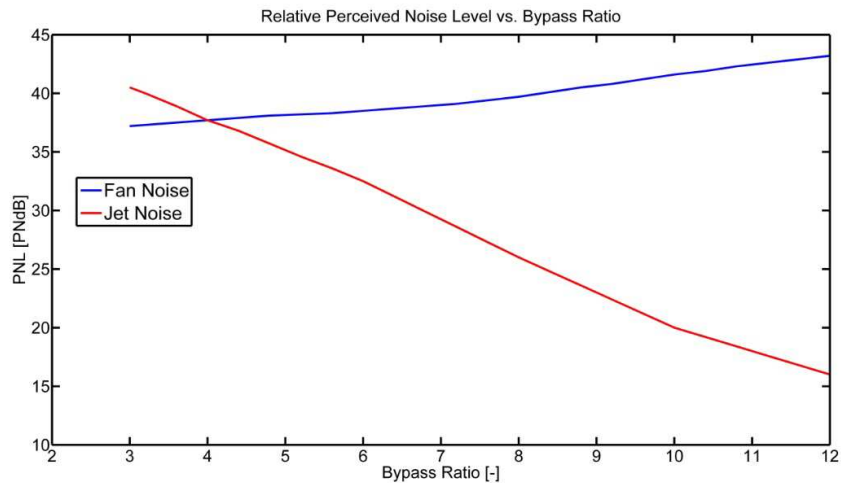


Figure 2.1: Variation of fan and jet perceived noise with bypass ratio reproduced from [23]

Two primary reasons can be identified for an alternate or improved approach to noise reduction and its assessment during conceptual aircraft design. Firstly, using metrics that better capture aircraft noise annoyance, an approach can be attempted towards lowering the annoyance experienced by the residents and making aircraft noise more acceptable. Secondly, by using metrics that better capture differences and changes in spectral content, focused reductions in particular noise components can be achieved by adjusting the spectral distribution of aircraft noise, which can reduce the later need for noise reduction technologies such as acoustic liner material or chevron nozzles.

The goal of any attempt to reduce the impact of aircraft noise on the community has to be to increase the acceptance of aircraft noise such that no serious resistance to current and projected growth in air traffic is posed. Since the societal benefit is strongly coupled with an economic benefit, this makes the situation one of considerable concern and interest currently [3], [4] and of major concern when projected to the future [25]. To increase aircraft noise acceptance, the annoyance aircraft noise causes therefore has to be reduced. This implies those components of aircraft noise that particularly contribute to listeners' annoyance have to be able to be identified and quantified so that aircraft, engines and flight procedures can be designed that ultimately produce minimal annoyance. The societal benefits of this approach will

result in economic savings as well, both at an air-transport level – by allowing air traffic to expand to meet the projected worldwide demand, but also at an aircraft level by aiding in identifying and preventing adverse sound effects at an early stage inherently by design.

The issue of increasing aircraft noise acceptance is directly connected with how aircraft noise is assessed. Changes in individual aircraft noise spectral characteristics can affect its perceived annoyance to varying extents. As such, improved metrics are required that capture the various characteristics of aircraft noise in a superior way to the currently used metrics. In order to do so, it is firstly necessary to clearly identify the deficiencies in metrics currently used to assess aircraft noise such that other improved metrics can be suggested which correspond better to the annoyance experienced by residents and may be more suitable for designing low annoyance aircraft in the future. As such, a brief analysis of the currently used metrics in the aerospace industry is presented next, followed by an identification of some aspects where improvements might be necessary.

2.1 Currently used metrics in the aerospace industry

Several metrics have been used in the aerospace industry for aircraft noise assessment and different approaches over the years led to different metrics being developed that would better reflect human response to the aircraft noise signatures [26] of that time. These metrics range from loudness based weighted Sound Pressure Level (SPL) metrics, annoyance based Perceived Noise Level (PNL) metrics and average level metrics both for single events (i.e. single aircraft movements) as well as for multiple events taking into account cumulative aircraft movements over a certain time period.

2.1.1 Loudness based weighted Sound Pressure Level metrics

The most commonly used weighted SPL metrics used in the aerospace industry are the A-weighted and C-weighted sound pressure levels.

1. *dBA or A-weighted SPL*

The A-weighted SPL, also referred to as the dB(A) or simply dBA metric, has been widely used for community noise assessment of all forms of outdoor environmental noise including noise due to different forms of transportation such as road, rail and aircraft. Its widespread use in the noise and acoustic community in general and the various measurement instruments available which measure A-weighted SPL values (such as simple sound level meters) also led to the use of the dBA metric in the aerospace industry. The A-weighting of the dBA metric was developed to approximate the fact that the human hearing system perceives high frequencies as louder than low frequencies. As such, the A-weighting applies a large reduction to low frequency noise so that the higher frequencies are more highly weighted than low frequencies below 500 Hz when assessing noise impact. The weightage is applied to individual frequencies and is shown for the 1/3 octave frequencies in Table 2.1 for both A-weighting as well as C-weighting.

Table 2.1: A- and C-weighting for 1/3 octave frequency bands

1/3 octave center frequency [Hz]	A-weighting correction [dB]	C-weighting correction [dB]	1/3 octave center frequency [Hz]	A-weighting correction [dB]	C-weighting correction [dB]
50	-30.2	-1.3	800	-0.8	0
63	-26.2	-0.8	1000	0	0
80	-22.5	-0.5	1250	0.6	0
100	-19.1	-0.3	1600	1	-0.1
125	-16.1	-0.2	2000	1.2	-0.2
160	-13.4	-0.1	2500	1.3	-0.3
200	-10.9	0	3150	1.2	-0.5
250	-8.6	0	4000	1	-0.8
315	-6.6	0	5000	0.5	-1.3
400	-4.8	0	6300	-0.1	-2.0
500	-3.2	0	8000	-1.1	-3.0
630	-1.9	0	10000	-2.5	-4.3

The A-weighting was chosen to approximate the 40 phon equal loudness curve from the equal loudness contours shown in Fig. 2.2. Since the equal loudness contours show that different SPL values will be perceived to have different loudness depending on their frequencies, a simpler approach was sought by the industry to be able to express the overall loudness of a spectrum with a single number and the 40 phon curve was chosen as a reference for this purpose. This relatively easy single value estimation of relative loudness was readily accepted by the industry for all outdoor noise assessment purposes, including by the aerospace industry. Another reason for the popularity of the dBA metric is the fact that it shows noise impact in numbers that are always lower than values shown in dB [27]. As lower numbers correspond better to the feeling of lower loudness psychologically, the industry is hesitant to depart from its use so easily.

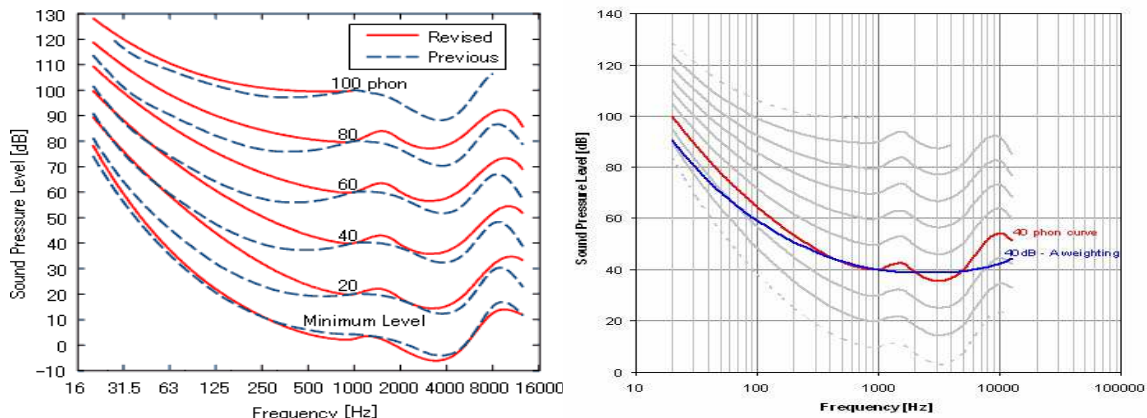


Figure 2.2: Equal loudness contours for pure tones of different levels and frequency (left), approximation of 40 phon loudness curve with A-weighting used for the dBA metric (right)¹

¹ Source of images: DiracDelta.co.uk – Science and engineering encyclopedia

2. dBC or C-weighted SPL

The C-weighted SPL or the dBC metric has also been used for the assessment of community noise around certain airports [28], [29] especially to focus on low frequency noise during takeoff operations. The C-weighting does not penalize low frequency noise as highly as the A-weighting and rather gives a small penalty to high frequency content above 4000 Hz. Since the dBC metric does not reduce low frequency noise values, it has been found to better correspond to community annoyance when the noise signatures are dominated by low frequency components such as those emanating from the jet. Furthermore, vibrations experienced in houses in airport vicinities are caused solely by noise below 250 Hz [29] and the dBC metric hence also corresponds better than the dBA metric in estimating noise induced house vibration thresholds. The C-weighting was developed to approximately follow the 100 phon equal loudness contour and was thus envisioned for assessment and measurement of louder noise levels than the dBA metric.

3. Sound Exposure Level (SEL or L_{AE})

Another metric used to describe the noise impact of single aircraft movements is the Sound Exposure Level (SEL), which integrates the noise impact in dBA for a single aircraft movement over the duration for which the noise impact is within 10 dBA of the maximum dBA value. A normalizing time constant T_1 of 1 second is then used according to Eq. 2.3 to calculate the SEL value in dBA:

$$L_{AE} = 10 \log_{10} \left[\frac{1}{T_1} \int_{t_1}^{t_2} 10^{\frac{L_A(t)}{10}} dt \right] \quad (2.3)$$

Here, L_{AE} is the SEL value, $L_A(t)$ is the time-varying noise impact in dBA during the course of a movement and t_1 and t_2 specify the time-interval during which noise impact is 10 dBA below the maximum dBA value L_{Amax} . The SEL value is thus intended to correspond to the constant sound level which has the same amount of acoustic energy in 1 second as the whole noise event. The SEL metric has been used not just for aircraft noise but also for other forms of transportation noise such as road and rail.

2.1.2 Annoyance based Perceived Noise Level metrics

1. Perceived Noise Level (PNL)

The perceived noise level metric was developed by K.D. Kryter [30] in the 1960s as part of efforts of the Federal Aviation Authority (FAA) of the US to develop a metric describing the annoyance experienced by residents living in airport vicinities [31]. The goal here was to develop a means of certifying aircraft for noise, an aspect which till then had not been part of the aircraft certification process [32]. An approach similar to the development of equal loudness contours (Fig. 2.2 (left)) was followed and it was reasoned that listeners perceive complex sounds containing high frequency components as more annoying than solely pure tones [33]. As such, a new annoyance scale analogous to the loudness scale was developed using psychoacoustic tests carried out on listeners in test environments for the ‘noisiness’ of aircraft sounds. This annoyance scale when described linearly was given the unit of *noy* (analogous to the linear loudness unit sone) and the overall noy value could be converted into the logarithmic perceived noise level PNL in units of Perceived Noise decibel, PNdB (analogous to the logarithmic loudness unit phon).

The equal noisiness curves developed for the PNL metric (shown in Fig. 2.3) correlate the perceived noisiness or annoyance experienced by listeners in test environments to the level and frequency of

complex sounds. A sound with random variation of pressure over time centered at 1 kHz in the 1000 Hz 1/3 octave band with an SPL of 40 dB was chosen as the reference sound for creating the equal noisiness curves. The goal was to obtain a single value from a given spectrum (1/3 octave or octave) representing the annoyance in PNL, which was performed quite simply using Eq. 2.4 and 2.5.

$$N = n_{max} + 0.15 \sum_{i=1}^m (n_i) - n_{max} \quad (2.4)$$

$$PNL = 40 + \frac{10 \log_{10} N}{\log_{10} 2} \quad (2.5)$$

Here, n_{max} is the maximum noy value in the spectrum, n_i is the noy value of the i^{th} band and m is the number of 1/3 octave bands, which together produce the overall noy value N . In Eq. 2.4, a multiplication factor of 0.3 instead of 0.15 is used for octave bands. Eq. 2.5 indicates that when the overall noisiness or annoyance N in noy doubles, then the PNL value increases by 10 PNdB. Furthermore, depending on the spectral distribution, two sounds with the same Overall Sound Pressure Level (OSPL) value, or A-weighted OSPL (OASPL) value in dBA, can have very different annoyance values expressed in PNL [6]. This observation indicates that the PNL metric was an improvement over previously used metrics when trying to capture spectral influence on annoyance.

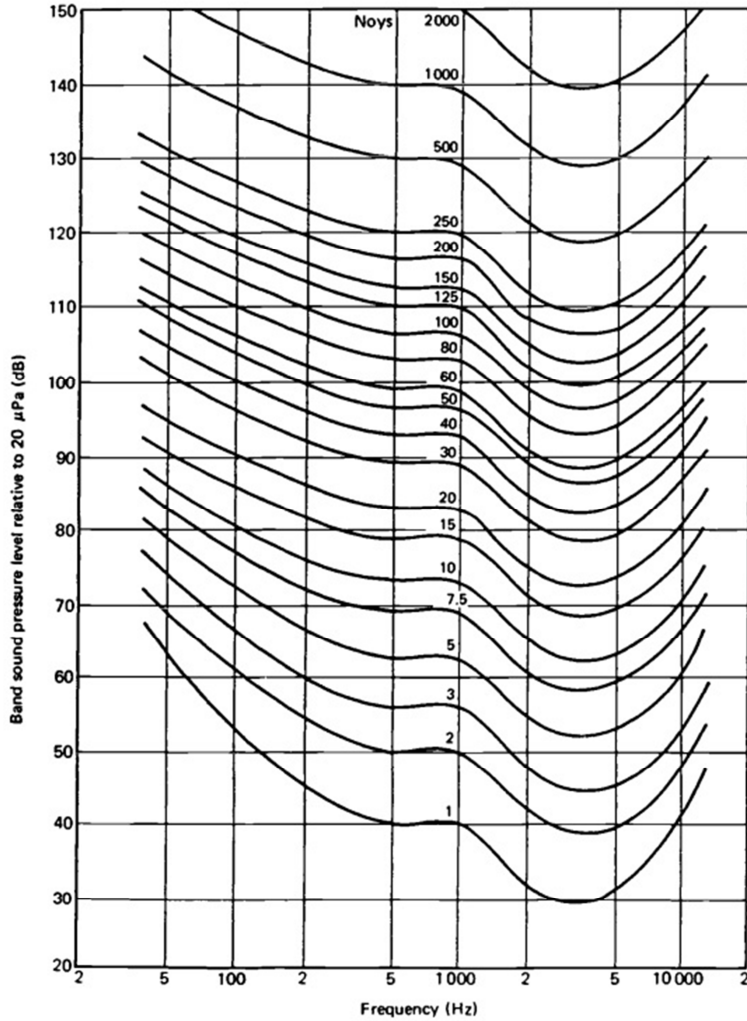


Figure 2.3: Equal noisiness curves used for PNL calculation

2. Tone-corrected Perceived Noise Level (PNLT)

After comparing the PNdB values with listener test results, it was reasoned that certain aspects of aircraft sounds hadn't been fully captured by the PNL metric and further improvement of the metric was sought. The human hearing system is very sensitive to the presence of discrete tones in a sound and can neglect broadband sounds in neighboring frequencies if any tones are detected in a particular band. The fact that the presence of discrete tones in otherwise broadband sounds makes the sound perceptually more annoying [34], led to the addition of a *tone correction* to the calculated PNL value. The Tone-corrected Perceived Noise Level (PNLT) metric was intended to approach the annoyance caused by aircraft noise in an improved way than the PNL metric and a tonal penalty was added to the PNL values if the presence of a strong protruding tone in the spectrum was detected. The tone correction, C is added to the PNL value to obtain the value in PNLT according to Eq. 2.6:

$$PNLT = PNL + C \quad (2.6)$$

The PNLT metric is based on 1/3 octave spectra ($m = 24$ bands) and the value of C depends on the frequency as well as level of the strongest protruding tone found in a 1/3 octave band, considering frequency bands from 80 Hz to 10000 Hz. The Effective Perceived Noise Level (EPNL) metric, which involves a time integration of the PNLT values obtained for each time-step of 0.5 seconds, is used for certification of noise and combines the individual effects of broadband and tonal aircraft noise components. The unconventional sound quality metrics also attempt to do the same (as will be explained in detail in Chapter 6) but in an alternate more detailed manner. In order to identify the areas where the EPNL metric could be improved and to allow a clear comparison with the alternate sound quality metrics, the procedure for calculating the PNLT values will be described in detail in this subsection. The PNLT and EPNL calculation involves ten steps in total, which will be explained now.

The first step in calculating PNLT values is to calculate the changes in SPL or the slopes s of the spectrum in the 1/3 octave bands, starting with the 80 Hz frequency band ($i = 3$):

$$\begin{aligned} s(3) &= \text{No value} \\ s(i) &= SPL(i) - SPL(i-1), \quad i = 4, 5, \dots, 24 \end{aligned} \quad (2.7)$$

where s is the change in SPL or the slope in dB and i is the third octave frequency band index. The second step involves identifying and encircling (or marking) those slope values s for which the change in slope Δs when compared to the previous third octave band slope $s(i-1)$ is greater than 5 dB:

$$|\Delta s(i)| = |s(i) - s(i-1)| > 5 \quad (2.8)$$

Three checks are then made for the encircled slope values s , based on which the original $SPL(i)$ values are marked or encircled:

- i. If the encircled slope value $s(i)$ is positive and algebraically greater than the previous slope $s(i-1)$, then $SPL(i)$ is encircled.
- ii. If the encircled slope value $s(i)$ is zero or negative and $s(i-1)$ is positive, then $SPL(i-1)$ is encircled.
- iii. For all other cases than i. and ii., no $SPL(i)$ or $SPL(i-1)$ values are encircled.

In the fourth step, new adjusted sound pressure levels $SPL'(i)$ are obtained according to the following three sub-steps:

- i. For the non-encircled sound pressure levels, the adjusted sound pressure levels are set equal to the original sound pressure levels i.e. they remain unchanged $SPL'(i) = SPL(i)$.
- ii. For the encircled sound pressure levels, the new adjusted sound pressure levels are set equal to the arithmetic average of the preceding and following sound pressure levels i.e.:

$$SPL'(i) = \frac{1}{2}[SPL(i-1) + SPL(i+1)] \quad (2.9)$$

- iii. If the SPL value in the 24th (i.e. 10 kHz) third octave band is also encircled, then the adjusted SPL value is calculated according to Eq. 2.10:

$$SPL'(24) = SPL(23) + s(23) \quad (2.10)$$

The fifth step in the calculation involves recalculating the slopes as s' , including a slope for an imaginary 25th third octave band:

$$s'(3) = s'(4) \quad (2.11a)$$

$$s'(i) = SPL'(i) + SPL'(i - 1), i = 4, 5, \dots, 24 \quad (2.11b)$$

$$s'(25) = SPL'(24) \quad (2.11c)$$

In the sixth step, an arithmetic average of three adjacent recalculated slopes s' is calculated according to Eq. 2.12 for the 1/3 octave bands from $i=3$ to $i=23$:

$$\bar{s}(i) = \frac{1}{3}[s'(i) + s'(i + 1) + s'(i + 2)] \quad (2.12)$$

In the seventh step, the final background 1/3 octave SPL values ($SPL''(i)$) are calculated starting from band $i=3$ to $i=24$ using Eq. 2.13:

$$SPL''(3) = SPL(3) \quad (2.13a)$$

$$SPL''(i) = SPL''(i - 1) + \bar{s}(i - 1), \quad i = 4, 5, \dots, 24 \quad (2.13b)$$

The eighth step involves the calculation of the differences, $F(i)$ between the original SPL values and the final background SPL values i.e. the so-called protrusion level:

$$F(i) = SPL(i) - SPL''(i) \quad (2.14)$$

The maximum tone correction factor from all the tone correction factors $C(i)$ computed for the protruding tones, is then the final tone correction factor C , that is added to the overall PNL value to obtain the PNLT value according to Eq. 2.6. Only differences $F(i)$ greater than 1.5 dB are considered as relevant for the annoyance computation (this value used to be 3 dB till the 1970s [6]) and the tone correction factors $C(i)$ are calculated according to Table 2.2 in the ninth step.

Table 2.2: Tone correction factors, C depending on frequency and protrusion level, F

Frequency, f [Hz]	Level difference, F [dB]	Tone correction, C [dB]
$50 \leq f < 500$	$1.5 \leq F < 3$	$F/3 - 0.5$
	$3 \leq F < 20$	$F/6$
	$20 \leq F$	3.333
$500 \leq f \leq 5000$	$1.5 \leq F < 3$	$2F/3 - 1$
	$3 \leq F < 20$	$F/3$
	$20 \leq F$	6.667
$5000 < f \leq 10000$	$1.5 \leq F < 3$	$F/3 - 0.5$
	$3 \leq F < 20$	$F/6$
	$20 \leq F$	3.333

3. Effective Perceived Noise Level (EPNL)

Another factor that could affect the annoyance experienced by residents due to aircraft noise was deemed to be the effect of duration [35]. It was reasoned by the industry experts and FAA representatives that the effect of annoyance would be enhanced the longer the residents were exposed to close to maximum PNLT values in the event of an aircraft flyover. Incorporation of a duration correction was then the final addition to the PNL metric that would ultimately yield a single value measure for the annoyance caused by aircraft noise for a single event (single departure or approach flight movement). Fig. 2.4 describes how the time integration for the duration correction is carried out, with PNLT values 10 PNTdB below the maximum PNLT value integrated for the aircraft movement and then normalized for a 10 second interval, in a similar way to the time integration performed for the SEL metric.

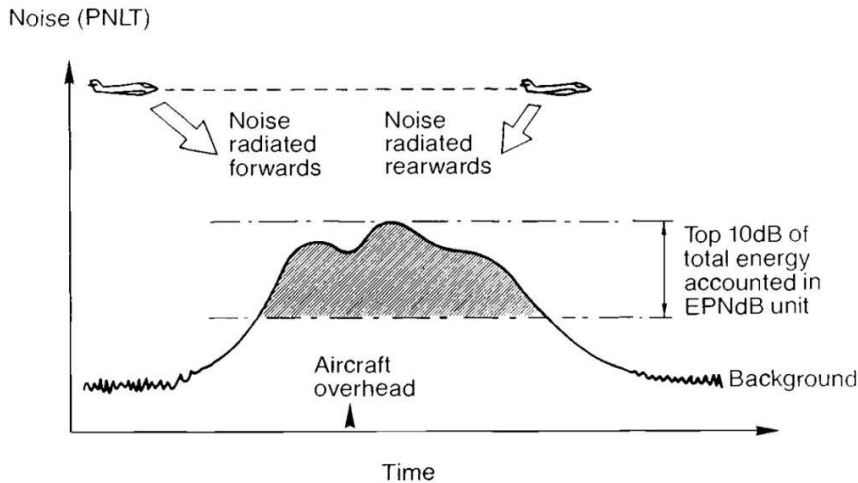


Figure 2.4: Duration correction for final EPNL calculation [6]

The duration correction D is calculated according to Eq. 2.15, leading to a final EPNL value using Eq. 2.16.

$$D = 10 \log_{10} [\sum_{k=0}^{2d} 10^{PNLT(k)/10}] - PNLT M - 13 \quad (2.15)$$

$$EPNL = PNLT M + D \quad (2.16)$$

In Eq. 2.15, k is the index for each time-step, given a standard value of 0.5 seconds for the certification process, d is the time-interval for which the tone-corrected perceived noise level value is 10 PNTdB below the maximum value $PNLT M$ for the movement in consideration. The value 13 is obtained due to normalization for the 10 second interval i.e. $10\log_{10}(0.5/10)$. It can be mentioned here that for takeoff procedures, the duration correction D at the flyover location 6.5 km from the point of brake release will in general be positive due to a longer flyover duration than the 10 seconds used for normalization. For approach movements at 2.3 km before touchdown, the correction will usually be negative as the flyover duration over the approach point is usually shorter than the 10 seconds due to the much closer location to the runway.

2.1.3 Multiple event average level metrics

In addition to the single event noise metrics most commonly used in the aerospace industry, certain multiple event metrics are also prevalent in making community noise assessment due to aircraft movements over longer durations of time. These metrics are intended to focus on residents living near airport vicinities and how they are affected by repeated aircraft movements over a specific time period, commonly 12 hours or 24 hours. The goal of using such metrics is to take into account, besides the effects of level, spectrum and duration also the effect of the background or ambient noise level, which varies over the course of the day and can also affect how much the residents are annoyed.

1. Average or equivalent A-weighted sound level ($L_{Aeq,T}$)

The SEL values mentioned in Section 2.1.1 for each single event can be summed energetically for a specified time period T to obtain an average or equivalent sound level for that period of interest. Eq. 2.17 shows the relation used for the $L_{Aeq,T}$ multiple event metric calculation:

$$L_{Aeq,T} = 10 \log_{10} \sum_{j=1}^N 10^{L_{AE}(j)/10} - 10 \log_{10} T \quad (2.17)$$

where N is the number of events in the time period T and $L_{AE}(j)$ is the SEL value for the j^{th} event. It was found during studies of noise exposure around European airports such as Heathrow in the 1960s [36] that $L_{Aeq,T}$ corresponded satisfactorily to noise exposure over longer durations of several hours and also to the sleep disturbance during night time, which depending on the airport is usually from 2200 or 2300-0700 hours.

2. Day-night average level (L_{DN})

The day-night average level (DNL) or L_{DN} was proposed by the US Environmental Protection Agency (USEPA) as a suitable noise descriptor for community noise impact and a correlation of L_{DN} with percentage of highly annoyed people was demonstrated by Schultz [26]. L_{DN} is a metric similar to $L_{Aeq,T}$ in that it also uses the integrated SEL values over specific intervals rather than instantaneous or peak-level values but adds a 10 dBA penalty (i.e. a doubling of perceived annoyance) to the average A-weighted sound level when the background or ambient noise is expected to be low, such as during night times.

$$L_{DN} = 10 \log_{10} \left[\frac{1}{24} \left[15 \left(10^{\frac{L_D}{10}} \right) + 9 \left(10^{\frac{(L_N+10)}{10}} \right) \right] \right] \quad (2.18)$$

In Eq. 2.18, L_D is the average A-weighted level during the day time (0700-2200) and L_N is the average level during the night time, both of which can be calculated using Eq. 2.17.

3. Day-evening-night average level (L_{DEN})

An extension of the DNL metric was proposed in Europe after studies indicated that besides noise intrusion being more severe during the night, the evening period was also an influencing factor as it was the time when the residents would be trying to fall asleep and any disturbance would prevent them from doing so. As such, as indicated in Eq. 2.19, an extra term for the average A-weighted level during evening time (1900-2200) is added to the calculation, with an addition of a 5 dBA penalty.

$$L_{DEN} = 10 \log_{10} \left[\frac{1}{24} \left[12 \left(10^{\frac{L_D}{10}} \right) + 3 \left(10^{\frac{(L_E+5)}{10}} \right) + 9 \left(10^{\frac{(L_N+10)}{10}} \right) \right] \right] \quad (2.19)$$

Several other metrics are also used by various local airport authorities around the world, such as the Noise and Number Index (NNI) in the United Kingdom (UK) and Noise Exposure Forecast (NEF) in Canada being a few known examples, which use the PNL metric and EPNL metric as their basis for averaging over specified time intervals respectively. These metrics will not be described here for conciseness and detailed information regarding them can be found in literature.

2.2 Deficiencies in currently used metrics and scope for improvements

Several metrics were described in the previous section that approached the subjective response of residents to aircraft noise in different ways, either by approximating loudness or annoyance estimated via psychoacoustic surveys. The goal of these metrics is to be able to quantify the subjective response of people to aircraft noise in the best way possible, such that a higher acceptance of aircraft and air traffic can be achieved when these metric values are reduced. By making use of metrics that can capture the varying characteristics of aircraft and engine noise that actually contribute to the resident's perceived annoyance, aircraft can also be designed that minimize annoyance.

The focus of this dissertation is on annoyance assessment during aircraft design, and therefore on usage of metrics that can capture aircraft design changes via corresponding noise impact values. Cumulative noise metrics such as $L_{Aeq,T}$ or L_{DEN} aren't suitable for this purpose as they require several (hundreds or thousands) flights to be assessed over a full day, with the noise impact averaged over different time spans. Since different aircraft types fly over the course of a day, the individual L_D , L_E and L_N values for the day, evening and night periods reflect noise impact for different aircraft arriving in or departing from an airport's airspace. As such, any changes in the cumulative metrics can at best only partly be attributed to an individual aircraft design change and the change in the cumulative metric value due to an individual design change will be reduced even further when averaged over several flights. Furthermore, no consideration of tonal content or low and high frequency noise division is made in these metrics and it has never been satisfactorily explained why a somewhat arbitrary universal doubling of annoyance (10 dB increase) is applied to the night time values [6]. As such, it is debatable if the $L_{Aeq,T}$ or L_{DEN} metrics even sufficiently correspond to aircraft noise annoyance [37], [38] as they neglect important characteristics of aircraft noise and *average* the values over multiple flight events. It is reasoned therefore that noise information averaged over thousands of flights by these metrics does not reflect reliably any aircraft design changes or also flight operation changes. The focus here will hence be placed on single event noise assessment metrics.

Looking at the loudness based single event metrics, both the dBA and dBC metrics are quite basic metrics that attempt to approximate human response to aircraft noise using single loudness curves. They neglect the many complexities of aircraft noise such as influence of tonal content, spectral balance or the fact that aircraft noise will have varying loudness impact depending on *both* its level and frequency, not frequency alone. This is based on the fact that aircraft noise for most situations will not correspond to a 40 phon loudness level curve as such low loudness levels are generally not observed in reality in airport vicinities [39].

The 100 phon loudness curve used for the dBC metric lies on the other extreme, representing response to very loud noise. The use of the dBC metric is highly limited as several noise components such as fan and low pressure (LP) turbine tones are present at high frequencies (1000 Hz and above) and this makes the dBC metric unsuitable for the complete aircraft noise spectrum range produced over various engine thrust settings. The use of the dBC metric has therefore quite rightly been limited, primarily to assess low frequency noise during start of takeoff. The dBA metric on the other hand has been used extensively for aircraft noise community impact analysis although it is known to be a poor indicator of experienced aircraft noise annoyance [9], [10], [11]. In general, dBA values present a correlation with relative loudness in a simple and easy way but the metric does not take into account various complex but present aspects of aircraft noise sound quality. It is for this reason that very different sounding spectra with very different subjective perceptions can have the same dBA value. An improvement over the dBA metric can be seen as necessary if community noise impact due to different aircraft, engines and flight procedures is to be expressed in a more comprehensive and accurate way.

The annoyance based single event metrics, namely PNL, PNLT and EPNL are definitely a step forward compared to the simpler dBA, dBC and SEL metrics. The PNL metric takes into account the fact that subjective response to aircraft noise varies both with the level of the sound as well as with frequency, by making use of the equal noisiness curves. Although complex sounds (i.e. broadband plus tonal sounds) were used for creating the equal noisiness curves, the specific presence of tones was not fully considered and the PNLT metric was thus designed to capture the tonal contribution to annoyance. Although the PNLT metric does provide a tonal penalty to the PNL values, it does this in a relatively basic way. The following deficiencies or aspects can be identified that can be improved upon:

- i. Only two divisions in the spectrum are made to account for different impact of the tones – between 500-5000 Hz tones carry a higher penalty and below 500 Hz or above 5000 Hz tones carry a lower penalty. This is a very broad and simplistic division and doesn't take into account many frequency dependent sensitivities of the human ear. It is not entirely accurate to say that a 1000 Hz tone would be perceived exactly as annoying as a 5000 Hz tone.
 - ii. Only tones that protrude by at least F equal to 1.5 dB are considered in the calculation, although when listening to sounds of aircraft noise, tones that don't protrude significantly above the broadband noise are not always completely masked and can still be audible.
 - iii. Tones below 500 Hz are given low tonal correction factors and are regarded as low contributors to annoyance. Low frequency tones however can contribute significantly to annoyance if they have high magnitudes, as low frequency tones are absorbed weakly by the atmosphere compared to high frequency tones. This is the case for instance for propeller and turboprop engine noise, as well as that of CROR engines, which are expected to enter the industry in the coming decades according to Airbus and Snecma [40]. The tones of these engines have their highest magnitudes at frequencies below 500 Hz (due to their low blade numbers and rotation speeds), which makes them more prominent for residents on the ground. Current very high bypass ratio geared turbofan engines, which have larger fans with lower blade numbers that rotate at slower speeds, also have their fan Blade Passage Frequency (BPF) being pushed to lower frequencies than what was the case for lower bypass ratio engines of the 1960s. With a view towards future aircraft engine sounds, it would be important to have a metric that better incorporates the annoyance of low frequency tones.
-

- iv. Another aspect not captured by the PNLT metric is the *number* of protruding tones present in the spectrum. The PNLT metric bases the final tonal correction factor only on the single most protruding tone, neglecting other tones and harmonics that may be present in the spectrum and could affect the annoyance perception. This fact had also been recognized during the creation of the tone-correction factor by certain studies [32].
- v. It was also found in studies carried out for Pratt and Whitney and Boeing [41] that the tone corrections as computed by the PNLT metric were actually half of what would be required in order to match the subjective response of listeners to aircraft noise recordings. Tones that protrude significantly above the broadband noise (F greater than 20 dB) are given the same constant penalty of either 3.33 or 6.67 dB. The tonal penalties are at times therefore *too low* and may lead to an underestimation of the perceived tonal impact. This scope for improvement to the tone-correction calculation was hence also recognized for the early generation aircraft and engines of the 1960s, albeit only in test environments using recorded aircraft noise.

It can be argued that a 1/3 octave frequency resolution is too broad and may not suffice in capturing all the tonal information such as number of tones and individual tone magnitudes in detail. For aircraft flying with turbofan engines, the tones (with the exception of buzzsaw tones explained later) will for most cases have a large frequency separation, exceeding the bandwidth of a 1/3 octave band. For the assessment of propeller or turboprop aircraft however, which have a very large number of tones populating the spectrum, a narrowband division of the spectrum will be necessary and tonal impact may be underestimated by only looking at 1/3 octave bands. As the focus in this dissertation is kept on turbofan engine aircraft, a 1/3 octave resolution is maintained for the analysis carried out. The alternate metrics which are suggested in later chapters are however capable of functioning for narrowband spectra just as well.

The incorporation of the effect of duration via integration over time of the noise metric values within a specific range of the maximum value is one that went through considerable discussion as the EPNL metric was being developed [32], [35]. It was indicated by some studies that a duration correction, as it was implemented for the EPNL metric, could in fact reduce the accuracy of the subjective ratings and could increase the error in correlation of objective results with subjective ratings [42]. A similar integration over time is also performed for the SEL metric as mentioned in the previous section. It would appear that a similar approach to the EPNL calculation as for the known and accepted SEL metric was chosen as a safe way to account for the duration factor, which many studies showed to be important although with some contradicting results from other studies [42]. As no better method of incorporating the effect of aircraft flyover time over an observer location was proposed, the EPNL calculation according to Eq. 2.15 and Eq. 2.16 was accepted by the FAA. It is however somewhat arbitrary that the calculation is normalized to a 10 seconds interval and it is also not fully clear why the maximum value is subtracted from the time-integrated PNLTdB values.

In general, it can be said that, as was argued for the cumulative metrics such as DNL, an integration of the values over time can remove the effects of individual changes which may occur during the course of the flight procedure. It has been found from psychoacoustic studies carried out both in the United States [43] and in Europe [44] in the years following the EPNL metric creation that the human response is affected more by the values that lie close to the maximum and are maintained for a short while, rather than values

statistically averaged over a certain time-span. It has been shown for instance that rather than the maximum value itself, a value below the maximum value exceeded and maintained for 5% of the exposure time actually presents the best correlation with the experienced subjective annoyance. New metrics that involve a time averaging over longer durations will therefore not be analyzed in this dissertation as this can lead to shorter term effects being neglected or being artificially averaged out. It is important from an aircraft design perspective to be able to foresee any worst case impact that may occur over any flight step (here every 0.5 seconds) due to a variation in thrust setting, flap or slat setting for instance, and not lose this information by integration over longer durations.

It can be noticed that the majority of the metrics described in Section 2.1 were developed over fifty years ago, for aircraft that were on the whole much louder, with dominating broadband jet noise, and components such as fan tones and airframe noise of much lower importance than what can be heard today. The metrics were developed using knowledge and expertise which for that time represented the state of the art in aircraft noise assessment, but are still being extensively used today the world over. Much more detailed knowledge regarding human response to aircraft noise has been accumulated since the time these metrics were developed and many of the deficiencies identified in this section can be improved upon by applying the knowledge that has been acquired over the past decades.

3 Current state of the art

It is useful to look at how various organizations have attempted to capture the complex characteristics of aircraft noise in a better way than via the conventional metrics currently used. Furthermore, it is also useful to look at how organizations have attempted to link the improved aircraft noise assessment with the aircraft design process, which is one of the goals of this dissertation. Looking at the state of the art in these fields gives an indication of which approaches have so far been successful and where there is a current scope for further research and analysis. The aim of this dissertation is to build on the current state of the art in aircraft noise annoyance assessment and its incorporation in the conceptual aircraft design process. As such, all the major organizations that are currently working in these fields and their relevant results which led to the foundations being developed for the current research work will be briefly summarized in this chapter.

3.1 State of the art in aircraft noise perception

With regards to research on the perception of aircraft noise and development of improved metrics, quite a few organizations both in Europe and the United States (US) have performed several psychoacoustic surveys with a variety of test-audiences over the years since the 1960s. In particular, advances in digital signal processing techniques [45] have made it possible for simulations of aircraft noise to focus on individual aspects and characteristics of aircraft noise which could not have been isolated fifty years ago using solely recordings of aircraft noise. The field of psychoacoustics, which in the 1960s was in its infancy has also progressed immensely, with expertise and theories being developed that can more accurately predict human response to sounds having very varied characteristics [44], [46].

In the past years, several studies such as [9], [10], [11], [47] showed that the commonly used metrics such as dBA were inadequate predictors of annoyance, in particular for sounds containing high levels of low frequency noise due to the negative weighting of low frequency noise values from the 40 phon curve used by the dBA metric, and also for sounds that contained prominent tonal components [12], [15]. The tonal correction factors used in metrics that currently attempt to account for tonal components in aircraft noise such as PNLT and EPNL have also been found to be insufficient in accurately describing the actual perceived tonal impact, as was explained in the previous chapter. Two studies on aircraft noise perception are of particular relevance for the research work in this dissertation – the study of Angerer et al. carried out at the Boeing noise laboratory [48] and that of More et al. at Purdue University [43], carried out very recently. These two studies and their major results will thus be briefly described in this section.

It was reasoned by Angerer et al. when investigating the annoyance experienced by passengers due to aircraft noise within the cabin that the currently used metrics for aircraft noise assessment were insufficient to meet the future needs of aircraft designers and of the airline industry. Their study, which involved psychoacoustic surveys of test sounds with varying spectral characteristics, indicated that a different approach would be required to assess aircraft noise, particularly in view of the advanced turboprop CROR engines that were being tested in the late eighties and early nineties, which have gained focus again in recent years. Since the tonal content would be much more prominent in the spectra

produced by these engines, it was reasoned that new metrics would be required that would capture the different spectra in a better, more holistic way.

In the study of Angerer et al., the research of Aures [49] and Zwicker [44], [50] on the perception and acceptability of sounds was regarded as the most logical and correct approach for capturing aircraft noise characteristics, as it focused on the elementary perceptual features of sound to explain and model how acceptable a sound is perceived to be. The approach took into account many identified individual characteristics of sound and made use of the *sound quality* metrics, each of which described specific characteristics of sound and furthermore, quantified the individual characteristics, which made their use very suitable for *sound engineering* purposes. These metrics were partly developed by Zwicker [44], [51] and Aures [49] as well as by other researchers in psychoacoustics such as von Bismarck [52] over several decades of research on perception of product sounds. Several other studies such as those by Scharf et al. [14], [53], Hellman et al. [10], [54], Genuit et al. [39], and more recently Berckmans et al. [17] have also incorporated the use of sound quality metrics to estimate the perceived annoyance of aircraft noise to varying extents, though they did not make use of all the sound quality metrics in a comprehensive way as was done by Angerer et al. The sound quality metrics used in the study of Angerer et al. were loudness, sharpness, roughness and tonality, which can be defined as follows^{*}:

- i. *Loudness*: Loudness is defined as the subjective perception of the magnitude of a sound and corresponds to the sound's overall intensity. It is a measure which is relevant for all sounds (not just of aircraft noise) and has been shown to be the largest contributor to the perceived annoyance of aircraft noise by various studies such as [16], [55].
- ii. *Sharpness*: Sharpness is a measure of the high frequency content of a sound and can be a useful metric where the sound is dominated by high frequency components [56].
- iii. *Roughness*: Roughness is the unpleasant sensation produced by sounds containing rapid amplitude fluctuations in the order of 15-300 Hz [49], [44].
- iv. *Tonality*: Tonality is a measure of the perceived strength of unmasked tonal energy present within a complex sound [49].

These sound quality metrics and how they can be implemented for performing aircraft noise annoyance assessment will be described in more detail in Chapter 6. The results of the study indicated that simple energy summations via OSPL and dBA metrics did not correlate to annoyance as well as the loudness based sound quality metrics. It was shown that the same dBA value could be obtained for different loudness values and an increase in loudness could be produced even though the dBA value would have decreased. It was shown in the study that the clearest correlation between experienced annoyance and the investigated metrics was shown by the *loudness* metric. The second most prominent correlation was observed between the experienced annoyance and the *tonality* of the sounds. This was an important result, which was specific to aircraft noise sounds and had not been accounted for by studies which had focused on other product sounds. The study found no clear correlation between annoyance values and the sharpness and roughness metrics. Based on the results of the study, Angerer et al. proposed an annoyance model which was a function of the loudness and tonality of aircraft noise, which yielded a prediction accuracy superior to that of the dBA metric. The correlation found between the annoyance of listeners in

* One sound quality metric not considered in the study was fluctuation strength, which is a measure of slow fluctuations in loudness of the order of 1-16 Hz, measured in the unit of vacil.

test environments and the loudness and tonality values of the tested interior noise sounds is shown in Fig. 3.1.

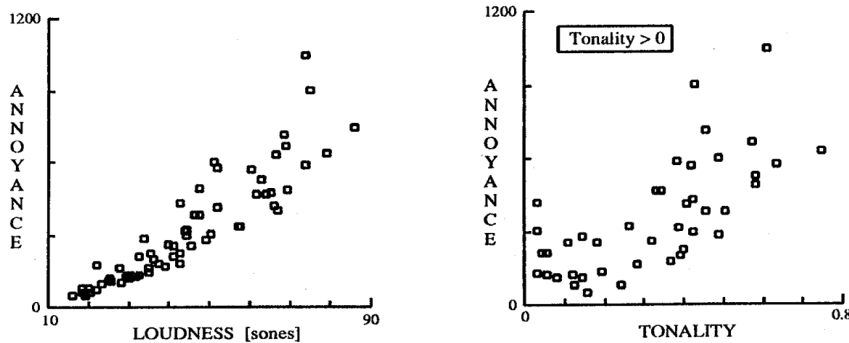


Figure 3.1: Correlation of aircraft interior noise annoyance of listeners in test environments to the loudness (left) and tonality (right) of the sounds from [48]. Tonality is defined from 0 – 1 tonality units (t.u.).

The results of the above mentioned study were said to be valid for aircraft interior noise, but covered a sampling space of sounds over a wide range of loudness, tonality, sharpness and roughness values, which could also be experienced for aircraft exterior noise of aircraft propelled with both turbofan and CROR engines. As such, the results are still of high relevance for the research work in this dissertation, which focuses on aircraft exterior noise impact.

The second important study on the influence of aircraft noise sound quality on *community noise impact* was carried out recently by More et al. of Purdue University [43], as part of the PARTNER[†] project. This study built on the findings from previous studies that from all the sound characteristics contributing to aircraft noise induced annoyance, loudness was the strongest contributor [16], [55], [48]. It was also known from studies by Västfjäll et al. for instance [57] that two sounds having equal loudness but different levels of other sound characteristics could sound significantly different and thus yield very different impressions of the perceived sound quality. It was thus likely that other sound characteristics in addition to loudness also affected people's subjective response to aircraft noise, as was indicated by Angerer et al.'s study. More et al. investigated using auralizations of aircraft noise (i.e. synthetic aural simulations [58]), the influence of the various aircraft noise sound characteristics on listeners' perceived annoyance. The range of loudness, sharpness, roughness and tonality variations was based on 40 aircraft noise recordings measured at two US airports, for civil aircraft takeoff and approach operations. The auralizations used in the study were based on the recorded noise of these aircraft, created using spectral decomposition of the tonal and broadband noise components [59]. The individual sound characteristics were in this way varied within the range of measured values obtained from the recordings, and used subsequently for subjective testing using psychoacoustic surveys of test listeners. The overall goal of this study was to develop a model for predicting the annoyance caused by aircraft noise in communities around airports more accurately than the currently used metrics and models.

One model that has been used for predicting the annoyance of product sounds is Zwicker and Fastl's Psychoacoustic Annoyance (PA) model (cf. Eq. 3.1-3.3) [44] which incorporates loudness (N), sharpness

[†] PARTNER – Partnership for Air Transportation Noise and Emissions Reduction

(S), fluctuation strength (F) and roughness (R) of the sound, but not its tonality (K). Since tonal components do not play as strong a part in the annoyance caused by most household products, the effect of tonal components was said to be accounted for these products solely by the loudness. In Eq. 3.1, N_5 is the loudness value exceeded for 5% of the time, w_s is the sharpness weightage term given by Eq. 3.2 and w_{FR} is the roughness and fluctuation strength weightage term given by Eq. 3.3.

$$PA = N_5 \left(1 + \sqrt{w_s^2 + w_{FR}^2} \right) \quad (3.1)$$

$$w_s = 0.25(S - 1.75) \log_{10}(N_5 + 10) \quad \text{for } S > 1.75 \quad (3.2a)$$

$$w_s = 0 \quad \text{for } S < 1.75 \quad (3.2b)$$

$$w_{FR} = \frac{2.18}{(N_5)^{0.4}} (0.4F + 0.6R) \quad (3.3)$$

As tonal content is however a very important factor affecting aircraft noise annoyance, this model therefore would not be immediately suitable for application to aircraft noise. The study of More et al. showed that a modified version of the PA model (cf. Eq. 3.4), which included the effect of tonality (Eq. 3.5), yielded the highest correlation with subjective tests results. The results of the study were somewhat similar to that of Angerer et al. in that loudness and tonality were found to be the two most relevant factors that contributed to the experienced annoyance. Roughness was in this study also found to be a possible relevant factor towards annoyance, although its contribution to the experienced annoyance was found to be of a much lower extent than loudness and tonality. The reason for roughness being found somewhat relevant by More et al. could be attributed to the fact that propeller noise recordings, which have much higher roughness values than turbofan engine aircraft, were included in the 40 aircraft noise recordings used as a basis for performing the roughness variation. Although only auralizations of turbofan engines were ultimately used while performing the surveys, the range of roughness variation of the test sounds thus included higher roughness values than are typically observed for turbofan engine aircraft. As seen by Angerer et al., no correlation between annoyance and sharpness or fluctuation strength was found in this study either.

$$PA_{mod} = N_5 \left(1 + \sqrt{\gamma_0 + \gamma_1 w_s^2 + \gamma_2 w_{FR}^2 + \gamma_3 w_T^2} \right) \quad (3.4)$$

$$w_T^2 = [(1 - e^{-\gamma_4 N_5})^2 (1 - e^{-\gamma_5 K_5})^2] \quad (3.5)$$

In Eqs. 3.4 and 3.5, PA_{mod} is modified Psychoacoustic Annoyance and w_T is the added tonality weightage term, based on the psychoacoustic survey results in the study of More et al. K_5 in Eq. 3.5 is the tonality value exceeded for 5% of the time and the coefficients γ_i ($i = 0, 1, 2, \dots, 5$) are empirical coefficients obtained from a best fit curve for the modified psychoacoustic annoyance model results and subjective annoyance ratings from the surveys.

Further work on perception of aircraft noise of relevance to this dissertation has been done by the National Aeronautics and Space Administration (NASA) of the US and the Dutch Aerospace Laboratory (NLR) of the Netherlands, by making use of aircraft noise auralizations and carrying out new psychoacoustic surveys of the sounds of current and future aircraft. NASA has made synthetic audible sounds of aircraft configurations expected to be used in the aerospace industry in the coming decades

such as Hybrid Wing Body (HWB) [60] and aircraft propelled by CROR engines [61] as well as Distributed Electric Propulsion (DEP) concepts [62]. Particularly for the latter two aircraft configurations and concepts, NASA has identified a need for improved metrics that would capture their very different sound signatures. NASA together with Purdue University has also investigated how synthetic rotorcraft noise may be perceived by listeners and which metrics would be best suited to capture rotorcraft noise impact [63]. The NLR has focused on aircraft operations by auralizing standard and noise abatement procedures and using the auralizations for performing psychoacoustic surveys towards investigating change in annoyance impact. White et al. for instance have investigated how noise abatement procedures such as the Continuous Descent Approach (CDA) correspond in terms of the annoyance they cause [64]. The NLR also performed a comparison of the sound produced by parametric models such as those used in this dissertation and measured sound at noise control points around Schiphol airport [65]. The differences were seen to be low to reasonable when expressed in the dBA metric although when comparing the audio, clear differences in the sounds could still be heard. This finding further hints at the need for using metrics that better capture the differences in sound produced by aircraft compared to current conventional metrics.

3.2 State of the art in low annoyance aircraft design

Several authors in the past have included certification noise and level based community noise considerations in a multidisciplinary aircraft design chain. Examples from literature are the works of Caves et al. [66], Manneville et al. [67] focusing on assessment of HWB aircraft as well as the work of Antoine et al. [68], which considered aircraft emissions and costs parallel to certification noise impact. Leifsson et al. [69] focused on airframe noise reduction during the conceptual aircraft design process and more recently Bertsch et al. [70] incorporated parametric noise models for low-noise conceptual aircraft design analyses. Although the organizations mentioned in Section 3.1 have worked on the perception and assessment aspects of aircraft noise, they have made no attempt currently to couple the annoyance modeling with the aircraft design process. This coupling of an annoyance modeling methodology with the capability to design aircraft that could yield aircraft designed to produce minimal annoyance to the residents, is the goal of the research work in this dissertation.

Two major research projects which broadly attempted to cover this and similar topics were the European Commission (EC) sponsored 6th and 7th Framework Program projects Sound Engineering For Aircraft (SEFA) [71] and Community Orientated Solutions to Minimize Aircraft Noise Annoyance (COSMA) [72] respectively.

SEFA was the first project of its kind to apply sound engineering methods to control aircraft exterior noise. It involved the identification of least preferred characteristics of aircraft noise via several listening tests, definition of preferred or ‘target’ aircraft sounds, and development of aircraft design criteria for obtaining the preferred aircraft sounds. The inspiration for the project was based on widespread use of sound quality analysis and optimization for automotive applications. Based on the results of psychoacoustic surveys of test subjects, SEFA identified certain acoustic and psychoacoustic parameters, which could allow the simulation of a typical listener’s subjective response to individual aircraft noise sounds. However, the prediction accuracy was deemed limited to the recorded sounds that formed part of the database used for the subjective testing and the virtual response was not suggested to be applicable to

any arbitrary aircraft. Target sounds were derived for each aircraft type and airframe and engine design guidelines for each individual aircraft were derived to achieve its target ‘weakly annoying’ sound. As such, design guidelines were developed only for each individual aircraft and global aircraft design guidelines could not be derived at the end of the SEFA project. Nonetheless, some very interesting and useful results with regards to aircraft noise sound quality optimization were produced, such as for instance:

- It was found for a quad-engine long-range aircraft that a reduction of the buzzsaw noise components (explained in more detail in Chapter 4) lead to large benefits for the perception of the aircraft sound during initial takeoff phase as less annoying, although they had only a minor influence on the overall EPNL value. This led to the recommendation that if the design LP spool speed was adapted (to reduce severity of supersonic shocks which constitute buzzsaw noise), then the sound quality would improve and the sounds would be deemed more acceptable. An alternate option to achieving the same goal would be to use a zero splice liner, as is seen for the Trent 900 and -1000 engines used on the Airbus A380 and Boeing 787 aircraft for instance.
- The effects of individual sound features such as fan tones were found to depend to a large extent on the overall sound composition of a flyover event i.e. the number and intensity of the other tonal and broadband components present in the sound spectra at a particular aircraft flight and engine setting. This implied that the interplay between the different aircraft noise spectral components would have an important influence on the experienced annoyance.
- The differentiation and scaling of aircraft sounds proved to be a very difficult task for typical listeners. One of the reasons was that full flyover events were played, which changed continuously over a typical 40 second duration used during the testing.

COSMA was a follow-up project to SEFA and intended a furtherance of the understanding of the effects of aircraft noise annoyance near airports. COSMA focused not only on the design of aircraft, but also on the flight operations in airport vicinities for lowering annoyance. It was reasoned for the COMSA project, as for its predecessor SEFA, that besides reducing the *level* of aircraft noise, one possible way to reduce annoyance around airports was to improve the *sound quality* of future aircraft. To focus on the sound quality aspect, an interactive Sound Synthesis Machine (SSM) was developed [73], which could allow test subjects to adjust the sounds of current aircraft to come up with sounds that they deemed less annoying or more acceptable. Faders were employed for this purpose for each major aircraft noise component identified from COSMA field and laboratory studies, using recorded and recording based synthesized noise. The test subjects could thus for instance adjust fan and turbine tonal components as well as jet, combustor and airframe broadband components to create a balance of sound that they preferred to the original sound. These improved sounds were then tested in comprehensive laboratory studies to see how they were perceived in terms of annoyance when applied to complete takeoff and landing procedures. The SSM had an automatic loudness equalizer programmed, which enforced the overall loudness level to remain constant. This was good for normalization of the sounds, but prevented significant deviations from current aircraft sounds, thereby restricting the scope somewhat of truly investigating a broad range of sounds such as was done by Angerer et al. and also by More et al.

It was also found during the work for the COSMA project that analysis of several studies around airports in the past had revealed that only a third of the variance in the *long-term* annoyance judgments could be explained by acoustic factors [74]. Many non-acoustic factors such as the resident’s mood, attitude

towards aircraft noise and feeling of being involved in the decision and policymaking process regarding noise in their neighborhoods also played an important role. These non-acoustic factors were seen to vary from airport to airport and could also vary with the time of day when the residents were exposed to aircraft noise. It was also stated that acting on the non-acoustic factors would produce faster results for long-term (i.e. multiple event) annoyance abatement and in increasing long-term acceptance of aircraft noise, as noise reduction technologies typically require decades before they can be implemented on a commercial aircraft. Nonetheless, it was stated that reducing aircraft noise and improving sound quality at the source would also confidently reduce the long-term annoyance experienced by the residents. In cognizance of the metrics described in the previous chapter, it can be stated that the analysis of the studies which showed only a third of the variance was accountable by acoustic factors had been carried out by the major European airports using the $L_{Aeq,T}$ metric. This metric, as was described in the previous chapter, is not a very suitable metric for predicting the annoyance caused by individual aircraft and it moreover makes use of the deficient dBA metric as its base metric. Other results may have been observed if improved alternate metrics had been used to construct the noise exposure curves were used in these studies. The work in this dissertation will not attempt to incorporate any non-acoustic factors in the design process, as they are as yet not sufficiently researched, and also to a large extent aircraft as well as aircraft design independent. The focus will therefore be kept here on single event or short-term annoyance.

The SEFA and COSMA projects also included important research work done by Diez and Iemma [75], where likely for the first time to the best of the author's knowledge, a link was made between a given weakly annoying target sound and the aircraft design parameters that could produce this target sound. Optimizations were made of a medium-range twin engine aircraft and parameters such as fan blade number, jet speeds and nozzle area ratio as well as wing sweep, span and flap area were adjusted to achieve the target sound. Alongside these design parameters, operational parameters such as fan LP spool speed, aircraft angle of attack, flap deflection angle among others were also varied to achieve the less annoying sound for an approach setting flyover. This methodology, although original and applicable for the kind of analysis intended to be carried out in this dissertation, has its limitations which are summarized as follows:

- i. The optimized design and operational parameters are only valid for the target sound they were trying to reproduce at a given observer location and are not suggested by Diez and Iemma to be considered as general guidelines for any generic commercial aircraft over any flight phase.
- ii. The approach varies *operational parameters* along with design parameters although in practice, approach and departure procedures are set by the local Air Traffic Control (ATC) authorities and cannot be varied as freely. At most, the flight path can be altered by slight amounts depending on the available thrust of the engine, which may allow steeper climb out or approach. The results are nonetheless demonstrative of the sound quality benefits that may be achievable via operational measures besides design parameter adjustment.
- iii. The effect of each individual design parameter towards the sound and corresponding annoyance on the ground is not quantified and it is not shown whether the presented adjusted values would always produce lower annoyance.
- iv. The design parameter values are adjusted solely from a numerical optimization perspective in order to meet the target sound. No use of known sound quality metrics which correspond to the subjective

annoyance experienced by listeners is made i.e. no quantification in measurable metrics is made in terms of the loudness, tonality, sharpness and roughness of the original and weakly annoying sounds.

Although both SEFA and COSMA did not ultimately provide general aircraft design guidelines for low annoyance aircraft design partly due to a limited recordings database to base conclusions upon, or perhaps a much broader overall scope, both were still very significant projects in the field of aircraft noise annoyance research.

The work in this dissertation will attempt to combine for the first time the detailed current knowledge of psychoacoustics and sound quality acquired over the past decades with the aircraft design process, an approach which till now has not been attempted by any other organization or author, to the best of the author's knowledge. This approach will be based directly on the fundamental knowledge of aircraft noise perception described concisely in this chapter and the known and tested multidisciplinary aircraft design and optimization process. The sound quality metrics mentioned here will be added to the conventional currently used metrics for assessing current aircraft for their noise impact. The research work will attempt to quantify the effects of each relevant aircraft and engine design parameter used as input in the source noise models on both the level and quality of the sound produced by current commercial aircraft. The results of this analysis will then allow optimizing aircraft designs at a very early stage such that they may produce less annoying and therefore more acceptable sounds inherently by design, and also indicate at a very early stage in which range of the parameter values any adverse sound effects might be expected. This approach ultimately has the dual goal of increasing aircraft noise acceptance by improving the general aircraft noise sound quality, and also to reduce the use of noise reduction technologies such as acoustic liners at a later stage, by preventing adverse sound effects from occurring already at an early stage.

4 Noise modeling for aircraft design and optimization

Various noise modeling methods and approaches exist in the aircraft noise and aeroacoustics fields today, with each method having its own purpose, accuracy and corresponding computational efficiency. Computational Fluid Dynamics (CFD) and Computational Aeroacoustics (CAA) based high-fidelity methods allow the modeling of the aerodynamics around a specific component and the subsequent computation of the near-field as well as far-field sound pressure disturbance produced by the aerodynamic source. This is done by solving the fundamental Navier-Stokes equations for fluid motion and the acoustic wave equation, which account for the aerodynamic sound source and the propagation of acoustic waves produced by this source through a given medium respectively. The numerical simulation methods generally provide results of a very high accuracy as they solve the governing flow equations from first principles with very few or minimal assumptions. Their application is however limited to aircraft components or relatively simple geometries due to their very high computational costs. A high-fidelity numerical simulation of jet noise using Large Eddy Simulation (LES) can easily take weeks to resolve all the high resolution temporal and spectral details. As such, they are at this stage not suitable for the purpose of aircraft design and for quantifying design sensitivities via extensive parametric studies, where hundreds of aircraft with slightly varying design parameters have to be designed and analyzed.

Use therefore has to be made of models that are relatively computationally inexpensive for noise modeling during aircraft design. These models must nonetheless offer a sufficient degree of accuracy and quite importantly for aircraft design purposes, reflect the physics behind the source noise generation via certain relevant design and operational parameters. These parameters can then be varied to analyze design sensitivities with regards to noise and annoyance impact, and subsequently be optimized to produce aircraft designs that minimize a certain noise specific objective. Such models are in general either purely empirical, based solely on measured data, or semi-empirical/semi-analytical, providing a link to noise generation physics via certain design and operation variables. They predict certain characteristics of aircraft noise such as directivity and spectral functions or the acoustic power analytically, and make up for any missing details or information by making use of an empirical database for the remaining noise characteristics. Before these more approximate methods more suitable for aircraft design purposes are presented and explained, a brief detour into aeroacoustic theory is made to develop an initial understanding of the physics behind aerodynamic noise generation. Subsequently, it will be shown what aspects of the first-principle theory could be retained or are reflected in the semi-empirical methods used for aircraft design and noise assessment in this dissertation.

4.1 The physics behind aircraft noise generation

The CAA methods are usually based on an ‘acoustic analogy’ where the governing fluid equations are rearranged to account for pressure disturbances in the flow due to acoustic sources. For this, the reference fluid is assumed to be unperturbed and the unsteady flow is assumed to occur only in a finite region surrounding the acoustic source. The remaining fluid is then assumed to experience small perturbations caused solely due to the passage of acoustic waves [76], [77]. This acoustic analogy was first developed by Lighthill [20], who derived from the exact equations of mass and momentum conservation a non-homogeneous wave equation, which then reduces to the classical homogeneous form outside of the source

region. Eq. 4.1 and Eq. 4.2 show the equations for conservation of mass and momentum respectively, as applied to an infinitesimal volume element:

$$\frac{\partial \rho}{\partial t} + \nabla \cdot \rho \mathbf{v} = 0 \quad (4.1)$$

$$\frac{\partial \rho \mathbf{v}}{\partial t} + \nabla \cdot \rho \mathbf{v} \mathbf{v} + \nabla \cdot \mathbf{P} = \mathbf{f} \quad (4.2)$$

In the above equations, the mass source term has been neglected (it would appear as Q_m and $Q_m \mathbf{v}$ on the right hand sides of Eq. 4.1 and 4.2 respectively) i.e. there is no mass injected into the system. Here, ρ , \mathbf{v} are the fluid density and velocity, \mathbf{f} is an external force field acting on the element and \mathbf{P} is the stress tensor of the fluid given by Eq. 4.3:

$$\mathbf{P} = p \mathbf{I} - \boldsymbol{\sigma} \quad (4.3)$$

where p is the fluid pressure, \mathbf{I} is the identity tensor or the Kronecker delta δ_{ij} such that $\delta_{ij} = 0$ if $i \neq j$ and $\delta_{ii} = 1$ if $i = j$. The term $\boldsymbol{\sigma}$ is the tensor corresponding to the viscous stress felt by the volume element in the fluid. If a time derivative of the conservation of mass equation is taken and the divergence of the conservation of momentum equation with no external force field present is subtracted from it, then Eq. 4.4 is obtained:

$$\begin{aligned} \frac{\partial^2 \rho}{\partial t^2} + \frac{\partial}{\partial t} (\nabla \cdot \rho \mathbf{v}) - \left[\nabla \cdot \frac{\partial \rho \mathbf{v}}{\partial t} + \nabla \cdot (\nabla \cdot \rho \mathbf{v} \mathbf{v}) + \nabla \cdot (\nabla \cdot \mathbf{P}) \right] &= 0 \\ \Rightarrow \frac{\partial^2 \rho}{\partial t^2} &= \nabla \cdot (\nabla \cdot \rho \mathbf{v} \mathbf{v}) + \nabla \cdot (\nabla \cdot \mathbf{P}) \end{aligned} \quad (4.4)$$

If the term $c_0^2 \nabla^2 \rho$ is then subtracted from both sides of Eq. 4.4 (c_0 being the speed of sound in regions outside the source region i.e. for the unperturbed fluid), then the following equation is obtained:

$$\frac{\partial^2 \rho}{\partial t^2} - c_0^2 \nabla^2 \rho = \nabla \cdot \nabla \cdot [(\rho \mathbf{v} \mathbf{v}) + (p - c_0^2 \rho) \mathbf{I} - \boldsymbol{\sigma}] \quad (4.5)$$

Eq. 4.5 is also written in the more compact form of Eq. 4.6:

$$\frac{\partial^2 \rho}{\partial t^2} - c_0^2 \nabla^2 \rho = \nabla \cdot \nabla \cdot \mathbf{T} \quad (4.6)$$

and also equivalently in Einstein summation convention as:

$$\frac{\partial^2 \rho}{\partial t^2} - c_0^2 \nabla^2 \rho = \frac{\partial^2 T_{ij}}{\partial x_i \partial x_j} \quad (4.7)$$

The tensor \mathbf{T} in the above equations is the so-called Lighthill's turbulence stress tensor and Eq. 4.6, Eq. 4.7 are two forms of the famous Lighthill's equation. This inhomogeneous wave equation was the first equation that theoretically accounted for the physical phenomenon of aerodynamic sound generation before experiments were accurate enough to verify it [77]. Since no approximations are made in deriving Lighthill's equation and it is simply a rearrangement of the governing equations, the equation is exact. The Lighthill's stress tensor \mathbf{T} accounts for the acoustic sources of the sound and depending on the flow conditions, each of the source terms can play a significant role in noise generation. The term $\rho \mathbf{v} \mathbf{v}$ (which

is the Reynold's stress) accounts for sound generation due to unsteady convection of the flow i.e. due to turbulence; σ describes sound generation due to viscous or shear stresses; $p - c_0^2 \rho$ accounts for sound produced due to convection of entropy perturbations i.e. a deviation from isentropic behavior of the flow.

Perturbations around mean values are now introduced such that $p' = p - p_0$ is the perturbation in pressure about its reference unperturbed value p_0 . The pressure perturbation p' is assumed to be of the form $p' = \hat{p} e^{i\omega t}$, where \hat{p} is a time-independent pressure amplitude of a traveling acoustic wave and p' has the properties that the mean value of the perturbation $\langle p' \rangle = 0$ and the mean-square value $\langle p'^2 \rangle \neq 0$. With ρ' the analogous perturbation of the fluid density about its unperturbed value ρ_0 , Eq. 4.6 can be written as:

$$\frac{\partial^2 \rho'}{\partial t^2} - c_0^2 \nabla^2 \rho' = \nabla \cdot \nabla \cdot \mathbf{T} = \nabla \cdot \nabla \cdot [(\rho \mathbf{v} \mathbf{v}) + (p' - c_0^2 \rho') \mathbf{I} - \boldsymbol{\sigma}] \quad (4.8)$$

It can be noted that outside the finite region around the source, \mathbf{T} will be zero and the inhomogeneous wave equation (Eq. 4.7) will reduce to the classical homogeneous form given by Eq. 4.9.

$$\frac{1}{c_0^2} \frac{\partial^2 \rho'}{\partial t^2} - \nabla^2 \rho' = 0 \quad (4.9)$$

Assuming isentropic flow, the pressure disturbance can be related to the density disturbance according to Eq. 4.10:

$$p' = c_0^2 \rho' \quad (4.10)$$

In this way, a similar derivation for pressure as for density can be carried out using Lighthill's acoustic analogy and the pressure form of Lighthill's acoustic equation can be obtained.

In order to solve Lighthill's equation for particular source terms, certain approximations have to be made. Lighthill reasoned that when the non-uniform entropy effects were negligible due to no change in temperature from the source region to the listener region, then the flow will produce sound at high velocities only i.e. at high Reynold's numbers. If this is the case, then the viscous effects will be negligible and the inertial effects will be dominant. The sound source will then be primarily due to the unsteady convection of the flow i.e. due to flow turbulence. The solution of Lighthill's equation in the far-field for free conditions is given by the following integral:

$$p'(\mathbf{x}, t) = \frac{\partial^2}{\partial x_i x_j} \int_{-\infty}^{\infty} \int_V \rho v_i v_j \frac{\delta(t - \tau - \frac{r}{c_0})}{4\pi r} dV d\tau = \frac{\partial^2}{\partial x_i x_j} \int_V \left[\frac{\rho v_i v_j}{4\pi r} \right]_{\tau=t_e} dV \quad (4.11)$$

In the above equation, \mathbf{x} is the vector for the receiver position, V is the volume of the source region, r is the distance between source and receiver such that $r = |\mathbf{x} - \mathbf{y}|$, where \mathbf{y} is the vector for the source position, t_e is the emission time at the source, t is the retarded time at the receiver ($t = t_e + r/c_0$) and δ is the Dirac-delta function. An estimate can now be obtained to indicate how the noise due to free turbulent jets scales with certain relevant geometrical and operational parameters of the jet flow. This is the crucial part of the above theoretical background, which will show the relevant aircraft design parameter correlation with the physics of the (aerodynamic) noise generation. In the far-field, the spatial derivative $\partial/\partial x_i$ is proportional to the temporal derivative $\partial/\partial t$ according to the following relations [77], [78]:

$$r \rightarrow |\mathbf{x}|, \frac{\partial}{\partial x_i} \rightarrow -\frac{1}{c_0} \frac{x_i}{|\mathbf{x}|} \cdot \frac{\partial}{\partial t}, \frac{\partial^2}{\partial x_i \partial x_j} \rightarrow \frac{1}{c_0^2} \frac{x_i x_j}{|\mathbf{x}|^2} \cdot \frac{\partial^2}{\partial t^2} \quad (4.12)$$

As such, the second order spatial derivative $\partial^2/\partial x_i \partial x_j \sim (1/c_0^2) \partial^2/\partial t^2$. Considering $\rho \approx \rho_0$ and that the flow velocity scales with the mean jet velocity u_{jet} , it can be written that $\mathbf{T} = \rho_0 \mathbf{v} \mathbf{v} = \rho_0 v_i v_j \sim \rho_0 u_{jet}^2$. An approximation for the temporal derivative term needs a consideration of turbulent flow as a sequence of eddies, with the characteristic frequency of the turbulence $f_c = 1/t_c$, where t_c is the time needed to convect an eddy over a characteristic dimension l with a convection speed u_c . In order to get these two terms in terms of the geometry and operational parameters of the jet, it can be said that the convection speed u_c of the eddy will also scale with the mean jet velocity u_{jet} and the characteristic dimension of the jet will be its nozzle diameter d_{jet} such that $f_c = 1/t_c \sim u_{jet}/d_{jet}$ and $\partial^2/\partial t^2 \sim u_{jet}^2/d_{jet}^2$. The volume V will then scale with the cube of the nozzle diameter i.e. $\int dV \sim d_{jet}^3$. Combining all the terms in order to approximate Eq. 4.11, the following relation for the far-field acoustic pressure fluctuation is obtained:

$$p' \sim \frac{\rho_0 u_{jet}^4 d_{jet}}{rc_0^2} \quad (4.13)$$

Since the acoustic intensity in the far-field $I = \frac{\langle p'^2 \rangle}{\rho_0 c_0}$ and acoustic power $\Pi = I \cdot A$, where A is the representative surface area surrounding the source, Lighthill's famous acoustic power law can once again be stated here (it was previously shown in its final form in Eq. 2.2):

$$I \sim \frac{\Pi}{4\pi r^2} \sim \frac{\rho_0 u_{jet}^8 d_{jet}^2}{c_0^5} \quad (4.14)$$

The above equation showed, as was mentioned in Chapter 2, that a free, cold, turbulent jet produced a noise intensity that varied theoretically with the eighth power of jet velocity and led to the noise reduction approach of reducing jet velocities by introducing bypass flow. It can be mentioned here that when the jet temperature is higher than the ambient temperature, entropy fluctuations are introduced which reduce the jet velocity exponent to between 6 and 8.

For other cases, where the turbulent flow is present around solid objects or boundaries, other generalizations of Lighthill's analogy were formulated. Curle [79] made an analogy for fixed solid surfaces in the flow, both compact such as cylinders (e.g. landing gear struts) and spheres (such as landing gear wheels) as well as for semi-infinite or large span thin bodies (such as wings), Ffowcs-Williams and Hall [80] applied a similar analogy to wing trailing edge noise. Ffowcs-Williams and Hawking (FWH) [81] formulated an analogy to predict aerodynamic noise due to rotating surfaces and flows, such as those due to the fan and turbine as well as subsonic propellers. The analogy separates the acoustic sources into a monopole source to account for volume displacement due to the object in the medium (so called *thickness noise*), a dipole source to account for aerodynamic loads on the rotating object (*loading noise*) and a quadrupole source to account for any turbulence related effects. For non-moving objects, the thickness noise term vanishes and the FWH analogy becomes similar to Curle's analogy, shown in Eq. 4.15. For both the FWH and Curle's analogies, all the acoustic source terms are added to the right hand side of the inhomogeneous wave equation, in addition to the Lighthill stress tensor.

As was shown for the noise due to free turbulent jets using Lighthill's equation, a similar correlation between the noise generated due to compact bodies in turbulent flows can be shown using Curle's equation, shown here at emission time t_e [77]:

$$p'(\mathbf{x}, t) = \frac{1}{4\pi c_0^2 |\mathbf{x}|} \frac{x_i x_j}{|\mathbf{x}|^2} \frac{\partial^2}{\partial t^2} \int_V T_{ij} dV + \frac{1}{4\pi c_0 |\mathbf{x}|} \frac{x_j}{|\mathbf{x}|} \frac{\partial}{\partial t} \int_S (P_{ij} + \rho v_i v_j) n_i dS + \frac{1}{4\pi |\mathbf{x}|} \frac{\partial}{\partial t} \int_S (\rho v_i) n_i dS \quad (4.15)$$

Curle's equation shown above by Eq. 4.15, describes the aerodynamic sound generated by a solid object immersed in a flow field. Such rigid bodies generate additional noise due to the interaction of the object's surface with turbulence. The first term describes the aerodynamic noise solely due to turbulence in the free field, as was shown for the free turbulent jet; the second term describes the instantaneous force exerted from the object's surface on the surrounding fluid as a reaction of the surface to the force $F_j = - \int_S (P_{ij} + \rho v_i v_j) n_i dS$ exerted by the flow on it where S is the surface of the compact body and n_i is the i^{th} component of a vector normal to the object surface. The third term in Eq. 4.15 is due to the displacement of volume by the object, moving with velocity v_n ($= \mathbf{v} \cdot \mathbf{n}$).

For a fixed rigid compact body, $v_n = 0$ and the third term as well as the second part of the middle term will vanish. Similar to the free jet case, the characteristic frequency $f_c = 1/t_c$, where t_c is the time needed by the sound signal to travel across the largest dimension D of the object. The characteristic frequency then is given as $f_c = c_0/D$ and if frequencies below f_c are considered, then the emission time differences over the object's dimensions can be neglected and the body can be regarded as 'compact'. For compact bodies, the surface related sound source representing the net aerodynamic force acting on the object reduces to $(1/(c_0 |\mathbf{x}|))(dF_x/dt)$, where F_x is the component of the aerodynamic force in the receiver's direction. This sound source is therefore directly proportional to the time rate of change of the aerodynamic force acting on the object. The aerodynamic force itself scales as $F \sim \rho U^2 D^2$, where U is the flow speed. Analogous to the free turbulent jet, it can be written that $d/dt \sim 1/t_c = U/D$. The far-field acoustic pressure fluctuation and the corresponding sound intensity for such fixed, rigid compact sources in a flow field are given by Eq. 4.16:

$$p' \sim \frac{\rho U^3 D}{rc_0}, \quad I = \frac{\langle p'^2 \rangle}{\rho c_0} \sim \frac{\rho U^6 D^2}{r^2 c_0^3} \quad (4.16)$$

This shows that the noise generated due to solid objects in a turbulent flow will have an intensity proportional to the sixth power of flow velocity (not eighth as for a free turbulent jet) and also will be c_0^2 or M^2 stronger than the turbulence induced noise implying it dissipates less strongly than jet noise (note: this result is valid only for low subsonic Mach numbers [78]). The turbulence induced noise has a *quadrupole* nature ($p \sim M^4$) while noise due to a solid object in a turbulent flow will have a *dipole* nature ($p \sim M^3$) [78]. For objects in unsteady flows which are not compact, such as thin bodies with relatively large spans, the scaling of aerodynamic noise with flow speed obtains a different exponent. Ffowcs-Williams and Hall [80] showed that the far-field noise intensity due to interaction of turbulent flow with a semi-infinite plate of negligible thickness at zero angle of attack scales with the fifth power of flow speed. This analogy is applicable to aircraft lifting surfaces such as the trailing edge of a wing or flap/slat trailing edge, and the $I \sim M^5$ or equivalently $p \sim M^{5/2}$ scaling with flow speed implies that trailing edge noise is a source lying between a monopole ($p \sim M^2$) and a dipole source [77]. Ffowcs-Williams and Hall found that the noise directional pattern from a trailing edge varied as $\sin^2(\theta/2)$ in the far-field, where θ is the polar directivity angle (angle with reference to the aircraft forward axis). It was shown that the far-field

noise intensity per unit volume of the acoustic source at the trailing edge of the wing could be given by [82]:

$$I \sim \frac{\rho U^5 \cos^3 \beta D(\theta, \psi)}{2\pi^3 r^2 c_0^2 l} \quad (4.17)$$

where β is the trailing edge sweep angle of the wing, l the characteristic dimension for turbulence, and $D(\theta, \psi)$ is the directional pattern or simply, the *directivity* of the noise, given for this source by Eq. 4.18 with ψ being the azimuthal angle (angle with reference to a straight line pointing downwards perpendicular to the forward axis):

$$D(\theta, \psi) = 2 \sin^2 \left(\frac{\theta}{2} \right) \sin \psi \quad (4.18)$$

In order to solve Lighthill's equation as well as those of Curle and Ffowcs-Williams and Hawking, the use of numerical CAA methods is made, which are coupled with time-accurate flow field aerodynamic data describing the source obtained a-priori either from Reynolds Averaged Navier Stokes (RANS) or LES solutions for instance. The acoustic equations are then solved to propagate the noise to the far-field.

The field of aeroacoustics thus describes in detail the various sound generating mechanisms, and although still young, it has become considerably vast over the years with applications made to various noise sources such as turbofan engine components, airframe geometry, CROR engines, rotorcraft etc. The goal of the above theoretical background was simply to give a feel of the physics which governs how the sound from aircraft and their engines is generated. The correlations of the intensities of various sources with geometric and operational parameters shown here correspond to some extent to the simpler semi-empirical and semi-analytical parametric methods explained in the next section. Many of the correlations such as those with jet velocity or flow speed, or the directivity patterns for instance, will be seen in the parametric models as well, thereby showing that the physics has indeed been *partly* retained in these models. Judging that the models must simulate highly complex phenomena of noise generation from a multitude of sources, the slight loss of accuracy due to not using high-fidelity methods for a significant gain in computational speed as well as a parametric analysis and design optimization capability, is a necessary compromise for assessing aircraft designs for noise.

4.2 Aircraft source noise modeling using parametric models

Noise models developed for the purpose of aircraft design and assessment that are in widespread use today are usually based on NASA's Aircraft Noise Prediction Program (ANOPP) [83]. These were developed in the late 1970s and early 1980s to predict not just overall aircraft noise but also aircraft system or component noise. These models are predominantly semi-empirical, with some noise component models such as for the noise produced by the fan leaning towards a more empirical than semi-empirical approach, due to the difficulty in predicting the complex mechanisms and flow interactions that take place in the fan and compressor stages. On the other hand, models for the airframe lean towards a more semi-analytical approach, as will be shown later. The models are based on extensive measurements and tests carried out by various NASA departments in partnership with several engine manufacturers. The goal was to come up with a comprehensive noise prediction program which could enable faster aircraft noise

analysis, retain to some extent the physics behind the noise generation and yet maintain a reasonable degree of accuracy compared to measured aircraft noise.



Figure 4.1: Major aircraft noise sources as modeled using ANOPP based source noise models^{*}

The noise components accounted for by ANOPP are summarized in Fig. 4.1. These include models of the engine fan and compressor based on the work of Heidmann [84], combustor and LP turbine noise using the method of Emmerling et al. [85] and Matta et al. [86], jet noise based on the method of Stone [87] and airframe noise (composed of wing trailing edge, flap edge, slat, landing gear and stabilizers) using the method of Fink [88]. These models have been regularly updated by NASA to reflect the advances in noise reduction technology. NASA is also planning a second version, ANOPP2, which retains all the functionalities of the original and adds the effects of separated sources, advanced shielding effects, detailed propagation effects and also provides the possibility to model propeller as well as CROR noise, and also other unconventional configurations by linking the ANOPP infrastructure with other NASA tools and codes [89]. The parametric source noise models used for engine noise modeling will be described first in this section, followed by the airframe noise models.

^{*} Source of images – Julian Herzog on www.en.wikipedia.org/wiki/Airbus_A320_Family (top) and PW1000 series geared turbofan on www.a320neo.com last accessed on 23rd March 2015.

4.2.1 Fan noise

The method of Heidmann predicts the free-field noise from the fan and LP compressor of a turbofan (or also turbojet) engine. Since the aeroacoustic phenomena occurring in the fan and compressor stages of the engine are highly complex (turbulence and unsteady flow interaction between fan rotor blades, vanes, supersonic effects at blade tips, both tones as well as broadband noise), fan noise prediction is most suited to a semi-empirical estimation. The method predicts the following five components of fan noise, which is radiated both in forward as well as aft directions from the engine:

- i. Inlet broadband noise
- ii. Discrete tones from inlet
- iii. Combination tones (or ‘buzzsaw’ tones) from inlet
- iv. Exhaust broadband noise
- v. Discrete tones from the exhaust

The original Heidmann model has been adapted to a form by Zorumski, which generalizes all the source noise modeling methods to one form used in ANOPP [83]. This form of the methods is logically constructed and is a more elegant form of the original methods upon which ANOPP is based. The mean-square acoustic pressure in the far-field $\langle p^2 \rangle$ according to this approach is given for each component by:

$$\langle p_{i,fan}^2 \rangle = \frac{\Pi_i}{4\pi r^2} \frac{S(\eta)_i D(\theta,\psi)_i}{(1-M_\infty \cos\theta)^4} \rho_\infty c_\infty \quad (4.19)$$

where Π_i is again the acoustic power of the fan noise source i , $S(\eta)_i$ is the spectral weighting function for the specific noise component, with η a frequency parameter given by Eq. 4.20 for the case of the fan. $D(\theta,\psi)_i$ is the directional weighting function i.e. the directivity of the i^{th} noise source. Both $S(\eta)$ and $D(\theta,\psi)$ for all components in Heidmann’s model have been determined empirically using the spectra and directivities observed in the measurements for various fans carried out by NASA. The factor $(1-M_\infty \cos\theta)^4$ is the forward flight effect factor, which increases the magnitude of the acoustic pressure when the noise source (i.e. the aircraft) is in motion, with M_∞ the aircraft’s freestream Mach number. The index ∞ refers throughout to freestream conditions.

$$\eta = (1 - M_\infty \cos\theta) \frac{f}{BPF} \quad (4.20)$$

BPF in the above equation is the Blade Passage Frequency (BPF) of the fan, which in turn depends on the fan LP spool rotation speed N and the number of rotor blades B the fan has (cf. Eq. 4.21). The term $(1 - M_\infty \cos\theta)$ accounts for the Doppler effect due to forward motion of the aircraft.

$$BPF = N \cdot B \quad (4.21)$$

The method of Heidmann predicts the spectrum shape, spectrum level as well as the directivity for each of the above mentioned fan noise components. Fan noise does not vary with azimuthal angle ψ but the convention is kept in Eq. 4.19 for keeping the format consistent for all aircraft noise components (Eq. 4.18 showed for instance that airframe trailing edge noise varied with azimuthal angle ψ). In fact, all engine noise components are seen to vary with polar angle θ only and are therefore radially symmetric

(i.e. $D(\theta, \psi)$ is equivalent to $D(\theta)$ for engine noise). The acoustic power in Eq. 4.19 for the fan is given by the following relation:

$$\Pi_i = \left(K' \cdot G(I, J) \left(\frac{s}{c} \right)^{-a(K, L)} M_m^b M_x \left(\frac{\Delta T}{T_{\infty}} \right)^2 F(M_r, M_m) \right)_i \rho_{\infty} c_{\infty}^3 A_{fan} \quad (4.22)$$

The constant K' has different values for each component determined empirically. $G(I, J)$ is a matrix that depends on two factors – the presence of Inlet Guide Vanes (IGV) and fundamental tone cut-off. Index $I = 1$ indicates a fan with no IGV and $I = 2$ a fan with IGV. Whether the fundamental fan tone is being cut-off or not is determined via the tone cut-off factor δ :

$$\delta = \frac{M_t}{|1 - \frac{V}{B}|} \quad (4.23)$$

M_t is the fan rotor tip Mach number given by Eq. 4.24, V is the number of stator vanes behind the rotating fan (the rotating rotor blades exert force on the airflow, the fixed stator vanes transfer the loads to the surrounding structure). The fundamental tone cut-off occurs if δ has a value less than 1.05. Tone cut-off basically implies that depending on the ratio of stator vane number to rotor blade number, and the operating condition via M_t , certain tones are strongly damped in the duct and do not propagate as strongly out of the duct, thereby essentially being ‘cut-off’. Index $J = 1$ corresponds to $\delta > 1.05$ and $J = 2$ corresponds to $\delta \leq 1.05$.

$$M_t = \frac{\pi N d}{c_{\infty}} \quad (4.24)$$

In Eq. 4.24, d is the fan rotor diameter. In general, the number of stator vanes will have to exceed the number of rotor blades in order to cut-off specific tones. This can be expressed using the relation:

$$V = 1.1(1 + M_t) \cdot nB \quad (4.25)$$

This relation implies that for the fundamental tone ($n = 1$) to be cut-off if the tip Mach number is approximately sonic, the number of vanes will have to be 2.2 times the number of rotor blades [6]. How this cut-off mechanism occurs depends on the fan and compressor initial stage geometry, and on the fan rotation speed. The mechanism can be explained using ducted fan acoustic theory. The pressure field in a cylindrical duct containing an axial flow fan consists of a spinning pattern with a characteristic, repetitive shape. Such rotating pressure field patterns whose shape can be described by a characteristic function at one specific frequency are referred to as a ‘mode’. Single frequency patterns like these in the circumferential direction are called ‘ m -modes’ and in the radial direction are called ‘ n -modes’ (not same as harmonic number n , which has same notation). Fan acoustic modes can be generated via the rotor alone or via rotor-stator interaction. Rotor alone modes are generated as circumferential modes with m -numbers which are integer multiples of B (i.e. nB). For rotor-stator interaction modes, an inflow disruption is added of spatial order equal to V , with the circumferential mode now given by $m = nB - kV$, with k being any integer and n the harmonic number. Positive m -numbers indicate mode rotation in the same direction as the fan and negative m -numbers indicate rotation in the opposite direction. Modes rotating in the opposite direction to the fan are attenuated as they must travel against the rotating flow and through the ‘obstructing’ rotating blade rows. They thus have a higher likelihood of decaying within the duct, thereby not propagating to the far-field. In order to reach the far-field, the modes must in addition have a

minimum critical spin rate, which is called the cut-off rate, below which the modes decay in amplitude exponentially with distance from the source. So the modes superimpose in circumferential and radial directions to produce the overall pressure field pattern in the far-field. Knowledge of the modes, their order and spin rate is essential in controlling which tones are to be damped and also how much acoustic liner treatment has to be applied on the duct.

Fig. 4.2 shows the sample case of an imaginary fan, for the simplified case of just 4 rotor blades and 3 and 5 stator vanes respectively. Real commercial turbofan fans and compressors can have anywhere between 20 (for larger engines) to 50 (for smaller engines) rotor blades. On the left, for the case of 3 stator vanes, one revolution of the fan rotors produces 12 interaction pulses at the location of each stator and the relevant circumferential mode rotates at 4 times the fan rotational speed in the same direction as the fan ($m = 4 - 3 = 1$ for $n = 1$ and $k = 1$). This mode will be able to pass through the rotating blade rows towards the front of the engine. On the right however, one revolution of the rotor blades will produce 20 interaction pulses at each stator location and the circumferential mode will rotate also at 4 times the fan speed but this time in the *opposite* direction ($m = 4 - 5 = -1$ for $n = 1$ and $k = 1$). This mode will not be able to propagate through the blade rows as easily and will be attenuated in the duct. By choosing the right number of vanes therefore for a given number of blades, the overall pressure pattern that results in the tone can be adjusted such that the tone is damped as it propagates out of the engine duct. To cut-off the fundamental tone for 4 blades, based on Eq. 4.25, 9 vanes or more will be required ($8.8 \approx 9$). Heidmann's method takes this cutoff effect only grossly into account, owing to the complexity of the combination tone generation mechanism and the limited database used during the testing for Heidmann's method development. The tone cutoff factor δ here accounts for a reduction in the fundamental tone's intensity by approximately 8 dB, if the ratio of V to B and the value of M_t in Eq. 4.23 produce a $\delta < 1.05$.

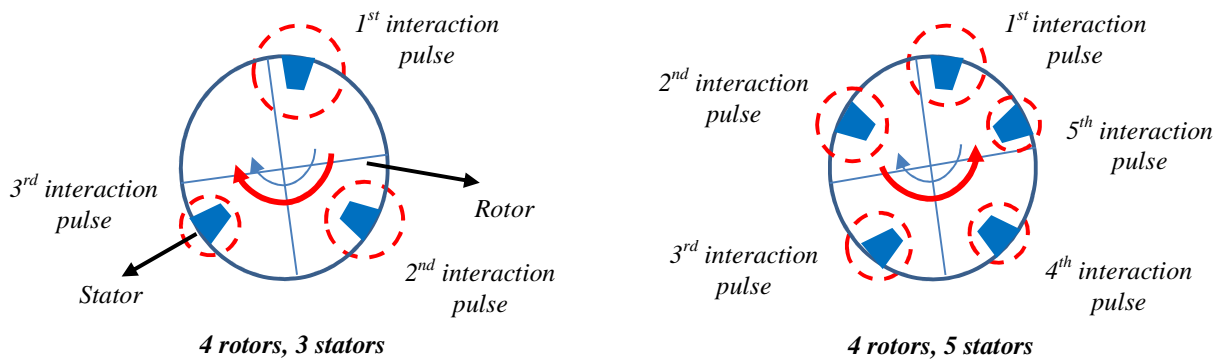


Figure 4.2: Mode propagation for sample case of fan with 4 rotors and 3 stators (left) and 5 stators (right) [6]. Blue arrow denotes fan rotational direction and red arrow denotes mode spin direction. Fundamental tone is attenuated on the right.

The factor s/C represents the effect of the rotor-stator spacing, s with C being the mean chord of the rotor blades. If the rotor blades and stator vanes are placed too close to each other, then very strong discrete tone generation will occur towards the front of the engine due to the cyclic interaction of the pressure fields of the rotors with the stators, and also due to cyclic fluctuations of the stators' lift distribution as they receive the rotor blade wakes. The rotor-stator spacing is a very important parameter for fan noise

control and in general an as high as possible spacing is strived for, keeping structural and size constraints in consideration. The exponent $a(K,L)$ will have different values for each relevant fan noise component with index $K = 1$ for $s/C \leq 1$ and $K = 2$ for $s/C > 1$. Index L corresponds to the presence of Inlet Flow Distortion (IFD), which can occur when the aircraft is on the ground due to additional turbulence around the engine inlet when in proximity to the ground. $L = 1$ implies no IFD is present and $L = 2$ implies that IFD is present i.e. the aircraft is on the ground.

The parameter M_m is termed the design point Mach number index and is obtained as the maximum value from 1 and the design value of the tip Mach number $M_{t,d}$ of the fan blades ($M_m = \max(1, M_{t,d})$). The exponent b gives the effect of M_m on each fan noise component. The factor $F(M_r, M_m)$ is the power function and varies for each fan noise component. It is a function of the relative tip Mach number and the design point Mach number index. The relative tip Mach number M_r is obtained using the actual tip Mach number and the axial flow Mach number M_x according to Eq. 4.26:

$$M_r = (M_t^2 - M_x^2)^{1/2} \quad (4.26)$$

where the axial flow Mach number is the ratio of the local mass flow to the inlet mass flow, given by:

$$M_x = \frac{\dot{m}}{\rho_\infty c_\infty A_{fan}} \quad (4.27)$$

A_{fan} is the fan inlet area, which in ANOPP convention is also the reference area of the engine, A_e . In order to specify the generated noise in terms of commonly used fan and compressor variables, Heidmann used equivalent terms for shaft power via the product of inlet mass flow and temperature rise and specific work done by the fan via just the temperature rise term. As such, terms with the fan mass flow \dot{m} (via the axial flow Mach number M_x) and ΔT also appear in the fan acoustic power equation in Eq. 4.22.

Once all the terms and factors from Eq. 4.22 are known or have been computed, the acoustic power Π_i can be substituted into Eq. 4.19 for obtaining the mean square acoustic pressure of each component as a function of frequency f and polar directivity angle θ for a 1 meter radius sphere at the source (taking $r = 1$ m in Eq. 4.19). All broadband noise components are provided as 1/3 octave band data and the tonal components are computed at their exact discrete frequencies. Since all ANOPP methods however use a 1/3 octave band spectral format, the tones are rounded to the nearest 1/3 octave band frequency value and added to the corresponding broadband component value. The component mean-square pressures can then be added linearly and the sum $\langle p_{fan}^2 \rangle$ converted to an SPL value using Eq. 4.28 by dividing by the square of the reference pressure p_{ref} , which has a value of $2 \cdot 10^{-5}$ Pascal.

$$SPL_{fan} = 10 \log_{10} \frac{\langle p_{fan}^2 \rangle}{p_{ref}^2} \quad (4.28)$$

With the *overall* method of computing fan noise parametrically based on the method of Heidmann described above, some attention can be given to the five individual fan noise components that the method of Heidmann predicts.

- i. *Inlet broadband noise:* Inlet broadband noise is caused by unsteady flow or turbulence in the flow around the fan and initial compressor stages. Sources of this unsteady flow are turbulence in the boundary layers, blade wakes and vortices, as well as unsteady flow in the inlet. The method does not predict the detailed individual inlet broadband sources but gives an estimate of the total broadband flow radiated from the inlet of the engine. Other than the matrix G , all terms from Eq. 4.22 are relevant for calculating the inlet broadband noise acoustic power.

The rotor-stator spacing exponent $a(K,L)$ is given by Eq. 4.29 and accounts for the inverse relationship between rotor-stator spacing and acoustic power except when IFD effects dominate when $s/C > 1$.

$$a(K,L) = \begin{bmatrix} 0.5 & 0.5 \\ 0.5 & 0 \end{bmatrix} \quad (4.29)$$

The power function F is given by Eq. 4.30, directivity values for D are determined empirically and can be obtained from [83], [84] in tabular form.

$$F = 1 \text{ for } M_r \leq 0.9; \quad F = 0.81M_r^{-2} \text{ for } M_r > 0.9 \quad (4.30)$$

The polar directivity angle resolution for all ANOPP based methods is 10 degrees and when finer resolutions are required then the directivity function values have to be interpolated. This has for instance been done in order to make the noise metric contours for complete departure and approach flight paths, described in Chapter 5. The spectral weighting function for inlet broadband noise is provided by the following semi-empirical or semi-analytical relation:

$$S = 0.116 \cdot \exp \left\{ -0.5 \left[\frac{\ln(\frac{n}{2.5})}{\ln(2.2)} \right]^2 \right\} \quad (4.31)$$

- ii. *Discrete tones from inlet:* Discrete tones are generated due to lift fluctuations on rotor blades or stator vanes, which are cyclical and repeat themselves with each blade passage. These lift fluctuations are caused by the blades encountering the wakes from inlet guide vanes or by the rotating wakes from the blades impinging on the stator vanes and disrupting the pressure field distribution in a repeating manner. The fundamental tone or frequency at which this pressure disturbance repeats itself is the BPF, given by Eq. 4.21. Along with the fundamental tone, higher harmonics are also formed at integer multiples of the BPF. The matrix G accounting for the effect of IGVs and tone cut-off logically plays an important role in inlet discrete tone modeling, as does the exponent a of the rotor-stator spacing term. As mentioned earlier, the discrete tones as well as their harmonics are modeled at their exact frequencies and then rounded to the appropriate 1/3 octave frequency value. The spectral function S for the tones therefore is also a discrete function, with separate values for the fundamental tone ($n = 1$) and for the subsequent harmonics ($n > 1$). The spectral intensity of the tones is furthermore affected by the presence of IGVs and tone cut-off and their effect is included additionally in the determination of the spectral weighting of the tones. Eq. 4.32 shows the function S as used in the method of Heidmann by Zorumski (indices I and J are for IGV presence and δ respectively). All the remaining terms such as F , D have also been determined empirically and can be found in [84].

$$S(1,I,J) = \begin{bmatrix} 0.499 & 0.136 \\ 0.799 & 0.387 \end{bmatrix}; \quad S(n,I,J) = \begin{bmatrix} 0.250 & 0.432 \\ 0.101 & 0.307 \end{bmatrix} \cdot 10^{-0.3(n-2)} \quad (4.32)$$

iii. *Combination tones*: Combination tones or ‘buzzsaw noise’ (as mentioned earlier in Chapter 3) are formed when the relative tip Mach number becomes supersonic, as a result of which shock waves are formed at the leading edge of each rotor blade. These shock waves propagate as Mach waves in the forward direction from each blade and coalesce in the inlet duct such that the repetition in pressure disturbance occurs not at each blade passage but rather with each complete rotation of the fan. As such, the tones are referred to as ‘combination’ tones and occur at each multiple of the shaft speed. Since the sound generated by the multiple combination tones is similar to that of a two-stroke motorbike or of a sawmill, the noise is also referred to as buzzsaw noise.

From tests carried out for various fans while developing Heidmann’s method, it was observed that buzzsaw noise spectra were characterized by peaks at three distinct frequencies. The method of Heidmann computes the acoustic power of combination tones at these three harmonics of the shaft rotational speed, expressed as fractions ($1/8^{\text{th}}$, $1/4^{\text{th}}$ and $1/2$) of the fundamental tone at BPF. The acoustic power in this case takes into account the effect of IGVs, which can prevent the combination tones from propagating and provides a different power function $F(M_r)$ and spectral function S for each $1/8^{\text{th}}$, $1/4^{\text{th}}$ and $1/2$ fundamental tone, both given as semi-analytical functions of relative Mach number M_r and frequency parameter η respectively. The spectral functions for combination tones are given by Eq. 4.33 for the three combination tones in ascending order and the directivity function D is provided empirically in tabular form in [83].

$$S(\eta) = 0.520(4\eta)^5 \text{ for } \eta \leq 0.125; \quad S(\eta) = 0.405(8\eta)^{-3} \text{ for } \eta > 0.125 \quad (4.33a)$$

$$S(\eta) = 0.520(4\eta)^5 \text{ for } \eta \leq 0.25; \quad S(\eta) = 0.520(4\eta)^{-5} \text{ for } \eta > 0.25 \quad (4.33b)$$

$$S(\eta) = 0.332(2\eta)^3 \text{ for } \eta \leq 0.5; \quad S(\eta) = 0.332(2\eta)^{-3} \text{ for } \eta > 0.5 \quad (4.33c)$$

iv. *Exhaust broadband noise*: The broadband noise emitted from the bypass exhaust is generated by the same mechanisms as described for inlet broadband noise. The main difference is that the presence of IGVs doubles the acoustic power of the radiated fan exhaust broadband noise. The power function F is similar to that of the inlet broadband noise, the spectral function S is the same and the directivity function D is again provided in tabular form.

v. *Discrete tones from the exhaust*: The tones that propagate from the engine bypass exhaust are produced by the same mechanism as the inlet tones. As such, they are predicted in an analogous way, with most functions and terms having the same values as for the inlet tones. The directivity function D is of course now more dominant towards the aft of the engine.

Fig. 4.3 shows a typical fan and compressor arrangement (only upper half) from [6], with the five primary fan noise sources described above shown in forward and aft directions.

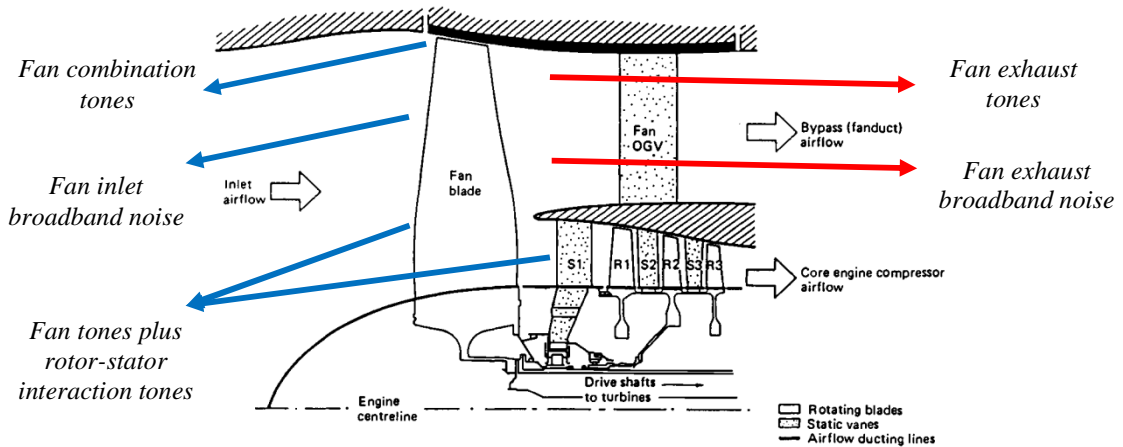


Figure 4.3: Primary noise sources originating from the fan (Fan configuration from [6])

The original method of Heidmann was seen to over-predict the intensity of fan tones when compared to more modern turbofan engines [90] and as such, the method was updated by Kontos et al. to reduce the fan tonal intensity due to improved blade designs of today. The updates to the empirical values used in the fan source noise models have been implemented in the current work as well. Furthermore, the effect of acoustic liners, which are used on all high bypass ratio engines, was also modeled by Kontos et al. in a second update to Heidmann's method [91], which further reduce the intensity of fan tones and broadband noise predominantly in the frequency range of 1000 Hz to 5000 Hz. The noise suppression depends on engine dimensions such as duct diameter and the length of the acoustic treatment area applied on the fan inlet and exhaust ducts. Sample values are shown in Fig. 4.4 for the CF6-80C2 engine and for the International Aero Engines V2527-A5 engine used on short to mid-range aircraft. The purpose of the plots for two quite different engines is to show the method's applicability for aircraft design purposes, where a generalization of methods is required. Since the actual data specific to liner technology is manufacturer sensitive, the validity of these results can be based on the fact that engines comparable to these commonly used engines were used in the measurements carried out by NASA and the duct diameters and liner area length for both engines have been taken for these comparable engines. In summary for the parametric fan noise prediction model for aircraft design and assessment purposes, Table 4.1 shows the geometric and operational parameters that the model requires as input.

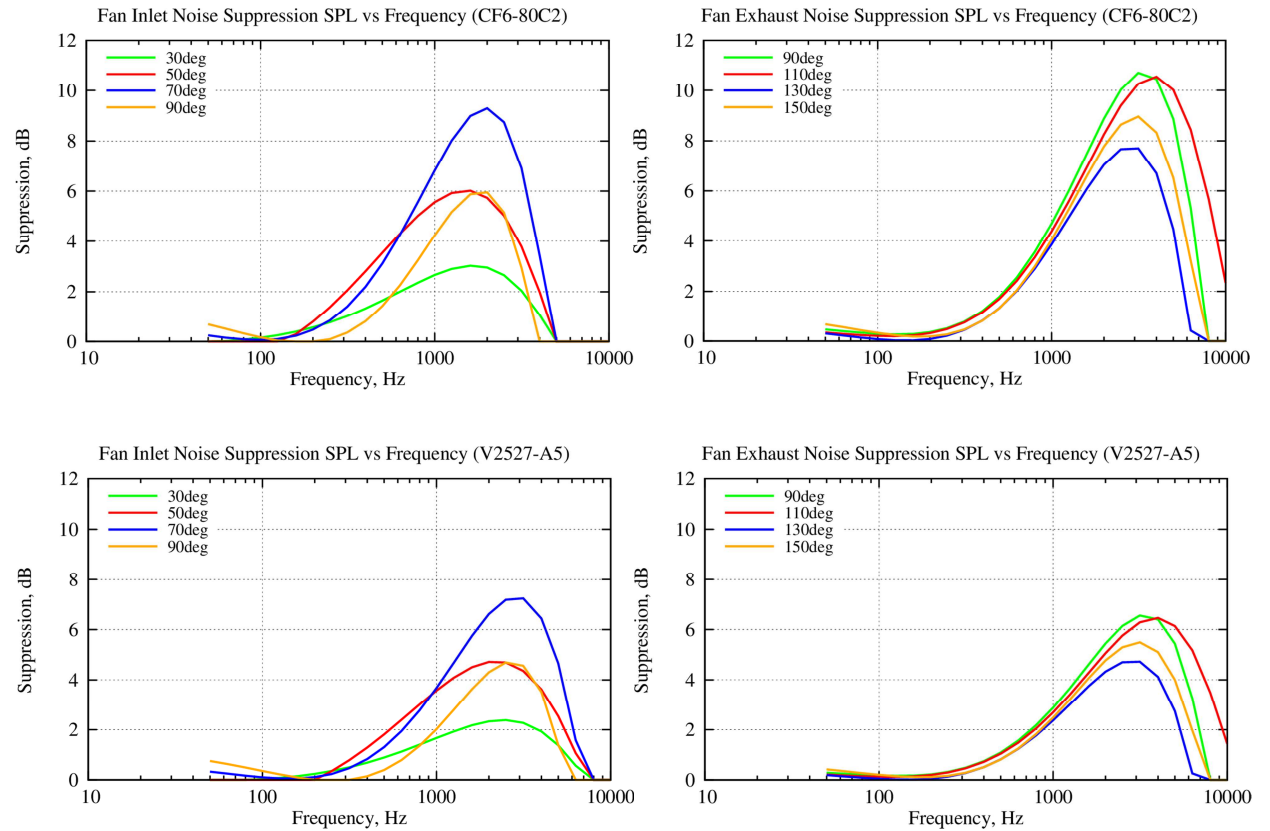


Figure 4.4: Noise suppression due to acoustic liner technology for two sample engines – CF6-80C2 (top) and V2527-A5 (bottom)

Table 4.1: Summary of geometric and operational parameters required for parametric fan noise prediction

Fan Noise Inputs	
Parameter Name	Symbol
Geometric Parameters	
Fan inlet area	A_{fan}
Number of rotor blades	B
Number of stator vanes	V
Fan rotor diameter	d
Fan rotor tip Mach number at design point	$M_{t,d}$
Rotor-stator spacing	s/C
Inlet Guide Vane index	IGV
Operational Parameters	
Fan mass flow rate	\dot{m}
Fan (LP) rotational speed	N (also NI)
Total temperature rise across fan	ΔT

It can be noted that for noise prediction using such parametric semi-empirical methods, both geometric as well as operational parameters for each component have to be provided as inputs. Many of the required inputs are however proprietary information, which are not publically disclosed by the engine manufacturers. As such, the input parameters have to be estimated via other means, which may not be a one hundred percent match to actual data, but still may provide a sufficient accuracy for a conceptual or preliminary design phase. For this purpose, the engine is modeled using the gas turbine design software Gasturb [92] in order to obtain the thermodynamic (operational) parameters required for fan noise prediction, and the geometric parameters are obtained using an empirical database for noise relevant engine geometry parameters created for work related to this dissertation. The geometric parameters are in this case sized via empirical relations based on the Sea-level Static Thrust (SLST) of the engine, following a ‘rubber-engine’ approach. The empirical functions developed for estimating the engine geometry parameters from the empirical database of current turbofan engines are shown in Appendix A.

The above described model for fan noise prediction was implemented for the research work carried out in this dissertation and the results of the model in terms of spectra in the forward and aft directions were compared with the spectra shown by Kontos et al. [90] for both an experimental quiet Energy Efficient Engine (E^3) of GE and NASA, as well as for GE’s CF6-80C2 engine used commonly on mid to long-range aircraft. The spectra were shown for both measured data as well as simulated data produced by NASA using their ANOPP code. The spectra have been shown for overall engine noise as well as for fan, combustor, LP turbine and jet noise for both engines and were used to validate the models, as implemented in this dissertation’s work. Fig. 4.6 to Fig. 4.8 in Section 4.2.5 show the simulated spectra for the E^3 engine made for the current research work and how they compare with measured and NASA’s simulated spectra.

4.2.2 Combustor noise

Noise produced from the combustion chamber of modern turbofan engines has gained prominence in the past decades due to the reduction in other major noise components such as the fan and jet. This has led to quite recent investigations into the current nature of combustor noise and its components [93]. It is known that the noise from the combustion chamber is purely broadband and is produced by the fuel heating process carried out in the combustion chamber. This noise due to fuel combustion can be direct – due to gas expansion in the chamber, which interacts with the surrounding flow and produces sound waves; and the noise can also be indirect, due to convection of entropy fluctuations from the combustion chamber to the turbine stages.

For current commercial aircraft, combustor noise is still dominated by other broadband components for departure and approach procedures (by jet noise during departure and airframe during approach), although at low thrust settings such as during approach, the combustor noise can make an increasingly significant contribution to the overall engine noise. Although combustor noise does not play as important a role for community noise impact currently, it can be expected to become significant in the coming decades, especially with new combustors entering the industry intended to produce very low gaseous emissions to meet the ACARE[†] Vision 2020 [94] and NASA N+2 and N+3 goals for noise and emission reduction [95].

[†] ACARE – Advisory Council for Aviation Research and Innovation in Europe

Combustor noise for the work in this dissertation is modeled parametrically using the method of Emmerling et al. [85]. The method predicts the overall broadband combustor noise in SPL according to Eq. 4.34:

$$SPL_{combustor} = 10 \log_{10} \frac{\langle p_{combustor}^2 \rangle}{p_{ref}^2} \quad (4.34)$$

where the mean-square acoustic pressure in the far-field due to the combustion process is given by Eq. 4.35:

$$\langle p_{combustor}^2 \rangle = \frac{\Pi_{combustor}}{4\pi r^2} \frac{S(\eta)D(\theta)}{(1-M_\infty \cos\theta)^4} \rho_\infty c_\infty \quad (4.35)$$

All the terms in Eq. 4.35 are as were explained for the fan noise calculation. The acoustic power $\Pi_{combustor}$ has been related parametrically to the combustor entrance and exit state variables according to Emmerling et al. and is given by Eq. 4.36.

$$\Pi_{combustor} = (8.85 \cdot 10^{-7}) \left(\frac{\dot{m}_{in}}{\rho_\infty c_\infty A_{combustor}} \right) \left(\frac{T_{t,out} - T_{t,in}}{T_{t,in}} \right)^2 \left(\frac{p_{t,in}}{p_\infty} \right)^2 \left(\frac{\Delta T_{des}}{T_\infty} \right)^{-4} \rho_\infty c_\infty^3 A_{combustor} \quad (4.36)$$

The value $8.85 \cdot 10^{-7}$ is an empirical constant determined from the measurements carried out for turbofan, turbojet as well as turboprop combustors. Index *in* denotes combustor entrance parameters and index *out* denotes combustor exit parameters, with T_t the total temperature and p_t the total pressure. The term ΔT_{des} is the design point temperature extraction from the turbine and corresponds to the temperature difference between combustor exit and turbine entry temperatures, at the engine design point.

The directivity function $D(\theta)$ and the spectral function $S(\eta)$ for combustor noise are given as functions of polar angle θ and logarithm of base 10 of the frequency parameter η in [83] in tabular form. The parameter η is determined using Eq. 4.37, where 400 Hz corresponds to the frequency around which the combustor noise was seen to peak by Emmerling et al.

$$\eta = (1 - M_\infty \cos\theta) \frac{f}{400} \quad (4.37)$$

The inputs required for combustor noise calculation as implemented in this dissertation are shown in Table 4.2.

Table 4.2: Summary of geometric and operational parameters required for parametric combustor noise prediction

Combustor Noise Inputs	
<i>Parameter Name</i>	<i>Symbol</i>
Geometric Parameters	
Combustor entrance area	$A_{combustor}$
Operational Parameters	
Combustor entrance mass flow rate	\dot{m}_{in}
Combustor entrance total temperature	$T_{t,in}$
Combustor exit total temperature	$T_{t,out}$
Combustor entrance total pressure	$P_{t,in}$
Turbine temperature extraction at design point	ΔT_{des}

4.2.3 Turbine noise

LP Turbine noise is predicted using the method of Matta et al. of GE [86], which has been integrated in ANOPP and predicts both the broadband as well as tonal components of turbine noise. The mechanisms of turbine noise generation are similar to those of the fan exhaust noise - discrete tones are generated due to cyclic pressure disturbances or lift fluctuations arising from blade wake interaction with the vanes; broadband noise is generated due to turbulence or unsteady flow occurring around the turbine rotors and stators. It can be mentioned that the noise generated from the High Pressure (HP) turbine does not radiate effectively out of the engine unit and is thus dominated by the LP turbine noise. As such, the method of Matta et al. only considers the LP turbine noise prediction.

Turbine noise in terms of SPL is calculated according to Eq. 4.38 and the mean square acoustic pressure in the far-field due to overall turbine noise $\langle p_{turbine}^2 \rangle$ is computed using Eq. 4.39. Since turbine noise has two components, the acoustic pressure due to both sources $\langle p_{i,turbine}^2 \rangle$ is first added linearly, before the overall turbine pressure is converted to its SPL value.

$$SPL_{turbine} = 10 \log_{10} \frac{\langle p_{turbine}^2 \rangle}{p_{ref}^2} \quad (4.38)$$

$$\langle p_{i,turbine}^2 \rangle = \frac{\Pi_i}{4\pi r^2} \frac{S(\eta)_i D(\theta)_i}{(1-M_\infty \cos\theta)^4} \rho_\infty c_\infty \quad (4.39)$$

- i. *Turbine broadband noise:* The acoustic power of the broadband noise radiated from the turbine is given by Eq. 4.40:

$$\Pi_{BB,turbine} = (8.589 \cdot 10^{-5}) \left(\frac{T_{t,in} - T_{out}}{T_{t,in}} \right)^{1.27} \left(\frac{\pi N d_{turbine}}{c_\infty} \right)^{-1.27} \rho_\infty c_\infty^3 A_{turbine} \quad (4.40)$$

where the value $8.589 \cdot 10^{-5}$ is again an empirical constant. In the second term in Eq. 4.40, T_t as the total temperature and T is the static temperature, with index *in* corresponding to the turbine entrance values and index *out* corresponding to the turbine exit values. The second term represents the ideal work extraction from the turbine and the third term represents the influence of the rotor tip-speed (analogous to the rotor tip Mach number for the fan blades). The broadband spectral function $S_{BB,turbine}(\eta)$ as well as the directivity function $D_{BB,turbine}(\theta)$ are provided in tabular form in [83]. The spectral function S is again a function of the frequency parameter η , which in turn depends on the ratio of the frequency f to the turbine BPF.

$$\eta = (1 - M_\infty \cos\theta) \frac{f}{BPF_{turbine}} \quad (4.41)$$

- ii. *Turbine discrete tones*: The acoustic power for the turbine tonal noise is given by Eq. 4.42, consisting of the same parameters as in Eq. 4.40, but with different empirical constants and exponents.

$$P_{Tone,turbine} = (1.162 \cdot 10^{-6}) \left(\frac{T_{t,in} - T_{out}}{T_{t,in}} \right)^{1.46} \left(\frac{\pi N d_{turbine}}{c_\infty} \right)^{-4.02} \rho_\infty c_\infty^3 A_{turbine} \quad (4.42)$$

The tonal spectrum function $S_{Tone,turbine}$ is given as a discrete function by Eq. 4.43 since, as was shown for fan discrete tones, the turbine discrete tones are modeled at their individual frequencies (the fundamental tone at BPF i.e. $n = 1$ and its harmonics at integer multiples, $n > 1$). The tone and the harmonics are then rounded to the nearest 1/3 octave band frequency values for further computation.

$$S_{Tone,turbine}(n) = 0.6838 \cdot 10^{-(n-1)/2} \quad (4.43)$$

The overall turbine noise far-field acoustic pressure as well as SPL can then be calculated using Eq. 4.38 and Eq. 4.39 after adding the broadband and tonal turbine noise components. Table 4.3 summarizes the inputs required for turbine noise calculation using the method of Matta et al.

Table 4.3: Summary of geometric and operational parameters required for parametric turbine noise prediction

Turbine Noise Inputs	
<i>Parameter Name</i>	<i>Symbol</i>
Geometric Parameters	
Turbine rotor diameter	$d_{turbine}$
Turbine inlet area	$A_{turbine}$
Turbine rotor blade number	$B_{turbine}$
Operational Parameters	
Turbine (LP) rotational speed	N (also NI)
Turbine entrance total temperature	$T_{t,in}$
Turbine exit static temperature	T_{out}

4.2.4 Jet noise

As was mentioned in Section 4.1, jet noise is a major source of aircraft noise particularly during takeoff and was the dominating noise source of aircraft of the past, leading to the development of the field of aeroacoustics by Lighthill. It was also mentioned that high-fidelity CFD and CAA based methods weren't suitable for aircraft design purposes currently, due to their extreme computational times. A semi-empirical parametric model that would retain some of the physics and would produce faster results with a slight loss of accuracy would thus be a necessary compromise. The need to retain some of the physics stems from the fact that if the model is based on more theoretical foundations, then it has the potential to be applicable to a wider variety of engines and not just ones which were used during the measurements. This is a crucial aspect when considering the right model for aircraft design purposes. One such method that has been widely used for aircraft design and noise assessment purposes is the method of Stone [87], which is also an integrated part of ANOPP.

The far-field noise from the jet or exit nozzle of the engine has been modeled for this dissertation using Stone's model, which can model the mixing noise as well as shock induced noise of turbojet and turbofan engines for both single stream as well as coaxial nozzle engines (typical for all modern turbofan engines). The mixing noise is produced when the high-velocity jets exiting the core (primary) and bypass (secondary) nozzles mix with the ambient air as well as with each other. This causes both large and small scale turbulence, with the resulting noise having a broadband character and peaking at low frequencies (typically 100-200 Hz for most turbofan engines).

Stone used measurements of several engines to come up with a semi-empirical jet noise prediction model and attempted to correlate the measured data with Eq. 4.13, which was Lighthill's acoustic power law. He found that although for large scale turbulence further downstream of the engine, a correlation of the acoustic power with jet velocity (from now on referred to as simply v_j) raised to eighth power could be found, for the other source regions closer to the engine a good match with the measurements couldn't be found with a v_j^8 correlation. This was attributed to the fact that Lighthill's acoustic power law was valid for *cold* jets where the temperature of the jet was comparable with the ambient temperature. For the measurements carried out for the model's development, a lower exponent of 7.5 yielded the highest correlation of predictions with measurements, likely due to the tested jets being 'hot' and not cold as would be theoretically required for a v_j^8 variation. The exponent value of 7.5 is nonetheless very close to the theoretical value of 8 and demonstrates the strength of Lighthill's theoretical jet noise prediction based on fundamental equations of fluid mass and momentum conservation.

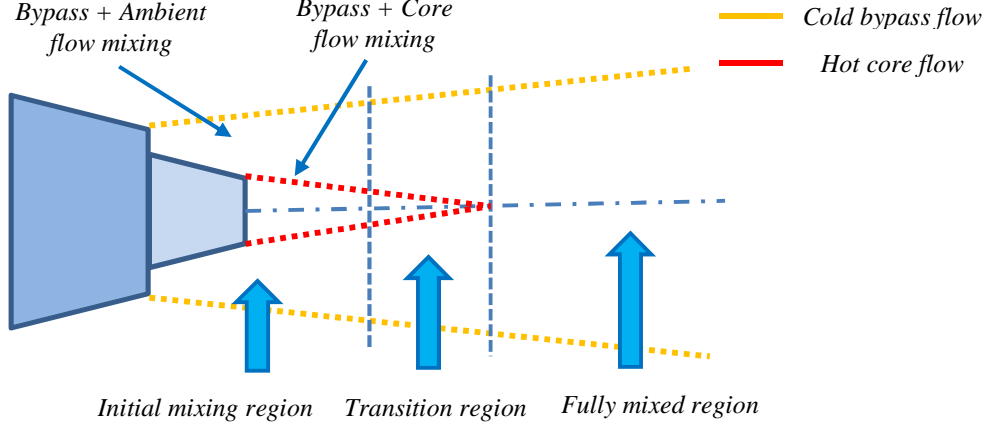


Figure 4.5: Jet mixing noise and the various mixing regions near the nozzle exit

Jet noise prediction according to the model of Stone takes into account a number of geometric and thermodynamic parameters. The predicted jet noise strongly depends on the nozzle areas (both bypass and core), the densities and temperatures at the nozzle exits as well as on both primary and secondary jet velocities. Once again, the approach outlined by Zorumski has been used to implement Stone's model. Since shock noise is usually not encountered for current civil turbofan engines which are analyzed in this dissertation, the shock induced noise is not described in this dissertation for conciseness. Shock induced jet noise has however been implemented in the parametric jet noise model for this dissertation and can be applied if required to turbojet jet noise prediction. The jet mixing noise calculation starts off with the computation of the mean-square acoustic pressure due to a single stream stationary jet, at a reference distance l_{ref} from the nozzle exit (which in Zorumski's approach is taken to be equal to $\sqrt{A_e}$) and at a polar directivity angle of $\theta = 90^\circ$. All jet parameters are henceforth referred to with the index j .

$$\langle p^2(l_{ref}, 90^\circ) \rangle = \frac{2.502 \cdot 10^{-6} (A_{j,1}/A_e) (\rho_{j,1}/\rho_\infty)^{\omega_0} (v_{j,1}/c_\infty)^{7.5}}{(1 + (0.124 v_{j,1}/c_\infty)^2)^{3/2}} \rho_\infty^2 c_\infty^4 \quad (4.44)$$

In Eq. 4.44, $A_{j,1}$ is the fully expanded primary jet area, $\rho_{j,1}$ is the primary jet density, and the density exponent ω_0 has been determined empirically by Stone as:

$$\omega_0 = \frac{2(v_{j,1}/c_\infty)^{3.5} - 0.6}{(v_{j,1}/c_\infty)^{3.5} + 0.6} \quad (4.45)$$

The value of the reference mean square acoustic pressure from Eq. 4.44 is then corrected for directivity via the term D_m , spectral weighting according to the function F_m and forward flight effects via the term H_m . The reference mean square acoustic pressure is then converted to that for a coaxial nozzle via the factor G_c such that the far-field pressure disturbance due to a coaxial jet and not just a single jet can be computed. The effect of a plug nozzle via the factor G_p is also considered in the far-field jet noise prediction. According to this approach, the far-field mean square acoustic pressure due to jet mixing noise is calculated using Eq. 4.46, after combining all of the mentioned functions and factors:

$$\langle p^2 \rangle = \frac{\langle p^2(l_{ref}, 90^\circ) \rangle}{4\pi r^2} \left[\frac{1 + \left(\frac{0.124v_{j,1}}{c_\infty} \right)^2}{\left(1 + \frac{0.6v_{j,1}\cos\theta}{c_\infty} \right)^2 + \left(\frac{0.124v_{j,1}}{c_\infty} \right)^2} \right]^{\frac{3}{2}} D_m(\theta') F_m(S_m, \theta') H_m(M_\infty, \theta, \frac{v_{j,1}}{c_\infty}, \frac{\rho_{j,1}}{\rho_\infty}, \frac{T_{j,1}}{T_\infty}) G_c G_p \quad (4.46)$$

For jet mixing noise (represented by index m), Stone found that the spectral function was not only a function of the Strouhal number S_m , but also of the modified polar directivity angle θ' . The modified polar angle has been used instead of the actual polar angle in this case to take into account refraction effects due to the high temperatures that exist in the nozzle flows. Contrary to other engine noise sources therefore, the jet mixing noise spectral function is not just a function of frequency but also of directivity. The directional characteristics of the mixing noise are in addition accounted for by the directivity function $D_m(\theta')$, as for the other noise sources, and the function has been provided as empirical values for each θ' angle value in [83], [87]. The modified polar directivity angle is given by $\theta' = \theta(v_{j,1}/c_\infty)^{0.1}$ and the Strouhal number for the spectral function F_m is given by Eq. 4.47:

$$S_m = S_{m,1} \cdot S_{m,2} \cdot g_c g_p \quad (4.47a)$$

$$S_{m,1} = \frac{\left(\frac{f\sqrt{A_e}}{c_\infty} \right) \left(\frac{d_{j,1}}{\sqrt{A_e}} \right) [1 - M_\infty \cos(\theta - \delta')] \left(\frac{T_{j,1}}{T_\infty} \right)^{0.4(1+\cos\theta')}}{c_\infty \left(1 - \frac{M_\infty c_\infty}{v_{j,1}} \right)} \quad (4.47b)$$

$$S_{m,2} = \left\{ \frac{\left(1 + 0.62 \left(\frac{v_{j,1}}{c_\infty} - M_\infty \right) \cos\theta \right)^2 + \left(0.124 \left(\frac{v_{j,1}}{c_\infty} - M_\infty \right) \right)^2}{\left(1 + 0.62 \left(\frac{v_{j,1}}{c_\infty} \right) \cos\theta \right)^2 + \left(0.124 \left(\frac{v_{j,1}}{c_\infty} \right) \right)^2} \right\}^{1/2} \quad (4.47c)$$

In the above equation, the term $f\sqrt{A_e}/c_\infty$ is the Helmholtz number, $d_{j,1}$ is the primary jet diameter, δ' is the angle between the flight vector and the engine inlet axis and $T_{j,1}$ is the primary stream temperature. g_c , g_p are configuration factors for a coaxial nozzle and for a nozzle with a plug respectively. Stone found that the frequency distribution of jet mixing noise was different for coaxial nozzles than for single stream nozzles (due to additional mixing of the core flow with bypass flow besides mixing with ambient flow) and was also affected by the presence of a plug at the nozzle exit. These two factors are accounted for by Eq. 4.48 and Eq. 4.49.

$$g_c = 1 \text{ for single nozzle;} \quad (4.48a)$$

$$g_c = \frac{1}{\left(1 - \frac{T_{j,2} f_s}{T_{j,1}} \right)} \text{ for coaxial nozzle} \quad (4.48b)$$

$$g_p = 1 \text{ for nozzle without plug} \quad (4.49a)$$

$$g_p = R_d^{0.4} \text{ for nozzle with plug} \quad (4.49b)$$

In Eq. 4.48, the term f_s is the frequency shift parameter, which is an empirically determined function of the area ratio parameter $1 + (A_{j,2}/A_{j,1})$ and $v_{j,2}/v_{j,1}$, and $T_{j,2}$ is the secondary jet temperature; the term R_d is the ratio of the plug nozzle hydraulic diameter $d_{h,1}$ to the equivalent jet diameter, with $d_{h,1}$ given by Eq. 4.50:

$$d_{h,1} = (d_{j,1}^2 - d_p^2)^{1/2} - d_p \quad (4.50)$$

The first term on the left side of Eq. 4.50 is the equivalent jet diameter and d_p is the plug diameter. The forward flight effects factor H_m is given by Eq. 4.51:

$$H_m(M_\infty, \theta, \frac{v_{j,1}}{c_\infty}, \frac{\rho_{j,1}}{\rho_\infty}, \frac{T_{j,1}}{T_\infty}) = \left\{ \frac{(1+0.62(\frac{v_{j,1}}{c_\infty})\cos\theta)^2 + (0.124(\frac{v_{j,1}}{c_\infty}))^2}{(1+0.62(\frac{v_{j,1}}{c_\infty}-M_\infty)\cos\theta)^2 + (0.124(\frac{v_{j,1}}{c_\infty}-M_\infty))^2} \right\}^{3/2} \cdot \frac{(1-\frac{M_\infty}{v_1})^5 (\frac{\rho_{j,1}}{\rho_\infty})^{\omega-\omega_0}}{1-M_\infty\cos(\theta-\delta)} \quad (4.51)$$

where the density exponent for forward flights effect is given by Eq. 4.52.

$$\omega - \omega_0 = \frac{1.8 \left\{ \left(\frac{v_{j,1}}{c_\infty} \right) \left[1 - \left(\frac{M_\infty c_\infty}{v_{j,1}} \right) \right]^{2/3} \right\}^{3.5} - \left(\frac{v_{j,1}}{c_\infty} \right)^{3.5}}{\left\{ 0.6 + \left\{ \left(\frac{v_{j,1}}{c_\infty} \right) \left[1 - \left(\frac{M_\infty c_\infty}{v_{j,1}} \right) \right]^{2/3} \right\}^{3.5} \right\} \left(0.6 + \left(\frac{v_{j,1}}{c_\infty} \right)^{3.5} \right)} \quad (4.52)$$

The forward flight effects factor H_m has been normalized such that it becomes unity for $M_\infty = 0$. The two remaining terms from Eq. 4.46, required to describe the mean-square acoustic pressure due to jet mixing noise are the configuration factors for a coaxial nozzle G_c and for a plug nozzle G_p . These are given by Eq. 4.53 and Eq. 4.54 respectively.

$$G_c = 1 \text{ for single nozzle} \quad (4.53a)$$

$$G_c = \left(\frac{T_{j,1}}{T_{j,2}} \right)^{1/2} \left\{ \left(1 - \frac{v_{j,2}}{v_{j,1}} \right)^m + \frac{1.2 \left(1 + \frac{A_{j,2} v_{j,2}^2}{A_{j,1} v_{j,1}^2} \right)^4}{\left(1 + \frac{A_{j,2}}{A_{j,1}} \right)^3} \right\} \text{ for coaxial nozzle} \quad (4.53b)$$

$$G_p = 1 \text{ for nozzle without plug} \quad (4.54a)$$

$$G_p = \left(0.1 + \frac{2R_d^2}{1+R_d^2} \right)^{0.3} \text{ for nozzle with plug} \quad (4.54b)$$

As for the other engine noise models, jet (mixing) noise in terms of SPL can be obtained from the mean square far-field acoustic pressure using Eq. 4.55. If shock noise is present due to supersonic flow at the nozzle, then the mean square pressure due to shock noise can be added linearly to the mixing noise acoustic pressure before conversion to SPL values.

$$SPL_{jet} = 10 \log_{10} \frac{\langle p_{jet}^2 \rangle}{p_{ref}^2} \quad (4.55)$$

The parameters that Stone's jet noise model requires as input for jet noise calculation are summarized in Table 4.4. It can be seen that besides the nozzle areas, the thermodynamic variables at both nozzles (which depend on the engine thrust setting) play a crucial part towards the magnitude, spectrum and directivity of jet noise.

Table 4.4: Summary of geometric and operational parameters required for parametric jet noise prediction

Jet Noise Inputs	
<i>Parameter Name</i>	<i>Symbol</i>
Geometric Parameters	
Primary jet area	$A_{j,1}$
Secondary jet area	$A_{j,2}$
Plug diameter	d_p
Engine inlet axis angle	δ'
Operational Parameters	
Primary jet Mach number	$M_{j,1}$
Primary jet temperature	$T_{j,1}$
Primary jet velocity	$v_{j,1}$
Primary jet density	$\rho_{j,1}$
Secondary jet Mach number	$M_{j,2}$
Secondary jet temperature	$T_{j,2}$
Secondary jet velocity	$v_{j,2}$
Secondary jet density	$\rho_{j,2}$

4.2.5 Engine noise validation at source

The engine noise models above were checked for their veracity by comparing the results with publically available references, such as the published spectra for the experimental E^3 engine of GE in [90]. The implemented code was firstly verified by providing as inputs the same values for all engine components for the E^3 engine; secondly, the E^3 engine was modeled using the software Gasturb and for the engine settings specified in [90], the required thermodynamic inputs were obtained from Gasturb. These simulated inputs were then used to predict the same spectra, both in a sample forward arc direction ($\theta = 50^\circ$) and in a sample aft direction ($\theta = 150^\circ$). The results from the models implemented for this dissertation's work were compared both to NASA's ANOPP simulated values as well as with measured values for the E^3 engine. The published spectra from are shown in the top part of Fig. 4.6 and Fig. 4.7 for the forward and aft directions respectively. The middle part of these figures shows the simulated spectra compared with NASA's ANOPP using reference values from [90]; the bottom figures show the comparison using Gasturb simulated values of the simulated spectra with the NASA ANOPP spectra (shown by cyan curve with legend entry 'NASA ANOPP Sum').

It can be observed from Fig. 4.6 and Fig. 4.7 that the models for engine noise as modeled for this dissertation produce spectra of a comparable fidelity to NASA's ANOPP. The small differences (1-2 dB) for reference value spectra can be attributed to different interpolation schemes or slightly different curve fitting functions made of the tabulated data for the various spectral and directivity functions. The spectra for the E^3 engine simulated using thermodynamic parameters obtained from Gasturb also show a very close match to the reference spectra, and based on Fig. 4.6 and 4.7, the use of Gasturb can be judged as more than suitable for aircraft noise estimation during a conceptual design and analysis phase. As NASA's ANOPP is still considered the state of the art in parametric aircraft engine noise prediction, the

prediction accuracy of the implemented models can therefore be deemed to be comparable to the current state of the art.

Fig. 4.8 shows the comparison of predicted spectra with measured engine noise spectra (shown by gray curve with legend entry ‘Measured Data’). It can be observed that qualitatively, the semi-empirical methods reflect overall measured spectra (orange curve of predicted ‘Engine Noise Sum’ compared with gray curve for ‘Measured Data’) reasonably well, although differences up to 8 dB for certain frequency ranges can be observed. This value, although somewhat high, is still not unreasonably far off from measurements and has been deemed to be as good as the models currently can be [65], [96]. The third octave spectra for all engine noise components were obtained in a matter of seconds for the complete 180 degree source noise spheres, thereby displaying the immense gain in computational efficiency for the slight loss of accuracy which was mentioned earlier as a necessary compromise.

The comparison with measured data highlights how challenging aircraft noise prediction is – one has to choose between a computational time of weeks to get highly accurate component level source noise data using CFD/CAA based methods, or approximate data in a matter of seconds for an entire aircraft using semi-empirical/semi-analytical methods. What is however very important for the purposes of this dissertation is that the models capture differences between broadband and tonal noise components of different engines and aircraft sufficiently well. A hundred percent match with measured data is not essentially necessary for parametric design studies, as long as the effects of the parametric variations are captured in the spectra produced for each variation. The models of Heidmann, Stone, Emmerling and Matta are seen to fulfill this requirement well, and as such their use has been made for aircraft design assessment and optimization for noise as well as annoyance in the subsequent chapters.

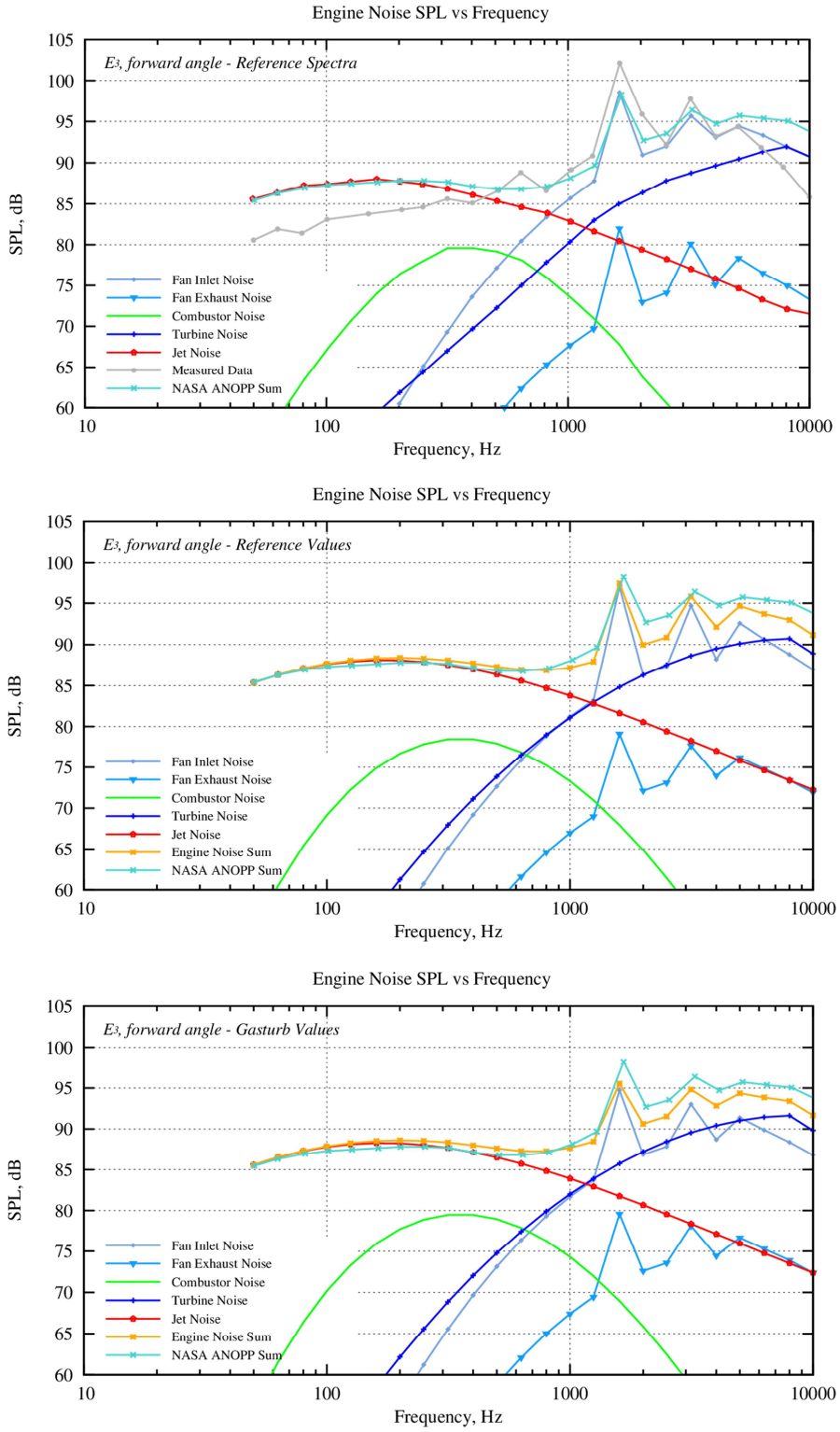


Figure 4.6: Comparison of implemented models with NASA's ANOPP from [90] in forward arc, $\theta = 50^\circ$ – reference spectra (top); simulated spectra with ref. values (middle); simulated spectra with Gasturb values (bottom)

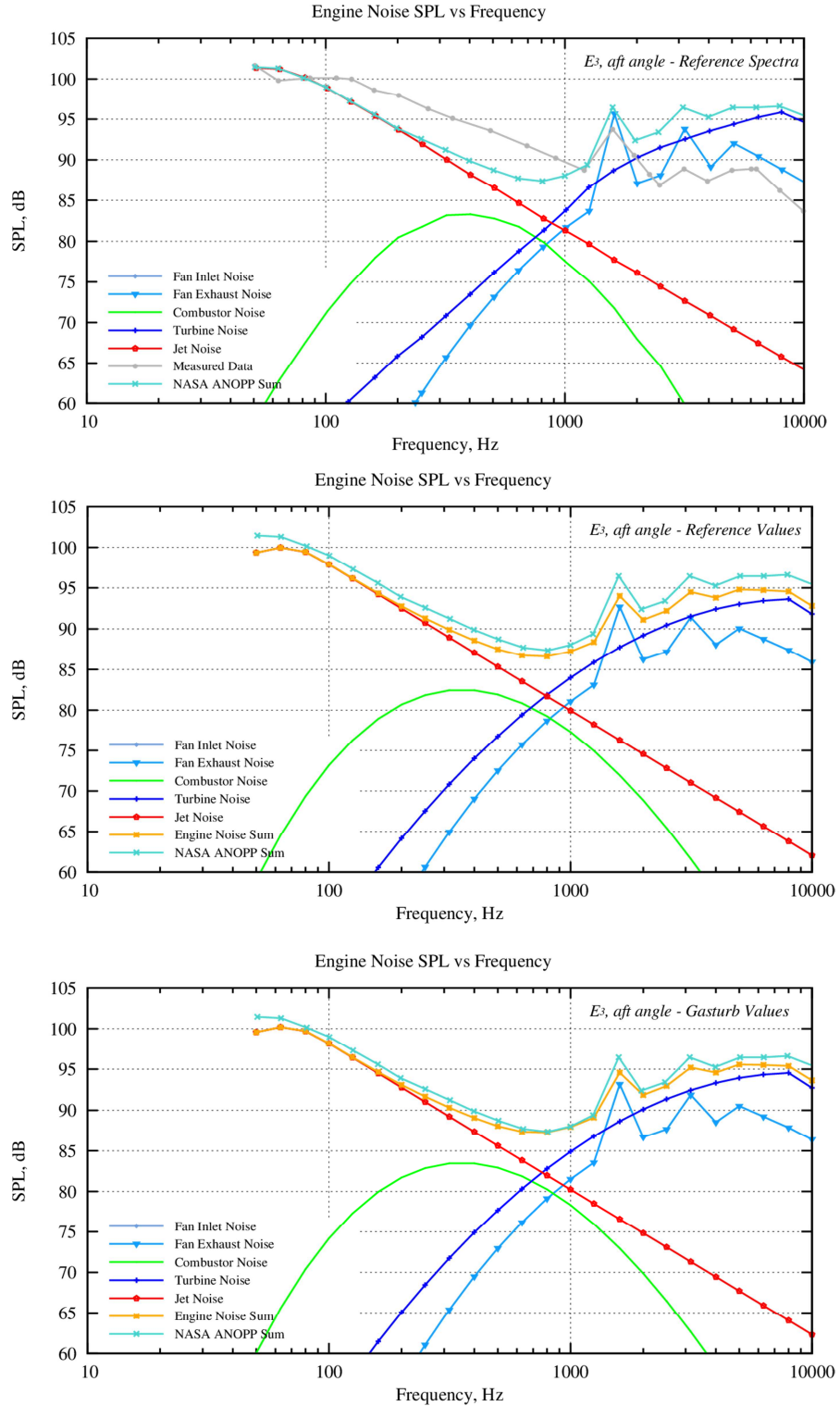


Figure 4.7: Comparison of implemented models with NASA's ANOPP from [90] in aft arc, $\theta = 150^\circ$ – reference spectra (top); simulated spectra with ref. values (middle); simulated spectra with Gasturb values (bottom)

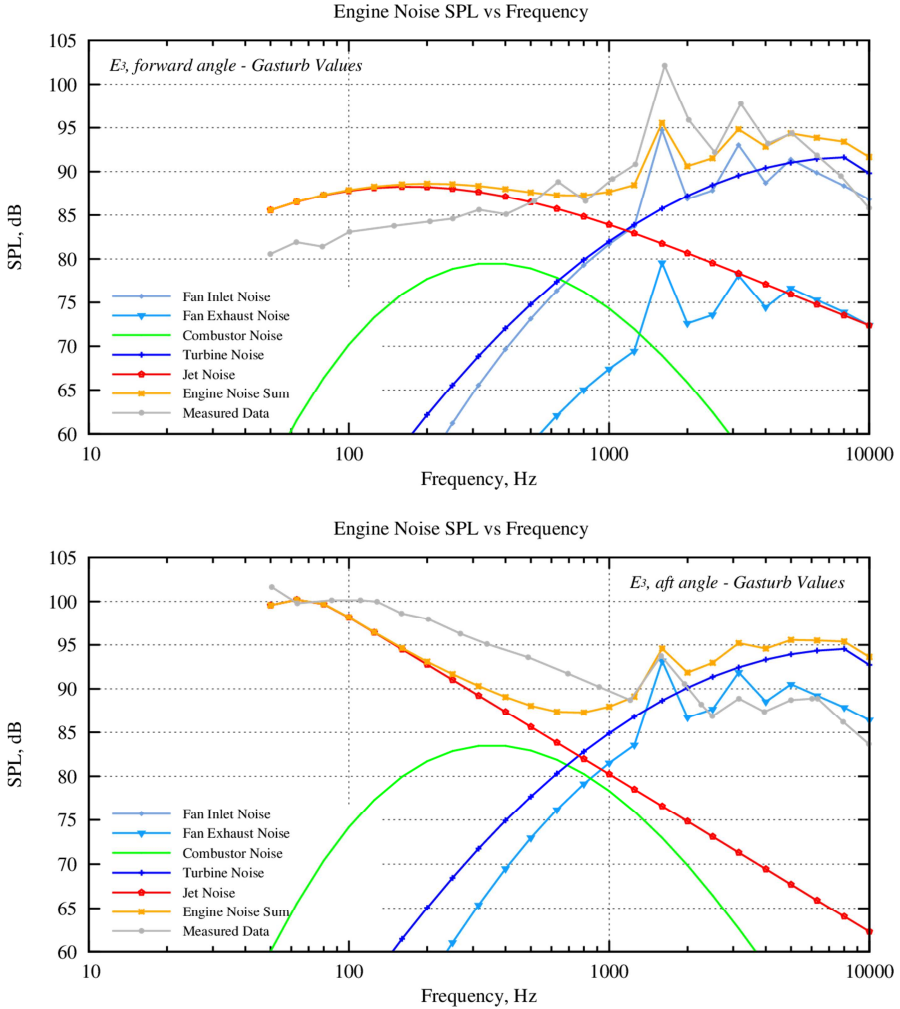


Figure 4.8: Comparison of implemented models with measured values from [90] – forward arc, $\theta = 50^\circ$ (top); aft arc, $\theta = 150^\circ$ (bottom)

4.2.6 Airframe noise

It was mentioned in Section 4.1 that turbulent flow over trailing edges and over compact bodies is also an important aircraft noise source and is the dominant broadband noise source during approach. The theoretical approach of Ffowcs-Williams and Hall and Curle was used to predict the far-field acoustic pressure created due to turbulent flow around thin sharp edges such as wing or slat trailing edges, and over compact bodies such as landing gear wheels and struts. The parametric model developed by Fink [88] of United Technology Research Center for the US FAA for predicting noise due to the aircraft airframe, is a model in wide use [65], [67], [97] and is an integrated part of ANOPP. The model predicts the broadband noise from the dominant components of the aircraft airframe, which include clean wing trailing edge noise, flap noise, slat noise, main and nose landing gear noise as well as aerodynamic noise from the stabilizers (as illustrated in Fig. 4.1). The model was developed specifically to predict overall airframe noise trends for commercial aircraft for carrying out aircraft level studies and as such, is highly

suitable for the purposes of this dissertation. The model makes use of empirical functions (from measurements of several aircraft flyovers in flight idle setting) and assumed theoretical functions to produce airframe noise spectra for each component as a function of third-octave frequency, polar directivity angle and azimuthal directivity angle. As was indicated via Eq. 4.18, noise from the airframe is not radially symmetric and also varies with aircraft azimuthal angle ψ .

Similar to the engine source noise models, the approach of Zorumski [83] will be used for predicting the far-field noise due to the airframe components. This is given by the familiar form of Eq. 4.56:

$$\langle p_{i,airframe}^2 \rangle = \frac{\Pi_i}{4\pi r^2} \frac{F(S)_i D(\theta, \psi)_i}{(1 - M_\infty \cos \theta)^4} \rho_\infty c_\infty \quad (4.56)$$

In Eq. 4.56, $F(S)_i$ is the spectral function for each airframe component and S is the Strouhal number, defined as:

$$S = (1 - M_\infty \cos \theta) \frac{fL}{M_\infty c_\infty} \quad (4.57)$$

where f is the frequency and L is the characteristic dimension of the airframe noise source. The acoustic power of each component is given by Eq. 4.58.

$$\Pi_i = K_i (M_\infty)^{a_i} G_i \rho_\infty c_\infty^3 b_w^2 \quad (4.58)$$

In the above equation, K_i is an empirical constant and a_i is a power coefficient, relating the radiated acoustic power with the flow speed. G_i incorporates the effect of airframe component geometry on the acoustic power and is different for each component. The term b_w corresponds to the wing span of the aircraft under consideration. Using Eq. 4.58, the acoustic power for each aircraft geometry component can be computed, and together with the directivity function D_i and spectral function F_i for the component, the mean-square acoustic pressure in the far-field can be determined. Some attention will now be given to the individual airframe noise sources and how they are predicted using the model of Fink.

i. *Clean trailing-edge noise:*

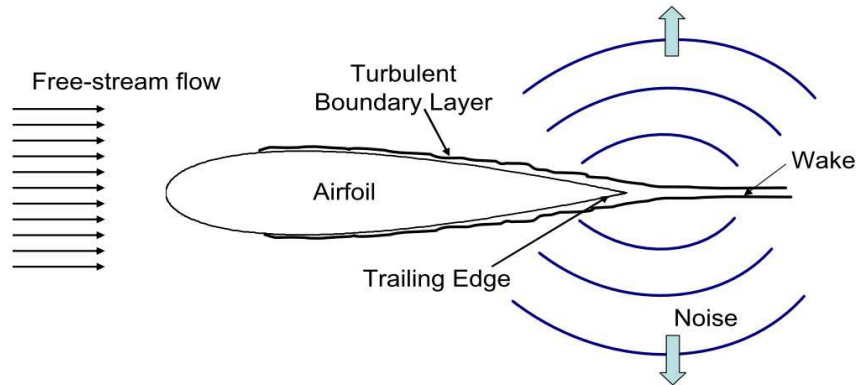


Figure 4.9: Clean trailing edge noise generation due to convection of turbulent flow over trailing edge [98]

In Fink's model, trailing edge noise over a clean wing and tail surfaces is caused by the convection of the turbulent boundary layer past the surface trailing edge. The turbulence length scale is taken to be the boundary layer thickness. The directivity function D is assumed to be of dipole form, aligned with the lift dipole and the spectral function F has been determined empirically. The acoustic power from trailing edge noise over conventional wings is given by Eq. 4.59, which is a specific form of Eq. 4.58 for the wing. The correlation of wing trailing edge noise acoustic power with fifth power of flow speed, as was shown in Eq. 4.17 can be noted.

$$\Pi_w = (4.464 \cdot 10^{-5})(M_\infty)^5 \delta_w^* \rho_\infty c_\infty^3 b_w^2 \quad (4.59)$$

where δ_w^* is the dimensionless turbulent boundary layer thickness and is computed by assuming a standard flat plate turbulent boundary layer according to Eq. 4.60.

$$\delta_w^* = 0.37 \frac{A_w}{b_w^2} \left(\frac{\rho_\infty M_\infty c_\infty A_w}{\mu_\infty b_w} \right)^{-0.2} \quad (4.60)$$

A_w in the above equation is the wing area and μ_∞ is the ambient dynamic viscosity of air. For the horizontal and vertical tail surfaces, the appropriate stabilizer area has to be substituted into Eq. 4.60 and for the acoustic power, Eq. 4.59 has to be multiplied by the ratio of spans b_h^2/b_w^2 or b_v^2/b_w^2 depending on the type of stabilizer surface (index h refers to the horizontal stabilizer and v refers to the vertical stabilizer). The directivity function for the clean wing and horizontal tail is given by Eq. 4.61 and for the vertical tail by Eq. 4.62.

$$D_{w,h}(\theta, \psi) = 4 \cos^2 \left(\frac{\theta}{2} \right) \cos^2 \psi \quad (4.61)$$

$$D_v(\theta, \psi) = 4 \cos^2 \left(\frac{\theta}{2} \right) \sin^2 \psi \quad (4.62)$$

The forms of directivity variation are also here similar to the form predicted theoretically by Ffwoocs-Williams and Hall, as was indicated in Eq. 4.18. The empirically determined spectral function F is given as two separate functions – one for rectangular wings and one for delta wings, according to Eq. 4.63 and Eq. 4.64 respectively:

$$F_{w,rect}(S) = 0.613(10S)^4((10S)^{3/2} + 0.5)^{-4} \quad (4.63)$$

$$F_{w,delta}(S) = 0.485(10S)^4((10S)^{1.35} + 0.5)^{-4} \quad (4.64)$$

In the above equations, the Strouhal number is calculated using Eq. 4.57, where the characteristic dimension L is taken to be the product of the dimensionless turbulent boundary layer thickness (δ_i^* from Eq. 4.60) and the span b of the surface under consideration (i.e. wing, horizontal or vertical stabilizer).

- ii. *Leading edge slat noise:* Fink accounts for the increased noise due to slat deployment by accounting for two mechanisms – the increment in wing trailing edge noise due to the interaction of the deployed slat with the boundary layer of the wing, and the trailing edge noise produced by the slat itself. For the first mechanism, the acoustic power radiated from the wing trailing edge when the slat is deployed is assumed to double. For the second mechanism, the slat noise acoustic power is assumed to be equal to

the clean wing trailing edge acoustic power. The main difference to wing trailing edge noise is that the spectral function $F_s(S)$ for the slat has a different weighting, also determined empirically and given by Eq. 4.65.

$$F_s(S) = 0.613(2.19S)^4((2.19S)^{3/2} + 0.5)^{-4} \quad (4.65)$$

iii. *Flap trailing edge noise:* The overall airframe noise increases with the extension of flaps due to the turbulent flow encountering the flap surface. The noise increases with increase in the flap deflection angle and its directivity according to Fink's models is assumed to be aligned with the lift dipole of the deflected flap. Fink also assumes that single and double slotted flaps have one value of acoustic power weightage (constant K from Eq. 4.58) and triple slotted flaps have another slightly higher weightage, accounting higher flap noise due to higher number of slots. These flap noise acoustic power equations are given by Eq. 4.66 and 4.67 for single/double slotted flaps and triple slotted flaps respectively.

$$\Pi_{f,1-2\text{slots}} = (2.787 \cdot 10^{-4})(M_\infty)^6 \frac{A_f}{b_w^2} \sin^2 \delta_f \rho_\infty c_\infty^3 b_w^2 \quad (4.66)$$

$$\Pi_{f,3\text{ slots}} = (3.509 \cdot 10^{-4})(M_\infty)^6 \frac{A_f}{b_w^2} \sin^2 \delta_f \rho_\infty c_\infty^3 b_w^2 \quad (4.67)$$

It can be noticed that the acoustic power radiated due to flap noise depends on the flap area A_f and on the flap deflection angle δ_f . The M_∞^6 term indicates a dipole noise source for the flap and not a noise source between a dipole and a monopole as is the case for wing and slat trailing edge noise. This is due to the fact that the flap, being completely immersed in turbulent flow from the onset, can be treated as a compact body, unlike the trailing edges, which are semi-compact bodies with turbulent flow passing only over their trailing edges. The directivity function D for flap noise is given by:

$$D_f(\theta, \psi) = 3(\sin \delta_f \cos \theta + \cos \delta_f \sin \theta \cos \psi)^2 \quad (4.68)$$

The spectral function for flap noise has been determined empirically by Fink for single or double slotted flaps and for triple slotted flaps separately. These depend on the flap Strouhal number, which is computed using Eq. 4.57 with the characteristic dimension for flap noise assumed to be the flap area divided by the flap span (A_f/b_f). The spectral functions can be found in [83], [88].

iv. *Landing gear noise:* Landing gear noise generation mechanisms are usually very complex and are dependent on the landing gear's specific geometry and configuration. Fink makes the simplifying assumption that there are two primary noise sources on the landing gear – the strut of the gear and the wheel(s). This assumption was made by Fink based on experimental data from the flyover measurements of several aircraft. The various interaction effects of the wheels and strut with each other as well as with the wing or fuselage are hereby neglected, being gear geometry specific. The model of Fink differentiates between gears with one or two wheels and gears with four or more wheels.

For landing gears with one or two wheels, typically seen on a Nose Gear (NG), the acoustic power function for wheel noise is given by Eq. 4.69, and for landing gears with four or more wheels, seen commonly on a Main Gear (MG), the acoustic power for wheel noise is given by Eq. 4.70:

$$\Pi_{wheel,NG} = (4.349 \cdot 10^{-4})(M_\infty)^6 n \left(\frac{d_{NG}}{b_w} \right)^2 \rho_\infty c_\infty^3 b_w^2 \quad (4.69)$$

$$\Pi_{wheel,MG} = (3.414 \cdot 10^{-4})(M_\infty)^6 n \left(\frac{d_{MG}}{b_w} \right)^2 \rho_\infty c_\infty^3 b_w^2 \quad (4.70)$$

where d is the wheel diameter and n is the number of wheels per landing gear. For strut noise originating from struts of both main and nose gears is given by Eq. 4.71:

$$\Pi_{strut} = (2.753 \cdot 10^{-4})(M_\infty)^6 \left(\frac{d}{b_w} \right)^2 \left(\frac{l}{d} \right) \rho_\infty c_\infty^3 b_w^2 \quad (4.71)$$

where d is again the wheel diameter and l is the strut length. The directivity functions are also the same for both one or two wheel gears and for four wheel gears, provided by Eq. 4.72 for wheel noise and by Eq. 4.73 for strut noise.

$$D_{wheel}(\theta, \psi) = \frac{3}{2} \sin^2 \theta \quad (4.72)$$

$$D_{strut}(\theta, \psi) = 3 \sin^2 \theta \sin^2 \psi \quad (4.73)$$

The wheel and strut spectrum functions are again empirically determined functions and are different for nose gears and main gears. They depend on the landing gear Strouhal number determined using Eq. 4.57, using the wheel diameter d as the characteristic dimension L .

The airframe noise components described above can be combined to compute the overall airframe noise far-field mean-square acoustic pressure using Eq. 4.56, which can be converted to SPL using Eq. 4.74.

$$SPL_{airframe} = 10 \log_{10} \frac{\langle p_{airframe}^2 \rangle}{p_{ref}^2} \quad (4.74)$$

It can be observed that airframe noise calculation according to Fink's model requires the input of a large number of aircraft geometry parameters. These parameters, as well as the operational parameters are summarized in Table 4.5.

Table 4.5: Summary of geometric and operational parameters required for parametric airframe noise prediction

Airframe Noise Inputs	
Parameter Name	Symbol
Geometric Parameters	
Wing span	b_w
Wing area	A_w
Flap span	b_f
Flap area	A_f
Horizontal tail span	b_h
Horizontal tail area	A_h

Vertical tail span	b_v
Vertical tail area	A_v
Main gear wheel diameter	d_{MG}
Nose gear wheel diameter	d_{NG}
Main gear strut length	l_{MG}
Nose gear strut length	l_{NG}
Operational Parameters	
Flap setting	-
Flap deflection angle	δ_f
Slat setting	-
Landing gear setting	-

Although Fink's airframe noise model is a suitable model for parametric prediction of noise radiated from the aircraft geometry, it predicts the primary airframe noise sources in a simplified yet efficient manner. There are however other important airframe noise sources such as those from the flap side edge, from spoilers and also from cavities and fuel vents in the wing that produce additional noise, but are not incorporated in Fink's model. A few other semi-empirical airframe noise models such as PROFAN of the German Aerospace Center (DLR) [96] are capable of predicting flap side edge and spoiler noise but not the parasitic noise from cavities (the cavity noise is often tonal in nature, in contrast to the broadband nature of all other airframe sources). The other models are however organization specific and are either not public, or are made publically available with limited functionalities. Since Fink's model is publically available and provides the control of several relevant aircraft geometry parameters for airframe noise studies, it has been the preferred choice for the current study. Although it simplifies the airframe noise generation theory to a great deal, it is still a state of the art model and predicts airframe noise of most current aircraft with correct trends and sufficient accuracy for conceptual design and assessment purposes. Fig. 4.9 shows two sample spectra for airframe noise at the source produced by a short range commercial aircraft (A320-200 comparable) for departure and approach flight settings, at a polar angle of 40° and azimuthal angle of 0° . It can be noticed that the overall airframe noise in this case is about 10 dB higher during approach than during departure, which is typical for commercial aircraft. Combined with the fact that the engine during approach is at flight idle setting, this makes airframe noise during approach a very significant noise source.

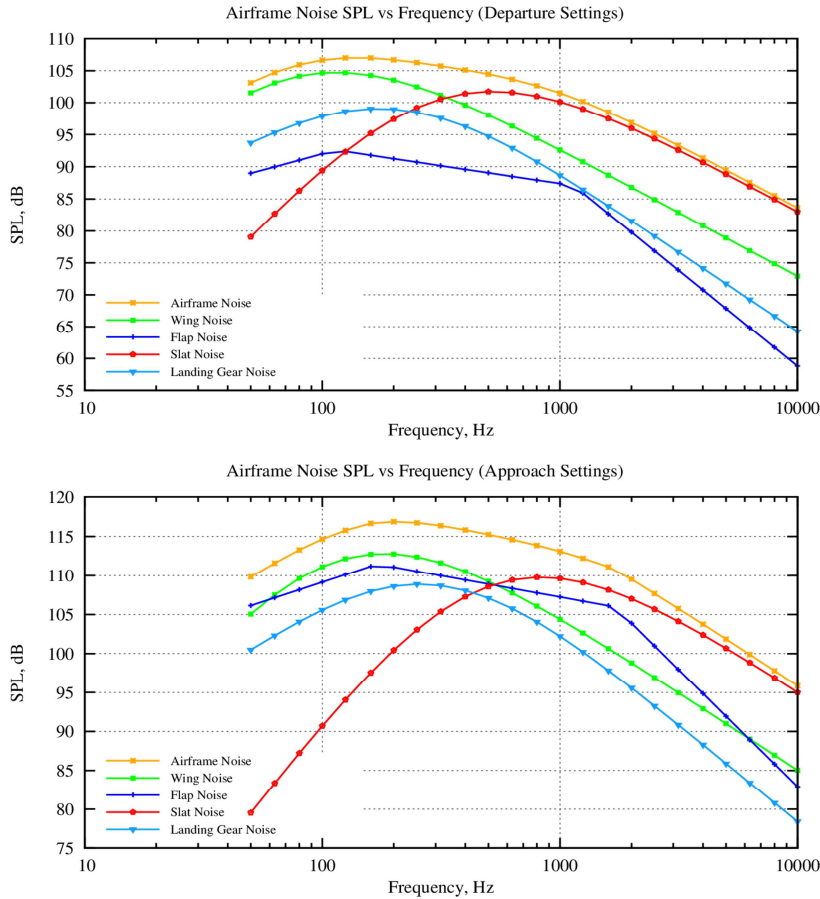


Figure 4.10: Sample spectra of airframe source noise for departure settings (top) and approach settings (bottom) at $\theta = 40^\circ$ and $\psi = 0^\circ$

4.2.7 Noise validation on the ground

Simulated and measured aircraft noise spectra were then compared to perform a validation of the implemented models. Both departure and approach flight setting flyovers of the DC-10 aircraft flying with the PW JT9D-59A turbofan engine, as published by Kapper et al. [99], were used for the comparison. In order to see how well the individual simulated airframe noise spectra presented here compare with those simulated by Kapper et al. using NASA's ANOPP, the reader is referred to [99]. The spectral comparison here focuses on the comparison of simulated spectra of aircraft noise as implemented for this dissertation with aircraft flyover measurements on the ground. The propagated noise spectra, which have undergone the various atmospheric and ground reflection and attenuation effects can be seen in Fig. 4.11 and Fig. 4.12.

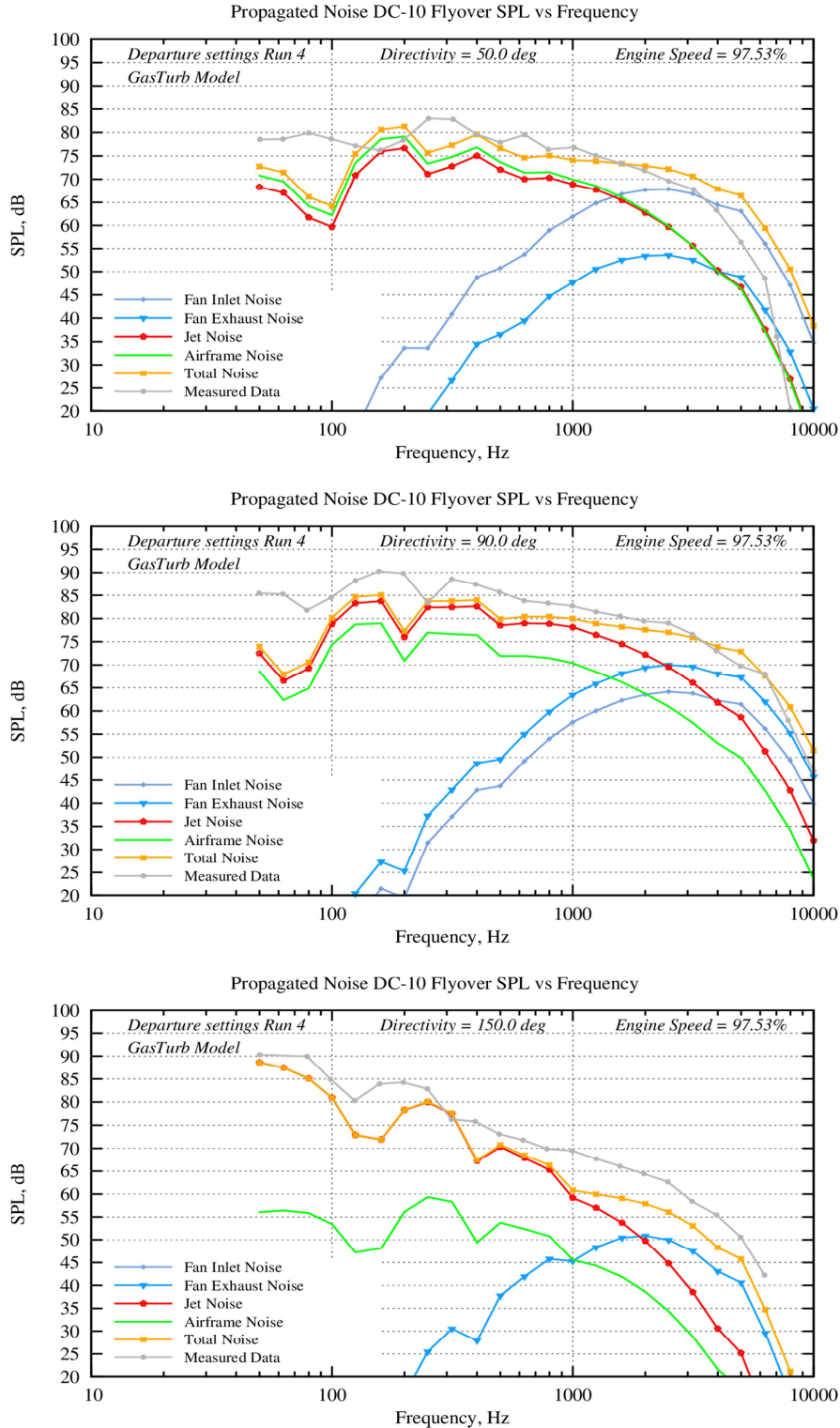


Figure 4.11: Comparison of simulated spectra on ground with DC-10 measured spectra from [99] for departure settings – $\theta = 50^\circ$ (top); $\theta = 90^\circ$ (middle); $\theta = 150^\circ$ (bottom)

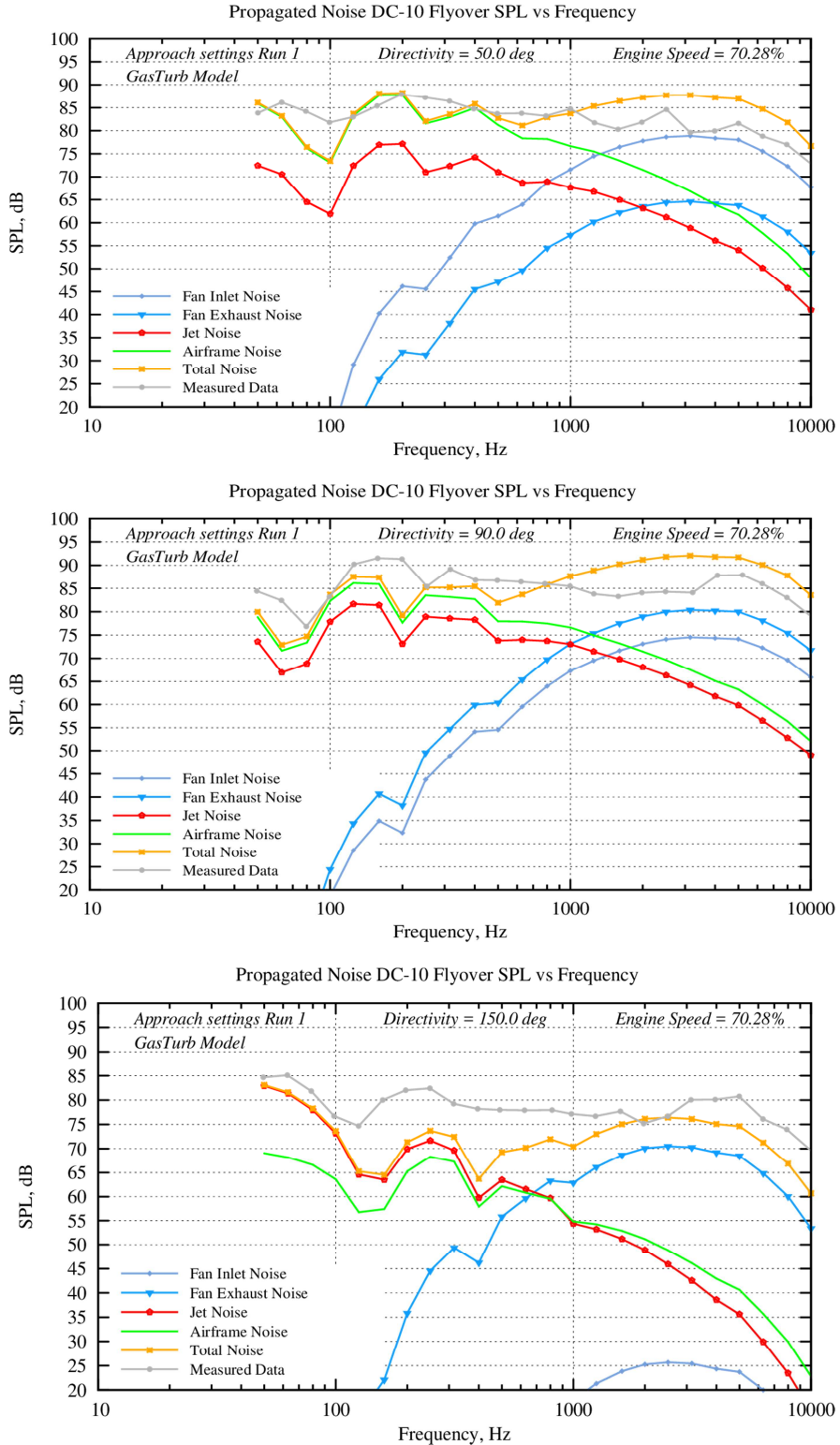


Figure 4.12: Comparison of simulated spectra on ground with DC-10 measured spectra from [99] for approach settings – $\theta = 50^\circ$ (top); $\theta = 90^\circ$ (middle); $\theta = 150^\circ$ (bottom)

The peaks and troughs seen in the spectra on the ground, which are not seen at the source, are characteristic of reflection of acoustic waves by the ground surface. This propagation effect will be explained in more detail in the next chapter. Furthermore, it can be observed in the spectra on the ground that the magnitude of the SPL values is much lower than that observed at the source, due to the propagation effects of geometric spreading and atmospheric absorption, whereby the acoustic energy is absorbed by the atmosphere as the sound waves travel from the aircraft to the observer on the ground. It can be seen that for most polar angles for both departure and approach settings, a good to reasonable match to the overall measured aircraft noise spectra is obtained (though the accuracy of the models is clearly limited). The engine cycle for the JT9D-59A engine has been modeled using the software Gasturb to obtain all the thermodynamic inputs for the source models. The DC-10 airframe geometry parameters have been obtained from [99]. The DC-10 aircraft was flying at an altitude of 363.1 m with an airspeed of 100.53 m/s for the departure setting flyover and at an altitude of 119.3 m and airspeed of 84.22 m/s for the approach setting flyover. The measurement microphone was located at a height of 1.2 m above the ground.

With regards to spectral composition of aircraft noise, it is useful to note that for the departure setting in Fig. 4.11 that in the forward directions, airframe noise is often of comparable magnitude to jet noise whereas jet noise is dominant by a large margin in the aft directions during departure. During approach, airframe noise remains the dominant broadband noise component in all polar directions, being slightly louder than jet noise even in aft directions. This is due to the aircraft flying at low engine thrust settings during approach. It can also be noted for both departure and approach settings, fan inlet noise is the dominant tonal component in the forward arc whereas fan exhaust noise begins to dominate from $\theta = 90^\circ$ onwards. This spectral composition is typical for current commercial aircraft flying with turbofan engines, and helps in understanding many of the effects on the sound quality of aircraft noise described in Chapter 6 to Chapter 8.

As the spectra published by Kapper et al. were for the now retired DC-10 aircraft, an additional validation of the noise simulated using the models implemented for this dissertation's research work was performed with the more modern Boeing 747 aircraft flying with the CF6-80C2 engine. For this, simulated SPL values in the dBA metric were compared with measured dBA values at a chosen noise measurement point near Schiphol airport Amsterdam. These results are not presented in this dissertation due to the flight paths being a property of Schiphol airport and the Dutch Aerospace Laboratory NLR, but it can be said that comparable differences to those presented in [65] were observed (the results can be made available by the author upon request). These differences are of a similar magnitude to the differences observed in the comparison of the DC-10 spectra in Fig. 4.11 and Fig. 4.12.

The atmospheric propagation and ground effects that affect aircraft noise reaching the observer on the ground, which were only briefly mentioned towards the end of this chapter, will be explained in more detail in the next chapter.

5 Development of an aircraft noise prediction and assessment environment

The source noise models described in the previous chapter were selected for their applicability to aircraft design and assessment at both aircraft and system level. The fact that the models are parametric allows the possibility to optimize current aircraft designs for noise as well as annoyance impact, by firstly seeing what effect their parametric variations have on the generated noise, and then selecting a combination of parameters that minimizes the noise impact. Crucial for optimizing aircraft designs for *annoyance* is the use of appropriate metrics, which actually correspond to the annoyance experienced by residents. The implementation of suitable annoyance metrics shall be described in the next chapter. The current chapter focuses on the development of an environment for predicting and assessing aircraft noise of current aircraft using the aforementioned source noise models for both certification and community noise impact. Furthermore, the chapter also describes the integration of this environment into an aircraft design and optimization chain with which the aircraft designs can be assessed and optimized for noise impact. The noise assessment will be shown in the current chapter in terms of conventional metrics that are currently used in the aerospace industry, as described in Chapter 2.

It can be understood that in order to design aircraft and assess them for noise impact, the noise prediction environment has to be either fully integrated or fully compatible with the aircraft design environment. The aircraft design environment has to provide all the relevant noise inputs at a system or component level and the noise prediction environment has to be capable of providing the noise impact in suitable metrics as feedback to the aircraft design environment for optimization purposes. The aircraft design software therefore has to be capable of providing all the aircraft geometry parameters as well as all operational parameters over complete departure and approach flight paths. The aircraft design environment used for the work in this dissertation is ILR's Multidisciplinary Integrated Conceptual Aircraft Design and Optimization environment (MICADO) [100], which has been developed over past several years for designing and optimizing commercial aircraft for various target criteria such as block fuel or costs. The MICADO environment was complemented over the course of the work for this dissertation with an aircraft noise prediction and assessment environment - ILR's Noise Simulation and Assessment Module (INSTANT) [101], [102], [103]. This chapter will describe briefly the MICADO aircraft design environment and the various system level design tools it comprises in Section 5.1. The subsequent sections will focus on the aircraft noise prediction environment INSTANT and how it can be used to assess aircraft for both noise certification as well as community noise impact.

5.1 The aircraft design environment MICADO

The MICADO environment was developed at the ILR of RWTH Aachen University in order to produce an aircraft design software that could design and assess aircraft with a minimum of user input in an automated way, based on certain typical top-level requirements such as the design range, payload, cruise Mach number and altitude for instance. An important characteristic of the MICADO environment is the capability to perform large scale parameter studies and optimizations over large parameter spaces, with relatively low computational costs. This allows not just top-level aircraft requirements to be varied and

optimized for assessment criteria such as block fuel or costs, but also system or component level parameter variations and optimizations. In this regard, parameters such as the wing sweep, aspect ratio or the available engine thrust can for instance be varied and the impact of each variation on target functions such as fuel consumption, weight and costs can be assessed.

The overall MICADO environment consists of a series of modules or sub-programs with a modular build up, which are linked to each other via a central parametrized and structured file in Extensible Markup Language (XML) format. Each module is intended to perform a specific aircraft design or analysis task such as estimate the aerodynamics of the aircraft, its performance, estimate its system level weight and overall weight and compute its costs and aircraft emissions. Based on the top-level aircraft requirements and certain design specifications (such as number of engines, position of wing), the aircraft geometry components such as the wing, fuselage, landing gear and stabilizers are sized yielding a preliminary first estimate design. This is followed by an analysis of the aircraft aerodynamics, weights, block fuel and performance among others, for a specified typical flight profile or a ‘mission’ of the aircraft. The process is iterated, going through all sizing and analysis modules till a convergence of key representative aircraft design parameters such as the Maximum Takeoff Weight (MTOW) and Operating Weight Empty (OWE) is achieved. This converged aircraft design is then assessed against selected evaluation criteria and used for further analyses and studies. A specific MICADO module named the *parameter study manager* allows parameter variation studies as well as optimizations to be carried out. For system level parametric studies, the module executes a specific design or analysis module for each required variation of the parameter of interest, and for aircraft level parametric studies, the module executes the entire convergence loop consisting of all the aircraft design and analysis modules. As such, this tool is a very powerful tool for quantifying sensitivities of specific design parameters on the target functions of interest. The parameter study manager has been used in this dissertation for quantifying the sensitivities of noise relevant aircraft and engine parameters on the noise and annoyance impact on the ground, which are shown in Chapter 7.

5.1.1 Aircraft design and assessment methodology

Fig. 5.1 shows the aircraft design and assessment methodology of the MICADO environment and shows how the various modules are structured such that a converged aircraft design is produced after input of the Top-Level Aircraft Requirements (TLARs) and design specifications. The TLARs include, besides the parameters mentioned earlier, the aircraft takeoff field length, time to climb, landing distance required and approach speed among other parameters that specify the aircraft’s flight envelope. The TLARs have to be provided for a design mission to design the aircraft and also for a ‘study mission’ for off-design assessment. The design specifications that need to be specified also include the type of engine being used (propeller or jet), the empennage configuration (conventional or, T-tail) and gear configuration (on wing or fuselage) among others.

After providing the TLARs and design specifications, the automated design process is begun with the initial sizing of the aircraft, where the overall aircraft design parameters - the thrust to weight ratio, T/W and wing loading W/S are estimated based on the takeoff, climb, cruise and landing requirements. During initial sizing also a first value of aircraft MTOW is calculated, for which the aircraft geometry is preliminarily sized and this value is compared with the reference MTOW value at the end of one cycle of the convergence loop to check for design convergence. Parallel to the initial sizing of the aircraft, the

fuselage design module sizes the fuselage and determines the fuselage cross-section, cabin and cargo layout (based on the design specifications). The initial sizing and fuselage design modules are run only once, with the fuselage geometry and layout not being changed iteratively. The iterative design process then begins with the design of the main aircraft components. As can be seen in Fig. 5.1, these include firstly the sizing of the wing, including its planform, 2D and 3D geometry as well as sizing of the high-lift devices (trailing edge flaps and leading edge slats) on the wing. The horizontal and vertical stabilizers are then sized by the empennage sizing module followed by sizing and placement of the engines as well as of the landing gear. The engine sizing module also creates engine performance decks for the selected engine, which are several engine cycle parameters such as thrust, mass flow, station temperatures and pressures provided as functions of LP spool speed, Mach number and altitude. The aircraft component geometries as determined by each of the respective modules, are written in the central aircraft XML file for data keeping and also so that other analysis tools can readily access the parameter values they require as inputs. It can be seen that the MICADO design loop also allows the option of performing more detailed component design and analysis. This includes designing the aircraft system architecture by estimating the system masses and power consumption over the mission for the electrical, hydraulic, pneumatic systems for instance, or also a stability and control analysis which sizes the aircraft control surfaces according to certification requirements.

Once the sizing of the major aircraft components has been completed, an analysis of the aircraft performance is carried out. This is done firstly via the mass estimation module, which estimates the system and component masses and with it the aircraft OWE and the center of gravity locations. Secondly, aerodynamic analysis via the polar module is performed, which determines the drag polars for all phases of the mission. Thirdly, the block fuel and mission fuel for the standard design mission of the aircraft are calculated using the thrust values from engine performance decks, the drag of the aircraft from the polars and the OWE from the mass estimation module. The sum of the calculated block fuel, OWE and the design payload from the TLARs results in a new value of the MTOW, which is then fed back to the start of the sizing and analysis tools and the entire process is iterated via the so-called convergence loop. A check for convergence is then made for the values of the MTOW, OWE, block fuel and center of gravity locations. Once convergence of the designed aircraft has been achieved, a check is made with regards to the TLARs and if a certain requirement has not been met, then this is recorded in the central aircraft XML file. The fully converged aircraft design can then be assessed in detail for various evaluation criteria such as block fuel over specific ‘study’ missions, aircraft operating and lifecycle costs, pollutant emissions as well as noise impact, which has been the contribution of the research work in this dissertation.

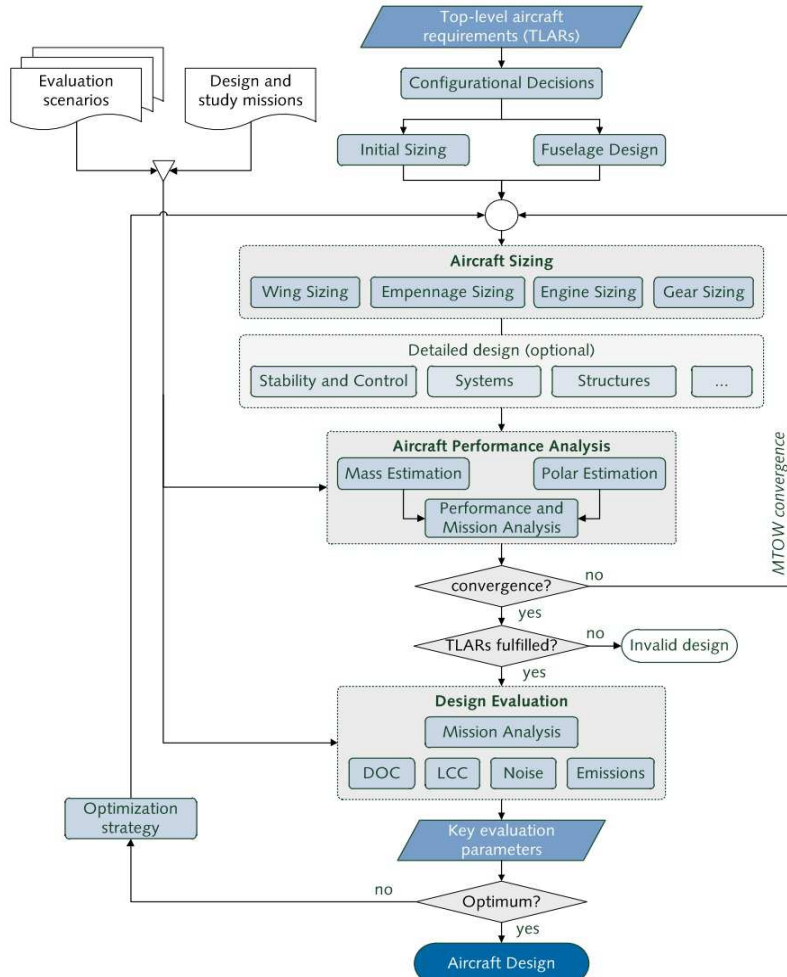


Figure 5.1: Aircraft design and assessment methodology of the MICADO environment [100]

The MICADO environment, as was mentioned earlier, also provides the possibility to perform design parameter variations for capturing design sensitivities and to optimize aircraft for the above mentioned criteria by performing Multidisciplinary Design Optimizations (MDO) for various target functions. Each parametric variation or each optimization evaluation point within the MICADO environment is a fully converged aircraft design. In the next sub-section, the MICADO aircraft design and analysis modules which are of relevance for the current dissertation are briefly described.

5.1.2 Aircraft design and analysis modules

The MICADO modules which are of relevance for this dissertation's research work are the aerodynamic analysis module, engine sizing module, performance and mission analysis module and the parameter study manager. These modules are used to not only compute the departure and approach flight paths for noise source calculation but also provide inputs for the various airframe and engine noise source models. Since engine noise is a major aircraft noise component, modeling of the engine thermodynamic cycle such that the engine thermodynamics is correctly represented is a crucial part of the noise prediction

process. As such, the methodology followed for modeling the engines using Gasturb is given special attention.

i. Aerodynamic analysis module:

The aerodynamic module of MICADO uses a mixture of semi-empirical and analytical models to predict flight polars of arbitrary aircraft for all flight phases i.e. departure, climb, cruise, approach and landing. These flight polars span the subsonic and transonic flight regimes and are used to compute the total drag of the aircraft as the sum of viscous drag, induced drag and wave drag. The module is linked to the potential flow theory based DLR tool LIFTING_Line [104] via a wrapper and uses LIFTING_LINE to calculate the aircraft lift, induced drag and the pitching moment. Since the tool is based on potential flow theory, it neglects the effects of flow separation and other non-linear effects that may occur. The maximum lift coefficient of the aircraft is computed semi-empirically using the methodology detailed by known aircraft design references such as Roskam [105] and Raymer [106] and the calculated value is corrected for compressibility using the Prandtl-Glauert correction.

For the overall drag coefficient calculation, the viscous drag coefficient is calculated for each relevant aircraft component from its skin friction coefficient and form factor described by Raymer [106]. The skin friction coefficient is estimated using a flat plate-turbulent flow approximation and makes use of the local Reynold's number for each aircraft component such as the wing, horizontal and vertical stabilizers, fuselage and nacelle. After taking interference effects for each component into account, the overall viscous drag is obtained as the sum of the viscous drag of each of the mentioned components. The remaining drag component, namely wave drag, is computed using Lock's fourth power approximation [107] of the difference between the freestream Mach number and the critical Mach number. The critical Mach number is obtained using the drag divergence Mach number, which is calculated using Korn's equation [108], extended with simple sweep theory. A more detailed description of the MICADO aerodynamics module can be found in [109].

ii. Engine performance module:

Most engine performance modeling tools used for aircraft design and assessment purposes are based on a full thermodynamic engine cycle analysis and make use of various software that can model the engine performance for all phases of flight. As mentioned earlier, the gas turbine cycle analysis program Gasturb has been used in this dissertation work to model the engine cycle. The process for modeling engines used on current commercial aircraft using Gasturb and the integration of the cycle data in the engine performance module of MICADO is outlined in the following steps.

1. Engine cycle modeling at design point:

Engines typically used by current commercial aircraft are mid to high bypass ratio turbofan engines and engines used in this dissertation's research work are the V2527-A5 engine, CF6-80C2 engine and the GE90-85B engine. These engines have been modeled using Gasturb as geared unmixed turbofan engine models (cf. Fig. 5.2) and the design point has been chosen to be the start of cruise phase (or equivalently end of climb phase). The reason for this choice of design point is mainly the correct estimation of the engine Thrust Specific Fuel Consumption (TSFC) for the cruise phase, which is a very critical parameter for aircraft design purposes. It is known from current as well as other research work [110] that engines modeled for the takeoff thrust setting (for which also most reference data is publically available) provide more reliable thermodynamic cycle values for departure and climb phases but offer less accurate prediction of thermodynamic state variables for the cruise and approach phases. Engines modeled for end of climb phase, where the thrust setting is here taken to 87.5% instead of 100% at takeoff, provide a better compromise for modeling all phases of flight. In order to model the engine at the design point (altitude 10-11000 m, Mach number 0.76-0.85 depending on the engine), pertinent engine design parameters have to be provided as inputs at the design point. These include among others - the bypass ratio, inner and outer fan pressure ratios, LP ad HP compressor pressure ratios, burner (combustor) exit temperature, fan mass flow and compressor and turbine polytropic efficiencies. The inputs should lie within realistic ranges for each design parameter and the values produced as output such as the cruise thrust and TSFC are checked whether they lie close to reference values or not. An iterative adjustment of the engine design parameters is usually necessary before the design point outputs match the reference values at design point.

2. Off-design point cycle check:

Since most relevant engine performance values are provided (very limitedly) for the takeoff thrust setting, the modeled engine's outputs are tested for the off-design case of takeoff thrust setting at ground level altitude and Mach number of zero. The outputs that are compared with values from known public references such as Jane's Aero-Engines [111] or [112] are, among others – the produced thrust, TSFC, fan mass flow, bypass ratio, overall pressure ratio, turbine entry temperature as well as the jet velocities and areas, which are of high importance for realistic jet noise calculation. The LP spool speed, $N1$ which corresponds to the maximum rated thrust is obtained from the specific engine's type certificate document and determines which spool speed value actually corresponds to takeoff thrust. Most engines in general can produce more thrust than their rated value (i.e. 101 - 115% $N1$) and as such a limiter on the LP spool speed to 100% has to be set in order to compare the off-design values with the reference catalog values. The off-design values will in general deviate significantly from the reference off-design values for the first run and the entire process (design point inputs, off-design checks) as such has to be iteratively repeated till a good match with all known reference values is obtained.

3. Comparison with ICAO emissions databank values:

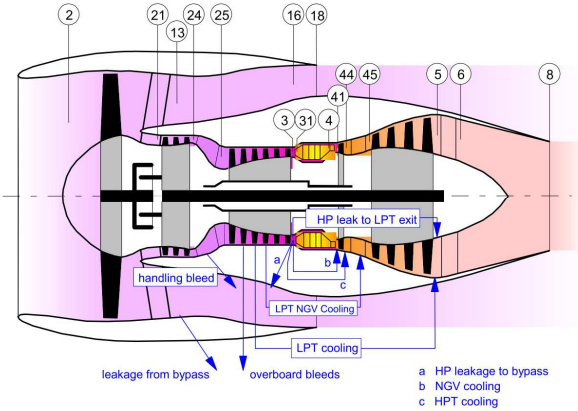


Figure 5.2: Geared turbofan unmixed model and thermodynamic station numbers as used in Gasturb [92]

Once the off-design cycle values are seen to match the reference values to a sufficient extent, another check is carried out to see how the engine performs for a series of thrust settings. For this purpose, the ICAO engine emissions databank for the specific engine being designed is used, which is made public by the respective aviation authority - FAA in the US, European Aviation Safety Agency (EASA) in Europe for instance. These documents contain actually measured data for the engine for sea-level static conditions and correlate the thrust setting for takeoff, climb out, approach and ground idle (7% of rated thrust value) conditions with the measured fuel flow in kg/s and the Emission Index (EI) in g/kg for each pollutant such as CO, NO_x and Unburned Hydrocarbon (UHC). Of interest for the engine comparison is the fuel flow value for each thrust setting. An ‘operating line’ is run in Gasturb, where the HP spool speed of the engine is varied in steps from minimum to maximum spool speed. As outputs, the calculated thrust and fuel flow are compared with the values contained in the engine emissions databank.

4. Creation of engine performance decks:

The earlier mentioned engine performance decks can then be created and exported from Gasturb for each relevant engine performance parameter such as the thrust, fuel flow, station mass flows, temperatures, pressures and jet velocities. For this purpose a parametric study is performed in Gasturb, where the LP spool speed is varied in steps of 5% from flight idle value (30-40% of rated thrust value) to 110%, and for each spool speed value the parameters of interest are calculated for altitude values of 0 m to 14000 m and Mach numbers of 0 to 0.95. In this way, required engine cycle values for performance and noise are made available for all thrust settings, flight altitudes and Mach numbers that may be of importance during computation over the entire aircraft mission. It is clear that commercial aircraft would not fly at Mach 0.9 at low altitudes but the goal of the engine decks is to attempt to cover the entire flight envelope of an aircraft, including flight regimes which in general may never be encountered. The simulated values from Gasturb are exported as Comma Separated Value (CSV) files, and these CSV files are then referred to as the ‘decks’, to be used by other aircraft design and analysis tools.

The operational limits of the engine such as the Exhaust Gas Temperature (EGT), fuel-to-air ratio, maximum and minimum LP and HP spool speeds and maximum allowable shaft power and bleed air offtakes are also accounted for by MICADO’s engine performance module. The module therefore allows the modeling of the effects of altitude, flight Mach number and flight phase dependent power offtakes on the engine performance and efficiency, while taking into account the engine’s operational limits. As is typical during conceptual and preliminary design, it is not possible to model a new exact engine for each aircraft design variation and the engine performance decks are therefore scaled based on the required takeoff thrust, obtained from the aircraft T/W ratio and MTOW value.

The three turbofan engines mentioned earlier (V2527-A5, CF6-80C2 and GE90-85B) are appropriately used and scaled depending on whether a short-range, mid-range or long-range aircraft is being designed. A scaling factor of 5-10% is seen to still offer a reasonable accuracy in performance and thermodynamic parameter values and known aircraft design references such as Torenbeek [113] suggest a scaling factor up to 20% as still providing sufficient accuracy for conceptual design purposes. Tables 5.1 and 5.2 show a comparison of key engine parameter values for the V2527-A5 and GE90-85B engines respectively, for Gasturb simulated and publically available reference values [111], [112]. The fan blade number and inlet diameter have been computed using the empirical engine geometry database, the empirical functions of which are provided in Appendix A. The accuracy of the modeled engines with regards to this dissertation

is to a large extent also representative of the accuracy of the engine noise modeled at the source, judging from the large number of thermodynamic parameters that are required for source noise calculation.

Table 5.1: Comparison of key Gasturb simulated and reference values for the V2527-A5 engine (TO represents takeoff thrust setting)

Parameter	Value - Simulated	Value – Reference	Deviation (%)
<i>Thrust Cruise</i> [kN]	19.79	25.6 (V2500 general)	-22.7
<i>SFC Cruise</i> [mg/Ns]	16.256	16.26 (V2500 general)	-0.025
<i>Thrust TO</i> [kN]	122.47	117.88	+3.89
<i>SFC TO</i> [mg/Ns]	10.026	10.206	-1.76
<i>BPR TO</i> [-]	4.565	4.75	-3.89
<i>FPR TO</i> [-]	1.8	1.7	+5.88
<i>OPR TO</i> [-]	32.37	27.4	+18.14
<i>Mass flow TO</i> [kg/s]	353.71	384	-7.88
<i>Fan blades</i> [-]	29	Not Available	-
<i>Fan inlet diameter</i> [m]	1.71	1.613	+6.01

Table 5.2: Comparison of key Gasturb simulated and reference values for the GE90-85B engine (TO represents takeoff thrust setting)

Parameter	Value - Simulated	Value – Reference	Deviation (%)
<i>Thrust Cruise</i> [kN]	58.31	77.85	-25.1
<i>SFC Cruise</i> [mg/Ns]	15.262	14.741	+3.53
<i>Thrust TO</i> [kN]	425.47	376.8	+12.92
<i>SFC TO</i> [mg/Ns]	8.264	9.18	-9.98
<i>BPR TO</i> [-]	8.06	8.4	-4.05
<i>FPR TO</i> [-]	1.698	1.65	+2.91
<i>OPR TO</i> [-]	41.95	39.3	+6.74
<i>Mass flow TO</i> [kg/s]	1377.56	1415	-2.65
<i>Fan blades</i> [-]	22	22	0
<i>Fan inlet diameter</i> [m]	3.05	3.12	-2.24

iii. Flight performance and mission analysis module:

The flight performance and mission analysis module of MICADO simulates the entire mission of the aircraft and calculates the fuel consumed over the mission. The module does this by regarding the aircraft as a point mass and analyzing Newton's laws of motion for small incremental discrete steps over the flight path. This is done by equating the net power produced by the engines with the sum of the rate of change of the aircraft's potential and kinetic energy according to Eq. 5.1 [114]:

$$(T - D)V = m_{ac} g \frac{dh}{dt} + m_{ac} V \frac{dV}{dt} \quad (5.1)$$

In Eq. 5.1, the left hand side represents the net power from the engines and right hand side represents the sum of the aircraft's potential and kinetic energy time rate of change. This relation can be rewritten in the form of Eq. 5.2, as has also been described by Oates [115].

$$\frac{dh}{dt} \left(1 + \frac{V}{g} \left(\frac{dV}{dh} \right) \right) = \frac{(T-D)V}{m_{ac} g} \quad (5.2)$$

Eq. 5.2 represents an initial value problem and requires firstly specific performance conditions to be set for each mission segment. These include parameter values such as the thrust setting, aerodynamic configuration, end altitude or flight level, required rate of climb and end Calibrated Air Speed (CAS) or Mach number for each flight segment. Since the aircraft thrust, drag and weight are not constant over the flight and vary with flight speed, altitude and time, Eq. 5.2 has to be solved iteratively for each mission increment. The primary inputs required for the simulation of each mission segment are the thrust available obtained from the engine decks, the aircraft drag obtained from the flight polars as function of aircraft Mach number and altitude, and the aircraft weight at each mission increment. A more detailed description of the mission analysis module of MICADO can be found in [114]. Flight paths for departure from brake release up to an altitude of 3000 m and for approach from an altitude of 3000 m to touch down on the runway are of relevance for ground noise impact and are extracted from the overall simulated mission flight path (taxiing noise is thus hereby neglected). As was mentioned earlier, the departure and approach flight paths thus produced by the flight performance and mission analysis module contain all the necessary operational and thermodynamic inputs for each mission step, required by the source noise models for source noise calculation.

iv. Parameter study manager:

The parameter study manager module of MICADO allows performing extensive parameter variation studies as well as optimizations both for the entire aircraft by executing the entire convergence loop, or also for individual components by executing only individual modules. In principle, any parameter present in the central aircraft XML file can be chosen as a free variable to be varied or also as an output to be followed during the parametric variations or optimizations. For parameter variation studies, the input parameter x_i which is to be varied in order to analyze its sensitivity on the output parameter y_i , is read from the aircraft XML file, the respective module or convergence loop is executed once for each variation, and the output y_i is then written to the aircraft XML file. As an example, Fig. 5.3 shows the parametric variation of two input parameters - the aircraft T/W ratio and wing loading W/S of a short-range aircraft and its effect on the fuel consumption by taking the block fuel as an output over a short-range study mission. Both the T/W and the W/S are hereby varied over discrete steps around the reference value for each input parameter. By looking at the impact on block fuel due to variation of both parameters, an optimum combination of the T/W and W/S for the short-range aircraft can be found. Another example can be taken to be the optimization of the same aircraft for minimizing the community noise impacted area on the ground in one of the noise metrics such as dBA or EPNL.

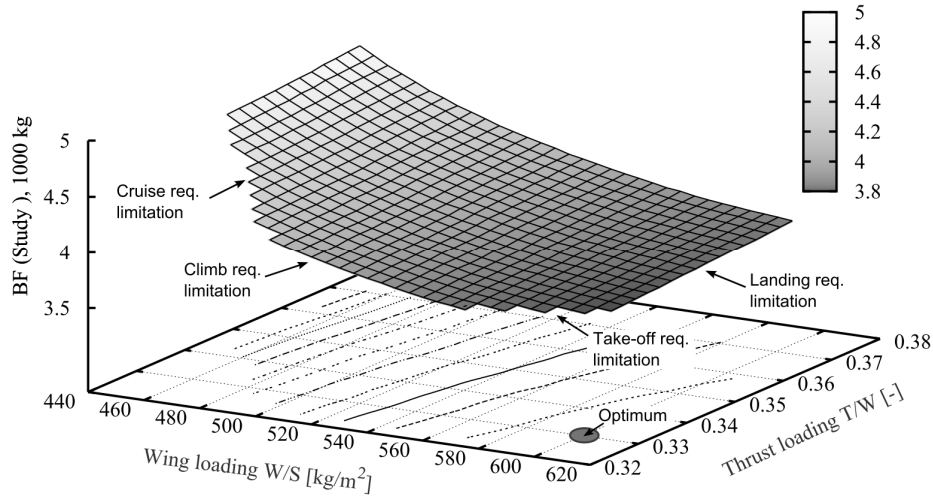


Figure 5.3: Parametric variation of T/W and W/S to analyze impact on block fuel over a study mission [100]

Fig. 5.3 also shows that the parameter study manager takes into account boundary conditions while performing the parameter variations and optimizations, which in this case were the takeoff field length, climb performance, cruise performance and the landing field length requirement. As was mentioned earlier, each evaluation point in Fig. 5.3 is a fully converged aircraft design.

The main difference between performing parameter variation studies and optimizations using the parameter study manager is the input parameter value or a combination of input parameter values is provided by the optimization algorithm instead of being read in discrete steps provided by the user. The MICADO toolchain involves a number of individual modules, each of which require their own inputs, use their own individual models and write their individual outputs. As such, there is no direct analytical function that connects the produced outputs with the input parameters that result in the required optimization. No derivative based optimization schemes can therefore be applied to the MICADO environment. For such applications, a ‘blackbox’ optimization is required and a well-known open-source blackbox optimization software that has been applied for aircraft design related MDO purposes [116] is the Nonsmooth Optimization by Mesh Adaptive Direct Search (NOMAD) software. The NOMAD software has been incorporated in the parameter study manager of MICADO and has been used to perform several parametric design studies and optimizations [100], [117].

Both the parameter variation studies as well as optimizations can be run parallelized on multiple processors by the parameter study manager, which reduces computational times considerably while finding global optima. Although bi-objective optimizations are also possible using the parameter study manager, only single objective optimizations have been employed in this dissertation. An explanation of the MICADO aircraft design approach, as well as some knowledge of the tools and models it uses in order to design current commercial aircraft presented in this section was necessary to give an idea of how the aircraft design and optimization process has been carried out in this dissertation. It was also necessary in order to understand how the inputs to the source noise models in the form of aircraft geometry and operational parameters over complete flight paths have been generated for the research work in this

dissertation. The next section describes the aircraft noise prediction module INSTANT and how it connects with the MICADO environment in order to simulate the noise impact on the ground for each aircraft design, which can then be assessed both for noise level and annoyance, either for certification or for community noise impact.

5.2 The aircraft noise prediction and assessment environment INSTANT

The aircraft noise prediction and assessment environment INSTANT was developed over the course of the research work for this dissertation to model and assess the noise produced by commercial aircraft. The overall goal was to develop a noise simulation capability which would be suitable for multidisciplinary aircraft design using ILR's MICADO environment and also provide a capability of assessing the mission level noise impact of commercial aircraft. The capability was required to be sufficient for current aircraft flying on both standard and noise abatement flight procedures and also be able to be extended to future concepts such as CROR propulsion or alternate aircraft configurations that minimize the emitted source noise via shielding of the noise for instance. With these overall goals in mind, the ILR Noise Simulation and Assessment module (INSTANT) was developed over the past several years at the ILR of RWTH Aachen University and has been used for several applications such as aircraft noise certification of aircraft designs, community noise impact analysis of both standard and noise abatement flight procedures as well as application to VR applications such as auralization and 3D visualization of aircraft noise in airport vicinities.



Figure 5.4: VR simulation achieved for the interdisciplinary VATSS project

With regards to VR applications, INSTANT was used for the interdisciplinary Virtual Air Traffic System Simulation - VATSS project, which was mentioned briefly in Chapter 1, for source noise simulation as well as community noise impact visualization. The VATSS project had the goal of making an immersive, interactive virtual reality simulation of aircraft noise by making use of 3D visualization as well as auralization of aircraft noise to make it more easily communicable to residents living in airport vicinities and to other non-experts [18], [19], [118] (cf. Fig 5.4). For this purpose, INSTANT provided both source noise data at each 0.5 seconds of flight for conversion to a directional audio file format for auralization purposes, and also noise impact data on the ground in the form of time-varying noise contours in a 3D visualization format. The auralization and visualization were then performed by two other specialized RWTH Aachen University institutes – the Institute of Technical Acoustics (ITA) and the Virtual Reality Group (VRG), resulting in a complex immersive VR aircraft noise simulation.

The current goal of INSTANT is to be able to model and assess the noise of all commercial aircraft from business jets to long-range airliners using standard as well as alternate noise assessment methodologies. The modeling is currently capable of assessing the noise of turbofan and turbojet powered aircraft,

although an extension to future propulsion technology such as CROR engines has already been initiated at the ILR [119], [120]. Fig. 5.5 shows the aircraft noise prediction and assessment methodology of INSTANT, parts of which have already been explained in Chapter 4 via the parametric source noise models used by INSTANT to predict engine noise and airframe noise, and also in Section 5.1, which explained the aircraft and engine design process as well as how the aircraft flight paths are simulated. The complete procedure to predict and assess aircraft noise using INSTANT consists of the following five main steps:

- i. *Aircraft and engine design:* Performed using MICADO and Gasturb respectively, with the integration of the engine performance decks into the MICADO toolchain. The engine geometry parameters needed for noise calculation are obtained from the empirical database as functions of the engine SLST as described in Appendix A.
- ii. *Flight path calculation:* Generated using the mission analysis module for standard (or noise abatement, if needed) departure and approach flight paths, providing all the operational and thermodynamic inputs required for airframe and engine noise calculation. The airframe geometry data such as the wing, flap spans and areas are obtained from the geometry classes made using the aerodynamic analysis module of MICADO.

Several noise abatement flight paths such as the Continuous Descent Approach (CDA) with varying glideslope angles and departures with thrust cutback have been simulated using the mission analysis module and assessed using INSTANT in [101]. The CDA procedure with 4° glideslope for a short-range as well as a long-range aircraft has been shown in Appendix B, along with the corresponding noise and annoyance impact produced over the CDA procedure to give an impression of the community noise impact changes due to such noise abatement procedures. It can be mentioned here that the flight paths need not always be simulated using MICADO's mission analysis module in order to be assessed for noise using INSTANT and can also be in the form of measured flight data, for aircraft flyover data measured using microphones placed at chosen observer locations. The goal of using measured data is then not aircraft design but rather community noise impact analysis around selected airports.

- iii. *Source noise calculation:* The engine component source noise models of Heidmann for fan noise, Emmerling for combustor noise, Matta for turbine noise and Stone for jet noise are used to calculate the engine noise for each mission step of the flight path. The model of Fink is used to calculate the noise due to the airframe geometry and its individual components such as wing trailing edge, flap, slat and landing gear. Since the ANOPP based models were developed intending to predict far-field noise, the overall aircraft (i.e. engine plus airframe) is hereby regarded as a point source in order to perform the propagation steps that follow source noise calculation.

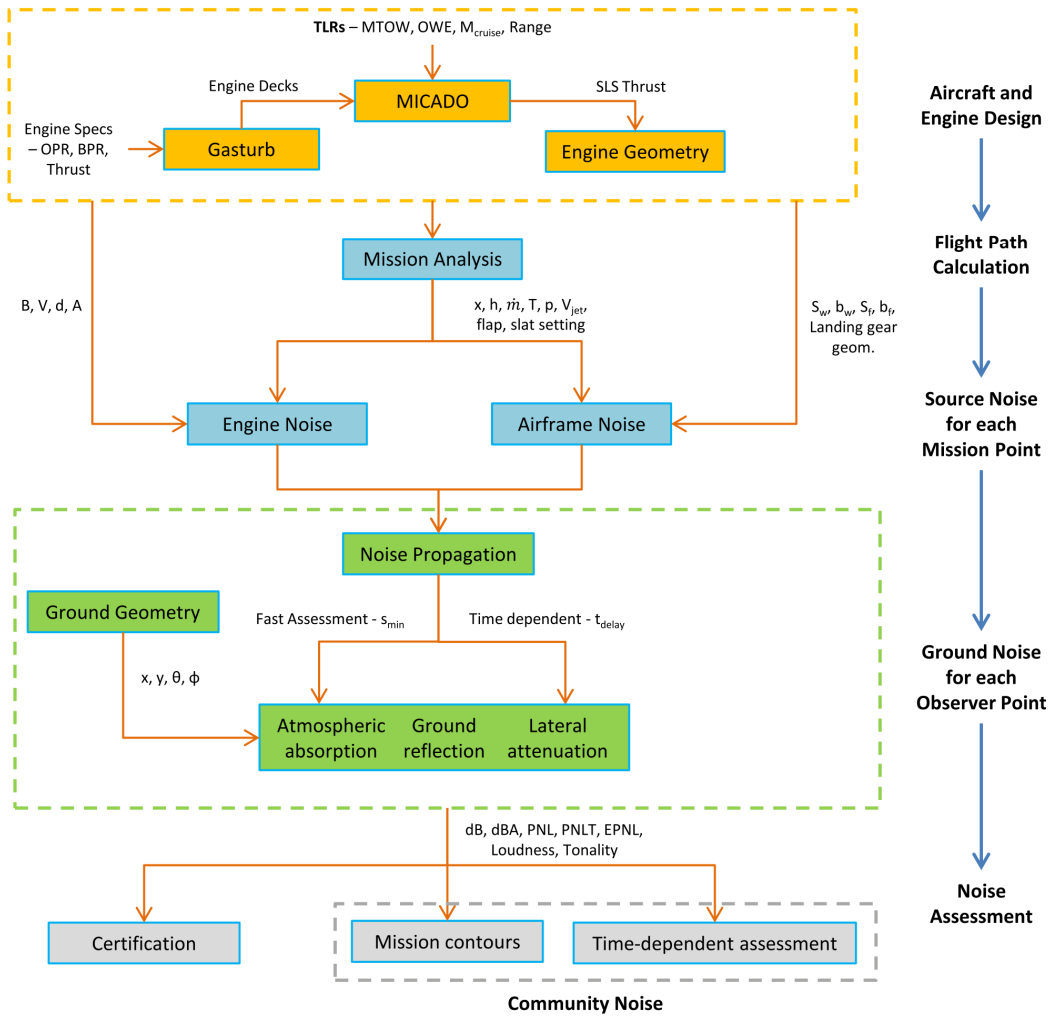


Figure 5.5: The ILR Noise Simulation and Assessment module INSTANT

- iv. *Propagation and ground noise calculation:* The aircraft source noise is propagated to the ground after applying the propagation and absorption effects of spherical (geometric) spreading, atmospheric absorption, ground reflection and lateral attenuation for user specified ground grids.
- v. *Noise assessment:* Depending on the specified ground geometry, the noise assessment can be performed for a single point for time-dependent noise prediction and simulation of virtual microphones on the ground; for an array of points for certification of aircraft designs for noise according to the ICAO Annex 16 methodology [7]; or for a full grid of points for mission level assessment in the form of noise contours displaying maximum values at each ground point in various conventional and alternate metrics.

The parts of the methodology dealing with the propagation of source noise to observers on the ground and the various assessment approaches implemented in INSTANT will now be explained in a bit more detail.

5.2.1 Propagation of source noise to the observer on the ground

The noise at the source is of relevance as it creates the pressure disturbance which travels through the atmosphere and is then felt by residents on the ground. Source noise values at the aircraft's position are only of relevance for interior (cabin) noise analysis but are of little meaning for community noise i.e. the noise impact actually felt by residents. One could say therefore that the noise at the source truly gains a meaning when it is propagated to the ground. Since this dissertation does not deal with the issues of aircraft interior noise, how the noise from the aircraft is propagated and which damping effects it undergoes have to be modeled correctly such that the annoyance due to aircraft noise experienced on the ground can be estimated correctly. The primary propagation and damping effects that aircraft noise undergoes on its way to the observer are those due to geometric spreading, atmospheric absorption and ground reflection and attenuation.

i. Geometric spreading:

Geometric spreading is the spreading of sound energy from a sound source, as the wavefronts of the sound wave which emanates from the sound source expand in the surrounding medium. For propagation purposes, as was mentioned earlier, the aircraft is regarded as a point source producing spherical sound waves in a uniform medium such as air and the geometric spreading is then regarded to be *spherical* spreading. A line source such as a busy road or highway with continuously moving automobiles can be regarded as a line source, which then results in cylindrical rather than spherical spreading of the sound energy. For the point source, the sound energy is assumed to radiate equally in all directions in free-field conditions (free of obstacles or boundaries) and the sound pressure level is then seen to reduce according to the inverse-square law by 6 dB per doubling of distance from the source. This occurs due to the fact that the acoustic power radiated from the sound source must remain constant from a source radius r_s to an observer radius r_o . As acoustic power is the product of acoustic intensity I (with $I = \frac{\langle p^2 \rangle}{\rho c}$ as mentioned in Chapter 4) and the surrounding surface area, the following relations can be said to hold for spherical sound waves originating from a point source (using here $\langle p^2 \rangle = p^2$):

$$\left(\frac{p^2(r_s)}{\rho c_s}\right) 4\pi r_s^2 = \left(\frac{p^2(r_o)}{\rho c_o}\right) 4\pi r_o^2 \quad (5.3)$$

$$p^2(r_o) = p^2(r_s) \left(\frac{\rho c_o}{\rho c_s}\right) \frac{r_s^2}{r_o^2} \quad (5.4)$$

If the source radius is taken to be 1 m (as is done for the aircraft source noise models described in Chapter 4) and replacing the observer radius r_o with simply r , and c_o with c , Eq. 5.4 can be written as:

$$p^2(r) = p_s^2 \left(\frac{\rho c}{\rho c_s}\right) \frac{1}{r^2} \quad (5.5)$$

Eq. 5.5 shows that the mean square acoustic pressure will reduce as $1/r^2$ with distance r from the source and equivalently, the pressure will reduce as $1/r$. The $1/r^2$ relation can be expressed logarithmically in terms of SPL reduction according to Eq. 5.6.

$$SPL(r) = SPL(r = 1) + 20 \log \left(\frac{1}{r}\right) \quad (5.6)$$

A doubling of distance will therefore result in a dB reduction of -6.02 dB, which is the inverse-square law. This relation has been implemented in INSTANT's noise propagation component for the straight line distance r occurring in three dimensions, calculated as the norm of the vector connecting the time-varying aircraft position vector with the stationary observer vector, expressed in global coordinates with the origin located on the runway at the point of brake-release for departures and point of touch down for approach paths. The global coordinate system as used in INSTANT showing the aircraft and observer vectors, the flight path, runway and the vector \mathbf{r} connecting the aircraft and observer are shown in Fig. 5.6.

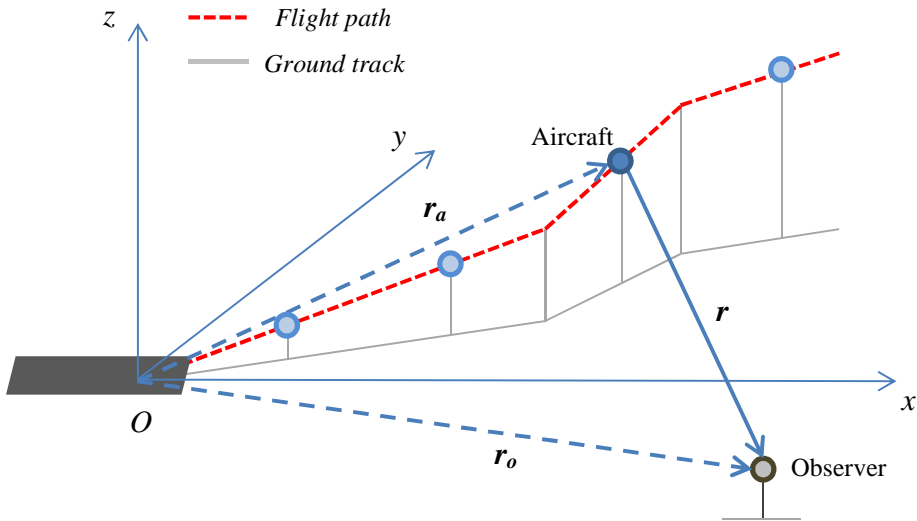


Figure 5.6: The global coordinate system with the aircraft and observer vectors as implemented in INSTANT

It can be expected that the distance between the aircraft and the observer is in general large and the atmosphere that would be contained within this large distance would not be uniformly constant throughout. It would actually contain various local wind and temperature changes that would give the path between the aircraft and observer a curvature, caused by refraction of the sound waves due to the locally varying speed of sound with which the sound waves travel. This curved sound path can lead to deviations in the magnitude of damping due to spherical spreading of the sound waves, and the curvature can also lead to certain 'shadow zones' [121] where the noise does not reach certain parts of the ground and reaches other areas which would not be impacted in the absence of wind and temperature gradients. These local wind and temperature gradient effects are however quite complex to model and require the solution of the wave equation via approaches such as the Fast Field Program (FFP), Parabolic Equation (PE) methods or ray-tracing [122]. The first two methods are frequency dependent and computationally very expensive and therefore not suitable for aircraft design and optimization purposes. The ray-tracing approach is computationally less expensive, being frequency independent but a ray-tracing implementation for modeling of detailed atmospheric propagation effects was beyond the scope of the current research work. As such, local wind and temperature effects have been neglected in the analysis presented in this dissertation and straight line propagation is assumed, in order to keep the computational costs involved in propagating source noise through the atmosphere at a level suitable for large scale aircraft design studies and optimizations.

ii. Atmospheric absorption:

The sound waves, as they propagate from the source, are attenuated due to absorption by the atmosphere besides undergoing reduction in magnitude due to geometric spreading. This atmospheric absorption is known to occur due to two primary mechanisms – classical absorption due to viscous effects and absorption due to the molecular composition of the atmosphere. The absorption due to air's molecular composition consists of molecular loss due to rotational and vibrational relaxation of the nitrogen and oxygen molecules present in air, which exchange energy from translational to rotational and vibrational modes as they collide with the expanding sound waves. The amount of energy transferred in this manner has been seen to be proportional to the amount of time it takes for the molecules to return to their equilibrium state i.e. to the relaxation time [123], [124]. The individual atmospheric absorption mechanisms are expressed as absorption coefficients, which depend on the frequency of the sound as well as the temperature, pressure and relative humidity of the air. The sum of all absorption coefficients provides the total atmospheric absorption coefficient α .

$$\alpha = \alpha_{classical} + \alpha_{rotation} + \alpha_{vibration,N} + \alpha_{vibration,O} \quad (5.7)$$

Since the aircraft as a source is continuously changing position as well as altitude over its flight path, the temperature, pressure and absolute humidity h are computed for the local aircraft altitude for each mission step. The relative humidity h_r is used to calculate the local absolute humidity (which is the molar concentration of water vapor expressed as a percentage) at the local altitude based on the ambient pressure p , reference pressure p_{ref} and the saturation vapor pressure p_{sat} according to Eq. 5.8. The saturation vapor pressure for this is computed according to Eq. 5.9.

$$h = h_r \left(\frac{p_{sat}}{p_{ref}} \right) \left(\frac{p_{ref}}{p} \right) \quad (5.8)$$

$$p_{sat} = p_{ref} \cdot 10^{\left(-6.8346 \left(\frac{T_{01}}{T} \right)^{1.261} + 4.6151 \right)} \quad (5.9)$$

The reference pressure p_{ref} is taken to be the atmospheric pressure of the International Standard Atmosphere (ISA) at mean sea-level i.e. 101.325 kPa as suggested by ISO 9613 [125], and T_{01} is the triple-point isotherm temperature having a value of 273.16 K (+0.01°C). The vibrational relaxation absorption coefficients of the nitrogen and oxygen molecules depend on the relaxation frequencies of both elements, which are given by Eq. 5.10 and 5.11 respectively.

$$f_{r,N} = \frac{p}{p_{ref}} \left(\frac{T}{T_{ref}} \right)^{-1/2} \left[9 + 280h \cdot \exp \left(-4.170 \left(\left(\frac{T}{T_{ref}} \right)^{-1/3} - 1 \right) \right) \right] \quad (5.10)$$

$$f_{r,O} = \frac{p}{p_{ref}} \left(24 + 4.04 \cdot 10^4 h \left(\frac{0.02+h}{0.391+h} \right) \right) \quad (5.11)$$

The total atmospheric absorption coefficient in dB/m is then calculated for each aircraft altitude step over its flight path using Eq. 5.12.

$$\alpha = 8.686 f^2 \left(\left(1.84 \cdot 10^{-11} \left(\frac{p}{p_{ref}} \right)^{-1} \left(\frac{T}{T_{ref}} \right)^{\frac{1}{2}} \right) + \left(\frac{T}{T_{ref}} \right)^{-\frac{5}{2}} \cdot \left(0.01275 \cdot \exp \left(\frac{-2239.1}{T} \right) \left(f_{r,o} + \frac{f^2}{f_{r,o}} \right)^{-1} + 0.1068 \cdot \exp \left(\frac{-3352}{T} \right) \left(f_{r,N} + \frac{f}{f_{r,N}} \right)^{-1} \right) \right) \quad (5.12)$$

The atmospheric absorption constant is calculated with Eq. 5.12 for each aircraft position over its flight path. It was felt it would be more accurate if the distance between the aircraft and observer is divided into a number of aircraft altitude dependent segments. In this way, the use of an average absorption coefficient over the large distance between the aircraft and observer would be avoided and a local atmospheric absorption coefficient could be calculated for each segment height, using the local atmospheric values. The aircraft source noise would then undergo a slightly different atmospheric absorption for each segment until it reaches the observer on the ground. This segment division for atmospheric absorption calculation is visualized in Fig. 5.7. The overall absorption in dB is then be the sum of each segment's α multiplied by the segment distance. If the segments are equidistant, then the overall absorption can also be computed by Eq. 5.13, where n is the number of segments the distance is divided into.

$$\delta L_t(f) = \sum (\alpha_i \cdot r_i) = \sum (\alpha_i) \cdot \frac{r}{n} \quad (5.13)$$

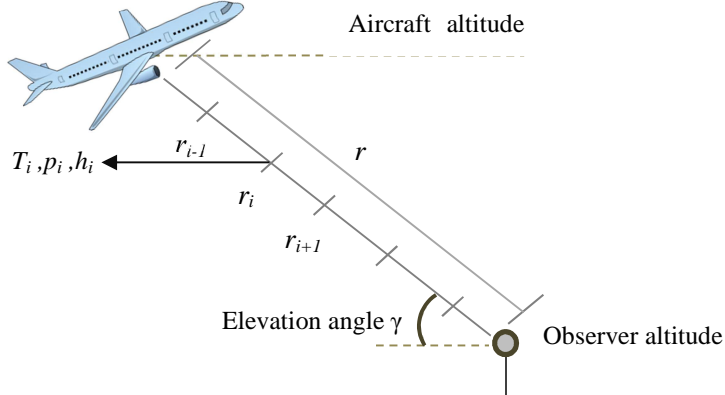


Figure 5.7: Calculation of atmospheric absorption by division of aircraft-observer distance into segments

One interesting and for this dissertation's work very important observation with regards to the magnitude of atmospheric absorption is that the atmosphere damps higher frequencies much more strongly than lower frequencies. This is one of the reasons why low frequency jet noise can be heard even at large distances from the aircraft as a low rumbling sound while the fan tonal noise is only prominent when the aircraft is relatively closer. This phenomenon is very important when considering the annoyance impact due to the spectral content on the ground. Pushing fan tones towards higher frequencies for instance would result in a higher absorption and therefore the resulting spectrum will have a lower prominence of the tones. Fig. 5.8 shows the variation of the atmospheric absorption magnitude with relative humidity, for several frequencies. It can be seen that the amount by which higher frequencies are damped is higher

than that for lower frequencies. It can also be seen that on hot and humid days the sound energy absorption by the atmosphere will be lower than on days when the humidity is low. The absorption is seen to peak at relative humidity values of around 10-20%.

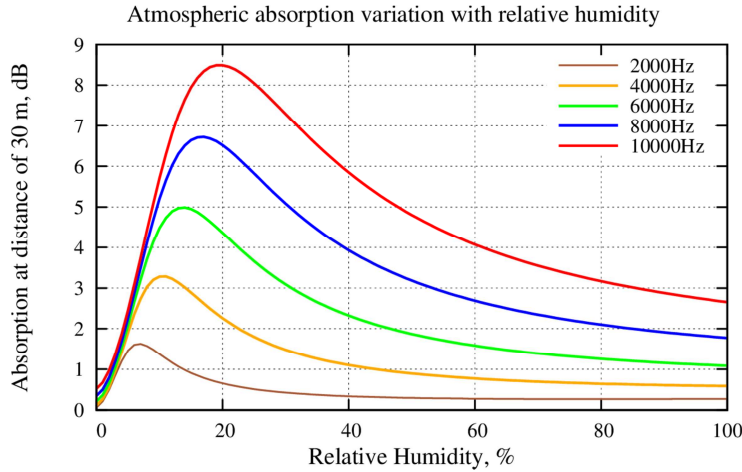


Figure 5.8: Variation of atmospheric absorption with relative humidity

iii. Ground reflection and attenuation:

The noise emanating from the aircraft not only reaches the observer directly after propagation through the atmosphere, but can also reach the observer after being reflected from the ground surface. The presence of the ground's surface results in a change in the spectrum of the sound due to reflection and attenuation of the sound waves, as well as due to the creation of surface waves. The amount of attenuation depends on the incidence angle (angle between the normal axis to the ground surface and the aircraft) and on the surface characteristics, expressed by the complex acoustic impedance of the surface. The sound waves which are not absorbed by the ground surface are reflected with a reduced or amplified magnitude, depending on the phase shift. The model used to estimate the ground reflection and attenuation is based on the Chien-Soroka theory [126], combined with the use of the Delany and Bazley impedance function [127], which estimates the ground impedance based on the frequency of the incident sound and the effective flow resistivity of the surface. The model assumes the ground is a locally reacting uniform plane and the source is a point source.

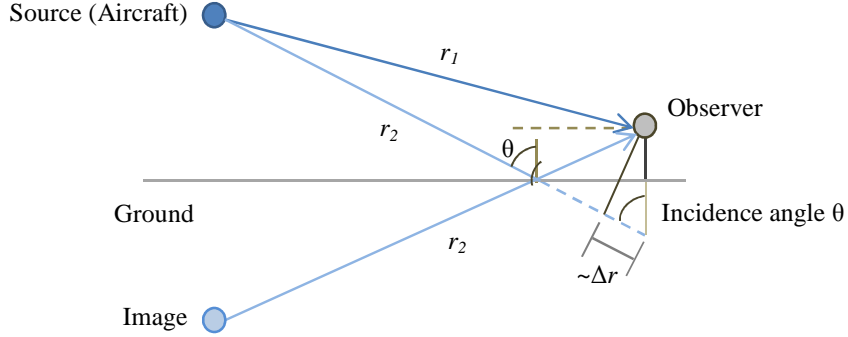


Figure 5.9: Geometry for ground reflection and attenuation calculation

Fig. 5.9 shows the aircraft-observer geometry (in two-dimensions), which will help in understanding how the ground reflection and attenuation is calculated. It can be seen that the sound arrives from the aircraft at the observer from a direct path having length r_1 and also from a reflected path from the ground having length r_2 , which appears to the observer to come from image source located in the ground. The parameter Δr is the path-length difference between the direct and reflected ray, with $\Delta r = r_2 - r_1$. The path length difference can be approximated as $\Delta r = 2h \cdot \cos\theta$. The distance $r_1 = r$ shown in Fig. 5.6 and 5.7, is obtained from the aircraft and observer position vectors and the distance r_2 can be computed using Eq. 5.14, where γ is the elevation angle from the observer to the aircraft. The cosine of the incidence angle required for calculating the path-length difference is also computed using the elevation angle via Eq. 5.15.

$$r_2^2 = r^2 + (2h)^2 - 2r \cdot 2h \cos(90^\circ + \gamma) \quad (5.14)$$

$$\cos\theta = \frac{rs \sin\gamma + 2h}{r_2} \quad (5.15)$$

The ground reflection and attenuation factor or simply the ground effects factor G is obtained from the Chien-Soroka theory, which obtains Eq. 5.16 and Eq. 5.17 from a solution of the wave equation, relating the mean-square acoustic pressure after undergoing ground effects with the free-field mean-square acoustic pressure.

$$\langle p^2 \rangle_{gr} = \langle p^2 \rangle_{ff} G \quad (5.16)$$

$$G = 1 + R^2 + 2R \exp(-(ak\Delta r)^2) \cos(\alpha + k\Delta r) \quad (5.17)$$

The parameter k in Eq. 5.17 is the wave number, calculated as $k = 2\pi f/c_0$ (where f is the frequency and c_0 is the speed of sound at observer altitude), R is the magnitude and α is the argument of the complex spherical-wave reflection coefficient and a is the incoherence constant. The term $\exp(-(ak \Delta r)^2)$ is a Gaussian approximation of the coherence coefficient C , which denotes the fraction of the acoustic energy in which phase relation has been maintained after reflection from the ground. The complex spherical-wave reflection coefficient, according to Chien-Soroka theory is given by the following relation:

$$Re^{i\alpha} = \Gamma + (1 - \Gamma)F(\tau) \quad (5.18)$$

where Γ is the complex *plane-wave* reflection coefficient given by Eq. 5.19 and $F(\tau)$ is a function accounting for the conversion from planar to spherical-wave shape.

$$\Gamma = \frac{\cos \theta - \nu}{\cos \theta + \nu} \quad (5.19)$$

The parameter ν is the complex specific *ground admittance*, which is the reciprocal of the complex specific ground impedance z . The expression for ν has been taken from the impedance model of Delany and Bazley, as mentioned earlier, which relates the admittance (and therefore impedance) with the frequency f and the surface effective flow resistivity σ , shown here via the dimensionless frequency $\eta = 2\pi f/\sigma$.

$$\nu = (1 + (6.86\eta)^{-0.75} + i(4.36\eta)^{-0.73})^{-1} \quad (5.20)$$

For an acoustically hard surface, $\eta = 0$ and therefore $\Gamma = 1$, $R = 1$ and $\alpha = 0$ i.e. all of the acoustic energy is reflected without any attenuation by the ground. In general, a part of the acoustic energy will be absorbed by the ground, depending on the value of the specific effective flow resistivity of the surface – snow would absorb more energy than grass, which would absorb more energy than asphalt or concrete. For the current research work, a grassy surface has been assumed, having a value of $\sigma = 250 \text{ kPa/m}^2 \cdot \text{s}$. Typical of ground effects is the creation of certain ‘dips’ in the noise spectrum, as was shown in Section 4.2.7, which occur due to the cancellation of sound intensity between the direct and reflected waves. If the reflected wave maintains its phase, then this results in sound intensity amplification of up to 6 dB. If the reflected wave arrives out of phase, then the sound intensity will experience an attenuation due to absorption by the ground surface.

As can be seen from Eqs. 5.14 to 5.20, the amount of reflection and attenuation depends on various factors such as the path length difference, incidence angle, wave number, specific effective flow resistivity, observer height above the ground as well as on the distance between the aircraft and the observer. Once the ground reflection and attenuation effects factor G has been calculated (cf. Eq. 5.17), it can be added logarithmically to the aircraft noise SPL, after the geometric (spherical) spreading loss and atmospheric absorption have also been added to the source noise to obtain propagated aircraft noise at the observer.

$$SPL_{observer} = SPL_{source} + 20 \log \left(\frac{1}{r} \right) - \delta L_t(f) + G \quad (5.21)$$

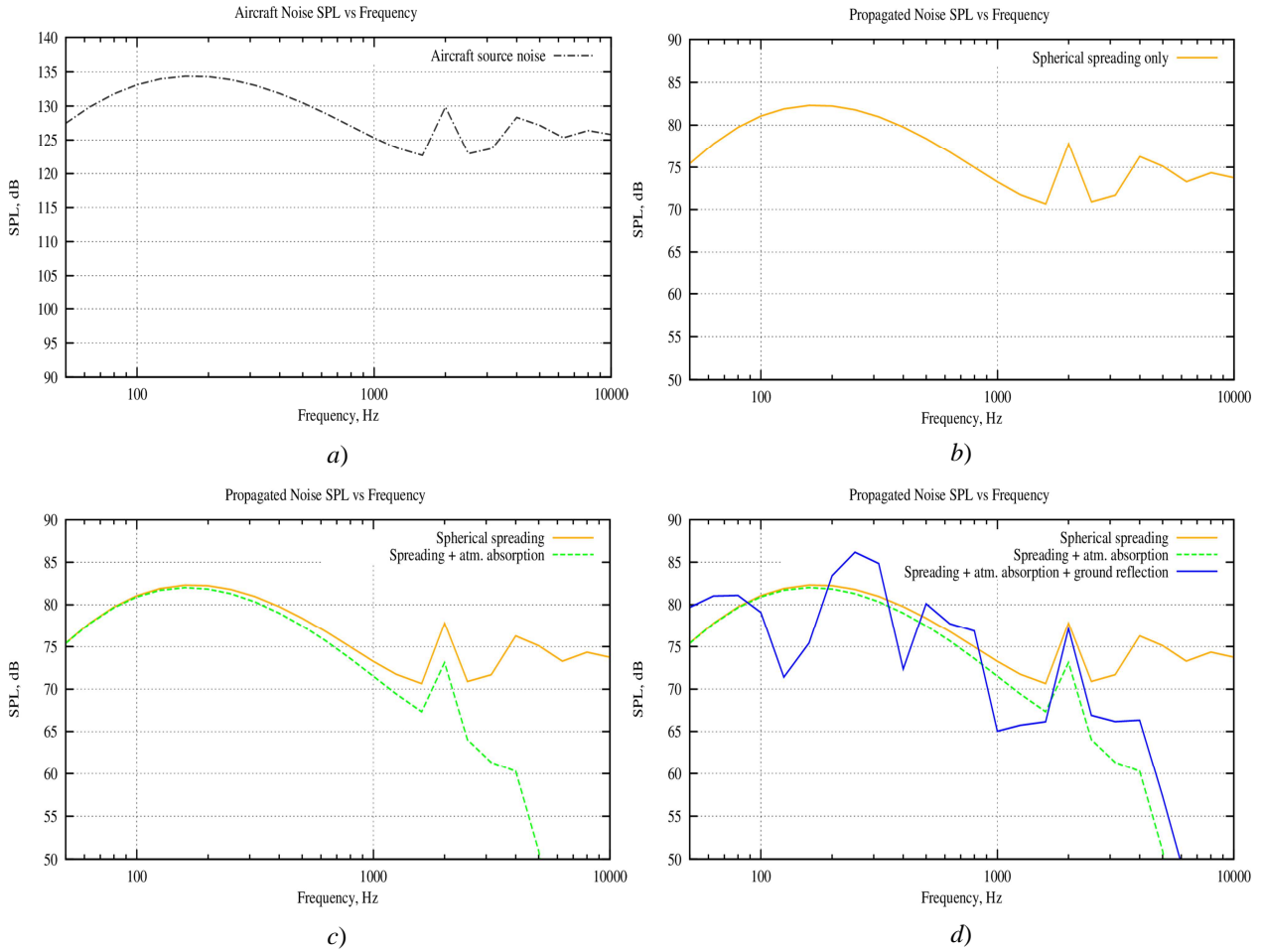


Figure 5.10: Aircraft noise spectra displaying propagation effects of spreading, atmospheric absorption and ground reflection

Fig. 5.10 shows a sample short-range takeoff aircraft noise spectrum at the source (Fig. 5.10a) and the gradual change in its spectrum as it undergoes the propagation effects of spherical spreading, atmospheric absorption and ground reflection, all calculated using the just described propagation models as they have been implemented in INSTANT. Table 5.3 shows the relevant geometric, atmospheric and ground surface parameters that result in the presented propagated spectra. It can be seen in Fig. 5.10b, the effect of spherical spreading on aircraft source noise results in a uniform

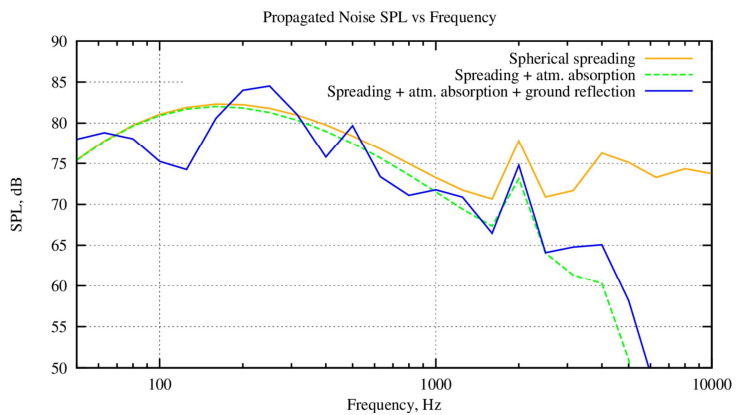


Figure 5.11: Propagated aircraft noise spectrum for a snowy ground surface

reduction for all frequencies by a value of 53.1 dB for the distance of 453.2 m between the source and observer. Fig. 5.10c shows that the atmosphere absorbs frequencies of 1000 Hz and above increasingly strongly, with the noise above 5000 Hz reduced to values below 50 dB from source values of around 125 dB. The lower frequencies can be seen to be absorbed much more weakly by the atmosphere, which would result in the longer persistence of broadband jet noise over larger distances, as was mentioned earlier. On the other hand, the higher harmonics of the fan tones would be quite strongly damped as they traverse the atmosphere, which would reduce the experienced tonal noise impact on the ground. The presence of the ground surface results in the previously mentioned spectral peaks and troughs due to acoustic energy cancellation and also amplification due to coherence of the direct and reflected sound waves. Fig. 5.11 shows the corresponding propagated spectrum on the ground, this time for a snowy surface, having a specific effective flow resistivity value of σ of 25 kPa/m²·s. It can be observed that the reflection effects i.e. the dips and peaks in the spectrum are of lower magnitude than those observed in Fig. 5.10d for a grassy surface.

Table 5.3: Relevant geometric and atmospheric data used for propagation in Fig. 5.10

Geometric and atmospheric data	
<i>Parameter</i>	<i>Value</i>
Aircraft altitude, h_a	55.4 m
Observer altitude, h_o	1.2 m
Distance, r	453.2 m
Reference temperature, T_{ref}	15 °C
Reference pressure, p_{ref}	101.325 kPa
Relative humidity, h_r	70%
Specific effective flow resistivity, σ	250 kPa/m ² ·s

iv. Lateral attenuation:

Although the Chien-Soroka theory shows for the most cases a fair to good match with measured aircraft noise, it often underpredicts the magnitude of the attenuation that the various frequencies undergo [128], [129]. It is thus regarded as a conservative estimate of the ground effects which aircraft noise experiences when close to the ground. It was observed over assessment of complete departure paths that particularly in lateral and aft directions when the aircraft is on the ground or very close to it, the predicted maximum noise values were higher than what would be expected by looking at dBA noise contours from references such as FAA's Integrated Noise Model (INM) [130]. In the aft directions, jet noise is the dominant source and since the simulated jet velocities and the corresponding jet noise were deemed to be in a realistic range (300-500 m/s and 120-135 dB at source respectively, for the V2527-A5 engine model), it was concluded that the absorption by the ground surface was lower than what would be observed in reality.

Various references such as [131] make use of an extra or ‘excess’ ground attenuation model to account for the lateral attenuation that occurs due to the presence of the ground surface, engine installation effects such as presence of the fuselage and wing which scatter the sound and also obstacles on the ground located between the aircraft and the observer. This excess ground attenuation was therefore also implemented in INSTANT. The method as described in SAE-1751 [132] was chosen to be applied since it

is the most widely used method and it determines the lateral attenuation according to purely empirical data obtained from measurements carried out for several commercial aircraft. There are however other more updated models, which have been developed at other international organizations [133], [134] but have only been internally used by the organizations. The SAE-1751 model determines the reduction in sound intensity when the aircraft is on the ground using Eq. 5.22, based on the horizontal distance l from the aircraft:

$$G(l) = 15.09 \cdot (1 - e^{-0.00274l}) \text{ for } 0 < l < 914 \text{ m} \quad (5.22a)$$

$$G(l) = 13.86 \text{ for } l \geq 914 \text{ m} \quad (5.22b)$$

If the aircraft is airborne and the horizontal distance from the aircraft is larger than 914 m, then the attenuation is calculated according to Eq. 5.23 based on the elevation angle:

$$G(\beta) = 3.96 - 0.066\beta + 9.9e^{-0.13\beta} \text{ for } 0^\circ \leq \beta \leq 60^\circ \quad (5.23a)$$

$$G(\beta) = 0 \text{ for } \beta > 60^\circ \quad (5.23b)$$

If the aircraft is airborne and the distance is less than 914 m, then Eq. 5.24 is used to compute the lateral attenuation based on both horizontal distance and elevation angle.

$$G(\beta, l) = \frac{G(l)G(\beta)}{13.86} \quad (5.24)$$

5.2.2 Assessment of aircraft noise

The aircraft source noise is thus propagated from the aircraft position at each mission step in its flight path where it is described using the parametric source noise models, and is successively adjusted in its intensity taking into account the damping with distance to the observer, the absorption by the atmosphere based on local weather conditions and the complex reflection and attenuation effects from the ground surface. The result is that for each aircraft mission step-observer combination, one spectrum is obtained at the observer position corresponding to the specific polar and azimuthal directivities and the aircraft-observer geometry at that time step. The next step then is to assess this aircraft noise spectrum in order to determine what influence it will have on the residents if they were to be living at that observer location. In Chapter 2 (cf. Section 2.1), the metrics which are currently used in the aerospace industry to assess aircraft noise were described, along with the at times detailed procedure of how some of these metrics are computed. One of the metrics - the EPNL metric, is a relatively complex metric as was shown in Section 2.1, having a lengthy computation procedure requiring firstly the prediction of PNL and PNLT metrics over 0.5 second steps of the flight path, followed by the time-integration for mission points lying up to 10 EPNdB below the maximum. All the single event loudness and annoyance based metrics from Chapter 2 have been implemented in INSTANT, namely – dBA, dBC, SEL, PNL, PNLT and EPNL using the earlier explained methodology. INSTANT provides a number of options of how the assessment is to be carried out, some of which include:

- Which metrics are required for the current assessment?
- Does the aircraft design have to be certified at ICAO specified certification points?

- Is a time-dependent assessment simulating a virtual microphone required at isolated ground points other than the certification points i.e. for community noise assessment?
- Is a mission-level assessment via noise contours for departure and approach flight paths required for community noise assessment?

These options have been implemented in INSTANT with slightly different algorithms depending on what the purpose of the assessment is. As can be seen in Fig. 5.5, the certification option is separated from the community noise assessment option in INSTANT. This has been done to have the option of assessing aircraft noise impact not only close to the runway and airport (via the certification points) but also further away from the runways where the residents actually live. As can be understood from the description of propagation mechanisms in the previous section, aircraft noise over large distances can undergo varying amounts of atmospheric absorption as well as ground effects depending on the observer location. The situation of ground noise impact at the certification points may not always be representative of the noise impact being felt by the residents living at larger distances from airport. The assessment using INSTANT is therefore divided fundamentally into two options – noise certification or community noise assessment. Community noise assessment is further divided into the simulation of virtual microphones ‘measuring’ aircraft noise over complete flyovers at observer locations other than the certification points; and assessment over large distances in airport vicinities via noise carpets or contours.

To facilitate the assessment process, two types of algorithms have been implemented in INSTANT – time-dependent assessment and mission level assessment, both of which shall now be briefly explained. As will be explained, the division has been made purely to save on the large computational costs that occur when the source noise spectra over complete departure and approach flight paths consisting of 500-1000 mission points (and therefore equivalent number of source noise spheres) have to be propagated to a large number of ground points in the order of 20000-60000 (depending on the desired ground grid resolution). The main difference between the two algorithms is that for time-dependent assessment all mission steps are taken into account to simulate a complete flyover over each observer point while for mission-level assessment, only those mission steps are considered for noise propagation which lie at a chosen factor times the closest distance to the observer.

1. Time-dependent aircraft noise assessment:

When a complete aircraft flyover has to be simulated over a measurement point on the ground, then the time-delay t_d between the time the noise was emitted (the emission time, t_e) and the time when the noise reaches the observer on the ground (the reception time, t_r) has to be taken into account. The reception time is therefore the sum of the emission time and the time-delay as shown by Eq. 5.25. The time-delay is calculated using the simplified straight line path distance (cf. Fig. 5.6 and Fig. 5.7) r and the speed of sound at the aircraft altitude c_a according to Eq. 5.26. Aircraft noise on the ground has to be expressed with reference to the observer and as such, the reception times on the ground are taken as the known value, for which, based on the time-delay t_d the corresponding *retarded emission times* are calculated according to Eq. 5.27. The retarded emission time is therefore the time at which the noise was emitted at the source, for a given time on the ground. It is clear from Eq. 5.27 that for $t_r < t_d$ starting from $t_r = 0$, the retarded emission time $t_{e,ret}$ will be negative.

$$t_r = t_e + t_d \quad (5.25)$$

$$t_d = \frac{r}{c_a} \quad (5.26)$$

$$t_{e,ret} = t_r - t_d \quad (5.27)$$

If the retarded emission time value is negative, then the noise for this value is set to a minimum value (e.g. 0 dB) as noise at the source is only known for emission times starting from zero and there is no noise produced before the first emission time. For the retarded emission times that are positive, an interpolation is made between neighboring emission times for which the noise is known. For example, if the aircraft is at a distance of 500 m from the observer, then a time delay of 1.47 s will occur before the noise at the source reaches the observer on the ground (assuming a constant speed of sound of 340 m/s in this example). This implies that for a t_r of 0 s, the retarded emission time $t_{e,ret}$ is -1.47 s and for a t_r of 2 s, the $t_{e,ret}$ is 0.43 s. If the emission time is known for values of 0 s and 0.5 s, then the noise at these two emission times has to be interpolated to obtain the noise corresponding to the t_r of 2 s. The noise at the source found in this way is then propagated to the ground by applying the aforementioned propagation effects and a noise value on the ground is obtained for the current reception time, at the current ground point. This process is then repeated for all the points on the ground for which time-dependent noise assessment is required to be performed.

Time-dependent assessment is performed in INSTANT when aircraft designs are to be assessed for certification purposes and also when community noise assessment is required to be performed at selected observer points simulating measurements of aircraft flyovers via virtual microphones, as was mentioned earlier.

i. *Certification of aircraft for noise:*

According to ICAO Annex 16 [7], all aircraft that enter the market have to be certified for noise for both departure and approach flight phases by ensuring that the aircraft's noise impact expressed in EPNdB values is below specified values depending on the aircraft Takeoff Weight (TOW) for both departure and approach procedures. These correlations between the aircraft takeoff weight and maximum allowable EPNdB value according to ICAO Chapter 3 regulations are presented in Eq. 5.28 for the lateral (sideline) and flyover certification locations:

$$EPNdB_{sideline} = \begin{cases} 94 & \text{for } TOW \leq 35 \cdot 10^3 kg \\ 80.87 + 8.51 \log(TOW) & \text{for } 35 < TOW < 400 \cdot 10^3 kg \\ 103 & \text{for } TOW \geq 400 \cdot 10^3 kg \end{cases} \quad (5.28a)$$

$$EPNdB_{flyover} = \begin{cases} 89 & \text{for } TOW \leq 48.1 \cdot 10^3 kg \\ 66.65 + 13.29 \log(TOW) & \text{for } 35 < TOW < 385 \cdot 10^3 kg \\ 101 & \text{for } TOW \geq 385 \cdot 10^3 kg \end{cases} \quad (5.28b)$$

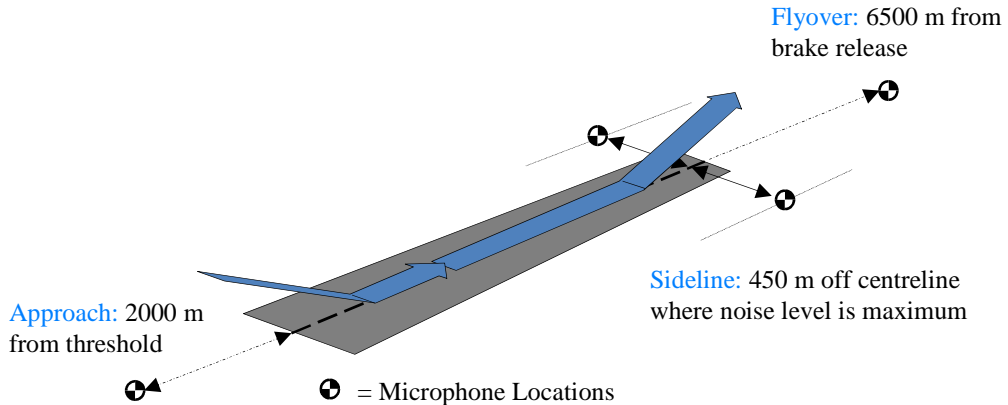


Figure 5.12: ICAO specified aircraft noise certification points

Eq. 5.29 shows the corresponding EPNL metric value correlation with takeoff weight for the approach certification point:

$$EPNdB_{approach} = \begin{cases} 98 & \text{for } TOW \leq 35.10^3 kg \\ 86.03 + 7.75 \log(TOW) & \text{for } 35 < TOW < 280.10^3 kg \\ 105 & \text{for } TOW \geq 280.10^3 kg \end{cases} \quad (5.29)$$

In January 2006 the more stringent ICAO Chapter 4 regulations for noise were introduced, which require a minimum EPNdB difference of 2 dB at each certification location between the maximum Chapter 3 allowed value and the measured value and a minimum 10 dB difference between the maximum cumulative allowed values and the cumulative measured values. The EPNdB values are computed using INSTANT at the approach certification point located 2000 m from the runway threshold (equivalently 2300 m from the point of touchdown) directly below the flight path, at the sideline location 450 m lateral to the runway where the maximum EPNdB value occurs, and at the flyover measurement point located 6500 m below the flight path from the point of brake release (cf. Fig. 5.12).

Table 5.4 shows the simulated EPNL values in EPNdB and maximum certification EPNL values as specified by ICAO for an Airbus A320-200 aircraft powered with a V2527-A5 engine model. The aircraft has been designed using the MICADO environment, the engine modeled using Gasturb and integrated in MICADO via engine performance decks, the departure and approach flight paths have been computed using the mission analysis module and the noise prediction at the certification points in the EPNL metric have been performed using INSTANT. The designed aircraft has a MTOW of 74014 kg (compared to the reference value of 73500 kg) and it has a modeled MLW of 62323 kg (compared to the reference value of 64500 kg). It can be seen that the simulated noise in the EPNL metric of the modeled aircraft and engine combination is within a realistic range and lies below the Chapter 3 certification limits and almost below those of Chapter 4 at all measurement locations except for the approach certification point. This is the case for acoustic liner technology activated, as is the norm for modern turbofan engines. Without acoustic liner technology however, the noise prediction is seen to be above Chapter 3 limits for the lateral and

approach points. The primary reason for the over-prediction is fan noise, which is reduced by the use of acoustic liners by 3-5 EPNdB for both departure and approach engine settings in both forward and aft directions. It is known that Heidmann's model over-predicts fan noise but the reductions in fan noise due to acoustic liner technology, being based on measured data of modern turbofan engines, are nonetheless representative of how the more stringent noise regulation requirements would not be met by the engine manufacturers without use of acoustic liner material. This aspect will be analyzed in a bit more detail in Chapter 8, where annoyance optimized aircraft designs without acoustic liner material will be compared with current designs with acoustic liner material present.

Table 5.4: Simulated and reference EPNL values for the A320-200 aircraft with V2527-A5 engine model

With acoustic liner technology			
<i>Noise certification point</i>	<i>EPNL Simulated [EPNdB]</i>	<i>EPNL ICAO limit [EPNdB]</i>	<i>Margin [EPNdB]</i>
Sideline	93.7	96.8	-3.1
Flyover	86.4	91.5	-5.1
Approach	99.0	100.5	-1.5
Without acoustic liner technology			
Sideline	97.0	96.8	+0.2
Flyover	89.2	91.5	-2.3
Approach	102.2	100.5	+1.7

Fig. 5.13 shows the PNLT vs. polar directivity (equivalently PNLT vs. time) variation at the sideline, flyover and approach certification locations, as simulated using INSTANT for the short-range aircraft, by making use of the time-dependent assessment algorithm.

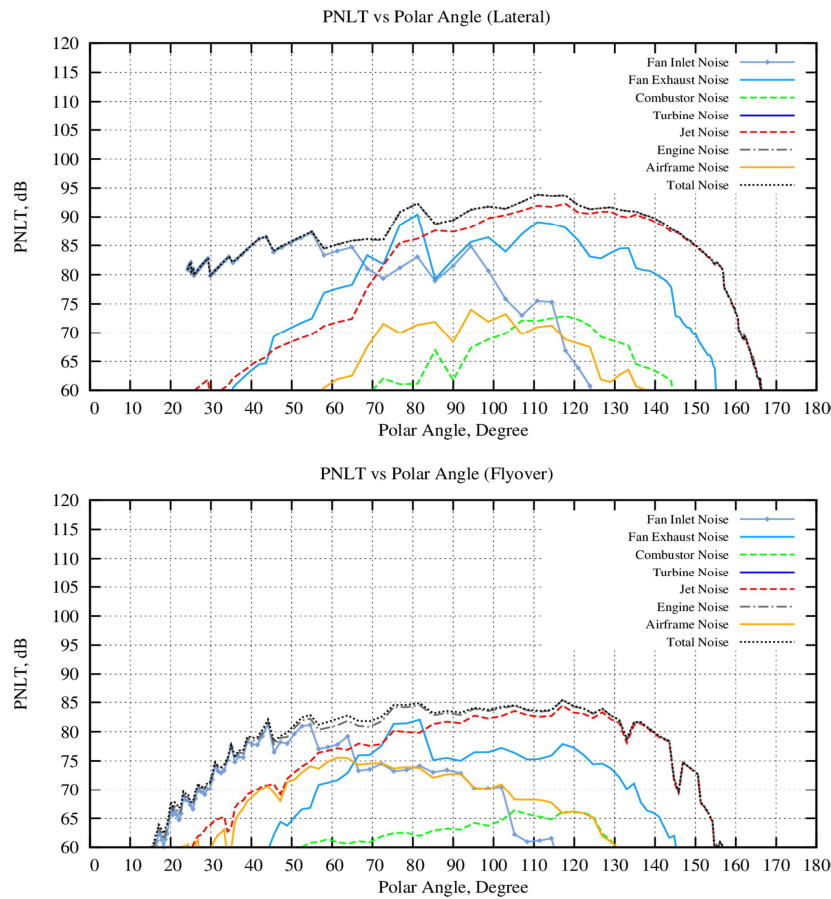


Figure 5.13: PNLT vs. polar directivity variation at the sideline and flyover points for a short-range aircraft

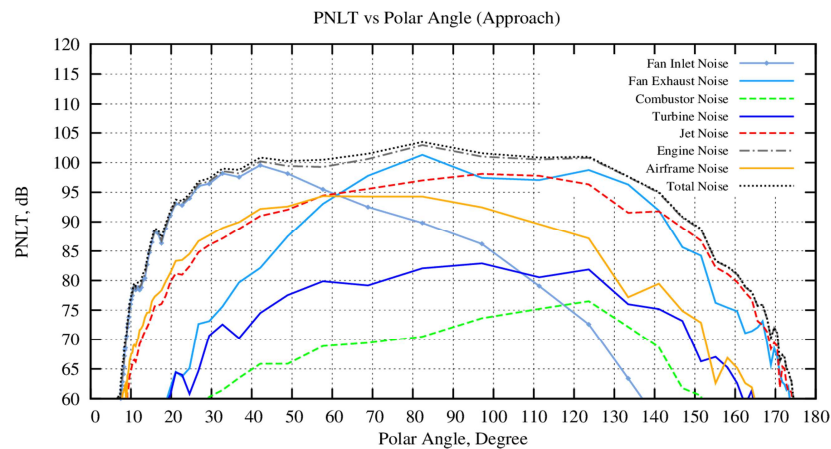


Figure 5.14: PNLT vs. polar directivity variation at the approach point for a short- range aircraft

Fig. 5.13 shows that for the departure flight setting, the jet noise is the most dominant aircraft noise component in aft directions from polar directivity angles of 90° onwards, and the fan inlet is the dominant component in the forward directions. Airframe noise, as expected, is much lower than the engine noise components. Fig. 5.14 shows the PNLT variation with polar directivity for the approach setting at the approach certification point, where it can be seen that fan noise is much more dominant (even with acoustic liner material activated) and airframe noise in the forward directions till 60° polar directivity is the most dominant broadband noise component, for the short range aircraft modeled here. For long range aircraft such as the Boeing 777 or 747 variants, airframe noise has a higher contribution due to the much larger airframe geometry of the long-range aircraft. Fan noise during approach can be seen to be the dominant component even in the aft directions as the engine thrust setting is at flight idle, which results in low jet velocities and hence low jet noise. It can be mentioned that the above presented PNLT variation plots are only valid for the certification points and do not represent the aircraft noise spectral composition further away from the runways.

ii. *Time-dependent community noise assessment:*

As mentioned earlier, the time-dependent assessment algorithm is also applied to community noise assessment, besides its application to simulate aircraft noise certification of the designed aircraft. Two sub-options exist regarding the time-dependent assessment that can be performed – simulating flyovers at selected individual measurement points or simulating flyovers over a grid of points showing the noise impact variation over time as the aircraft flies above. The first sub-option shows in detail how the noise impact in terms of the chosen metric varies over time at isolated observer locations, as shown in Fig. 5.15 and Fig. 5.16 for a standard departure and approach procedure respectively, of the same short-range A320-200 similar aircraft with the V2527-A5 engine model. The figures show the variation of the overall aircraft noise as well as of the major aircraft noise components, namely fan noise, jet noise and airframe noise in the dBA metric.

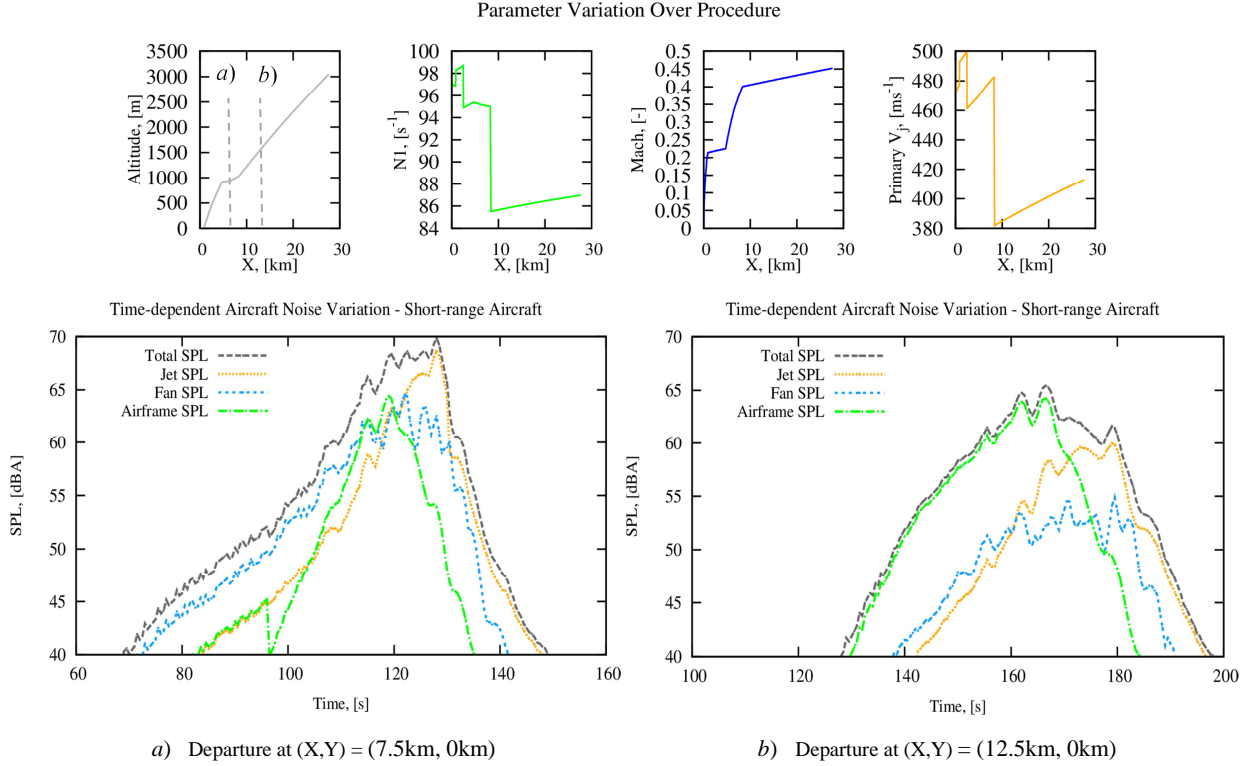


Figure 5.15: Time-dependent community noise assessment for a short-range aircraft standard departure flight path

Fig. 5.15a shows the SPL variation at a point 1 km beyond the flyover point and it can be seen that for the takeoff condition, fan noise is dominant to the front, jet noise to the aft and airframe noise lies generally below both components. Fig. 5.15b however shows the time-dependent variation at 12.5 km directly below the flight path and it can be seen that the individual spectral contributions have changed somewhat, with the aircraft being slightly higher and the thrust setting being reduced to maximum climb from maximum takeoff (cf. Fig. 5.15 top part showing the variation of relevant parameters such as LP spool speed (N_1) and primary jet velocity over the flight procedure). The fan noise has decreased considerably and the airframe noise is now dominant towards the front of the aircraft. The aircraft noise due to the short-range aircraft with a medium bypass ratio engine is therefore dominated by broadband noise further away from the runway.

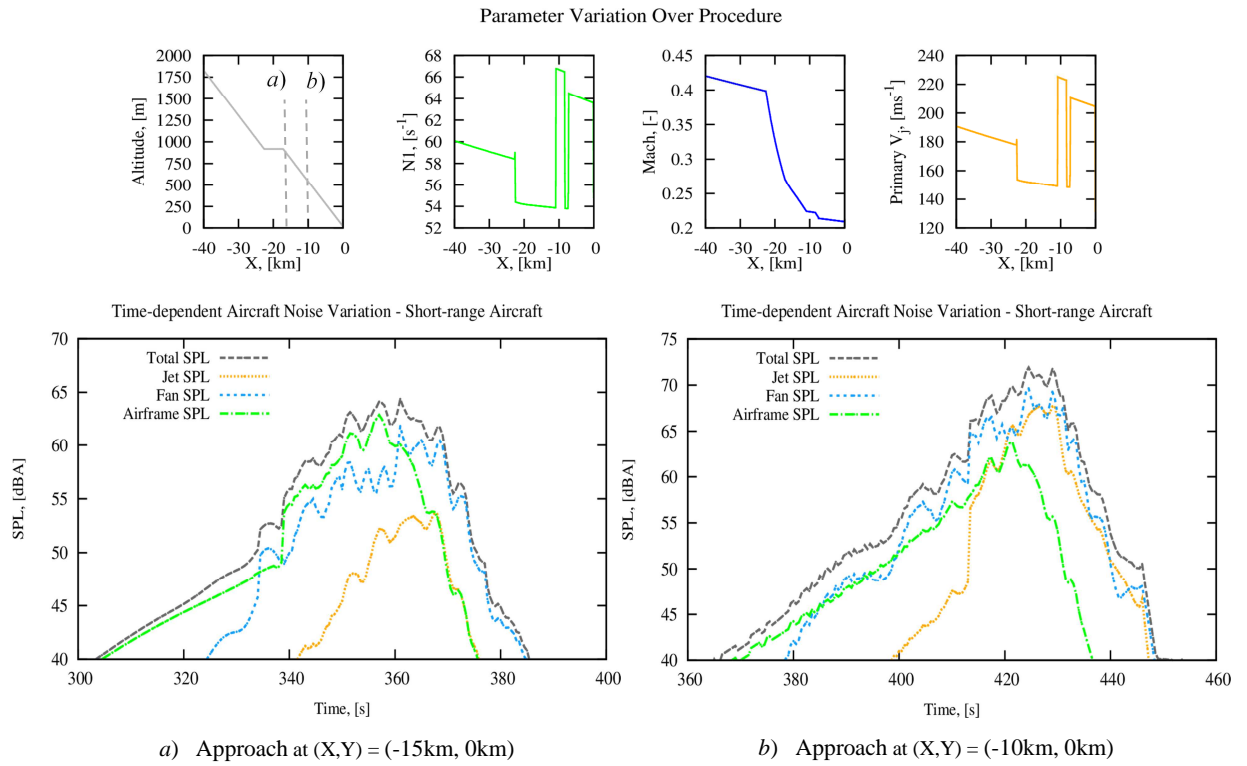


Figure 5.16: Time-dependent community noise assessment for a short-range aircraft standard approach flight path

Fig. 5.16 shows the corresponding variation for a standard approach procedure at two observer locations further away from the runway – at -15 km and -10 km from point of touchdown directly below the flight path. At (-15 km,0 km), the airframe noise is the dominant broadband component and fan noise is the strongest component aft of the aircraft. Since the jet velocities are much lower for the flight idle setting (cf. top part of Fig. 5.16), the jet noise is quite low further away from the runway. Fig. 5.16b shows the time varying noise impact at (-10 km,0 km), where the engine setting has been increased during the final approach (the engine setting alternates between flight idle and approach) and this leads to higher jet velocities and higher corresponding jet noise. The fan noise in Fig. 5.16b can also be seen to have increased by about 8 dBA at the second location closer to the runway. It can be noted that since the fan noise is much more prominent during the approach phase, the fan tones which constitute fan noise to a large extent, will be more audible during landing than during takeoff, particularly at larger distance from the runway where residents often live. This will have an impact on the annoyance impact experienced by the residents, as will be explored in subsequent chapters. It can also be mentioned that since the time-dependent noise impact variation plots have been shown in the widely used dBA metric, the jet noise which peaks at lower frequencies has been in effect under-weighted by the A-weighting.

Fig. 5.17 shows the second time-dependent community noise assessment sub-option in INSTANT – time-dependent noise contours on the ground for individual flight paths. The time-dependent noise contours are shown for the short-range aircraft over a standard departure flight path, over an area of 10 km x 10 km,

shown for selected reception times on the ground. The plots show from Fig. 5.17a to 5.17f, the noise impact over the ground for several reception time values and how it spreads with successive reception time steps, gradually reaching ground points located further away from the flight path and its corresponding ground track. When the noise from a 1 m radius source sphere around the aircraft exactly reaches each ground point depends, as explained earlier, on the time-delay and on which emission time corresponds to the current reception time on the ground. Time-dependent noise contours such as those presented in Fig. 5.17 are quite well suited for demonstration purposes by showing visually how airport vicinities are affected by individual aircraft as they depart and approach the airport over resident communities. This approach of time-dependent noise impact visualization was also applied for the previously mentioned VATSS project, where the noise contours for each reception time-step were converted to a 3D visualization format and implemented for creating the VR simulation of air-traffic in airport vicinities. The exact methodology with which the time-dependent noise contours were converted to the 3D visualization format and integrated in the VR toolchain for the VATSS project has been detailed by the author in [18], [19].

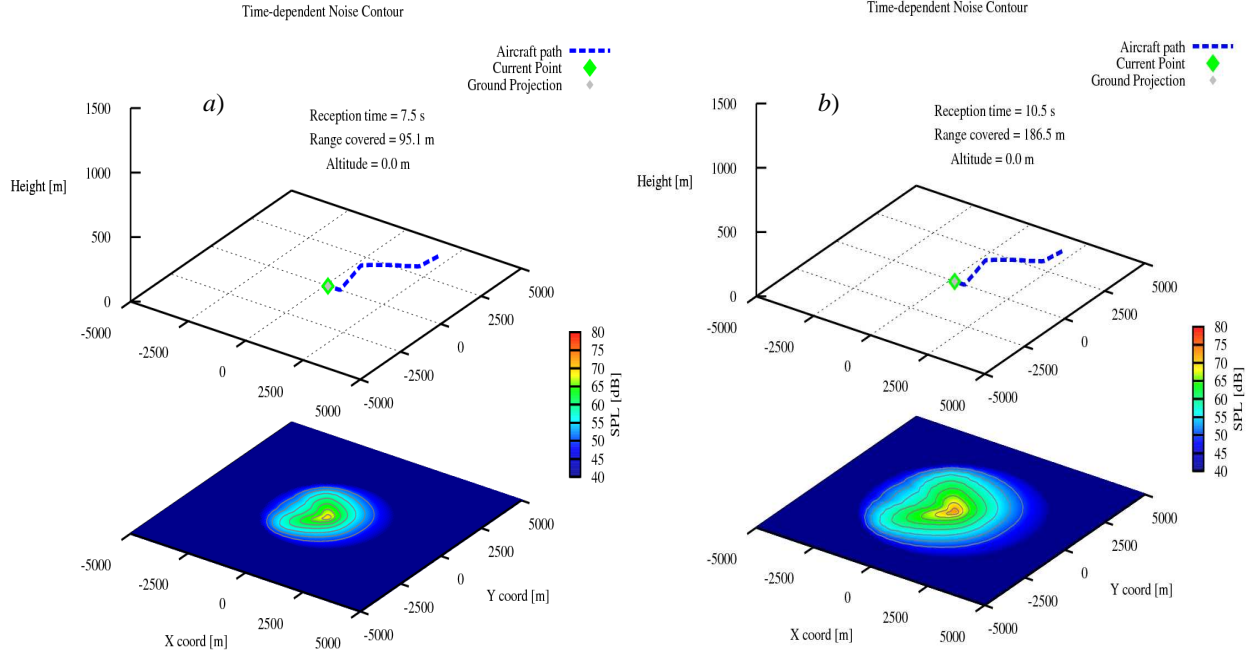


Figure 5.17: Sample time-dependent noise contours made using INSTANT – (1)

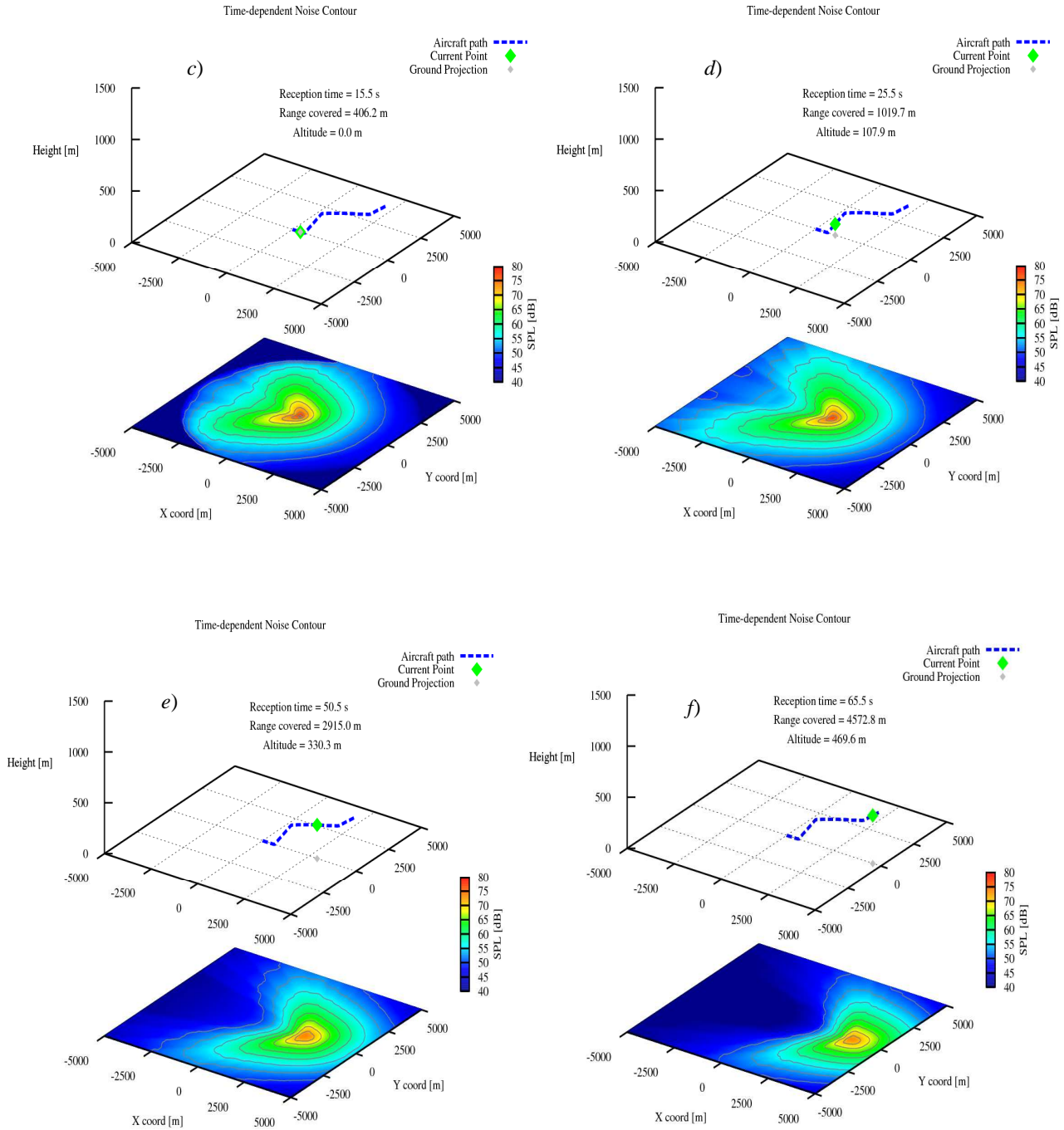


Figure 5.17: Sample time-dependent noise contours made using INSTANT – (2)

2. Mission-level aircraft noise assessment:

Time-dependent assessment is useful for detailed analysis at specific ground points or for time varying noise impact assessment over several observer points in airport vicinities via the time-dependent noise contours. For aircraft design optimization purposes however, the information displayed by the time-dependent noise impact analysis at each ground point has to be conveyed as a single value which is representative of the ground noise impact caused by the aircraft over its entire flight path. Conventionally, several researchers have used the cumulative EPNdB values at certification points for optimizing aircraft designs for noise or for performing trade-offs between noise, emissions, fuel, weight and costs [68], [135] during the preliminary or conceptual design phase. As can be observed from Fig. 5.15 and Fig. 5.16 for the short-range aircraft, the noise impact close to the runways, where the certification points are located may not necessarily be representative of the noise impact at larger distances where the residents actually live. An attempt will be made in this dissertation therefore to incorporate community noise impact of aircraft during the design phase by showing aircraft noise and annoyance design sensitivities (in Chapter 7) and aircraft design optimizations for community noise impact (in Chapter 8). While developing a means to incorporate community noise impact in the aircraft design and optimization process, two possible options can be to use the OSPL value in dBA or the EPNdB value at specific individual ground points further away from the runways, or to incorporate the complete *noise exposure* of the aircraft over departure and approach flight paths by using the noise impacted area in km² in any of the conventional or alternate noise metrics (via a maximum or close to maximum metric values). The latter approach is considered more representative of overall community noise impact as it captures the noise impact over entire flight paths and over ground locations both close to and far away from the aircraft's flight path.

This is done using INSTANT's mission-level aircraft noise assessment option, whereby noise contours over the complete flight paths for each designed aircraft are made displaying the maximum value that occurred at each ground point over the complete flight procedure. The choice of using the maximum noise impact value over the ground point has been made instead of average values as the residents' perceived annoyance is known to be determined by the maximum noise impact over a given time period, or by a value lying close to it [43], as was mentioned in Section 3.1. Isocontour lines are made for a range of noise impact values in the metric chosen for assessment and the area contained within the isocontour line for a specific metric value can then be attempted to be minimized for optimization purposes. Since these 'mission' contours require the maximum metric value at each ground point to be known but not necessarily the complete time-dependent variation, a mission-level assessment algorithm has been applied in order to construct the mission contours. Mission-level assessment is intended to be made over very large distances around the airport, for flight paths with a large number flight points and the calculation of source noise spectra in all the polar and azimuthal directions as well as their propagation to the multitude of observers can become a computationally expensive task. Especially for performing aircraft design parameter variation studies and optimizations, a faster computation is desirable as several hundred designs at times need to be assessed.

The mission-level assessment algorithm in INSTANT searches for the mission point over the flight path which is located closest to the current ground point and then selects only those mission points for propagation to the current ground point which are located within a selected range of the closest mission point i.e. a factor times the shortest observer-aircraft distance r . This is based on the knowledge that the noise intensity peaks when the aircraft is closest to the ground and this saves considerable computational

time, producing noise contours for complete aircraft movements in the order of a few minutes. From the geometry module of ANOPP [83] a distance of eight times the minimum distance between aircraft and observer is said to reduce the intensity due to geometric spreading alone to close to background noise levels. From experience while making noise contours using INSTANT, a distance of five times the minimum distance has been seen to provide accurate results for maximum noise impact values on the ground.

Fig. 5.18 shows the mission noise contour for the standard departure procedure of the A320-200 similar aircraft flying the flight path shown in the parameter variation of Fig. 5.15 (top part), in the dBA and EPNL metrics. Fig. 5.19 shows the corresponding mission contours for the standard approach procedure that was shown in Fig. 5.16.

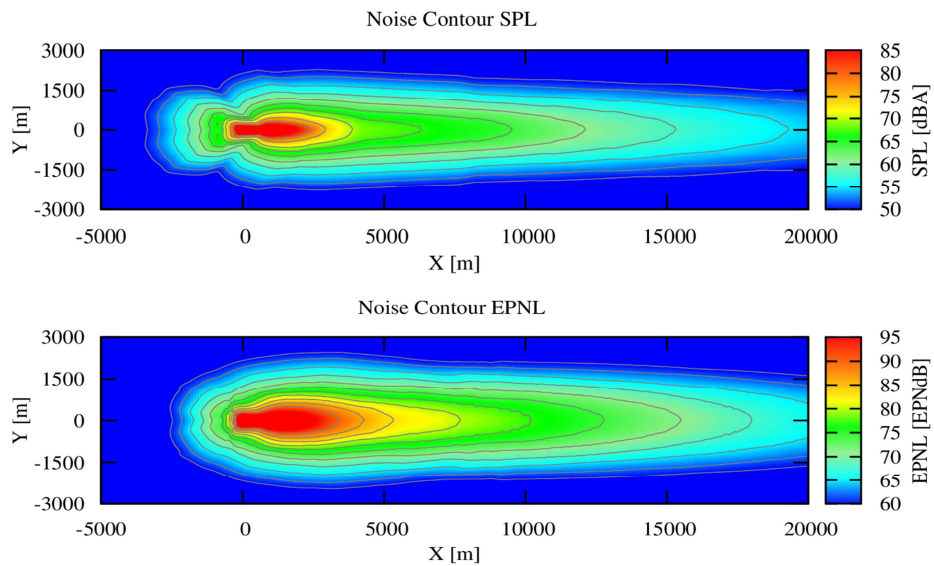


Figure 5.18: Maximum value noise contours made using INSTANT for a standard short-range aircraft departure procedure in the dBA metric (top) and EPNL metric (bottom)

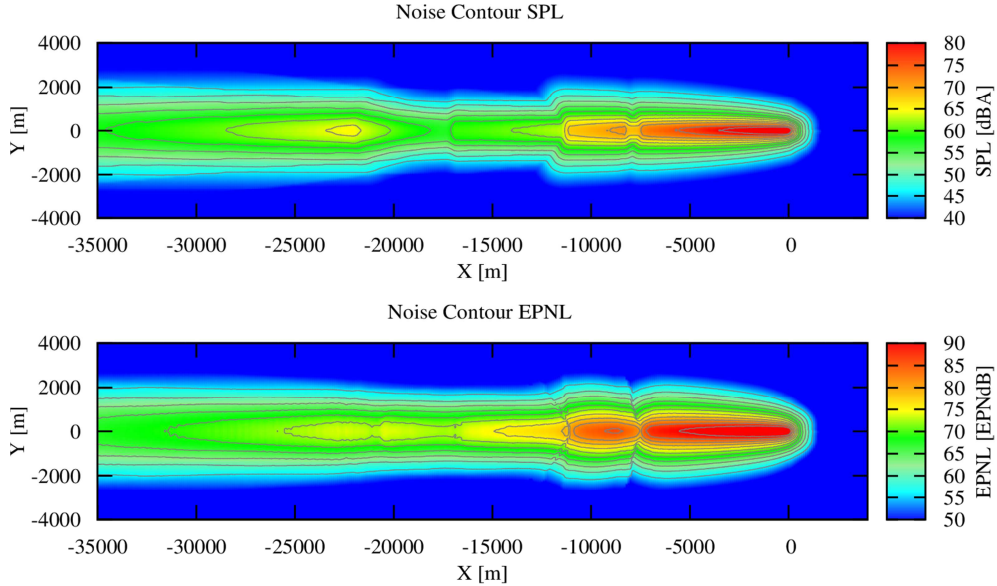


Figure 5.19: Maximum value noise contours made using INSTANT for a standard short-range aircraft approach procedure in the dBA metric (top) and EPNL metric (bottom)

As mentioned earlier, the impacted area within these contours presents the potential for minimization for community noise abatement. If the impacted area is used as a design constraint or requirement during the design process, then aircraft can be designed as well as optimized that also satisfy community noise requirements, besides the performance and efficiency requirements. For the assessment of aircraft noise on the ground, INSTANT can produce mission contours in the conventional noise metrics of decibel, dBA, PNL, PNLT and EPNL, as well as in the sound quality metrics of loudness, tonality and sharpness, which are explained in the next chapter.

6 Annoyance assessment using sound quality metrics

In Chapter 3, it was described how various organizations involved in the field of aircraft noise perception and annoyance research have approached quantification of the annoyance impact of current and future aircraft. Most research made use of sound quality metrics to quantify aircraft noise annoyance, which were developed for sound perception in general and were applicable to all product sounds, not just to those of the aircraft. This approach can be regarded as a logically sound approach as the metrics that were borrowed from the field of psychoacoustics for quantifying the sound characteristics of aircraft noise have been widely verified and applied to the sound engineering of products from well-established industries such as automotive and industrial design engineering. The organizations that did not make use of sound quality metrics, relied on their own psychoacoustic survey results of test audiences using either recorded or auralized sounds. Since performing new psychoacoustic surveys of aircraft noise for annoyance quantification with test audiences was beyond the scope of the current research work, it was decided to develop a capability of being able to assess the annoyance due to aircraft noise via the sound quality metrics which were briefly mentioned in Section 3.1. This is based on the findings of [48] and [43] that loudness followed by tonality best correlate with the actual psychoacoustic annoyance experienced by listeners in test environments, followed by roughness and sharpness. The observation that aircraft sounds that were both loud and tonal were perceived to be exceptionally annoying was also backed by listening to aircraft noise auralizations made for the VATSS project, where the tonal content was particularly unpleasant to hear if it also had a high intensity.

For this purpose, the noise assessment capability of INSTANT was extended to assess the aircraft noise spectra in terms of their loudness, sharpness and tonality. The sound quality metric of roughness was left out of the current implementation due to two main reasons – firstly, the temporal resolution of the flight paths created using the mission analysis module of 0.5 seconds is not small enough to capture the fast fluctuations in loudness that the metric requires; secondly, roughness of turbofan aircraft, which are the focus in the current work, is not as strong an annoyance factor as it is for propeller based aircraft. The psychoacoustic surveys performed by [43] found roughness to be the third relevant factor for annoyance experienced due to aircraft noise with loudness and tonality the more dominant factors and [48] indicated no clear correlation of annoyance with roughness of the test sounds. The methodology with which the sound quality metrics of loudness, sharpness and tonality were implemented will be explained in Section 6.1 and Section 6.2 will show community noise annoyance results for two current commercial aircraft.

6.1 Implementation of the sound quality metrics

1. Loudness:

As was mentioned in Section 3.1, loudness is the subjective perception of the magnitude of a sound. It has been shown to be a function of both intensity and frequency of the sound [51], as well as of time when the sounds are transient in nature [136]. For the current research, temporal changes in loudness in time-spans less than 0.5 s are currently neglected as the temporal resolution of aircraft noise spectra generated using INSTANT is 0.5 seconds and more detailed resolution of the flight path below 0.5 s is not realistic during a preliminary or conceptual aircraft design phase. The sound is thus assumed to be stationary over 0.5

second intervals for the simulated flight paths. For simple sounds such as pure tones, the loudness can be quantified via experiments where test subjects can estimate the magnitude of a sound on a numerical scale from low (quiet) to high (loud) or by adjusting and matching the subjective loudness of the tone with a reference tone such as a 1 kHz pure tone having a given level. The sound matching approach was used to define the loudness level, L_N of a sound by Barkhausen in the 1920s, which was defined as the sound pressure level of a 1 kHz tone that is perceived to be as loud as the given sound. The loudness level was given the unit of ‘phon’. This definition of loudness level implies that a sound which is perceived to be as loud as a 1 kHz tone having an SPL of 60 dB would have a loudness level of 60 phon. The matching approach was also used to construct the ‘equal loudness contours’, which display the *non-linear frequency sensitivity* of the human ear [137], and were shown previously in Fig. 2.2.

The equal loudness contours capture some important aspects of the human hearing system regarding how loudness is perceived. They show for instance that the threshold of hearing (shown in Fig. 2.2 as ‘minimum level’) is lowest from 3000 to 4000 Hz, indicating that the human ear is most sensitive at and around these frequencies. The equal loudness contours also show that at low frequencies, the threshold of hearing is higher, implying that low frequency sounds have to have higher levels before they are noticed by the human ear and also that low frequency sounds have to have higher levels to be considered as loud as higher frequency sounds. One important aspect the contours also show is that at 1000 Hz and above, the spacing between the individual curves is about 10 dB whereas the difference at frequencies below 1000 Hz, particularly at 200 Hz and below, the spacing between the individual contours is much lower. This implies that an increase in level at low frequencies will be perceived as a higher change in loudness than at high frequencies. Applied to aircraft noise, this observation implies that fan tones typically occurring at 1000 Hz and above could have an increased level and still be perceived as loud as before, while low frequency jet noise would be perceived as clearly louder with the same increase in level. The loudness level expressed in phon is on a logarithmic scale. Stevens [138] proposed the unit of ‘sone’ for loudness, N when it is to be expressed linearly.

Another important characteristic to consider while determining the perceived loudness of a sound is the *masking* of sounds due to the presence of other sounds. Masking is the decrease in the audibility of one sound due to the presence of another sound. In general low frequency sounds mask high frequency sounds if they both are present at the same time. A tone or a narrowband sound will mask a range of frequencies located around it, with frequencies which lie above the center frequency being masked much more effectively than frequencies that lie below the center frequency.

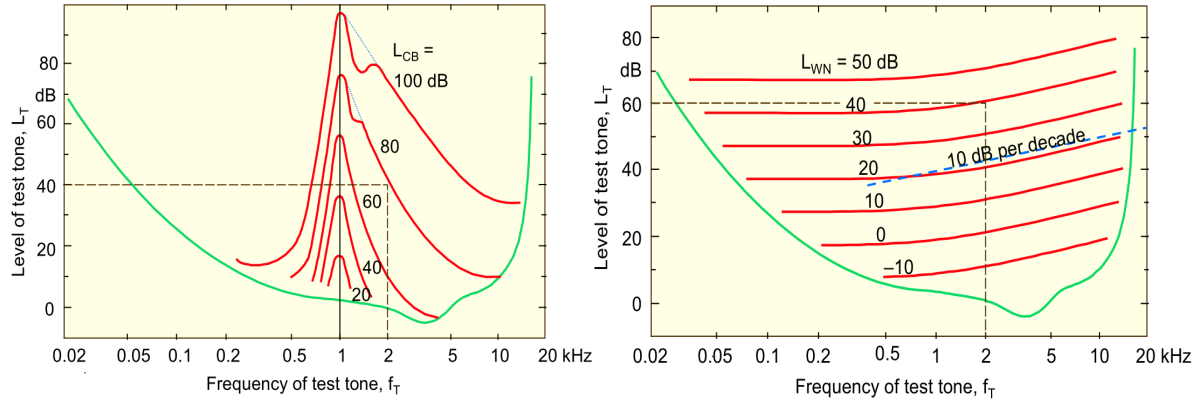


Figure 6.1: Masking of a 2 kHz test tone due to narrowband noise centered at 1 kHz (left) and due to white noise (right) [139] – CB refers to the critical band and WN to white noise

The left part of Fig. 6.1 shows this phenomenon for a test 2000 Hz pure tone having a level of 40 dB. It can be seen that the masking narrowband noise centered at 1000 Hz will mask this tone if it has a level of 80 dB or above, thereby displaying the ‘upward’ spread of masking. Any other tone or narrowband noise will have its own masking pattern (more effective to the right) and will affect the audibility of tones that lie at higher frequencies in the spectrum. For aircraft noise this implies that any fan or LP turbine tone that occurs will have the potential to either completely or partially mask other tones and harmonics that lie at higher frequencies than its own frequency. The right part of Fig. 6.1 shows the corresponding masking effect of white noise. Broadband white noise is seen to mask all frequencies, with a horizontal curve till approximately 500 Hz and a 10 dB per decade slope for frequencies above 500 Hz. It can be seen that a 2000 Hz tone having a level of 60 dB will in this case be masked by white noise having a lower level of 40 dB. The implication of this observation is that broadband noise such as jet noise is very effective in masking pure tones or narrowband sounds such as fan tones. The two observations that tones can mask each other and that surrounding broadband noise can mask individual tones will also have an influence on the tonality of the sound, as will be explained later in this section.

For complex sounds such as those produced by the aircraft and engine (consisting of both broadband and multiple tonal noise components), the *critical band* and *critical bandwidth* come into play, which are important for determining the masking effects and also for computation of the overall loudness experienced by the human ear. The human hearing system divides the audible frequency range into a series of frequency bands which are called critical bands (or ‘Frequenzgruppen’ originally in German) and the critical bandwidth of each critical band corresponds to the frequency resolution of the ear. Two tones present within the same critical band will not be heard as two separate sounds and the sounds will affect each other’s perception due to masking. The perception of loudness for a narrowband noise is seen to be unchanged if the bandwidth of the noise is less than the critical bandwidth, but once the bandwidth becomes wider than the critical bandwidth, the sound is perceived to be louder at the same overall level. This is demonstrated in Fig. 6.2 for a band-pass noise centered at 2000 Hz and having an overall level of 47 dB. The bandwidth of the noise is gradually increased till it exceeds the critical bandwidth (at around 250 Hz), resulting in an increase in perceived loudness from that point onwards.

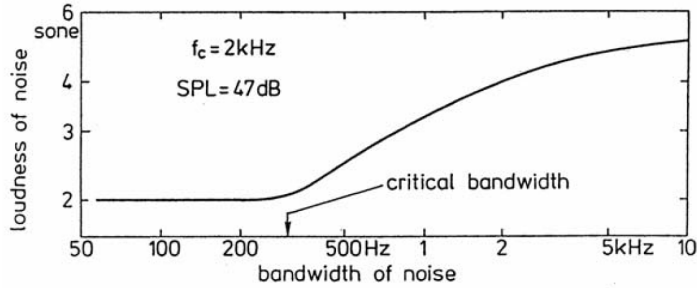


Figure 6.2: Effect of critical bandwidth on the loudness perception of band-pass noise [140]

The critical band scale has a range from 0 to 24 and critical bands (with symbol z) are measured in the unit Bark. On the Bark scale, which is used by most loudness calculation methods to compute the overall loudness, the level is plotted against frequency on a linear scale from $z = 0$ to 24 rather than logarithmically when frequency in Hz is used as the abscissa. The first critical band covers the frequency range of 0 - 100 Hz while the last critical band covers the high frequency range of 12000 – 15500 Hz. Up to a frequency of 400 Hz, the critical bandwidth has a constant value of 100 Hz and for all frequencies above 500 Hz, the critical bandwidth gradually increases as a percentage of the center frequency, roughly approximated as 20%, as is shown in Fig. 6.3. The contiguous critical band number z in Bark corresponding to the given frequency in Hz can be computed using Eq. 6.1, and Eq. 6.2 computes the critical bandwidth, CBW .

$$z = 13 \tan^{-1} \left(0.76 \frac{f}{1000} \right) + 3.5 \tan^{-1} \left(\frac{f}{7500} \right)^2 \quad (6.1)$$

$$CBW = 25 + 75 \left(1 + 1.4 \left(\frac{f}{1000} \right)^2 \right)^{0.69} \quad (6.2)$$

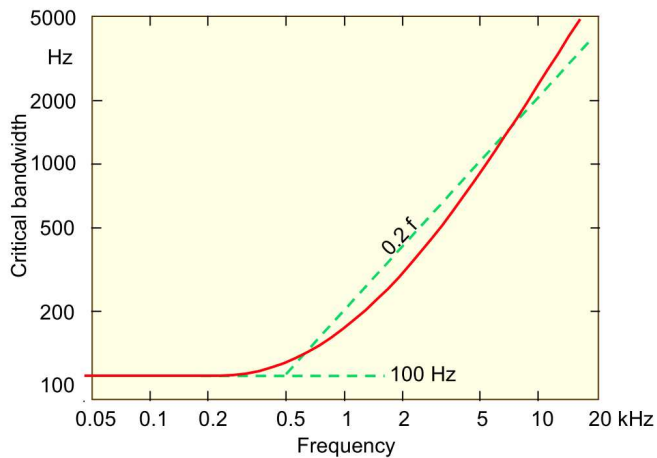


Figure 6.3: Critical bandwidth as a function of frequency [139]

The concepts of non-linear frequency sensitivity, masking and critical bands are essential in determining the loudness of a sound as experienced by the human hearing system. For the current research work, Zwicker's method as described in ISO532-B and DIN 45631 [51] has been used to calculate the loudness of the predicted 1/3 octave aircraft noise spectra on the ground. Zwicker's loudness calculation method estimates spectral masking effects besides using the knowledge on equal loudness curves, thereby providing a potential improvement over the conventional metrics by incorporating more detailed knowledge on the perception of sounds. The method was initially developed to be used graphically by manually reading predefined neural excitation level vs critical band rate curves and masking patterns, and summing up graphically the unmasked loudness contributions within each critical band to yield an overall loudness value in sone. This manual graphical procedure was automated by Zwicker et al. in [141] and then subsequently standardized.

The procedure begins with a conversion of the 1/3 octave band levels to neural excitation levels L_E in the critical bands, which is done using a correction curve for frequencies above 250 Hz. For frequencies below 250 Hz, the critical bands are broader than the 1/3 octave bands. This therefore requires summing up the 1/3 octave band levels for frequencies below 250 Hz to get excitation levels in dB representing the first three critical bands. Zwicker does this by adjusting the 1/3 octave frequency levels to levels at the critical band rate frequencies based on the corresponding equal loudness curve for that level. He then sums up the thus obtained levels till 80 Hz to get the excitation level for the first critical band, from 100-160 Hz to get the excitation level for the second critical band and from 200-250 Hz for the third critical band. The remaining 1/3 octave bandwidths correspond approximately to the critical bandwidth and the remaining 1/3 octave band levels are then also converted to neural excitation levels using the aforementioned correction curve. The method then corrects the levels according to the transmission characteristics of the outer ear and takes into account the excitation level at the threshold of hearing L_{TQ} for each critical band. This results in a *main* loudness value for each critical band, also referred to as the specific loudness N' in sone/Bark, as:

$$N'(z) = 0.0635 \cdot 10^{0.025L_{TQ}(z)} \left[(0.75 + 0.25 \cdot 10^{0.1(L_E(z)-L_{TQ}(z))})^{0.25} - 1 \right] \quad (6.3)$$

A check is made in the next step of loudness calculation, to see if the main loudness in each critical band is either partly or completely masked by the so-called *accessory* loudness, caused by the excitation over the current critical band from a sound focused on another critical band. The variation of the masking patterns as a function of the critical bands was found by Zwicker by playing pure tones surrounded by narrowband noise at varying frequencies to test audiences. The unmasked main loudness values in each critical band are thus determined and used to calculate the total loudness value N in sone, which corresponds to calculating the area under the unmasked specific loudness pattern, according to:

$$N = \int_0^{24} N'(z) dz \quad (6.4)$$

Physiologically, the summation of loudness over the critical bands corresponds to the summation of the overall neural activity evoked by the sound in the human ear. Zwicker's loudness method further takes into account whether the sound is created in a free-field (such that it approaches the observer from one specific direction), or in a diffuse field (with many reflecting surfaces corresponding to indoor environments). If a diffuse field is chosen, then a higher loudness value is observed. For the aircraft noise

spectra produced using INSTANT however, a free-field is always selected as no obstruction between the aircraft and observer is assumed.

The calculation procedure allows all 1/3 octave aircraft noise spectra propagated at the chosen ground points as produced by INSTANT to be assessed via an overall loudness value in sone, as well as in the corresponding loudness level in phon, obtained by using a logarithm of base 2 of the sone value and adding 40 phon as a minimum loudness level. The simulated loudness values have been validated using publically available references such as [142] and both reference and simulated values are shown for sample spectra in Table 6.1.

2. Sharpness:

Sharpness is a measure of the high frequency content of a sound and can be of relevance when a product's sound has considerable high frequency content. A sound is therefore perceived to be 'sharper' when it has more high frequency content than low frequency content. For aircraft noise, it was seen from other studies that sharpness is the fourth relevant sound quality attribute and although it doesn't show a clear correlation with the experienced annoyance due to aircraft noise, it is still a useful metric in that it shows when high frequency noise is starting to gain prevalence in the aircraft noise spectra. The primary high frequency aircraft noise components are the fan and LP turbine, as modeled in this dissertation. The sharpness metric can therefore show, in addition to the more important loudness and tonality metrics, when high frequency fan noise has increased relative to the dominant low frequency components such as jet noise and airframe noise. This will be shown by an increase in the sharpness value.

The sharpness metric has been implemented in INSTANT based on the method of von Bismarck [52], although since the sharpness metric has not been standardized as yet, other methods such as those of Zwicker and Fastl [44] and of Aures [49] also exist. Von Bismarck's method (as well as the other methods) makes use of a weighted first moment of specific loudness. A weighted partial first moment at critical band z is computed as $\int_0^{24} g(z)N'(z)z dz$ where $g(z)$ is the sharpness weighting function given by Eq. 6.5, as used in the method of von Bismarck. It can be seen that in the weighting function, all spectral content at or above 16 Bark (at least 2700 Hz and above) is weighted more heavily by the weighting function, which was determined using psychoacoustic tests carried out by von Bismarck. The overall sharpness value for a given spectrum is then calculated using Eq. 6.6, where the constant c has a value of 0.11. The sharpness metric has the unit of acum, such that a narrowband noise one critical band wide, centered at 1 kHz and having a level of 60 dB has a sharpness value of one acum.

$$g(z) = \begin{cases} 1 & z \leq 16 \\ 0.066 e^{0.171z} & z > 16 \end{cases} \quad (6.5)$$

$$S = c \left[\frac{\int_0^{24} g(z)N'(z)z dz}{N} \right] \quad (6.6)$$

As for the Zwicker's loudness metric, the sharpness values obtained using INSTANT have been validated using publically available references such as for the sharp and less sharp sound spectra shown in [56] and reproduced in Fig. 6.4. The comparison of simulated and reference sharpness values is also shown in Table 6.1.

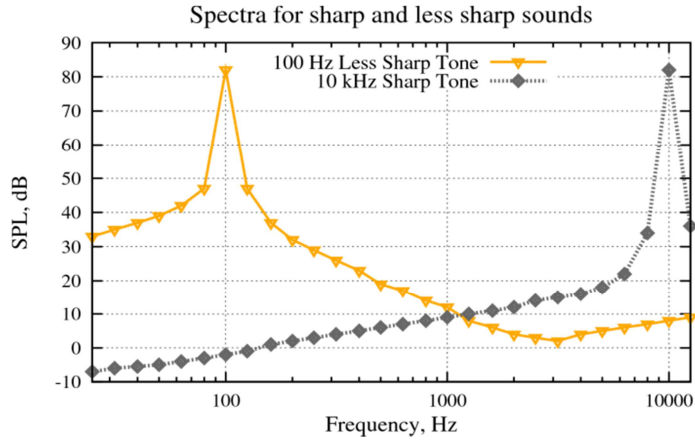


Figure 6.4: Sample spectra for sharp and less sharp sounds used for loudness and sharpness validation [56]

Table 6.1: Comparison of reference [56], [142] and INSTANT simulated OSPL, loudness and sharpness values for sample spectra from Fig. 6.4

	100 Hz tone spectrum		10000 Hz tone spectrum	
Metric	Value - Simulated	Value – Reference	Value - Simulated	Value – Reference
OSPL [dB]	82.0	82.1	82.0	82.3
Loudness [sone]	11.05	11.05	7.89	7.89
Sharpness [acum]	0.31	0.31	7.00	7.49

3. Tonality:

As was mentioned earlier, the tonal content of aircraft noise is a major contributing factor towards the annoyance experienced due to aircraft noise. The PNLT and EPNL metrics described in Chapter 2 account for the perceived annoyance due to aircraft tonal noise via the tone penalty, which depends quite broadly on the frequency and level of the strongest tonal component above the broadband noise. It was reasoned in Section 2.2 that accounting for the tonal content's contribution to actual perceived annoyance could be improved upon if the frequency of the tones, the tonal prominence level, the number of tones and the magnitude of the penalty added due to protruding tones were accounted for in a better way. From the annoyance studies carried out by Angerer et al. [48] and More et al. [43], it was found that the annoyance due to aircraft tonal noise could be predicted with a reasonably high correlation by the tonality metric developed by Aures in 1985 [49]. As such, Aures' tonality metric was implemented alongside the sound quality metrics of loudness and sharpness in order to attempt to capture the annoyance due to tonal content of aircraft noise in an alternate way compared to the PNLT and EPNL metrics. The goal here is to see if Aures' tonality metric can capture aircraft tonal characteristics in a better or more comprehensive way than the conventional metrics currently used in the aerospace industry, improving upon their identified deficiencies. Several methods of accounting for the tonal content of product spectra besides Aures' tonality metric also exist, such as the tone-to-noise ratio [143], prominence ratio [144] and Joint Nordic Method [145], each of which attempt to capture tonal content in slightly differing ways. From all of these metrics, Aures' metric was implemented in INSTANT's noise assessment component as it is a

recognized ‘sound quality’ metric and has been used for analyzing the sound quality of various products from the automotive and industrial design fields. Furthermore, Aures’ tonality metric is also one that attempts to use the most detailed knowledge of psychoacoustics and sound perception compared to the other tonal content metrics, and thus proposes the highest potential for a possible improvement over the tone-penalty method used in the PNLT and EPNL metrics.

The method developed by Aures for quantifying the tonality (‘Klanghaftigkeit’ in German) of noise has been outlined in [49]. Aures made use of a number of test sounds consisting of pure tones and band-pass noise with a small bandwidth of 30 Hz and a large bandwidth of 1000 Hz to quantify the influence of tonal prominence, frequency, bandwidth as well as loudness relative to overall spectral loudness on how tonal a sound was perceived to be. Based on the psychoacoustic survey results, he developed a method which could objectively predict with a high degree of correlation how tonal a sound is perceived to be subjectively.

The method firstly requires an identification of the tonal components present in the spectrum, when overall spectra are obtained from measurements. This is due to the fact that unless detailed knowledge of the source noise is available, it is not known beforehand which tonal components are present in the spectra and what their magnitudes are. The method thus requires the identification of pure tones as well as narrowband noises with bandwidth less than the critical bandwidth, which the human ear also perceives to be tonal by considering all spectral components which protrude by at least 7 dB above the levels of neighboring narrowband samples. This process of tonal identification is however simplified using parametric source noise models used in INSTANT as the tones from the fan and LP turbine are modeled at their individual frequencies already at the source noise modeling stage, before being propagated to the observer on the ground. This removes the need to ‘extract’ tonal components and estimate their magnitudes from the overall aircraft noise spectra, as is traditionally done when using Aures’ tonality metric.

The second step in Aures’ tonality calculation method is to identify the SPL excess of each tonal component so as to only consider those tones which are *aurally relevant* for tonality calculation. Aures based the SPL excess calculation on the procedure of Terhardt et al. [146], which is used in the calculation of the perceived virtual pitch of tonal sounds. The aural relevance of tones is determined based on their actual level, the mutual masking effects of all tones present in the spectrum, the masking effect of broadband noise surrounding each tone and the level above the threshold of hearing. The SPL excess ΔL_i in dB is calculated using Eq. 6.7 and only those tones are considered aurally relevant for which the SPL excess value is greater than zero.

$$\Delta L_i = L_i - 10 \log_{10} \{ [\sum_{k \neq i}^n A_{Ek}(f_i)]^2 + E_{Gr}(f_i) + E_{HS}(f_i) \} \quad (6.7)$$

In Eq. 6.7, L_i is the actual SPL of the i^{th} tonal component in dB, with $i = 1$ to total number of tones n . The term A_{Ek} is referred to as the amplitude of the secondary neural excitation at frequency f_i due to a k^{th} tonal component and is calculated using Eqs. 6.8 – 6.10. A_{Ek} is calculated for each tone to determine what excitation the current tone causes at other tonal or harmonic frequencies, thereby affecting their perceived magnitude. The sum of all the secondary excitations therefore takes into account the combined effect of all tonal components and how they may influence each other’s perceived intensity via mutual masking. $L_{Ek}(f_i)$ is the secondary excitation level at tonal frequency f_i , and is obtained using Eq. 6.9 where z_k and z_i

are the k^{th} and i^{th} critical band rates and L_k is the SPL of the k^{th} tonal component in dB. The term s is the steepness of the slope of the excitation level-critical band rate pattern in dB/Bark, given by Eq. 6.10 (note that the frequency f_k in Eq. 6.10 has to be provided in Hz).

$$A_{Ek}(f_i) = 10^{\frac{L_{Ek}(f_i)}{20}} \quad (6.8)$$

$$L_{Ek}(f_i) = L_k - s(z_k - z_i) \quad (6.9)$$

$$s = \begin{cases} 27 & f_i < f_k \\ -24 - \frac{230}{f_k} + 0.2L_k & f_i > f_k \end{cases} \quad (6.10)$$

The term E_{Gr} in Eq. 6.7, used for calculating the SPL excess, is the masking intensity of the broadband noise surrounding each tone. It is calculated as the sum of the broadband noise intensities surrounding the i^{th} tonal component from $z_i - 0.5$ Bark to $z_i + 0.5$ Bark i.e. one Bark around it. The remaining term in the SPL excess calculation is the intensity at the threshold of hearing, E_{HS} , which is calculated using Eq. 6.11 for each tonal frequency f_i expressed again in Hz.

$$E_{HS}(f_i) = 3.64 \left(\frac{f_i}{1000} \right)^{-0.8} - 6.5 e^{-0.6 \left(\frac{f_i}{1000} - 3.3 \right)^2} + 10^{-3} \left(\frac{f_i}{1000} \right)^4 \text{ dB} \quad (6.11)$$

All tones for whom ΔL_i is less than or equal to 0 are considered aurally irrelevant and are not used further for calculating the prominence weighting function $w_3(\Delta L_i)$, using Eq. 6.12. The exponent 0.29 in Eq. 6.12 was obtained by Aures after he optimized the results of the psychoacoustic surveys for determining the tonality of various sounds.

$$w_3(\Delta L_i) = \left(1 - e^{-\left(\frac{\Delta L_i}{15} \right)} \right)^{0.29} \quad (6.12)$$

Aures reasoned that the perception of how tonal a sound is would depend besides on its level or prominence also on the frequency of the tonal component as well as its bandwidth. The first effect, namely the dependence of tonality or tonal annoyance on frequency was acknowledged also for the conventional metrics such as the PNLT metric, although in a relatively broad way, as was explained earlier. Aures developed an analytical relation between the tonality and frequency of pure tones having only one tonal component (i.e. no harmonics) and converted this into a frequency weighting function $w_2(f_i)$ shown by Eq. 6.13.

$$w_2(f_i) = \left[\sqrt{1 + 0.2 \left(\frac{f_i}{700} + \frac{700}{f_i} \right)^2} \right]^{-0.29} \quad (6.13)$$

The equation relating the frequency weighting function with frequency presented in Eq. 6.13 has been applied by most psychoacoustic analysis software as well as organizations that have implemented Aures' tonality metric such as [147]. Fig. 6.5 (left) shows the variation of relative tonality (with reference to a 14 sone 1000 Hz pure tone) with frequency in the Bark scale visually, as was shown by Aures in his original paper. It can be seen that tonality peaks from around 5 Bark to 9 Bark (approximately 400-1000 Hz) and decreases by up to 40% for high frequencies of 7000 Hz (i.e. 21 Bark) and above. It can also be seen in

Fig. 6.5 (left) that the psychoacoustic results showed much lower tonality values for narrowband noises having a bandwidth of 30 Hz with peak values about half those for pure tones. Little to no tonal perception was observed for band-pass noises having a bandwidth of 1000 Hz and for high-pass noise with a lower cut-off frequency of 2000 Hz.

The effect of bandwidth on the tonality of sounds is shown in Fig. 6.5 (right) with the bandwidth Δz shown as a percentage of the critical bandwidth. It can be seen that a pure tone with $\Delta z = 0$ has the highest tonal perception and the tonality gradually decreases as the bandwidth is increased. This effect of bandwidth on the tonality of sounds was converted by Aures into a bandwidth weighting function $w_1(\Delta z_i)$, shown by Eq. 6.14.

$$w_1(\Delta z_i) = \frac{0.13}{0.13 + \Delta z_i} \quad (6.14)$$

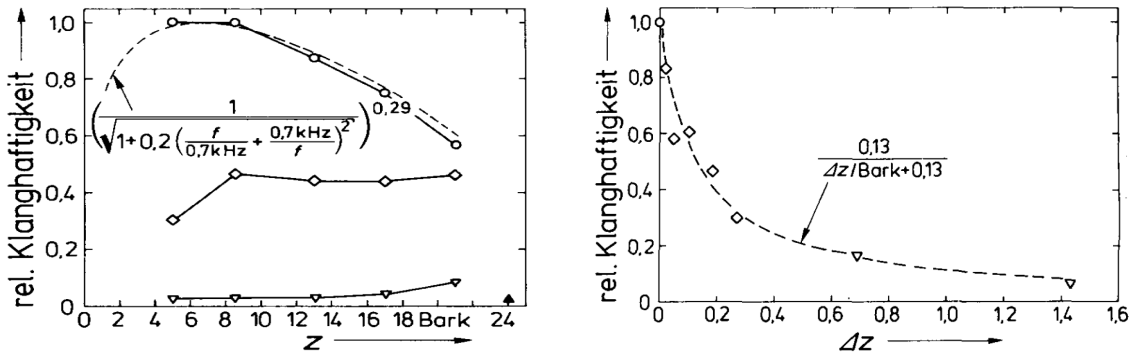


Figure 6.5: Variation of relative tonality with frequency in Bark (left) and bandwidth in Bark (right) for pure sine tones \circ , band-pass noise with bandwidth of 30 Hz \diamond , bandwidth of 1 kHz ∇ and high-pass noise with lower cut-off frequency of 2 kHz \blacktriangle from Aures' original paper [49]

The three weighting functions for the tonal prominence, frequency and bandwidth are then combined into an overall tonal weighting function w_T using Eq. 6.15, where w'_i ($i = 1, 2, 3$) is given by $w'_i^{1/0.29}$.

$$w_T = \sqrt{\sum_{i=1}^n [w'_1(\Delta z_i) w'_2(f_i) w'_3(\Delta L_i)]^2} \quad (6.15)$$

Aures found that the overall tonal weighting function w_T was able to predict the tonality of sounds that were composed predominantly of tonal components quite well but considerable deviations were observed for sounds that were composed of both broadband as well as tonal noise. A factor relating the loudness of the spectrum without tones, N_{Gr} was therefore introduced and its relation to the overall loudness of the spectrum composed of both tonal and broadband noise N was then used to calculate a loudness weighting function w_{Gr} according to Eq. 6.16.

$$w_{Gr} = 1 - \frac{N_{Gr}}{N} \quad (6.16)$$

This allowed the ultimate computation of the tonality K of any sound using Eq. 6.17 in tonality units t.u.:

$$K = c w_T^{0.29} w_{Gr}^{0.79} \quad (6.17)$$

The constant c in Eq. 6.17 is a calibration constant, which in order to obtain a tonality value of 1 t.u. for a reference pure tone of frequency 1000 Hz and having a level of 60 dB, has to be set equal to 1.09 [147].

In order to apply the tonality metric of Aures to the aircraft noise spectra produced by INSTANT, the procedure was automated and integrated in INSTANT's noise assessment component. This method of tonality estimation has till now never been applied to the spectra obtained using the parametric source noise models described in Chapter 4 and as such, if certain information was not available it had to be approximated.

The tones from the fan and LP turbine are obtained from the models of Heidmann and Matta and are modeled at the nearest 1/3 octave band frequency. This can affect slightly the tonal frequency weighting obtained using Eq. 6.13. However, looking at Fig. 6.5 (left), it can be seen that the frequency weighting does not change significantly for frequencies separated by less than 1 Bark. This implies that when the frequency of the tones is summed to the nearest 1/3 octave band, the error in frequency weighting towards tonality calculation would not be significant. The contribution of buzzsaw tones to the overall tonality has been neglected as they require a narrowband spectrum analysis to be performed, being more closely spaced in frequency than the more widely spaced interaction tones from the fan inlet and exhaust. The neglecting of buzzsaw tones was based on the fact that they only occur during departure when the engine has a maximum thrust setting, which occurs for a small portion of the entire departure procedure and not at all for approach procedures. As such, their analysis may require a separated focus solely on the early departure phases rather than the cumulative impact for complete departure and approach procedures as has been attempted in this dissertation. If multiple tones or harmonics are present in the same critical band, then they are summed to represent one tone with a combined SPL value. This assumption is also reasonable as tones present within the same critical band cannot be distinguished by the human ear.

The ANOPP based source noise models provide information on the tonal frequency and level, but provide no information on the bandwidth of the tonal components. A pure tone has a bandwidth of zero and with it, the highest tonal perception. The fan and LP turbine tones however are in effect complex tones as they also have their harmonics present in the generated spectra. Using a value of zero for the bandwidth Δz in Eq. 6.14 hence leads to a very high tonality value close to that of a pure tone with no harmonics. Few references are available which show tonality values of measured aircraft noise and More et al. [43] mention a measured tonality range of 0.01 to 0.4 t.u. for current commercial aircraft composing airliners, business jets and turboprop powered aircraft. Measured aircraft noise spectrograms also show that the fan tones undergo a ‘spectral broadening’ as they propagate through the atmosphere likely due to atmospheric turbulence. The tonal energy is therefore spread over a limited bandwidth around the tone rather than being focused only on one single frequency.

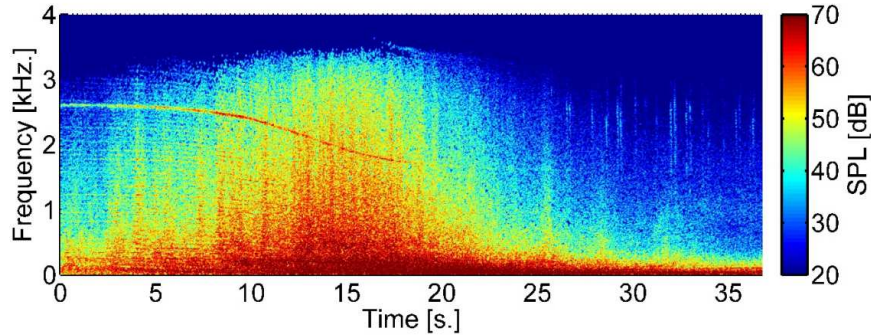


Figure 6.6: Sample spectrogram of an aircraft departure from [65]

Looking again at Fig. 6.5 (left), it can be seen that Aures presented two separate curves for the frequency weighting of a single pure tone and that of narrowband noise having a bandwidth of 30 Hz. It can be observed that the relative tonal perception of the narrowband sounds is considerably lower, between 30-50% of a pure tone's tonal perception, as mentioned earlier. As such, the tonality values of 0.01 to 0.4 t.u. can only be obtained if the engine tones are regarded as narrowband noises rather than as pure tones while calculating the tonality of aircraft noise spectra according to Aures' method.

Two tests were performed for Aures' tonality metric as implemented in INSTANT. Firstly it was verified if the metric as implemented gives correct values of tonality irrespective of bandwidth and secondly, a suitable value of the tonal bandwidth for aircraft noise spectra produced using INSTANT had to be chosen such that it would yield tonality values comparable to those produced by known commercial psychoacoustic analysis software. To test the tonality implementation independent of bandwidth, the bandwidth Δz was reduced to zero and a pure tone of frequency 1000 Hz and level 60 dB was input into INSTANT's assessment component. By definition of tonality K , a pure tone with frequency 1000 Hz and level 60 dB has a tonality of 1 t.u. and the test pure tone spectrum resulted in a tonality value of 0.9998 t.u.

Next, a calibration was decided to be performed with other software that make use of Aures' tonality metric. The tonality values produced by INSTANT for predicted aircraft noise spectra on the ground were compared with known psychoacoustic analysis software such as Sound Quality Analyzer (SQA) of Nelson Acoustic Software, for auralized audio of the same aircraft flying with the same settings, at the same ground location. The calibration showed that a constant percentage bandwidth Δz of 27.5% of the critical bandwidth around each tonal frequency yielded the best results. This corresponds to a bandwidth of 44 Hz for a 1000 Hz fundamental fan tone and to 88 Hz for the first harmonic which would occur at 2000 Hz. It was observed over the course of the research work that the fundamental tone's bandwidth was the determining bandwidth for the bandwidth weighting function $w_i(\Delta z_i)$ and a narrower bandwidth for higher frequency harmonics did not affect the overall tonality. The effect of bandwidth on tonality was also seen to primarily affect the *absolute magnitude* in t.u. but relative changes in tonality were seen to be independent of the tonal bandwidth when a constant percentage bandwidth of the tonal components was used. This implies that any relative trends in changes in tonality due to aircraft or engine design changes

will be consistent irrespective of the chosen bandwidth of the tonal components with reference to the tonality of the original design. The selection of the suitable bandwidth is however necessary to match the absolute tonality values in t.u. such that the tonality values can be used correctly in other metrics such as the modified psychoacoustic annoyance metric mentioned in Section 3.1 (see Eq. 3.4).

The comparison between tonality values for predicted spectra using INSTANT and for synthesized audio using the SQA software is shown in Table 6.2 for the 777-300 comparable Long Range (LR) aircraft powered with a GE90-85B engine model and the A320-200 comparable Short Range (SR) aircraft powered with a CFM56-5B engine. The comparison has been made for standard departure and approach flight paths simulated using the mission analysis module and simulated for ground noise impact using INSTANT. Both aircraft have been designed using MICADO and both engines have been modeled using Gasturb. The auralizations have been made using RWTH Aachen's auralization infrastructure developed for the VATSS project and tonality values exceeded 10% of the time, K_{10} have been used for the comparison.

Table 6.2: Comparison of tonality exceeded 10% of the time (K_{10}) for various aircraft and procedures between the SQA software for synthesized audio and INSTANT for predicted spectra

<i>Aircraft and procedure</i>	SQA tonality, K_{10} [t.u.]	INSTANT tonality, K_{10} [t.u.]	Difference, ΔK_{10} [%]
LR std. departure at (X,Y) = (10km, 0km)	0.19	0.20	+5.3
LR std. approach at (X,Y) = (-28km, 0km)	0.30	0.28	-6.7
SR std. departure at (X,Y) = (12km, 0km)	0.08	0.07	-12.5
SR std. approach at (X,Y) = (-30km, 0km)	0.09	0.08	-11.1

Table 6.2 shows that the INSTANT produced tonality values for propagated spectra compare well to the tonality values produced by the SQA software for synthetic audio of the same aircraft movements at the same observer locations. It can be mentioned here that the synthesized audio files do not contain airframe noise, which was not auralized during the VATSS project timeframe. The tonality values during approach, where airframe noise is the dominant broadband component, are therefore slightly higher for the synthetic audio files than for INSTANT predicted spectra which do include airframe noise. The calculated tonality values can be seen to lie within a realistic range (0.01-0.4 t.u.) and follow an expected logic such that for instance if the broadband jet noise decreases, then the tonality increases due to higher tonal prominence and reduced masking by low frequency broadband noise. The tonality is also seen to increase if more or stronger tones are present in the spectrum. Any changes in tonality can thus be explained by looking at the spectra on the ground. It is seen for the work presented in this dissertation, that the tonality of lower bypass ratio engines such as the V2527 is lower (due to the relatively higher jet noise compared to fan noise) than for a higher bypass ratio GE90 engine (for which fan noise is either as loud or louder than the jet noise due to much lower jet velocities). A similar trend is seen during the approach phase, where the tonality is much higher than during departure due to the engine thrust setting being close to flight idle and jet noise thus being much less dominant. This can also be observed in sample spectrograms of the SR and LR departure and approach flight paths, shown in Fig. 6.7 and Fig. 6.8 respectively.

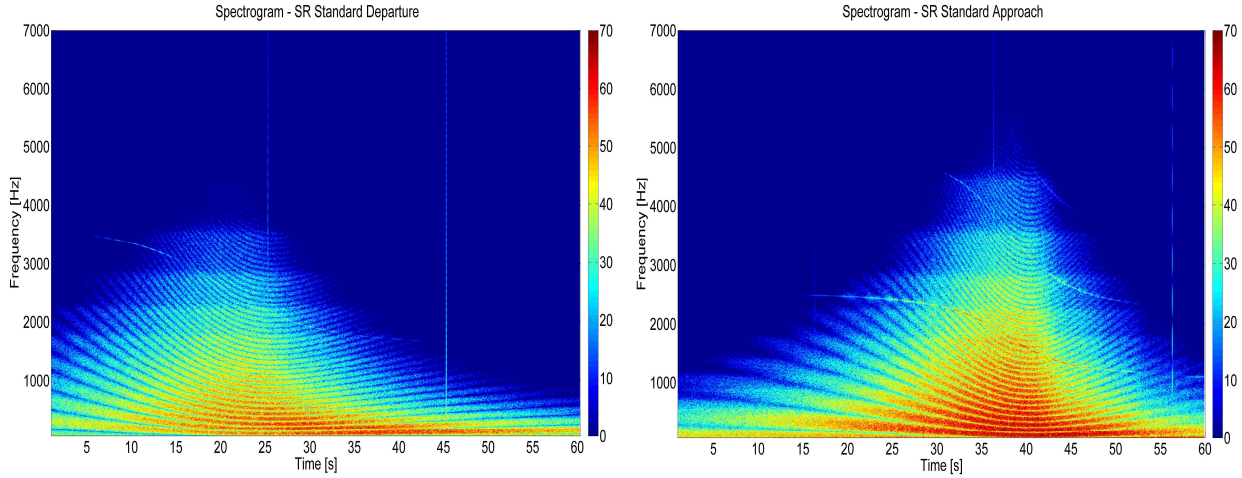


Figure 6.7: Sample spectrograms for the SR aircraft: standard departure (left) and standard approach (right)

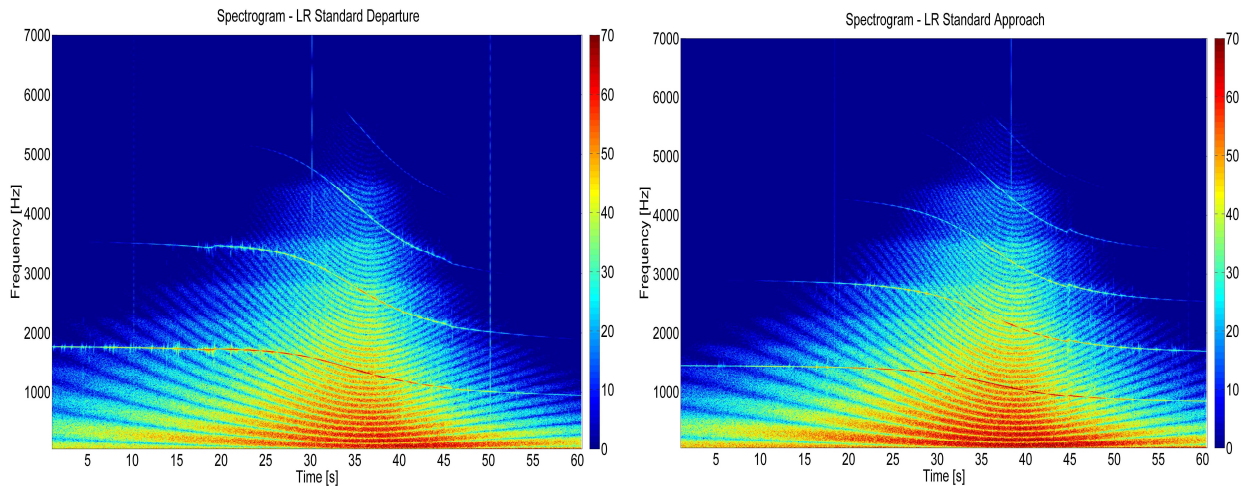


Figure 6.8: Sample spectrograms for the LR aircraft: standard departure (left) and standard approach (right)

By looking at the spectrograms, it becomes quite clear that the long-range LR aircraft is much more tonal than the short-range SR aircraft, with multiple strong tones and harmonics being present in the spectrograms (cf. Fig. 6.8). It can also be noticed in both Fig. 6.7 and Fig. 6.8 that the tones during approach are more in number and stronger in intensity than during departure for both aircraft. This fact is also reflected in the tonality values presented in Table 6.2 for both aircraft, and will also be seen in the maximum tonality value contours presented in the next section.

6.2 Community noise assessment in sound quality metrics

The sound quality metrics described in the previous section were applied to assess the annoyance impact of current commercial aircraft analogous to the community noise assessment in conventional metrics shown in Section 5.2.2. The sound quality assessment was implemented both at the certification points to see how the alternate metrics compare to the conventional metrics close to the airport and also for community noise impact for the annoyance caused further away from the airport. Figures 6.9 and 6.10 show the maximum value annoyance contours in the sound quality metrics of loudness, sharpness and tonality for the short-range A320-200 comparable SR aircraft (this time using a V2527-A5 engine model) for a standard departure and standard approach respectively. Fig. 6.11 and Fig. 6.12 show the corresponding annoyance contours for the long-range 777-300 comparable LR aircraft (using the same GE90-85B engine model used for the tonality comparison in Table 6.2). The flight profile via the altitude, LP spool speed N_1 , Mach number and primary jet velocity v_j is shown for each aircraft movement, in order to aid in understanding the corresponding annoyance impact on the ground.

Fig. 6.9 shows that for the standard departure of the SR aircraft, the maximum loudness value contour (or simply the loudness contour) in Fig. 6.9 (top) has a similar overall shape to the maximum dBA contour presented earlier in Section 5.2.2 (cf. Fig. 5.19). The contour, for the range of loudness values selected here (50-95 phon), shows a larger spread than that indicated by the dBA contour. The similarity in the dBA and loudness contour shapes can be expected as the dBA metric is based on a 40 phon loudness curve, although the loudness metric of Zwicker incorporates much more detailed knowledge of loudness perception as explained in the previous section. The maximum sharpness value contour in Fig. 6.9 (middle) gives a measure of the regions where high frequency content is dominant. It can be observed that the highest sharpness values occur immediately after brake release up until $X = 4$ km, where the engine has maximum thrust setting (shown via the N_1 variation). A cutback to maximum continuous thrust setting is made after that till $X = 9$ km, resulting in reduced sharpness values and the sharpness values decrease considerably after $X = 9$ km when the engine setting is reduced to the climb setting and the aircraft reaches higher altitudes, whereby higher frequency noise is absorbed more strongly.

The maximum tonality value contour in Fig. 6.9 (bottom) indicates that the SR aircraft during departure has a generally low tonality value, reaching a maximum of 0.09 t.u. close after brake-release in the forward direction. To the aft of the engine, tonality values are relatively low during departure due to the dominant jet noise, which masks the exhaust fan tones. The tonality values are seen to slowly reduce as the aircraft departs and reaches higher altitudes. The directivity pattern of the fan is also evident from the triangular shapes in the tonality contours showing that the maximum tonality during departure will frequently occur due to fan tones emitted in the forward directions which exceed the broadband airframe noise present in the forward axis. Airframe noise during the departure phase has a much lower intensity, as has been mentioned earlier.

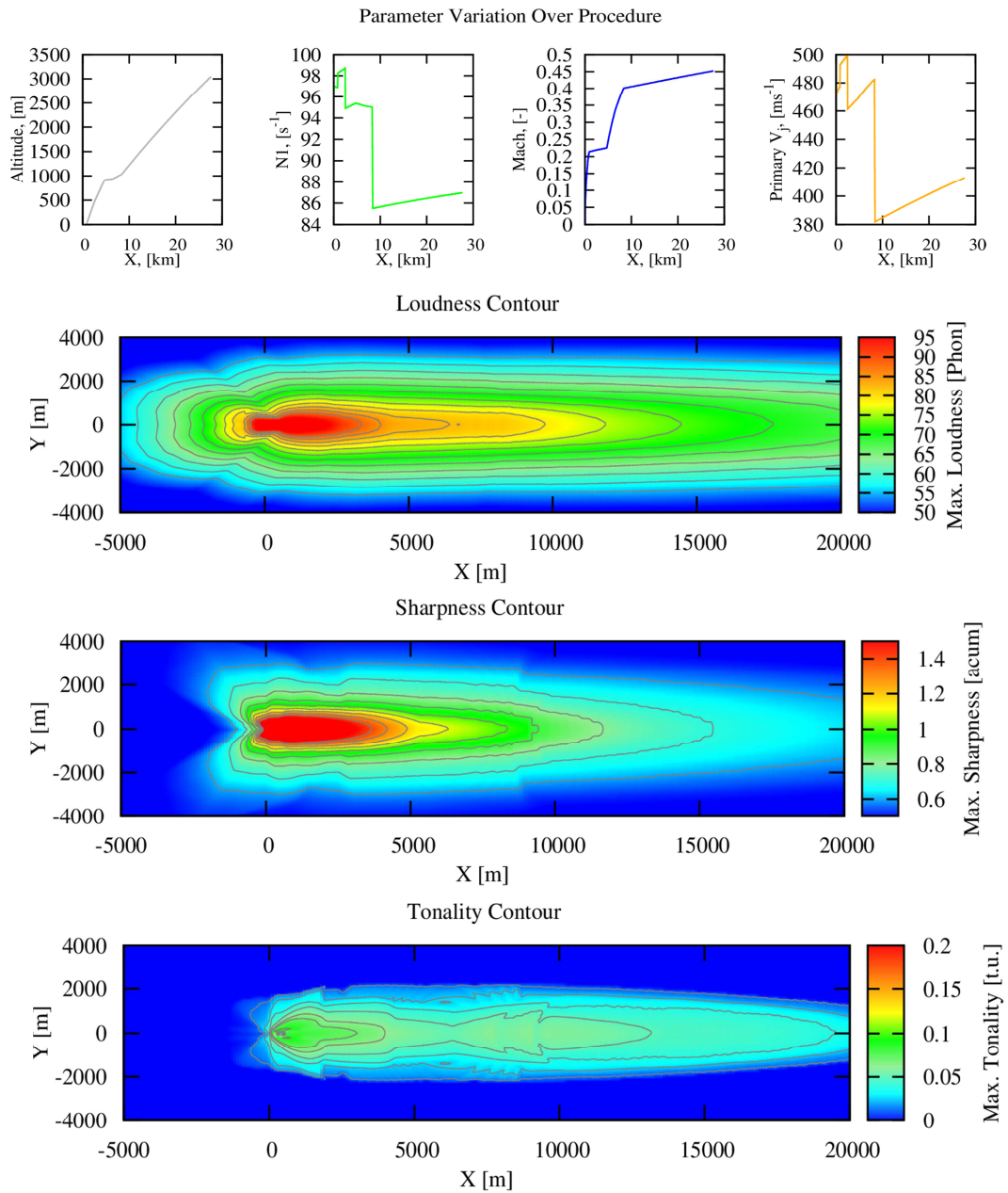


Figure 6.9: Sound quality contours for the SR aircraft standard departure: maximum loudness values in phon (top); maximum sharpness values in acum (middle); maximum tonality values in t.u. (bottom)

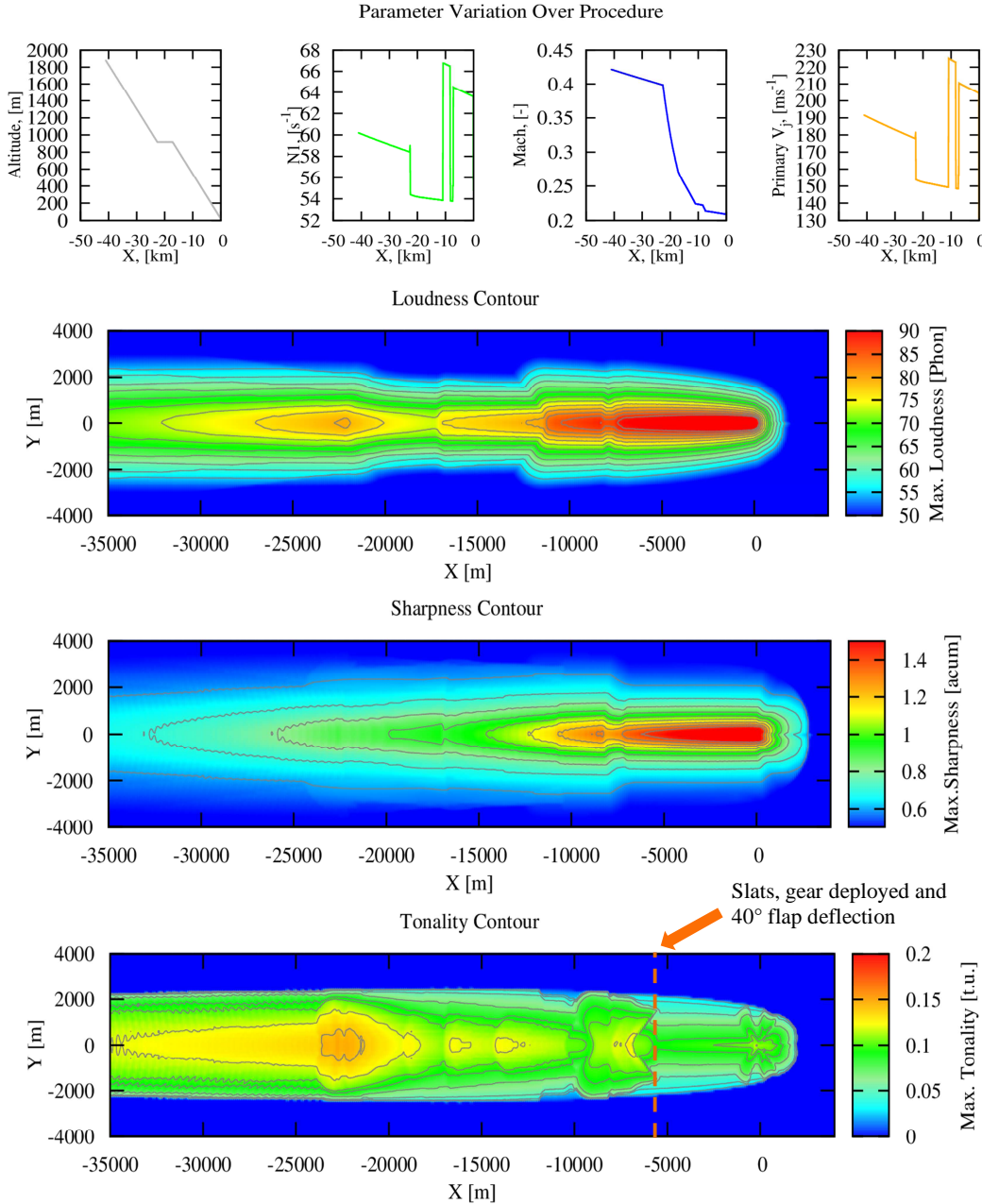


Figure 6.10: Sound quality contours for the SR aircraft standard approach: maximum loudness values in phon (top); maximum sharpness values in acum (middle); maximum tonality values in t.u. (bottom)

Fig. 6.10 shows the maximum loudness, sharpness and tonality value contours for the SR aircraft during a standard approach. Comparing with Fig. 5.20 where the maximum dBA contour for the same aircraft and movement was shown, it can be seen that the loudness contour shape during approach is even more similar to the dBA contour than what was observed for the SR departure. The spread of loudness during departure, particularly in lateral and aft directions, was seen to be greater than the corresponding dBA

contour spread, whereas it is of similar size during approach. This is explained by the fact that during departure low frequency jet noise is dominant and low frequencies are given a higher penalty by the dBA metric, thereby in effect under-predicting the low frequency impact over large distances to the side and aft of the aircraft. The loudness metric of Zwicker does not incorporate this ‘artificial’ reduction of low frequency noise. During approach, jet noise is minimal due to the low engine thrust setting and the difference between the dBA and loudness metrics then becomes less extreme, as can be seen in Fig. 6.10 (top). The sharpness contour shows that the aircraft noise becomes sharper as the aircraft descends and comes closer to the ground. Besides the sharpness increase due to increased thrust setting after $X = -9$ km, which pushes fan tones to slightly higher frequencies, the sharpness value increases in general due to the distance between the aircraft and the ground points becoming lower, thereby reducing the amount of atmospheric absorption the higher frequency components go through.

The tonality contour for the approach phase shows that the tonality values of aircraft noise spectra depend on the interplay between the broadband and tonal aircraft noise components. The tonality values increase each time the $N1$ value is reduced due to three main reasons: the shift of the fan tones to lower frequencies which are perceived as more tonal (cf. Fig. 6.5 (left)), the decrease in jet noise, which results in lower masking of the higher fan tones, and the general increase in prominence of the tones due to reduced broadband jet noise. Broadband airframe noise also affects the masking and prominence of the engine tones and in Fig. 6.10 (bottom) this is seen from a distance of $X = -5.5$ km till close to touchdown of the aircraft on the runway, where the slats as well as landing gear are deployed and the flaps have a maximum deflection of 40° . The inverse relationship between the engine setting and tonality can be seen in Fig. 6.10 (bottom) with an increase in tonality observed each time the engine setting is reduced (for instance at $X = -22.5$ km, $X = -8$ km) and an analogous decrease in tonality observed when the engine setting is increased.

The sound quality contours of the LR aircraft standard departure in Fig. 6.11 and standard approach in Fig. 6.12 show similar trends as the SR aircraft except with the metric values being significantly higher. It can be noted that the Y-axis values for the LR aircraft have been presented for 8 km on both sides of the aircraft while for the SR aircraft the lateral spread had been limited to 4 km. This is to be expected as the long-range aircraft are much heavier than short-range aircraft (the LR aircraft has an MTOW value of 299000 kg compared to the 77000 kg of the SR aircraft). Particularly the tonality values of the LR aircraft are much higher than the tonality values of the SR aircraft for both departure as well as approach, due to the higher bypass ratio of the GE90-85B engine than that of the V2527-A5 engine (cf. Table 5.1 and Table 5.2). This was also seen in the spectrograms for the LR aircraft presented in Fig. 6.8 where several strong tones were present for both departure and approach settings. The sharpness contours indicate that the LR aircraft’s sound is slightly less sharp as experienced on the ground than that of the SR aircraft, which is due to the lower optimum LP spool speed of the GE90-85B engine model (nominal $N1$ value of 2465 rpm, compared to 5650 rpm for the V2527-A5 engine model). The changes in tonality with changing thrust setting are even more evident for the LR aircraft as its fan tonal noise is at least as loud as the broadband jet noise during departure and as loud as airframe noise during approach, exceeding them for the most part. As such, the maximum tonality values during the LR approach are consistently high throughout the procedure over large distances and retain their prominence even when all airframe components have been deployed at their maximum settings from $X = -6$ km.

The goal of the sound quality or annoyance contours is to show what the annoyance impact on the ground is in terms of metrics that describe the perceived annoyance via the quality of aircraft sound, rather than simply via noise levels. Each metric contour focuses on different aircraft noise characteristics and gives an indication of the annoyance impact on residents living in airport vicinities during departure and approach procedures. By computing the area contained within contours of certain relevant threshold values of each metric, an impression can be obtained via parameter variation studies regarding how variations in aircraft design can affect the community annoyance. These parametric variations are the focus of the next chapter.

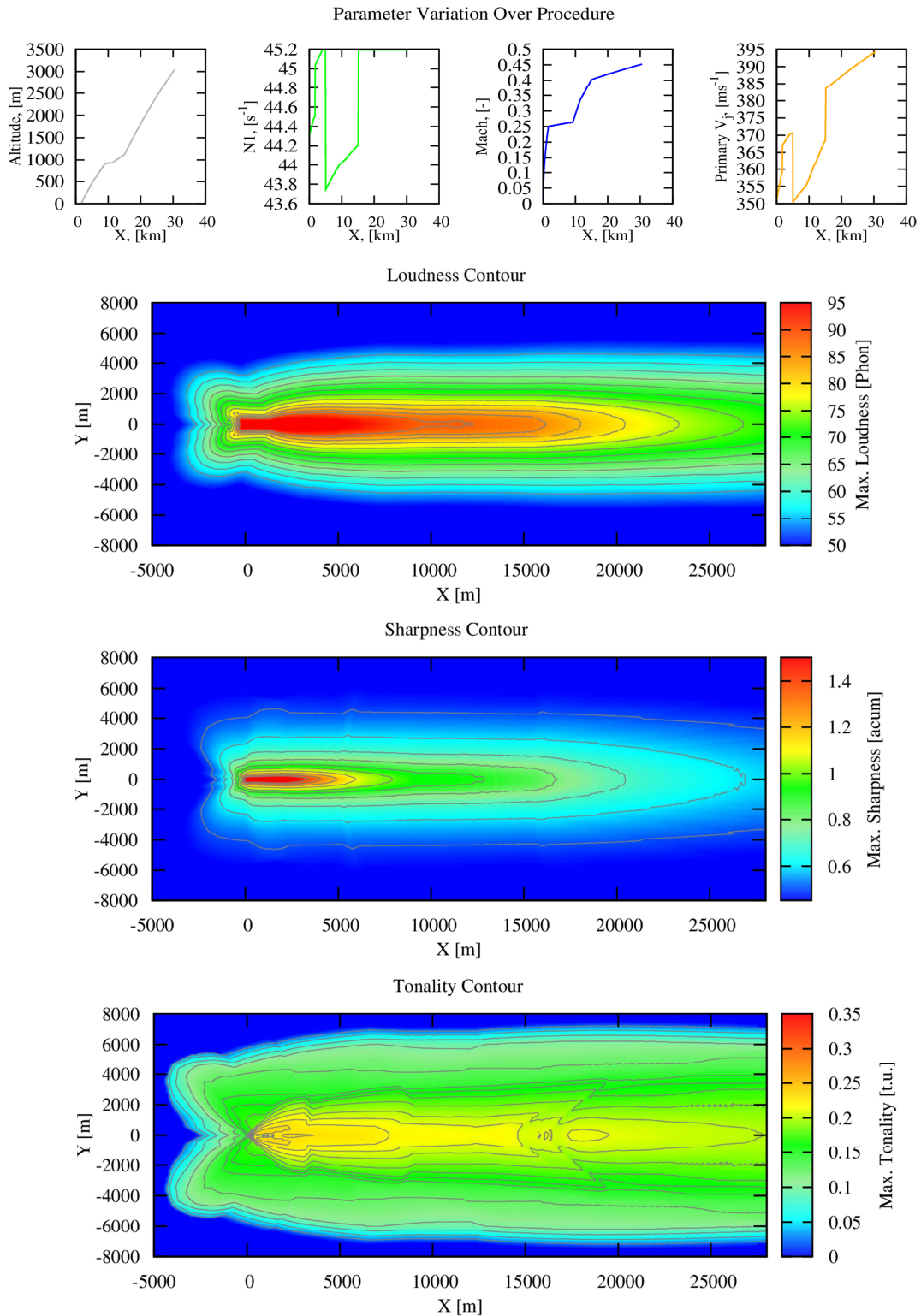


Figure 6.11: Sound quality contours for the LR aircraft standard departure: maximum loudness values in phon (top); maximum sharpness values in acum (middle); maximum tonality values in t.u. (bottom)

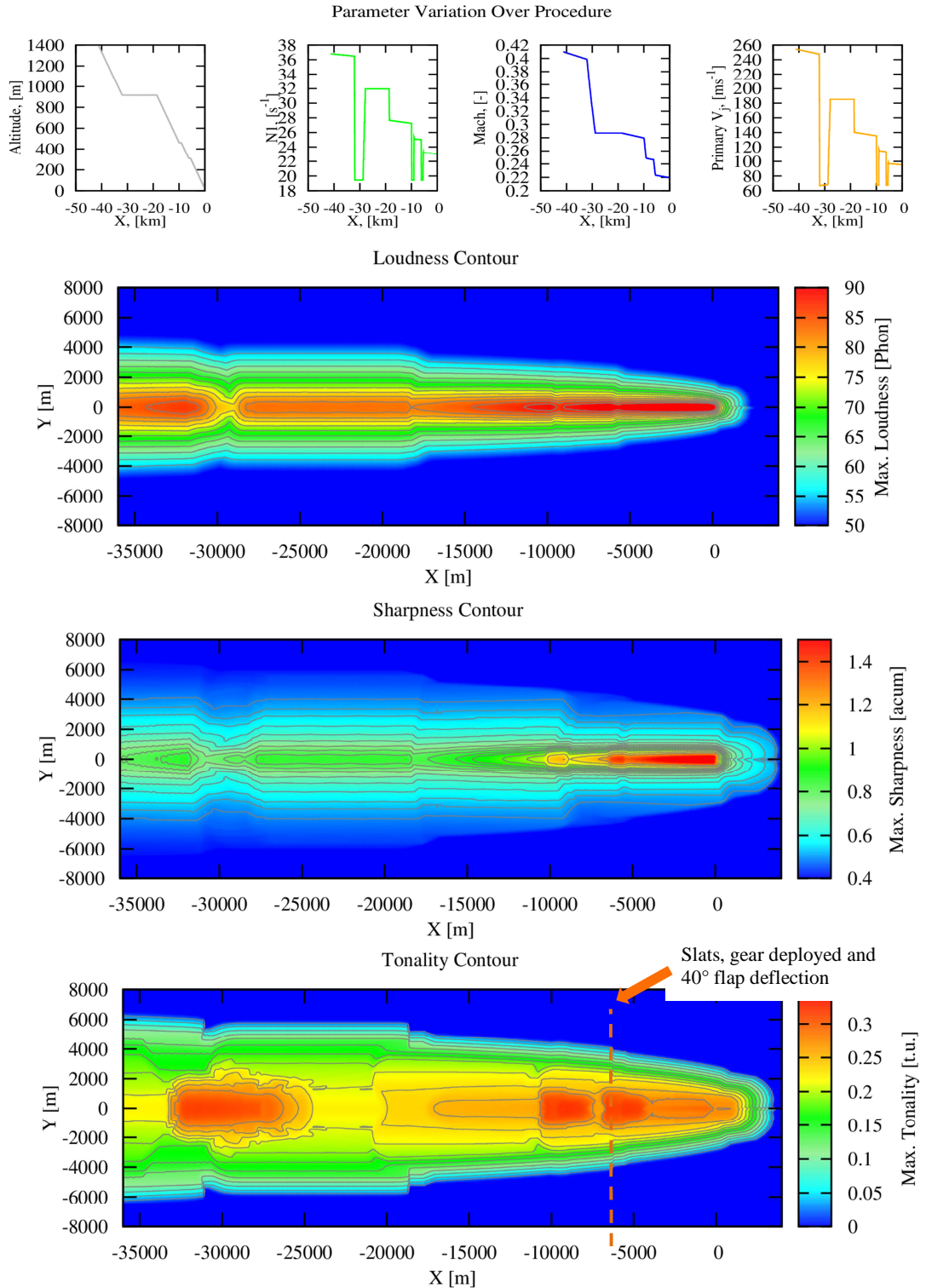


Figure 6.12: Sound quality contours for the LR aircraft standard approach: maximum loudness values in phon (top); maximum sharpness values in acum (middle); maximum tonality values in t.u. (bottom)

7 Design parameter sensitivity analysis

In the previous chapter, it was shown how aircraft noise can be assessed in an alternate way by making use of sound quality metrics that attempt to capture the annoyance due to aircraft noise by focusing on individual characteristics such as its loudness, sharpness and tonality. In order to assess aircraft noise, it was necessary to have a means of modeling the aircraft noise at the source using suitable models (as described in Chapter 4) and propagate the noise from the source to the observer on the ground (as described in Chapter 5). The source noise models as well as the propagation and assessment methodology in conventional and alternate metrics were integrated in the aircraft noise prediction environment INSTANT. In order to provide the necessary inputs to the source noise models in INSTANT over complete departure and approach flight paths, use of the aircraft design environment MICADO was made, as was explained in Chapter 5. It was explained in Section 5.1 that the *parameter study manager* module of MICADO allows the variation of relevant aircraft design parameters to follow their impact on any chosen evaluation criteria. This chapter focuses on the use of the parameter study manager module of MICADO to perform parametric variations using INSTANT of several noise relevant input parameters mentioned in Section 4.2.

Two overall aircraft design parameters – the aircraft wing-loading, W/S and the thrust to weight ratio, T/W are two primary parameters that can be varied during conceptual design and can be optimized for different goals such as fuel efficiency, range, costs or community noise impact, as was mentioned in Chapter 5. With regards to community noise impact, the wing-loading directly affects the wing and high-lift device area and hence the airframe noise produced by the aircraft and alongside this, it also affects the flight path of the aircraft. A larger wing can help in steeper departure and approach, which can lower the noise impact on the ground. The thrust to weight ratio scales the entire engine and has a very strong effect on the noise produced by the whole engine as well as by its individual components. This is due to the fact that the engine geometry parameters such as the fan diameter, number of blades and vanes, fan tip design Mach number as well as the primary and secondary jet areas among others are all scaled with the maximum producible thrust, as modeled in ILR's INSTANT. The change in geometry is also coupled with a change in the thermodynamics of the engine, which is adjusted for each design iteration by scaling the engine decks using the MICADO environment. A higher T/W can also alter the flight path by allowing the aircraft to climb out faster during departure for instance. It was found from initial overall parameter variation studies, where the T/W and W/S were varied simultaneously, that a number of changes in the ground noise impact occurred, but it was difficult to localize which design parameter had contributed to the overall change and to what extent. In this context, it was important to be able to distinguish between ground noise impact changes due to changes to the flight path, which occur if the W/S and/or T/W are changed, and changes due primarily to changes to the aircraft and engine geometry. For this purpose, two types of parametric variation studies were decided to be performed in this dissertation – uncoupled engine geometry variation studies for a constant flight path, and coupled W/S as well as coupled T/W variation studies with changing geometry and changing flight path combined. The parametric studies of engine geometry parameters were limited to the fan and jet input parameters as the combustor and LP turbine are for most community noise relevant flight phases of lower intensity than fan and jet noise. Changes in the airframe geometry are made via the wing area and span (as well as flap and slat spans and areas, as

percentage of the wing area) which are varied along with the aircraft wing-loading for the coupled parametric studies.

The analysis will focus on community noise impact (as most residents live at large distances from the runways, rather than at the certification points) with some results for noise impact at the certification points also presented. The parametric variations are shown here for the short-range SR aircraft for conciseness, with the knowledge from Section 6.2 that the trends shown by the smaller short-range aircraft also reflect the trends of the larger long-range aircraft, just with lower absolute metric values. Parametric variations for the long-range LR aircraft have been presented in a previous publication by the author [102], where it was observed for the LR aircraft that it was more difficult to reduce the much higher noise metric values of the LR aircraft via design variations, with *relative* changes being about half as large as those seen for the SR aircraft although the *absolute* reductions were on the whole as high or higher. Nonetheless, the trends in relative noise impact changes in conventional and sound quality metrics for the LR aircraft were analogous to the trends seen for the SR aircraft, when the same parametric design variations were performed.

7.1 Uncoupled parametric variation studies

In this section, the results of the uncoupled engine geometry parametric variation studies are presented, firstly for the noise impact in conventional and sound quality metrics at the flyover and approach certification points in Section 7.1.1 and secondly for community noise impacted area variation for certain threshold values of each metric in Section 7.1.2. As mentioned earlier, in order to isolate the effect of engine geometry changes from flight path changes, the flight path has been kept constant for both departure and approach analysis results in this section. To ensure that the assumption of a constant flight path for varying engine geometry remains valid, the engine geometry parameters are varied around their reference values by a maximum of 25 percent (above and below the reference SR value) such that the unchanged thermodynamics may still apply to the modified geometry of the engine fan and jet.

It was seen in Table 5.4 that acoustic liner technology plays a crucial role in the certification for noise of current commercial aircraft and considerable cumulative reductions of up to 9 EPNdB were seen to be achieved for the A320-200 similar SR aircraft. Since one of the aims of this dissertation is to see what optimization possibilities regarding annoyance due to aircraft noise exist via design changes, it was reasoned that the effect of acoustic liner material be turned off such that a comparison could be made of the gains via design changes as against gains due to the use of acoustic liner material. The parameter variation study results presented in this chapter are thus without the effect of modern acoustic liners, and lead to the design optimizations presented in Chapter 8 for both conventional and sound quality metrics. Ultimately the annoyance benefits obtained via optimized designs by considering the sound quality from an early phase are compared to those obtained via acoustic liner technology applied at a later stage.

7.1.1 Noise impact analysis at certification points

1. Departure

Figure 7.1 shows the results of the parametric variation of the fan inlet area, rotor blade number, stator vane number, fan tip design Mach number and the primary and secondary jet areas by 25 percent around

their reference values for the V2527-A5 engine model at the ICAO specified flyover certification location ($X = 6500$ m, $Y = 0$ m). The change in noise impact at the flyover point is shown by changes in the conventional EPNL and dBA metrics and also in the sound quality metrics of loudness in sone, tonality in t.u. and sharpness in acum. The reference parameter values are presented in Table 7.1 and the reference noise metric values are presented in Table 7.2.

Table 7.1: SR aircraft reference engine geometry values

Parameter Name	Symbol	Ref. Value
Fan inlet area [m^2]	A_{fan}	2.11
Number of rotor blades [-]	B	30
Number of stator vanes [-]	V	35
Fan rotor tip Mach number at design point [-]	$M_{t,d}$	1.43
Rotor-stator spacing [%]	s/C	2.75
Primary jet area [m^2]	$A_{j,1}$	0.201
Secondary jet area [m^2]	$A_{j,2}$	1.01

Table 7.2: SR aircraft reference noise metric values at the flyover certification point

Noise metric	Ref. Value
dBA	73.50
EPNL [EPNdB]	89.15
Loudness [Sone]	24.276
Tonality [t.u.]	0.0644
Sharpness [acum]	1.17

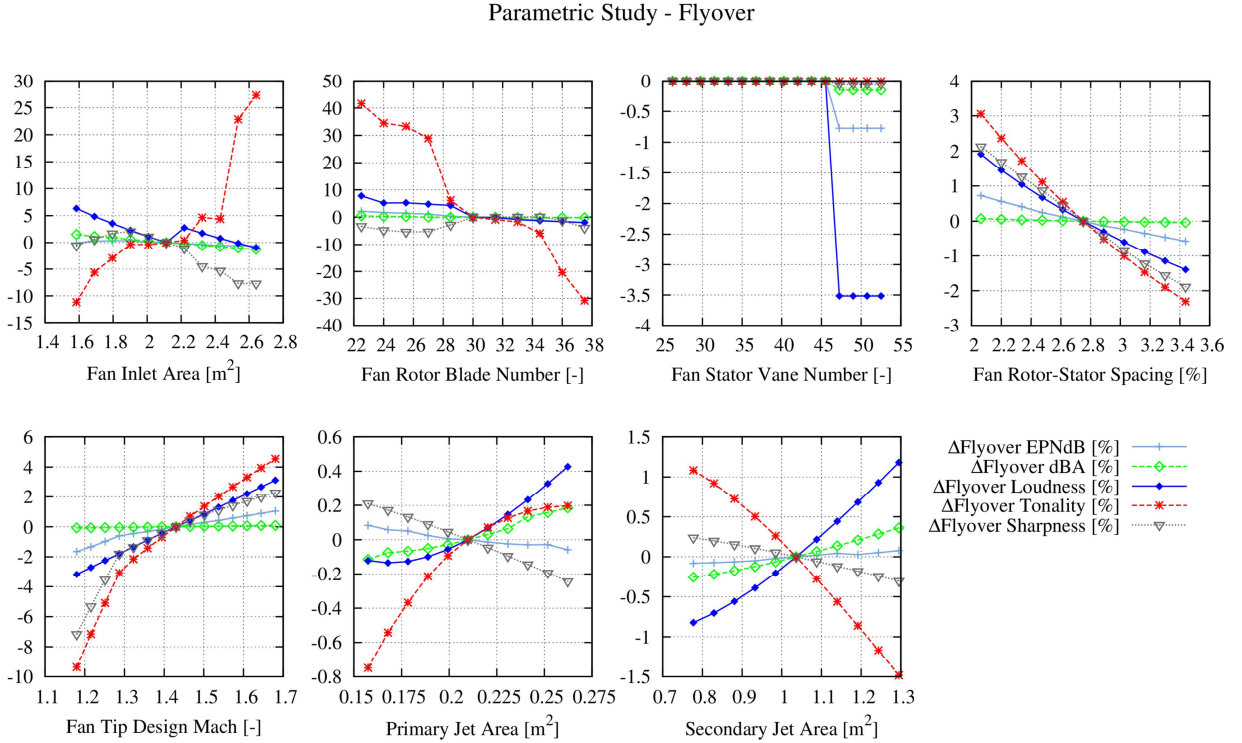


Figure 7.1: Engine geometry parameter variation results on noise impact at the flyover certification point

It can be noticed in Fig. 7.1 that for some parameters, the relative change in tonality (shown by the red curve with symbol x) is quite large, for instance due to a variation of the fan inlet area or the number of fan blades. The large changes in tonality are mainly due to the comparatively low tonality value of the SR aircraft for the takeoff engine setting (0.0644 t.u. at flyover), when the jet noise is more dominant and masks the tones more effectively, besides the tones being produced at higher frequencies due to the higher fan rotation speed. It can be seen that when the number of fan blades is increased from 30 to 38, a reduction in tonality of 32 percent to 0.0438 t.u. is observed and a reduction to 22 blades increases the tonality by 42 percent to 0.0914 t.u. This can be explained by the fact that for more blades the BPF (which is fan rotation speed multiplied by the number of blades, cf. Eq. 4.21) and all its harmonics are shifted to higher frequencies, which are weighted less strongly for tonality as was shown in Fig. 6.5 (left) by Aures' frequency weighting curve. Another reason for the higher frequency tones resulting in lower tonality values is that the higher frequencies are absorbed more strongly than lower frequencies by the atmosphere, as described earlier, and this also reduces the prominence of the fan tones as they reach the ground. The reverse is seen for lower blade numbers, which shift the fan tones to lower frequencies that are absorbed less strongly and are also perceived as more tonal. This effect was also partly seen for the tonality contours presented in Fig. 6.9 to Fig. 6.12, where it was the lower fan rotation speed during approach that shifted the tones to lower frequencies and higher tonality values. The sharpness variation (fraction of high frequency noise, shown by the gray curve with inverted triangle symbol), also aids in understanding the changes in the spectrum that occur due to lower blade numbers in that the high

frequency content is seen to reduce by up to 7%, indicating that more noise has shifted to lower frequencies.

The fan inlet area also has a strong effect on SR tonality and as the fan inlet area does not affect the frequency of the fan tones, the cause of the change in tonality is in this case the prominence of the tones as well as the masking effects of low frequency broadband noise on the higher frequency fan tonal noise. It can be seen that reducing the fan inlet area can increase the overall loudness of aircraft noise and reduce the tonality at the same time. This indicates that based on the parametric models used in this dissertation, a smaller engine is relatively louder and less tonal. It can also be seen in Fig. 7.1 that increasing the fan inlet area can increase the tonality of aircraft noise and in general will decrease the loudness, which is seen better at the approach certification point in Fig. 7.3 as well as for community noise impacted area changes in Fig. 7.4 and Fig. 7.5. This is in accordance with current trends in turbofan engines, where higher bypass ratios are being pursued which result in quieter engines having more pronounced fan noise (cf. Fig. 2.1). The use of acoustic liners to reduce the relatively higher fan noise then becomes essential. It is useful to look at the individual fan and jet noise variation at the flyover point in order to further understand what is causing the higher tonality for larger fan inlet areas. Fig. 7.2 shows the time-dependent component level variation of the noise impact in the dBA metric at the flyover certification point for the SR departure with the reference fan inlet area (left) and with the larger fan inlet area of 2.654 m^2 (right). It can be seen that the larger fan inlet area causes an approximately 2 dBA increase in the peak fan noise and a reduction by the same amount of the jet noise. This change in the spectral composition of engine noise results in the fan noise (including fan tones) becoming more prominent, resulting in the increased tonality values seen in Fig. 7.1.

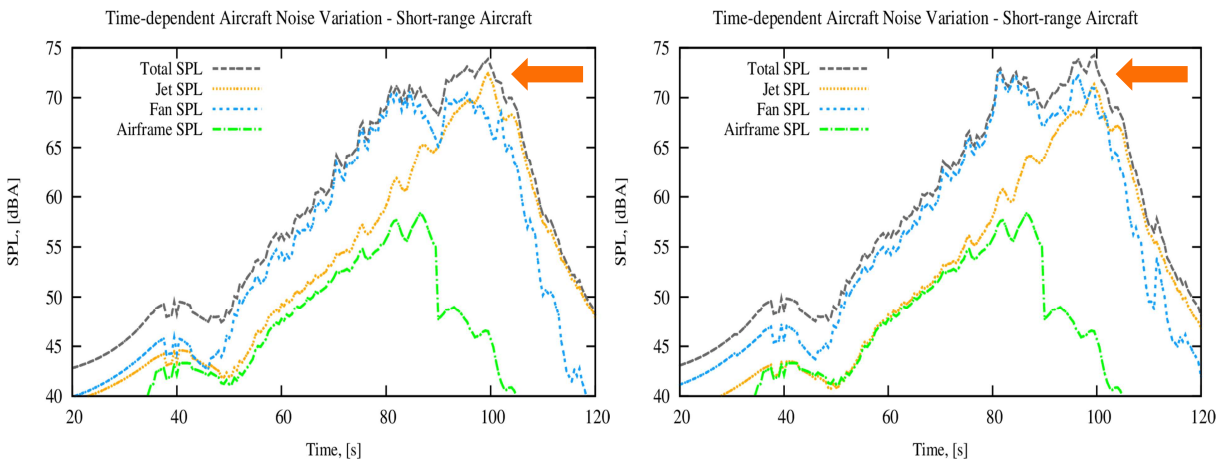


Figure 7.2: Time-dependent component level noise variation at the flyover certification point for reference fan inlet area (left) and for a larger fan inlet area (right)

The fan inlet area is an important parameter for engine noise computation and it is used in calculating the acoustic power equations for both fan noise (Eq. 4.22) as well as jet noise (Eq. 4.44) as the engine reference area A_e in Stone's model. In Eq. 4.22 it can be seen that the acoustic power radiated from the fan for all its components increases with an increase of the fan inlet area. Eq. 4.44 shows that the

reference mean square acoustic pressure for jet noise is calculated at a reference distance of $\sqrt{A_e}$. A larger fan inlet area therefore implies a larger reference distance, a reduction in the reference mean-square acoustic pressure and a reduction of the produced jet noise. Both these factors combine to increase the tonal prominence as well as in reducing the masking effects of jet noise on the fan tonal noise.

The parameters rotor-stator spacing and blade tip design Mach number present a reduction in all metrics i.e. a positive change to noise level as well as sound quality will be observed if the rotor-stator spacing is increased or the tip design Mach number is decreased. This is also consistent with current trends in the commercial engine industry, namely the fan blades being designed for lower tip speeds. An increase in the rotor-stator spacing reduces the strength of the interactions between the blade wakes and stator vanes as was mentioned in Section 4.2.1, and this reduces the radiated noise intensity from the fan. The stator vane number plays a role mainly on the tone cutoff factor δ (cf. Eq. 4.23) which decreases for a higher number of stator vanes if $V/B > 1$, which is typically the case for current turbofan engines.

Varying the primary and secondary jet areas has the primary effect of increasing or decreasing the jet noise intensity. This affects the overall loudness of the aircraft noise and it can be observed that the change in jet noise by changing the jet areas also affects the tonality, again via masking effects and altering the prominence of the fan tones. The effect of varying the primary jet area to alter the noise level or sound quality seems to be minimal at both the flyover and approach certification points (cf. Fig. 7.3). The effects are seen more clearly for community noise impacted area on the ground, especially for the approach phase in Fig. 7.4, which is shown in the next sub-section. Fig. 7.1 shows nonetheless that increasing the jet areas can increase the loudness of the aircraft noise and decreasing the jet areas can decrease the loudness (albeit only slightly at the flyover certification point). Variation of the secondary jet area also shows that a larger secondary nozzle could reduce the tonality by increasing the jet noise and reducing the fan tonal prominence. The fact that the jet noise intensity increases with the jet area is reflected in Stone's model in Eq. 4.44 and also from Lighthill's fundamental acoustic power relation in Eq. 2.2 and Eq. 4.13.

In general, for all the variation plots it can be observed that changes in the dBA and EPNdB metrics at the certification points are very minute (0-2% maximum). This could be due to the fact that the dBA and EPNdB metrics follow logarithmic scaling whereas loudness (in sones), tonality and sharpness are all scaled linearly. An approach could be to convert the dBA and EPNdB metrics to a linear scale using the relation $2^{10(\text{EPNdB}-40)}$, similar to the conversion of phon to sone. This approach was however avoided as any noise level reduction for certification is always expressed in differences of 'x' EPNdB and any other form of expressing differences in conventional metrics may not be understandable to most experts. It can also be noticed that the reductions in dBA and EPNdB metrics, although very minute for most parameters at the certification points, follow in general same trends as the loudness metric. This effect is also amplified when changes in the dBA and EPNdB metric areas on the ground are followed for design parameter sensitivities on community noise impact in Section 7.1.2.

2. Approach

Table 7.3 shows the reference noise metric values for the SR aircraft at the approach certification point (taken here as $X = -2300$ m, $Y = 0$ m). It can be noticed that all the metric values are much higher at the approach certification point than at the flyover point, which is primarily due to the approach point being

located much closer to the runway, and the aircraft being much closer to the ground ($h = 137$ m or 450 ft for the SR aircraft).

Table 7.3: SR aircraft reference noise metric values at the approach certification point

Noise metric	Value
dBA	89.56
EPNL [EPNdB]	102.20
Loudness [sone]	81.13
Tonality [t.u.]	0.106
Sharpness [acum]	1.74

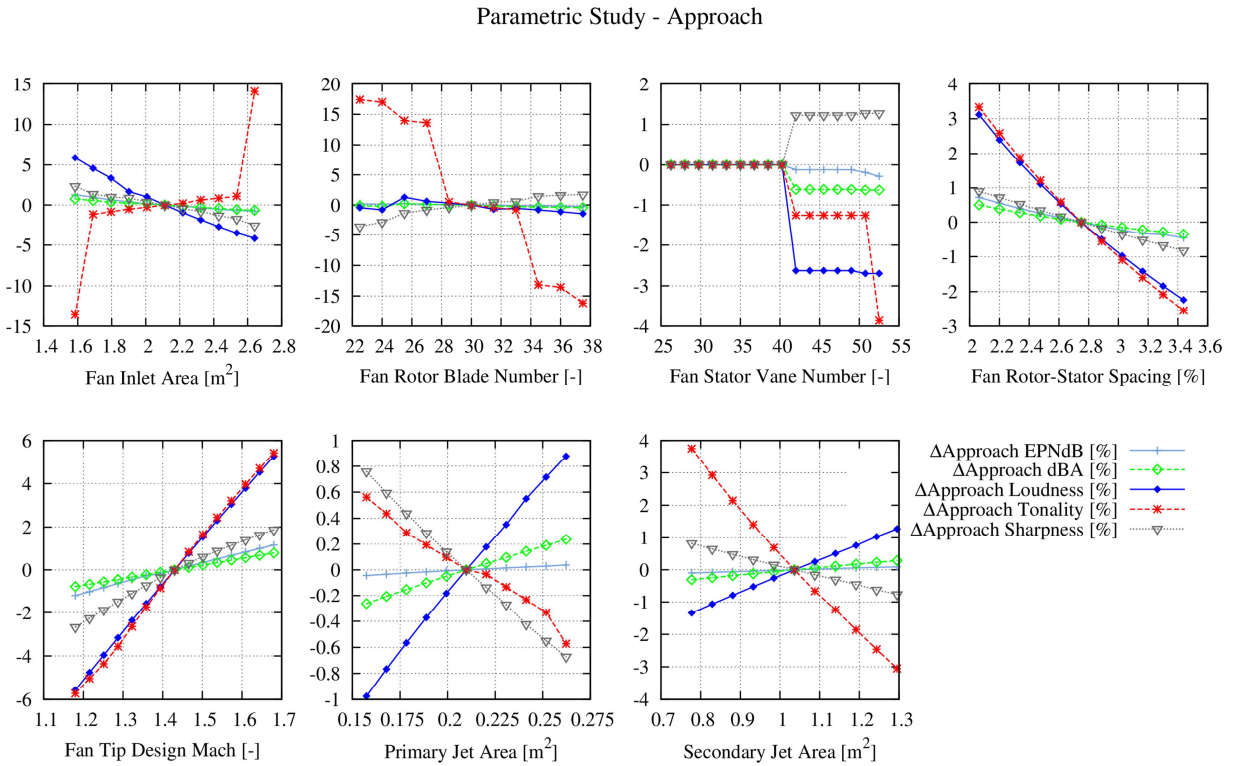


Figure 7.3: Engine geometry parameter variation results on noise impact at the approach certification point

Figure 7.3 shows the corresponding variation of engine geometry parameters and its effect on the metrics at the approach certification point. On the whole, similar trends as at the flyover certification point are observed. It is noticeable that the increase in tonality due to fan inlet area and rotor blade number changes is about half of the values observed at the flyover point for takeoff. This is explained by the fact that the maximum tonality at approach is greater (0.106 t.u.) in comparison to the maximum tonality at flyover (0.0644 t.u.) due to the relatively lower broadband jet noise and higher fan tonal noise during approach.

The relative reduction in tonality is also half as high due to changes in rotor blade number whereas it is comparable to the reduction at the flyover point if the fan inlet area is reduced. Fig. 7.3 also shows, as was seen at the flyover point, that a larger fan inlet area results in a quieter engine but also one that is more tonal. The variation of the stator vane number during approach shows that after a certain number of increased stator vanes, favorable noise reductions in most metrics can be observed, with a 4% reduction in tonality and 3% reduction in loudness. The change in primary jet area shows very small changes in the metrics at the approach point. The secondary jet area variation in Fig. 7.3 shows that a larger exhaust nozzle increases the loudness due to higher jet noise and reduces tonality due to masking and reduced tonal prominence effects. As was mentioned for the flyover point, the relative changes are still small at the approach *certification* point and are seen to be more pronounced for community noise impact.

7.1.2 Community noise impact analysis

This section presents the results of the parametric variations of the engine geometry parameters for the SR aircraft for community noise impact via the impacted area on the ground for each metric. The analysis makes use of complete departure and approach flight paths, which were simulated using the mission analysis tool, with the source noise modeled using INSTANT at each 0.5 s time-step. The propagation has been performed for observer points over a grid of 30 km x 20 km for departure paths and 40 km x 20 km for approach paths, with a ground point resolution of 100 m x 100 m. For each metric, the area in km^2 has been calculated at and above two chosen threshold values – 55 and 75 dBA for A-weighted level, 65 and 85 EPNdB for EPNL, 65 and 85 phon for loudness level, 0.075 t.u. and 0.1 t.u. for tonality and 0.75 and 1.0 acum for sharpness. Any change in the engine geometry parameter is shown by a corresponding change in the affected ground area for each metric. The main motivation to analyze community noise impact separately from noise impact at certification points was to see the effects of design variations over large distances as the certification may not be fully representative for the noise impact over large distances around the airport, as was explained earlier. The reference community noise impacted areas in each metric for the SR aircraft have been provided in Table 7.4 for a standard departure path and in Table 7.5 for a standard approach path.

1. Departure

Table 7.4: SR aircraft reference community noise impacted area for a standard takeoff flight path

Community noise impacted area [km^2]	Value
55 dBA threshold 1 area	50.4
75 dBA threshold 2 area	2.28
65 EPNdB EPNL threshold 1 area	79.56
85 EPNdB EPNL threshold 2 area	6.48
65 phon loudness threshold 1 area	84.92
85 phon loudness threshold 2 area	4.64
0.075 t.u. tonality threshold 1 area	1.84
0.10 t.u. tonality threshold 2 area	0
0.75 acum sharpness threshold 1 area	51.12
1.0 acum sharpness threshold 2 area	17.28

Fig. 7.4 shows the changes in community noise impacted area in the sound quality metrics for variations of the engine geometry. The most noticeable feature in Fig. 7.4 is the very large change in tonality impacted area for variations of the fan inlet area and number of rotor blades. Similar trends were seen at the flyover certification point, but the changes in the 0.075 tonality impacted area are much larger than the tonality changes seen at the flyover point. This is partly due to the 0.075 tonality area having a very low value of 1.84 km^2 , due to the low tonality of the SR aircraft during departure, as was seen in Fig. 6.9 (bottom). The community noise impact changes correspond nonetheless to what was observed at the flyover certification point, the main difference being in the magnitude of the changes. The variations suggest that a smaller engine (having a smaller fan inlet area) with a higher number of rotor blades could reduce the tonality impact on the ground by a considerable amount. This will be seen in a bit more detail in Chapter 8, where optimizations for minimal tonality are investigated together with optimizations for other metrics.

The trends for the variations of most engine geometry parameters are similar to the observations made at the flyover point. The loudness of the aircraft noise increases for a smaller fan inlet area, with the 85 phon impacted area increasing by up to 20%. A reduction in noise impact on the ground for all metrics is observed if the rotor-stator spacing is increased or if the fan tip design Mach number is reduced. Increasing the stator vane number results in a favorable reduction in loudness and tonality from a vane number of 47 onwards and increasing the primary and secondary exhaust areas can increase the loudness and reduce simultaneously the tonality. The effect on community noise impact of varying the primary jet area is again seen to be lower than that of varying the secondary jet area.

Parametric Study Community Noise - Takeoff

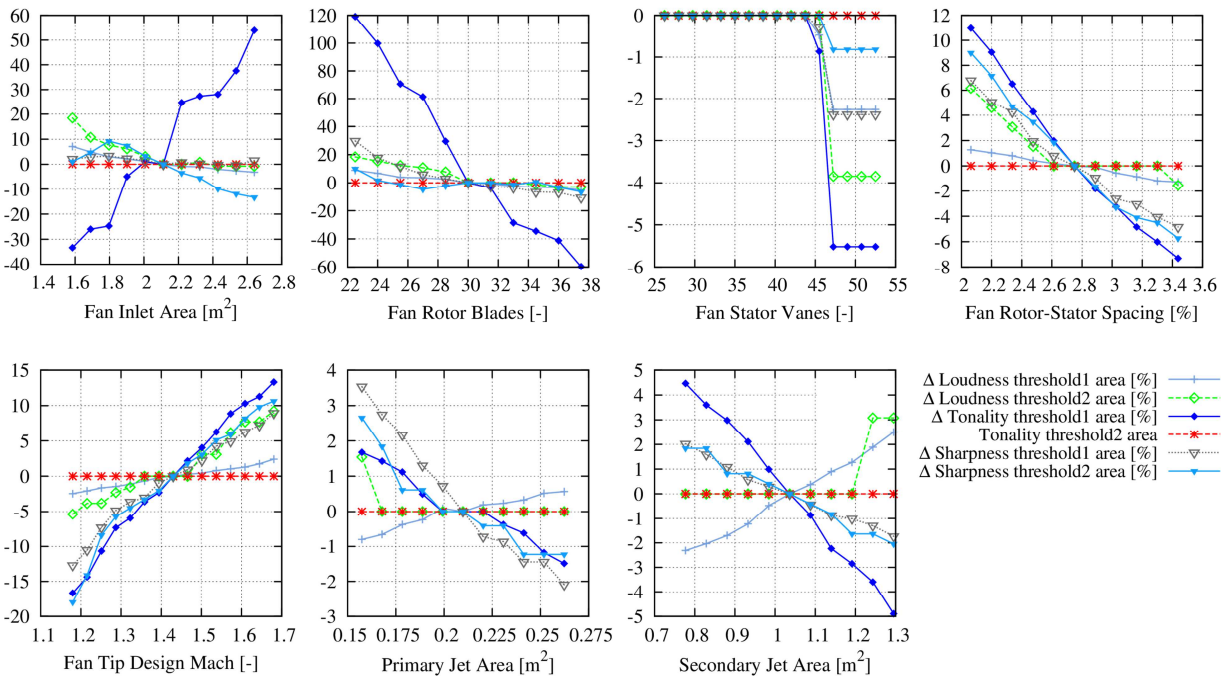


Figure 7.4: Engine geometry parameter variation results on community noise impact for a standard SR departure in sound quality metrics

Looking at the community noise impact over larger areas serves as an important confirmation of the trends seen at certification points, which showed much lower relative changes and if the motivation to make a certain geometry change was not conclusive via certification analysis, then community noise impact analysis provides the stronger evidence.

Figure 7.5 intends to show the community noise impact variation in the conventional dBA and EPNL metrics for a parametric variation of the engine geometry parameters. It can be noticed that although at certification points very minute variations in the conventional metrics were seen, the changes in terms of impacted area on the ground are more pronounced. For most parameters, it can be seen that both metrics show the same trends and when compared to the sound quality metrics, the trends follow similar variation to the loudness metric. The change in tonal content is not clearly captured by the EPNL metric as it is by the tonality metric for variations of the fan inlet area and rotor blade number. The changes in EPNL impacted area are seen to be comparable to the loudness impacted area changes for both these parameters. It can be reasoned that this occurs due to the less dominant tonal content of the SR aircraft, which does not yield high enough tonal SPL values to suffer the maximum tonal penalties in the EPNL metric. For the most part, the EPNL metric does not yield trends much different to the dBA metric in this case. Both metrics also do not show any information regarding high or low frequency content change in the spectra, information which is provided by the sharpness metric. One parameter whose variation has a significantly stronger effect on the EPNL metric is the stator vane number. An increase in the number of vanes to 47 yields a large reduction in both 65 and 85 EPNdB areas on the ground of 18% and 22% respectively.

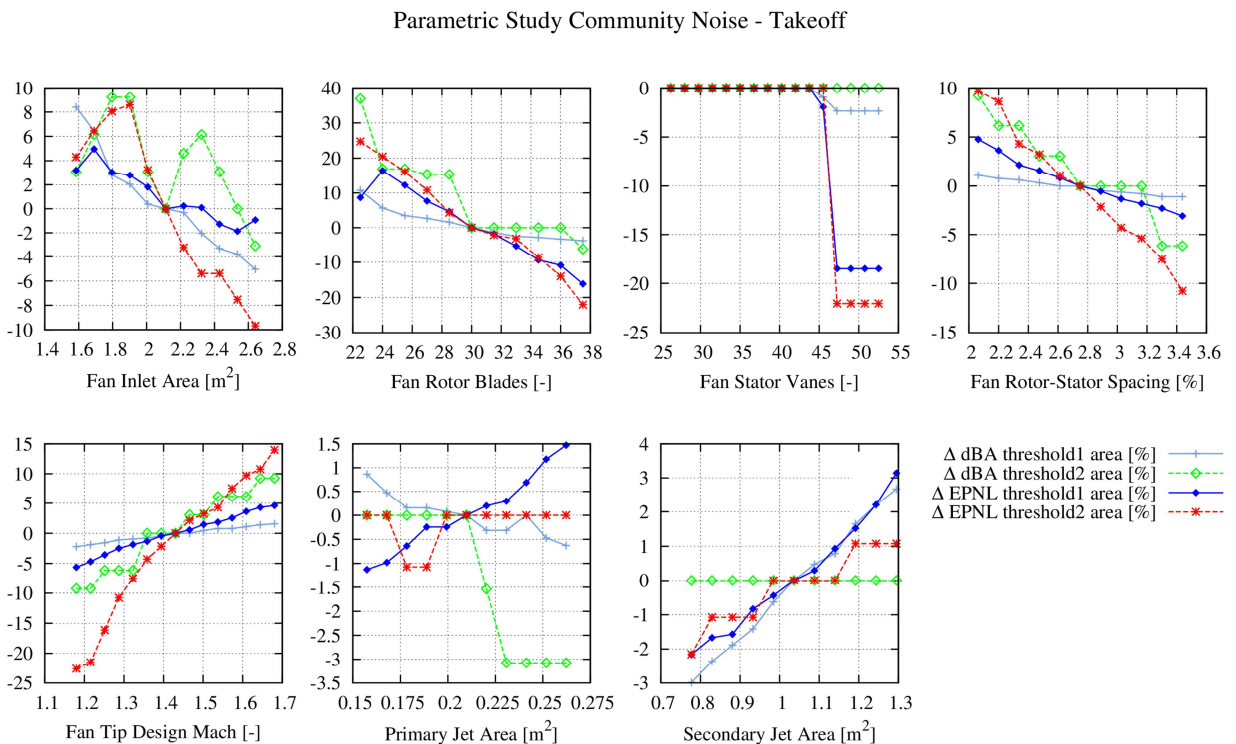


Figure 7.5: Engine geometry parameter variation results on community noise impact for a standard SR departure in the dBA and EPNL metrics

2. Approach

Table 7.5 shows, as was seen at the approach certification point, that the impacted area is larger for each noise metric during approach than during departure. The larger noise impact during approach is actually due to the slower aircraft speed and hence longer duration of a standard approach flight procedure. The aircraft remains for long distances below the 10000 ft altitude where the approach analysis starts and it is for this reason that a larger ground impact analysis area during approach of $40 \times 20 \text{ km}^2$ is taken compared to the $30 \times 20 \text{ km}^2$ during departure, where the aircraft reaches an altitude of 10000 ft already after a range of around $X = 25\text{-}30 \text{ km}$ (cf. 6.9).

Table 7.5: SR aircraft reference community noise impacted area for a standard approach flight path

Community noise impacted area [km^2]	Value
55 dBA threshold 1 area	67.2
75 dBA threshold 2 area	2.76
65 EPNdB EPNL threshold 1 area	93.8
85 EPNdB EPNL threshold 2 area	6.76
65 phon loudness threshold 1 area	102.24
85 phon loudness threshold 2 area	7.8
0.075 t.u. tonality threshold 1 area	172.48
0.10 t.u. tonality threshold 2 area	127.8
0.75 acum sharpness threshold 1 area	94.84
1.0 acum sharpness threshold 2 area	27.28

Figure 7.6 shows the effect on sound quality metric areas when the engine geometry parameters are varied for the approach phase. As for the departure phase, many of the trends are similar to those seen for certification at the approach point (cf. Fig. 7.3) but with larger relative changes from the reference values. As was seen in Fig. 6.10 (bottom), it can be noticed that the SR aircraft has a higher tonality during approach and as such, the 0.10 t.u. tonality threshold 2 area has a significant span on the ground. Some differences to the approach certification point can also be noticed in Fig. 7.6. The fan rotor blade number variation results in an asymmetric change in tonality impacted area – a larger reduction in tonality impacted areas for higher blade numbers is observed than an increase in tonality impacted area for lower blade numbers (-65% compared to +50%). The reduction in tonality impacted areas for stator vane numbers of 47 and above is also much higher than what was seen at the approach certification point. It can also be observed that although the 0.075 t.u. tonality threshold 1 area changes for variations of the primary and secondary jet areas are comparable to the changes observed for departure in Fig. 7.5, the 0.10 t.u. tonality threshold 2 changes are much more significant. This implies that larger exhaust nozzles could reduce the tonality impact on the ground during approach by a significant amount.

The changes for the other sound quality metric areas are similar to those observed in the previous engine geometry parameter variations in this sub-section, further confirming that the effect of these noise relevant parameter changes are more generally valid and not restricted to a particular flight procedure. In [102] it has also been shown that similar trends for both departure and approach phases are observed for the 777-300 similar LR aircraft, but with lower magnitudes of the relative changes. Fig. 7.7 shows the

corresponding community noise impact changes in the dBA and EPNL metrics, where both metrics are again seen to follow the loudness trends for all parameter variations.

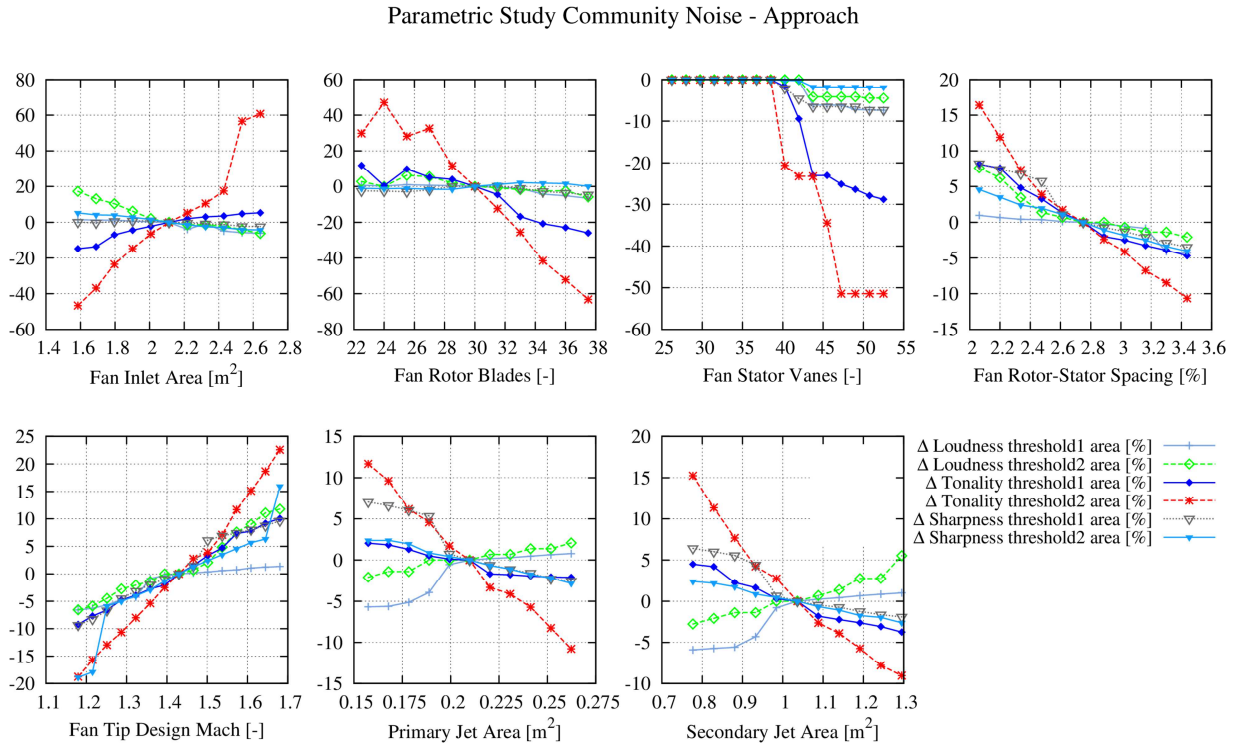


Figure 7.6: Engine geometry parameter variation results on community noise impact for a standard SR approach in sound quality metrics

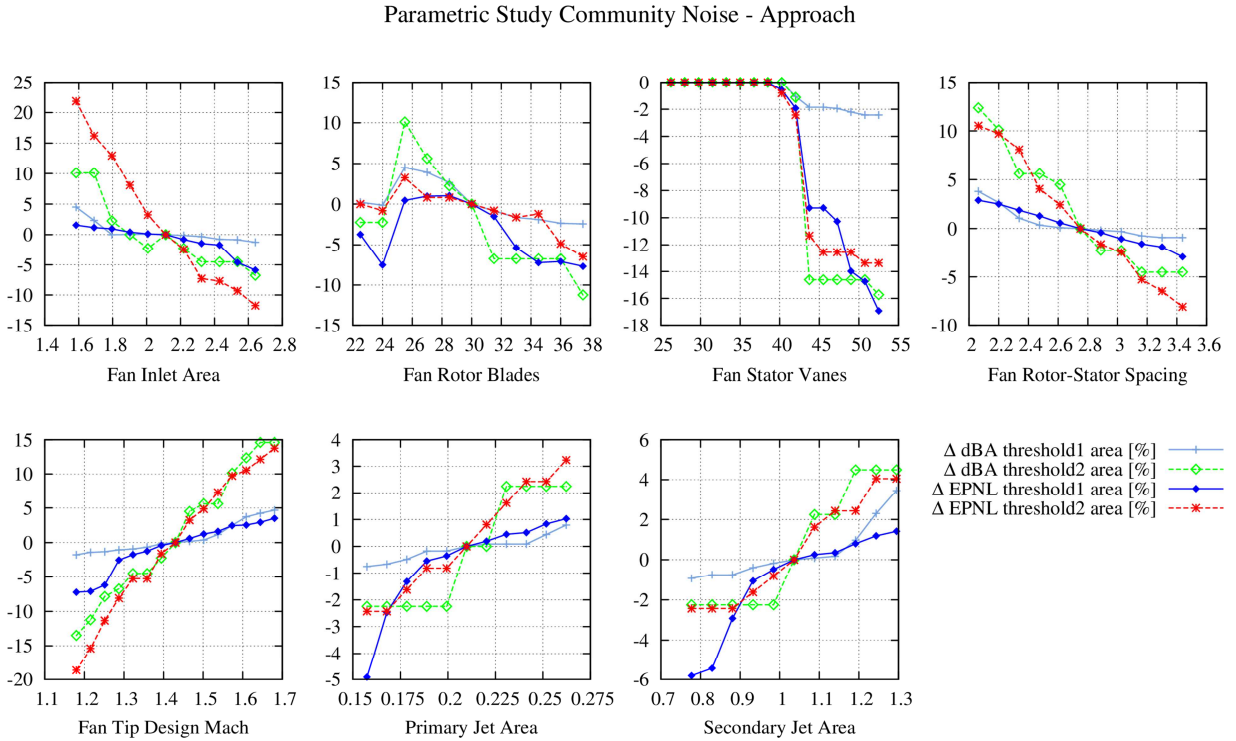


Figure 7.7: Engine geometry parameter variation results on community noise impact for a standard SR approach in the dBA and EPNL metrics

7.2 Coupled parametric variation studies

The individual engine geometry parameter variations in the previous section showed that each individual engine geometry parameter had an individual effect on the noise impact on the ground both in terms of level as well as sound quality. In order to quantify the effect of varying the engine geometry parameters, the flight path was kept constant in the previous section. During the aircraft design process however, a variation of the overall aircraft design parameters W/S or T/W will change the aircraft's flight path along with the airframe and engine geometry respectively. The individual effect of airframe geometry was chosen to be followed by varying the aircraft wing size and span by performing a coupled parametric variation of the aircraft wing-loading. This incorporates an automatic change of the wing noise via the changed wing area and wing span and change of flap noise via the changed flap area and flap span. A change in wing-loading can also change slat noise by changing the acoustic power of the slat by altering the slat boundary layer thickness (cf. Eq. 4.60). Each value of W/S also results in a new and altered flight path of the aircraft, for both departure and approach phases.

The landing gear geometry was not varied in the current analysis in order to keep the focus on the wing geometry, as landing gear noise only affects a small fraction of the approach phase (from around $X = -10$ km to touchdown for the aircraft modeled in this dissertation). Furthermore, the landing gear does not alter the flight path of the aircraft whereas the aircraft wing and high-lift elements such as flaps and slats can affect both the climb performance as well as aircraft approach speed. For each value of the wing-

loading W/S , the entire MICADO convergence loop was run iteratively via the parameter study manager module till a converged design with optimized aerodynamics and performance for the SR aircraft with new W/S value was achieved. Since the goal of the parametric variations was not to deviate too strongly from the reference SR design, each design variant aimed a convergence for the same MTOW and OWE values, as well as the same TLARs as the reference SR aircraft. For each wing-loading variation, the aircraft for the same MTOW has a larger or smaller wing size and flies slightly differently, which in turn varies the noise impact experienced on the ground.

The thrust to weight ratio variation changes all the engine geometry parameters shown in Section 7.1 for the uncoupled variation, as well as the other engine geometry parameters mentioned in Chapter 4 for the source noise models by scaling them for the modified SLST. Besides changing the engine geometry, the T/W variation also has a significant effect on the aircraft departure flight path and a higher T/W value (corresponding to a larger engine) results in a steeper climb out of the aircraft. A variation of the aircraft T/W will therefore combine all the individual effects seen in Section 7.1 with an additional altered ground noise impact due to changes to aircraft flight path. As for the wing-loading variations, the T/W variations aim a convergence for the same MTOW and OWE values as the reference SR aircraft design, for the same TLARs.

Section 7.2.1 will show the parametric variation of the SR aircraft wing-loading and its impact on certification and community noise; Section 7.2.2 will show the parametric variation of the thrust to weight ratio and the corresponding certification and community noise impact changes that the variation results in. Table 7.6 shows the reference SR aircraft W/S , T/W , SLST and airframe geometry values.

Table 7.6: SR aircraft reference W/S , T/W , SLST and airframe geometry values

Parameter Name	Symbol	Value
Wing-loading [kg/m^2]	W/S	629
Thrust to weight ratio [-]	T/W	0.312
SLST [kN]	F	113.34
Wing area [m^2]	S	117.68
Wing span [m]	b	33.39
Flap area [m^2]	S_f	8.48
Flap span [m]	b_f	8.51

7.2.1 Wing-loading variation

1. Noise impact analysis at certification points

Figure 7.8 shows the effect of wing-loading variation from the reference value of 629 kg/m^2 on the metric values at certification points. For both the flyover and approach points, very small effects on the metrics are seen. Particularly for the flyover point it is observed that the wing geometry will have hardly any noticeable influence on the ground noise impact. This is consistent with the fact that airframe noise during takeoff is much lower than the engine noise and the flight path at 6.5 km from brake release does not change by a considerable margin for changes in wing geometry for the same engine thrust. At the flyover point the only somewhat noticeable change is in the sharpness, which decreases for a larger wing (i.e. a

lower W/S) value by up to 1.5%. At the approach point, only a change in loudness is slightly noticeable with the loudness decreasing for a smaller wing and increasing for a larger wing. The reduction in loudness is primarily due to the reduction in airframe noise from a smaller wing due to a higher wing-loading. As modeled in the MICADO environment, a slightly smaller wing also results in smaller high-lift devices as the climb-requirements are still met comfortably and do not require an increase in the high-lift device areas. Overall it can be said that varying the wing geometry changes the metrics by very small amounts at the certification points and no clear trends are visible for most metrics. This encourages a check for community noise impact, as the flight paths beyond the certification points can show much higher differences.

2. Community noise impact analysis

Figure 7.10 shows the results for the wing-loading variation and its effect on community noise impact via impacted areas at and above the chosen threshold values for each metric. Many of the trends are more clearly visible while looking at community noise impact. For the approach phase, as was seen very slightly at the approach certification point, both the loudness threshold areas of 65 phon and 85 phon decrease for a higher wing-loading (i.e. smaller wing size) and increase for a lower wing-loading (i.e. larger wing size), which can be attributed to an increase in the airframe noise from the wing and high-lift elements. For departure however, it is observed that a decrease in the 65 phon (threshold 1) loudness impacted area is observed for a higher wing-loading, whereas an increase in the higher 85 phon (threshold 2) loudness impacted area is observed for a lower wing-loading. This observation is linked to how the wing size affects the flight path of the aircraft during departure, rather than the actual intensity of airframe noise it produces, which is of course significantly lower than engine noise during departure.

In order to elucidate how a higher wing-loading value can decrease the 65 phon loudness impacted area but increase the 85 phon loudness impacted area during takeoff, Fig. 7.9 shows three departure flight paths of SR aircraft variants having W/S values of 471.8 kg/m^2 , 629.1 kg/m^2 (which is the reference value) and 754.9 kg/m^2 . Fig. 7.9 (left) shows that the larger wing for the wing-loading value of 471.8 kg/m^2 allows the SR aircraft variant to climb out faster than the reference SR aircraft (shown in gray) in the initial departure phase, shown up to $X = 5.5 \text{ km}$. The smaller wing for the high wing-loading value of

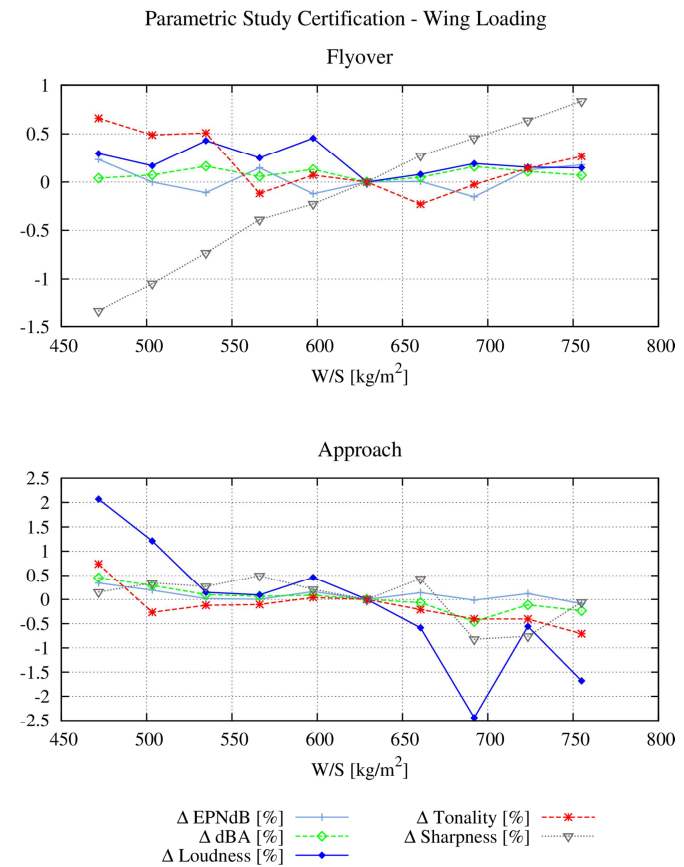


Figure 7.8: W/S variation results for noise impact of the SR aircraft at flyover and approach certification points

754.9 kg/m^2 on the other hand makes the SR aircraft variant require a longer ground roll, which results in the aircraft flying at lower altitudes initially compared to the reference SR aircraft. This results in the increased 85 phon threshold 2 loudness impacted area for the higher W/S values.

Over the whole procedure however, Fig. 7.9 (right) shows that at larger distances from the point of brake release, the smaller wing results in a slightly steeper climb out compared to the reference SR aircraft due to lower drag values produced by the smaller wing and the engine thrust remaining unchanged for the same T/W value. This results in the reduction of the 65 phon threshold 1 loudness impacted areas for high W/S values. A corresponding increase in 65 phon threshold 1 loudness impacted area is seen for low W/S values, for which the aircraft ends up flying at slightly lower altitudes at later departure phases due to higher drag values for the same available thrust, thus requiring a larger distance to reach an altitude of 10000 ft.

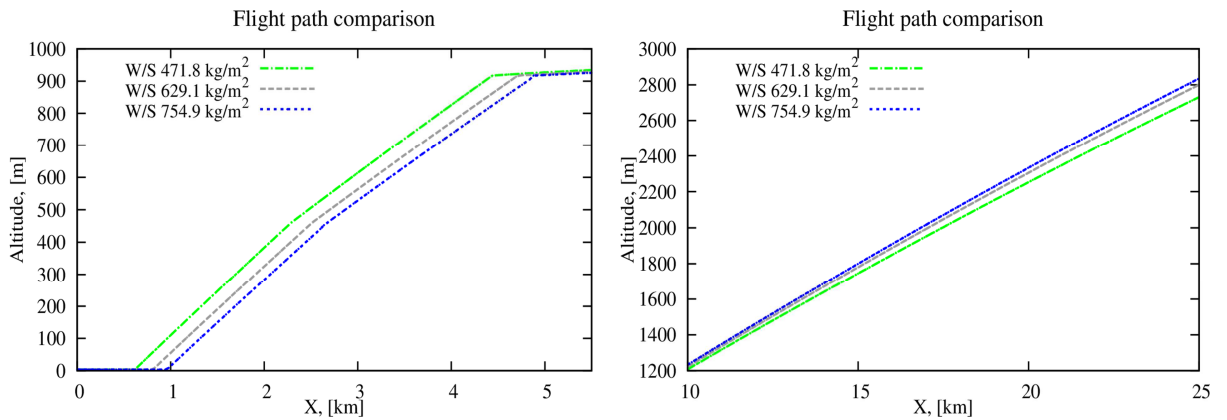


Figure 7.9: Flight path comparison of the SR departure for low and high wing-loading values – initial departure phase (left) and later departure phase (right)

Airframe noise during approach is the dominant broadband component and any change in its intensity can alter both the level as well as quality of the overall aircraft noise as well. It is for this reason that a higher wing-loading during approach decreases *both* the 65 phon and 85 phon loudness impacted areas whereas for departure it decreased only the 65 phon loudness impacted area. A lower wing-loading on the other hand is seen to increase the loudness impact during approach for both low and high loudness values quite considerably, by 10-15%.

An interesting observation in the wing-loading variation and its effect on the sound quality metrics in Fig. 7.10 is that a change in wing-loading can also alter the tonality of the aircraft noise. As airframe noise is purely broadband (as modeled in this dissertation), a change in the tonality of aircraft noise due to airframe noise variation is mainly due to how it affects the prominence of fan tones and how effectively it masks the fan tones. Fig. 7.10 shows that a smaller wing can increase both the low and high tonality value impacted areas during approach. This is because a smaller wing produces lower airframe noise, which in turn increases the tonal prominence. Increasing the wing area via a lower wing-loading is seen to reduce the 0.1 t.u. tonality impacted area, due to the opposite effect of increased airframe noise for a larger wing, which decreases the tonal prominence and also increases the masking effectiveness from the low frequency airframe noise components. The fact that low frequency noise increases for a larger wing is

seen via the sharpness metric trends, which show that both sharpness value impacted areas are reduced for a larger wing, indicating that the fraction of high frequency noise in the overall aircraft noise spectra has decreased.

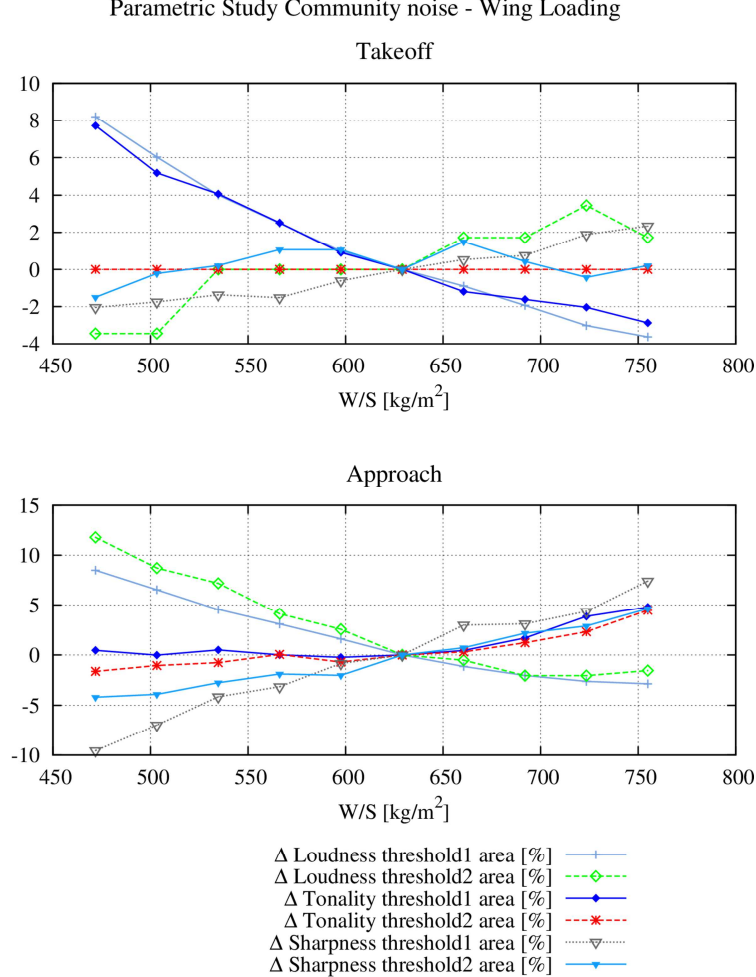


Figure 7.10: Wing-loading variation results for community noise impact of the SR aircraft for departure and approach flight paths in sound quality metrics

Fig. 7.11 shows the changes in community noise impact in the dBA and EPNL metrics. It can be seen that particularly the dBA metric is seen to follow exactly the same trends as the loudness metric. A smaller wing is seen to increase the 85 dBA impacted area during departure and a larger wing is seen to increase the 65 dBA impacted area. For approach, both metrics follow the loudness trends, with a larger wing increasing the impacted areas in both metrics by comparable amounts to the loudness metric. The observation that the dBA and EPNL metrics both follow the trends of the loudness metric was also observed for the engine geometry variations presented in Section 7.1.

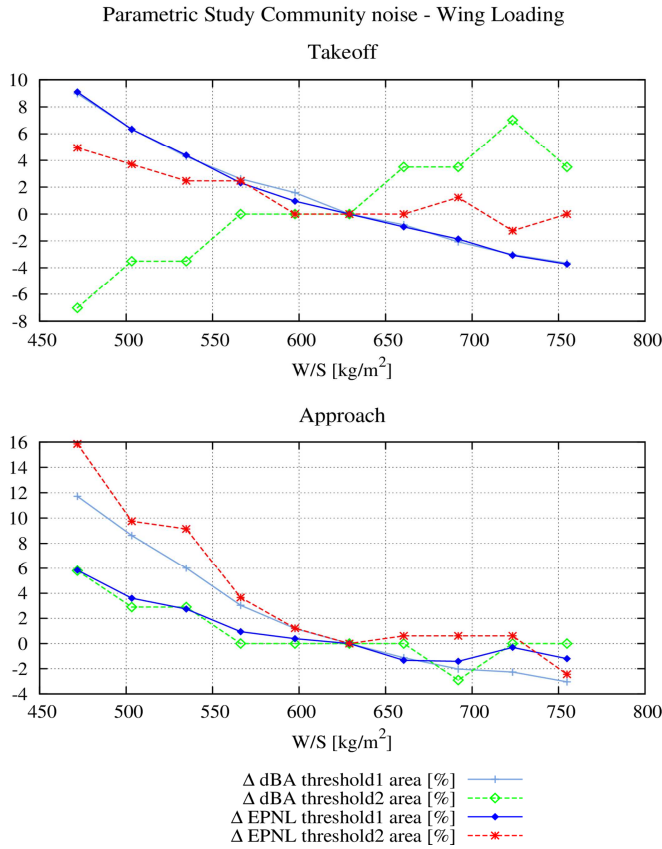


Figure 7.11: W/S variation results for community noise impact of the SR aircraft departure and approach flight paths in dBA and EPNL metrics

7.2.2 Thrust-to-weight ratio variation

Fig. 7.12 shows the coupled variation of the SR aircraft thrust to weight ratio around its reference value of 0.311 and its effect on community noise impact in sound quality metrics. In order to give an indication of how the noise relevant geometry parameters are varied with thrust according to the engine geometry database created during the course of the current research work (shown in Appendix A), Table 7.7 shows the relevant fan and jet engine geometry values for two SR variants – one with a high T/W ratio of 0.375 and one with a low T/W ratio of 0.265. Compared to the reference SR values presented in Table 7.1, it can be observed that the lower T/W value results in a smaller fan inlet area, smaller primary and secondary jet areas, a higher blade and vane number and a slightly reduced tip design Mach number. For the higher T/W value, the areas are correspondingly larger and the number of blades as well as vanes has decreased for the larger scaled engine. These parameter values for the SR variants help in explaining many of the effects the overall T/W variation has on the community noise impact in terms of each metric.

Table 7.7: SR aircraft engine geometry values for two T/W values

Parameter Name	$T/W = 0.265$	$T/W = 0.375$
Fan inlet area [m^2]	1.859	2.408
Number of rotor blades [-]	47	28
Number of stator vanes [-]	52	33
Fan rotor tip Mach number at design point [-]	1.40	1.45
Rotor-stator spacing [%]	2.75	2.75
Primary jet area [m^2]	0.165	0.258
Secondary jet area [m^2]	0.902	1.178

In Fig. 7.12, it can be seen that as was hinted by the engine geometry parameter variations in Section 7.1, a larger engine (having a higher T/W) is quieter but at the same time more tonal. The increase in tonality for higher T/W values is seen for both the departure as well as approach phase. The higher T/W value results in a larger fan inlet area, which increases the fan noise intensity, including that of the fan tones. The larger fan inlet area (which is also the engine reference area used for jet noise calculation) also reduces the broadband jet noise intensity due to a larger source reference distance $\sqrt{A_e}$, which further increases the tonal prominence and also reduces the intensity with which they are masked by the low frequency jet noise. The lower number of rotor blades also increases the tonality as the tones move to frequencies which are perceived as more tonal in Aures' metric and are absorbed less efficiently by the atmosphere. The larger jet areas increase the jet noise intensity as was shown in the previous subsection, and actually reduce the tonality of the produced aircraft noise. The increase in tonality for T/W values higher than 0.345 therefore begins to decrease from an increase of 60% to around 30% for the T/W value of 0.39, where the reduction in tonality due to larger jet areas begins to compensate for the increase in tonality due to the larger fan inlet area and lower blade number.

It can also be seen that the tonality of the SR aircraft during departure can be reduced to negligible amounts if the engine is scaled to a low T/W value of 0.265. Again, for this observation it has to be noted that the reference SR tonality during departure is already quite low and this implies that the much smaller scaled engine will have fan tones that completely lie below the broadband noise and will not produce any noticeable tonal perception. Keeping in mind the results from Fig. 7.4 and Fig. 7.6, the parameters that contribute to the reduction in tonality for a low T/W value are:

- Smaller fan inlet area: Large reductions seen for both departure and approach
- Larger rotor blade number: Very large reduction seen for departure, resulting in the complete removal of the 0.075 t.u. tonality impacted area on the ground i.e. the tones become much less prominent
- Larger stator vane number: Particularly during approach, large reduction observed as shown in Fig. 7.6
- Reduced tip design Mach number

For the approach phase, it was shown earlier that the SR aircraft has a higher tonality due to the engine being operated at flight idle setting and the jet noise being minimal. With regards to the tonality impacted area on the ground, a notable difference to the takeoff phase is that the tonality increase for high T/W values during approach does not decrease as strongly towards higher T/W values.

It can also be observed in Fig. 7.12 that during departure, the 0.1 t.u. tonality impacted area remains unaffected (due to the tonality value during departure not exceeding 0.1 t.u.) and the 0.075 t.u. tonality impacted area can be reduced to negligible amounts by scaling down the T/W ratio. For the approach phase however, the 0.075 t.u. tonality impacted area can only be reduced by up to 40% whereas the 0.1 t.u. tonality impacted area can be reduced to negligible amounts. This implies that the higher tonality during approach is harder to reduce than the lower tonality during departure, where the engine tones can be reduced in prominence more easily. To do the same during approach would require a much larger increase of the broadband noise components, which may not ultimately be beneficial in reducing the overall annoyance. The goal here is thus to find the right spectral balance at an early stage such that adverse effects are prevented at a later stage.

With regards to the loudness impact on the community, it can be observed that the loudness impacted area is increased for lower T/W values and decreased for higher T/W values, thereby supporting the observation that a larger engine is quieter (but more tonal). The change in loudness with thrust to weight ratio during approach is however lower than during departure, with an increase of up to 5% observed for low T/W values and a decrease of up to 10% observed for high T/W values (compared to changes of up to 20% observed during departure). This is also consistent with the loudness impact on the community presented in Section 7.1 for the approach phase – a larger fan inlet decreases loudness impact by around 10% whereas the larger primary and secondary jet areas increase the loudness by up to 5%. A factor that adds to the loudness reduction during departure is the effect on the flight path, which for a higher available thrust for comparable aircraft weight and drag allows a steeper climb out. This ultimately results in a reduced community noise impacted area on the ground due to an increased distance between the aircraft and the ground. This effect was also observed while analyzing noise abatement flight procedures with maximum thrust setting climb out in [101] whereby the community noise impact was reduced due to the aircraft reaching higher altitudes faster with more thrust being available. The noise abatement procedure analysis for approach flight paths such as the Continuous Descent Approach is presented concisely in Appendix B of this dissertation, to show the effect of *flight operations* on the level and quality of aircraft noise, besides the effect of design parameters presented in this chapter.

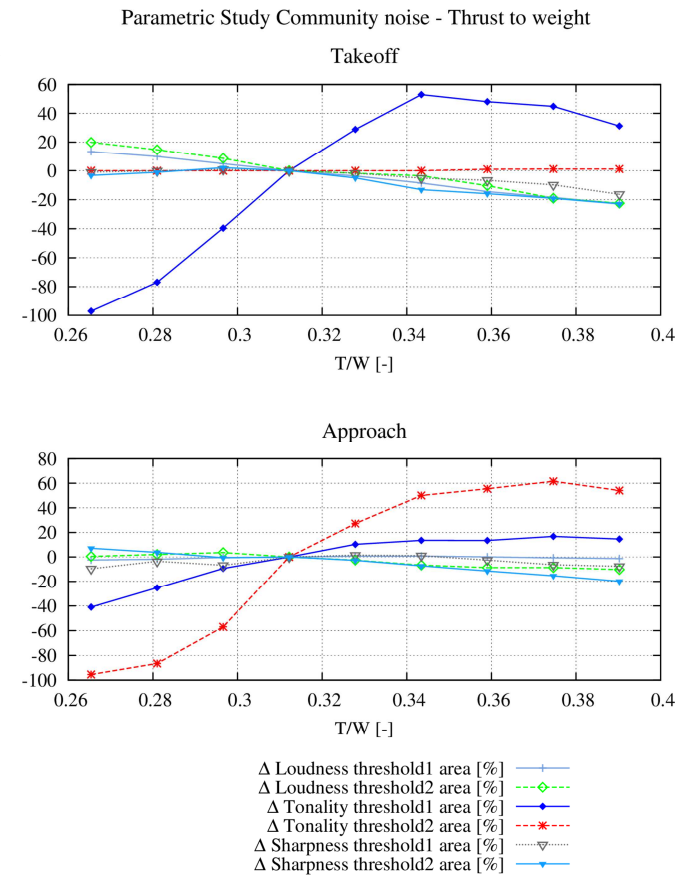


Figure 7.12: T/W variation results for community noise impact of the SR aircraft in sound quality metrics

Fig. 7.13 shows the corresponding community noise impact for the T/W variation in terms of the dBA and EPNL metric impacted areas on the ground, to once again show the community noise changes with engine size and available thrust in the more conventional metrics. All of the impacted area changes seen for both departure and approach phases can be directly linked to the parameter values provided in Table 7.7 and the individual parameter variations presented in Fig. 7.5 for takeoff and Fig. 7.7 for approach.

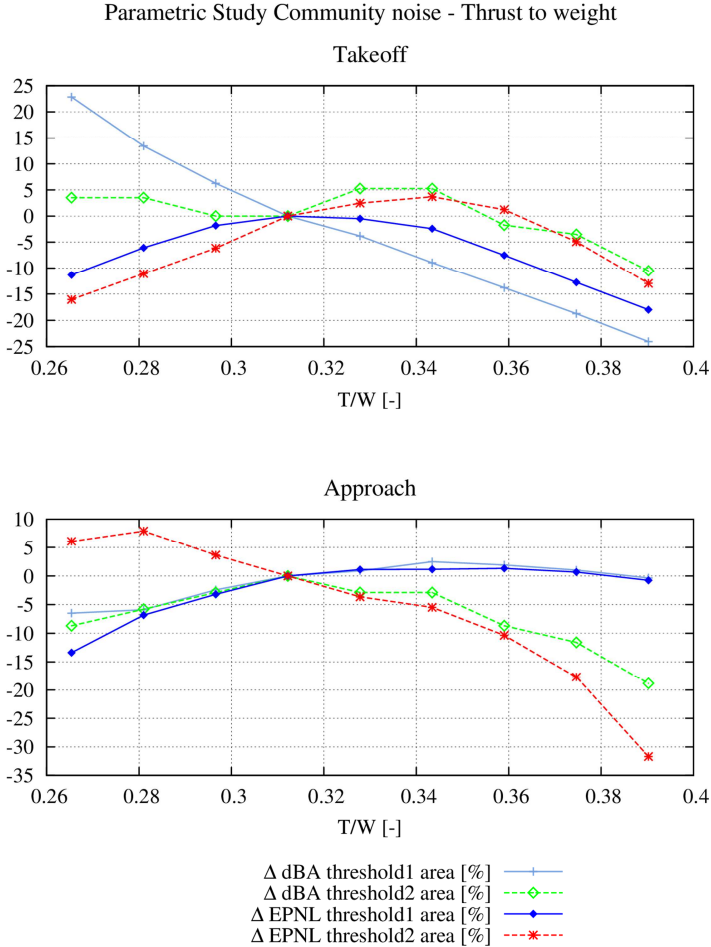


Figure 7.13: Thrust to weight ratio variation results for community noise impact of the SR aircraft for departure and approach flight paths dBA and EPNL metrics

8 Optimization possibilities for low annoyance aircraft design

This chapter will aim to combine all the background and analyses performed in the previous chapters of this dissertation and explore the possibility of low annoyance aircraft design i.e. the possibility of designing aircraft that are perceived as inherently less annoying due to having considered the quality of the aircraft noise as an optimization target. The parameter study manager module of MICADO will again be used to perform the optimizations of the SR aircraft for each target metric. The metrics that will be used as targets for analyzing optimization possibilities will be the EPNL metric, loudness metric and tonality metric. A preliminary optimization of the modified Psychoacoustic Annoyance metric briefly described in Section 3.1 is also attempted. Although the modified PA metric was said to be valid only for the 40 aircraft noise recordings used for the study by [43], it is a metric that nonetheless presents a possible way of including the three more established sound quality metrics of loudness, tonality and sharpness into one overall metric. Section 8.1.1 will show how the metric reductions presented for the optimized designs correspond to the actual sound produced by the optimized aircraft designs, by presenting spectrograms for approach and departure phases for each optimized design. Since one of the overall goals of the research work in this dissertation was to explore the possibility of reducing aircraft noise annoyance by design, thereby minimizing the need for late noise reduction measures such as acoustic liners, a comparison of the annoyance optimized designs with current aircraft having acoustic liner technology will also be presented in Section 8.1.2.

8.1 Comparison of optimized aircraft designs

The optimizations have been made by using the overall aircraft design parameters - the aircraft thrust to weight ratio and wing-loading as free variables, using the coupled variation approach of Section 7.2. The optimized designs have the same target MTOW and OWE as the reference SR aircraft and also have the same requirements. The requirements however have not been enforced as design constraints and the optimized aircraft design may in the end not fulfill all the top-level requirements, yet still lead to a plausible converged design variant of the SR aircraft. A hard constraint for requirements is undesirable for the analysis in the current research work as it limits the number of design options that the optimizer may have while searching for an optimum. The optimization target will be the cumulative community impacted area in km^2 for each target metric, summing both the departure as well as approach community noise impact for each flight path of the design variant. The analysis will also however cover the noise impact at the certification points, in order to see if designs optimized for community noise impact also result in reductions at the much closer to the runways certification points. In order to keep track of the effect of the optimizations for noise on the aircraft performance, changes in the aircraft MTOW, OWE as well as block fuel will also be presented. Further parameters of relevance to the aircraft's performance that will be followed include the requirements for the Takeoff Field Length (TOFL), the time to climb from 1500 ft to the Initial Cruise Altitude (ICA), the approach speed V_{app} and the Landing Distance (LDN). The required values of these parameters for the SR aircraft are: TOFL = 2200 m, time to climb to ICA = 35 min, V_{app} = 138 knots and LDN = 1850 m.

1. Optimized SR design for minimum 85 EPNdB community impacted area – minimum EPNL SR design: Table 8.1 shows the comparison of the SR reference design with the EPNL optimized SR variant i.e. the optimum design that produces the minimum cumulative 85 EPNdB impacted area on the ground. Table 8.1 shows the engine and airframe geometry parameter values for both the reference and minimum EPNL designs, to provide a link to the parameter variation studies presented in the previous chapter. It can be observed that the optimizer of the parameter study manager module attempted to minimize the noise impact in the EPNL metric by selecting an as large as possible engine by increasing the thrust to weight ratio to the maximum allowed value of 0.4. Furthermore, the optimizer also selected a slightly smaller wing than the reference design, in order to choose a design variant that minimizes the higher EPNdB values on the ground. The values of $T/W = 0.4$ and $W/S = 689 \text{ kg/m}^2$ and how they result in a design variant that minimizes the 85 EPNdB threshold 2 community impacted area can be linked to Fig. 7.11 and Fig. 7.13 showing the W/S and T/W parametric variations and their effect on the community noise impact in the dBA and EPNL metrics. Although the T/W value was only varied till 0.39 in Figs. 7.11 and 7.13, the optimizer was allowed to go up to a value of $T/W = 0.4$. The trends from Figs. 7.11 and 7.13 already indicate that a larger T/W would reduce the higher dBA and EPNdB value impacted areas further.

The choice of a larger engine reduces the EPNdB impacted area due to the larger engine being quieter and also as the larger engine allows a steeper climb out during the departure phase. A smaller wing primarily results in a reduction of the airframe noise, which also adds to the reduction in the EPNdB values. In Table 8.1, it is seen that a cumulative reduction in the 85 EPNdB impacted area of 45% is achieved for the $T/W = 0.4$ and $W/S = 689 \text{ kg/m}^2$ combination of the overall aircraft design parameters. Table 8.2 shows the more detailed noise and annoyance impact values for both aircraft designs for the departure and approach phases. It is seen that the minimum EPNL design reduces both the 65 and 85 EPNdB impacted areas on the ground and a close to 50% reduction in the 65 EPNdB impacted area during departure and 33% reduction during approach are produced. These reductions can once again be directly linked to the parametric variations in Fig. 7.11 and Fig. 7.13. The annoyance impact of the minimum EPNL design variant in terms of the sound quality metrics presented in Table 8.2 shows that the minimum EPNL design variant reduces the noise impact in all metrics, with only the tonality impact increased during departure. The reductions in the dBA and loudness impacted areas of the minimum EPNL design variant are also significant but predominantly occur during the departure phase. The reductions in the lower threshold impacted areas during approach for both the dBA and loudness metrics are much lower, between 8-10%. Slight reductions in the tonality impact during approach are also observed as well as slightly reduced sharpness values for both the departure and approach phases.

Table 8.1: Comparison of reference SR aircraft and minimal EPNL optimized designs

Parameter Name	SR-Ref	SR-Min. EPNL
Engine geometry parameters		
Fan inlet area, $A_{fan} [\text{m}^2]$	2.058	2.585
Fan rotor blades, $B [-]$	31	29
Fan stator vanes, $V [-]$	36	59
Fan tip des. Mach, $M_{t,d} [-]$	1.43	1.46
Primary jet area, $A_{jet,1} [\text{m}^2]$	0.201	0.285

Secondary jet area, $A_{jet,2}$ [m ²]	1.01	1.26
Airframe geometry parameters		
Wing area, S [m ²]	117.68	112.37
Wing span, b [m]	33.39	32.64
Flap area, S_f [m ²]	8.48	8.09
Flap span, b_f [m]	8.51	8.32
Aircraft design and performance parameters		
Wing-loading, W/S [kg/m ²]	629	689
Thrust-to-Weight ratio, T/W [-]	0.312	0.400
SLST [kN]	113.34	151.87
MTOW [kg]	74014	77428
OWE [kg]	40166	42047
Block fuel [kg]	13910	15235
TOFL [m]	1962.05	1553.56
Time to climb to ICA [min]	15.89	9.73
Approach speed, V_{app} [m/s]	138.05	144.0
LDN [m]	1517.45	1591.87
Cumulative community impact areas		
85 EPNdB EPNL area [km ²]	13.04	7.12
85 phon loudness area [km ²]	12.44	9.64
0.1 t.u. tonality area [km ²]	127.84	111.84

Table 8.2: Community noise impact comparison of reference SR aircraft and minimum EPNL optimized design

Community noise impact [km²]	Departure SR-Ref	Departure Min. EPNL	Approach SR-Ref	Approach Min. EPNL
dBA threshold 1 55 dBA area	50.4	34.72	67.2	60.56
dBA threshold 2 75 dBA area	2.28	2.04	2.76	1.68
EPNL threshold 1 65 EPNdB area	79.56	40.6	93.2	62.76
EPNL threshold 2 85 EPNdB area	6.48	4.28	6.56	2.84
Loudness threshold 1 65 phons area	84.92	58.2	102.24	93.8
Loudness threshold 2 85 phons area	4.64	3.44	7.8	6.2
Tonality threshold 1 0.075 t.u. area	1.84	12.44	172.24	141.68
Tonality threshold 3 0.10 t.u. area	0	0.52	127.84	111.32
Sharpness threshold 1 0.75 acum area	51.12	38.24	94.84	84.0
Sharpness threshold 2 1.0 acum area	17.28	13.96	27.28	21.44

In order to show the certification noise impact of the minimum EPNL design variant and how it compares to the reference SR aircraft design's noise impact at the certification points, Table 8.2 shows the noise impact at the flyover and approach certification points. It can be observed that the aircraft design which

has been optimized for minimum community noise impact in the EPNL metric produces a large EPNdB reduction of 8.26 EPNdB at the flyover certification point and a modest reduction of 1.96 EPNdB at the approach certification point. The lower reduction at the approach point can be partly attributed to the location of the approach point, such that the aircraft's altitude will change very little at this location, being so close to the runway. The changes in the SPL values in dBA at the certification points do not capture the differences indicated by the EPNL and sound quality metrics for the reference and minimum EPNL SR design.

Table 8.3: Certification noise impact comparison of reference SR aircraft and minimum EPNL optimized design

<i>Certification noise impact</i>	<i>Flyover SR-Ref</i>	<i>Flyover Min. EPNL</i>	<i>Approach SR-Ref</i>	<i>Approach Min. EPNL</i>
SPL [dBA]	73.50	72.13	89.0	88.25
EPNL [EPNdB]	89.15	80.89	99.07	97.11
Loudness [sone]	24.28	20.21	80.03	73.23
Tonality [t.u.]	0.064	0.072	0.106	0.123
Sharpness [acum]	1.17	1.06	1.74	1.68

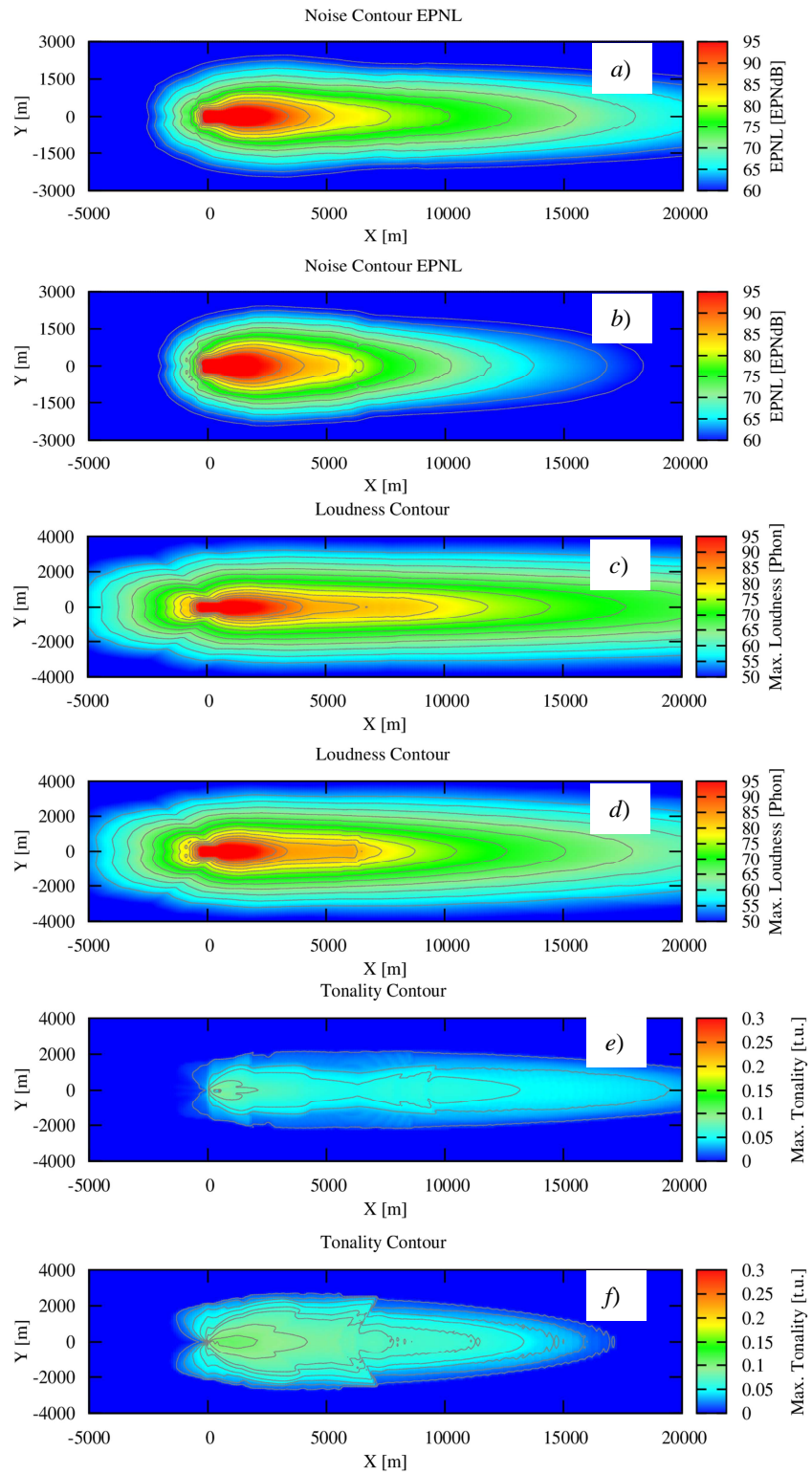


Figure 8.1: Departure noise contours of the SR-Ref and min. EPNL variants for – a) EPNL SR-Ref, b) EPNL min. EPNL, c) Loudness SR-Ref, d) Loudness min. EPNL, e) Tonality SR-Ref and f) Tonality min. EPNL

Fig. 8.1 shows the comparison of the noise contours for the reference SR aircraft design and the minimum EPNL design variant of the SR aircraft, for the departure phase. The contours for the metrics EPNL, loudness and tonality are presented, displaying the maximum values that occur over the flight procedure. The contours are intended to supplement visually the numerical results presented in Table 8.2, in order to show how the community noise impact in the various metrics for the optimized design compares to the reference design. As was mentioned in Chapter 7, the effect of acoustic liners has been deactivated for all optimizations presented in this chapter as well.

Fig. 8.1 shows that the minimum EPNL optimized design, as selected by the optimizer of the parameter study manager module, minimizes the EPNL impacted area considerably during the departure phase. This is due to the larger engine and smaller wing allowing a faster climb out over the complete departure procedure (cf. Fig. 7.9

(right)), as well as due to the lower EPNL values produced by a larger fan inlet and smaller airframe geometry. It is evident from Fig. 8.1 a) and b) that a steeper climb out can reduce the EPNL impact on the community by considerable amounts from a distance of $X = 6$ km onwards. This is in contrast to the current approach of flying with a reduced thrust setting (cutback) for a section of the takeoff procedure, as specified by ICAO. The

reduction in loudness impacted area is seen to be more modest comparing Fig. 8.1 c) and d), although with the reduced phon values evident from $X = 6$ km onwards as well. The reduction in tonality impacted areas in Fig. 8.1 e) and f) is seen to be comparable to the EPNL reductions, although a larger impacted area and higher tonality values compared to the SR-Ref tonality occur up to $X = 6$ km. The overall increase in the tonality impacted area for the minimum EPNL optimized design during the departure phase was also seen in Table 8.2, although the tonality contour provides the extra information that benefits to the community living beyond $X = 15$ km may be achieved via the minimum EPNL optimized SR design.

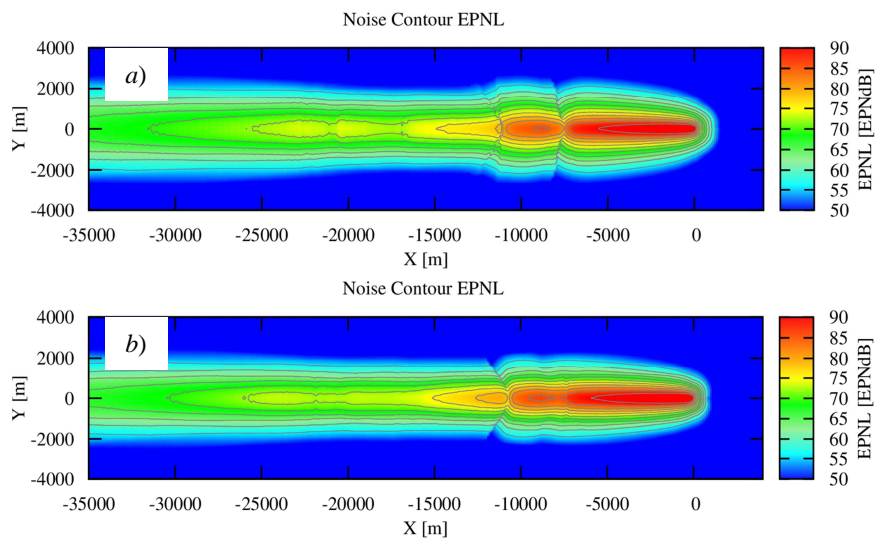


Figure 8.2: Approach noise contours of the SR-Ref and min. EPNL variants for – a) EPNL SR-Ref and b) EPNL min. EPNL - 1)

The corresponding noise contours comparison for the approach phase is presented in Fig. 8.2. It is immediately evident that the reductions in the various metrics are much more subtle during the approach phase. For the EPNL noise contour, the reduction is mainly in the lateral directions, with the minimum EPNL SR variant producing a narrower contour than the SR-Ref design when looking at Fig. 8.2 a) and b). The reduction in the higher 85 EPNdB impacted area is evident primarily from $X = -11.5$ km, whereby the 85 EPNdB and higher values occur later from $X = -10$ km for the minimum EPNL design variant. The

community noise impact comparison for the loudness metric in Fig. 8.2 c) and d) shows very little noticeable difference upon visual inspection and the differences numerically in Table 8.2 are also seen to be minimal implying that the minimum EPNL optimized SR variant will not produce much reduction in loudness to the residents during the approach phase. The tonality impact comparison however again shows some similarity to the EPNL metric impact changes, with the tonality contour in Fig. 8.2 f) being narrower for the minimum EPNL design than for the SR-Ref design in Fig. 8.2 e). These reductions in tonality impacted areas are also consistent with what was observed in Table 8.2.

By looking at the tonality and EPNL contours it appears that the EPNL metric, at least to some extent, does incorporate the tonal content present in the SR aircraft noise spectra. It will be shown slightly later however that the SR design optimized for minimum tonality impact does this in a quite different way compared to the EPNL metric, as would be evident from the very different methodologies with which the EPNL metric (cf. Section 2.1.2) and the tonality metric (cf. Section 6.1) were developed. It can be observed overall that the minimum EPNL optimized aircraft design produces on the whole reasonably large reductions in the EPNL metric, with some reduction in loudness during the departure phase and only slight overall reductions in tonality during the approach phase.

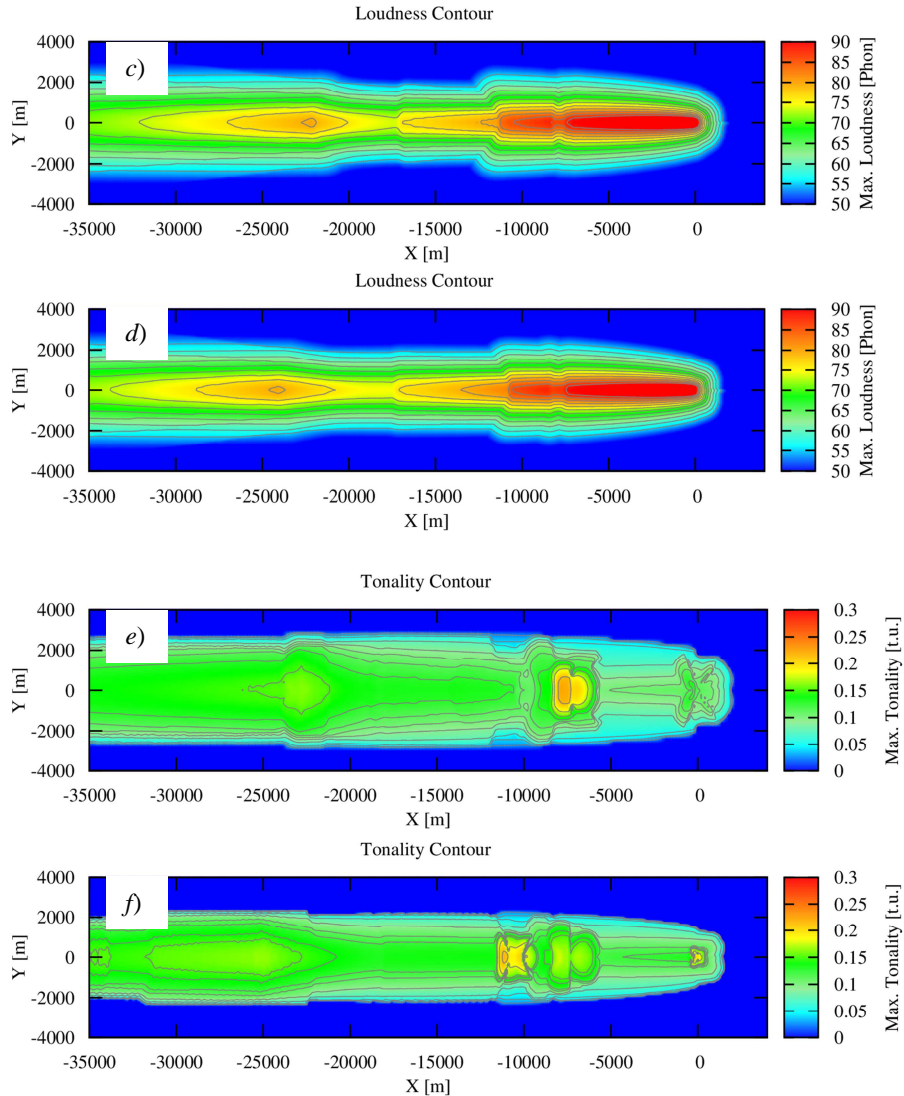


Figure 8.2: Approach noise contours of the SR-Ref and min. EPNL variants for – c) Loudness SR-Ref, d) Loudness min. EPNL, e) Tonality SR-Ref and f) Tonality min. EPNL - 2)

The analysis of the minimum EPNL optimized SR aircraft design variant above focused on the noise and annoyance impact of the optimized design. For aircraft design purposes, it is also important to consider the effect on aircraft performance that such optimizations for minimal noise may produce, in order to judge how realistically aircraft designers and industry may be willing to apply such an approach. Table 8.1 for this reason also showed some of the major aircraft design and performance parameters for the reference and minimum EPNL SR designs. It can be observed that in order to minimize the community noise impact in the EPNL metric, the SR aircraft will become heavier, due primarily to the choice of the larger engine. The MTOW value is seen to increase by 3414 kg and the OWE sees an increase of 1881 kg, along with an increase in the block fuel of 1325 kg. This indicates that an optimization for minimal EPNL impact for the community would adversely affect the SR aircraft performance. It can be mentioned here

that an increase in the engine size by 23%, as selected by the optimizer for the minimum EPNL optimized design is purely from a theoretical perspective in order to explore the optimization limits. As was seen in Table 8.2 and Table 8.3, the optimized design not only reduces the EPNL community noise impact by 45% cumulatively, it also results in a reduction of 10 EPNdB at the certification points. A smaller increase in engine size may be a more pragmatic approach, if such an optimization is desired to be pursued realistically. The minimum EPNL design variant also fulfills the TOFL, time to climb as well as LDN requirements, although the smaller wing results in an increase in the approach speed to 144 knots, which is over the required approach speed of 138 knots for the SR aircraft.

2. Optimized SR design for minimum 85 phon community impacted area –minimum loudness SR design: The second optimized SR design is presented for the loudness metric, whereby the target criteria was taken to be the cumulative 85 phon impacted area on the ground, summing the community noise impact for both the departure and approach phases. It can be observed in Table 8.4 that the optimized design that minimizes the 85 phon loudness area on the ground was selected by the optimizer to be very close to the EPNL optimized design. The optimizer again selected an as large as possible engine by selecting a value of $T/W = 0.4$ and a slightly smaller wing than the reference SR design by selecting a value of $W/S = 659 \text{ kg/m}^2$. This combination of T/W and W/S produces the minimum loudness impact on the ground based on the trends seen in Chapter 7 (cf. Fig. 7.10 and Fig. 7.12), reducing the cumulative 85 phon loudness impacted area by 23%. Since the optimization target was chosen to be the 85 phon impacted area, a slightly smaller wing than the reference wing size was selected as the optimal solution. It can be seen in Fig. 7.10 that had the target been minimization of the 65 phon impacted area, then the optimized design would have selected an even smaller wing size. That the loudness optimized design is ultimately very similar to the EPNL optimized design is not surprising as it was already seen in Chapter 7 that the conventional EPNL and dBA metrics followed the same trends as the loudness metric for most of the parametric variations.

It can also be mentioned here that optimizing the aircraft design by varying only the two top-level aircraft design parameters of thrust to weight ratio and wing-loading is limited in its range of possible designs, unlike a variation whereby all engine geometry parameters and airframe geometry parameters could be varied independent of each other. For the airframe, this is easier to perform as a change in the slat geometry will primarily change slat noise and will affect the lift generated by the wing, which will in turn modify the flight paths. For the engine geometry, an individual parametric variation will require a highly detailed simulation of the engine cycle for the actual geometry values, as a change in the number of fan blades will change the fan noise but will also modify the engine thrust and also the thermodynamics further downstream of the blades. Such a capability is usually not implemented during the conceptual design phase and an implicit coupling of the engine geometry with the thermodynamics is used. From the uncoupled variations presented in Chapter 7, it is nonetheless evident that the variation of individual engine geometry parameters can have a great effect on the sound produced by the engine. Such an optimization would be able to produce designs that differ significantly from the SR aircraft and could be optimized to an even greater extent for both the level as well as the quality of the sound. Such a capability would also allow a parallel optimization of the engine performance, besides the optimization for noise presented in this dissertation. The coupled T/W and W/S optimizations presented here nonetheless show at an early stage how the overall aircraft design could be influenced to minimize the noise impact either in

terms of level or quality, taking into account in parallel any adverse effects on performance that such an optimization may produce.

Table 8.5 shows the detailed certification noise impact and Table 8.6 the detailed community noise impact of the minimum loudness SR variant, which produces for most metrics a noise impact comparable to the minimum EPNL SR variant presented in Table 8.2 and in Table 8.3.

Table 8.4: Comparison of reference SR aircraft and minimal loudness optimized designs

<i>Parameter Name</i>	<i>SR-Ref</i>	<i>SR-Min. Loudness</i>
<i>Engine geometry parameters</i>		
Fan inlet area, A_{fan} [m ²]	2.058	2.58
Fan rotor blades, B [-]	31	29
Fan stator vanes, V [-]	36	59
Fan tip des. Mach, $M_{t,d}$ [-]	1.43	1.46
Primary jet area, $A_{jet,1}$ [m ²]	0.201	0.285
Secondary jet area, $A_{jet,2}$ [m ²]	1.01	1.26
<i>Airframe geometry parameters</i>		
Wing area, S [m ²]	117.68	117.17
Wing span, b [m]	33.39	33.32
Flap area, S_f [m ²]	8.48	8.45
Flap span, b_f [m]	8.51	8.50
<i>Aircraft design and performance parameters</i>		
Wing-loading, W/S [kg/m ²]	629	659
Thrust-to-Weight ratio, T/W [-]	0.312	0.400
SLST [kN]	113.34	151.46
MTOW [kg]	74014	77221
OWE [kg]	40166	42133
Block fuel [kg]	13910	15017
TOFL [m]	1962.05	1487.92
Time to climb to ICA [min]	15.89	9.74
Approach speed, V_{app} [m/s]	138.05	140.88
LDN [m]	1517.45	1552.46
<i>Cumulative community impact areas</i>		
85 EPNdB EPNL area [km ²]	13.04	7.24
85 phon loudness area [km ²]	12.44	9.56
0.1 t.u. tonality area [km ²]	127.84	112.72

Table 8.5: Certification noise impact comparison of reference SR aircraft and minimum loudness optimized design

Certification noise impact	Flyover SR-Ref	Flyover Min. Loudness	Approach SR-Ref	Approach Min. Loudness
SPL [dBA]	73.50	72.27	89.0	88.27
EPNL [EPNdB]	89.15	80.7	99.07	97.25
Loudness [sone]	24.28	20.2	80.03	74.6
Tonality [t.u.]	0.064	0.073	0.106	0.123
Sharpness [acum]	1.17	1.07	1.74	1.69

Table 8.6: Community noise impact comparison of reference SR aircraft and minimum loudness optimized design

Community noise impact [km²]	Departure SR-Ref	Departure Min. Loudness	Approach SR-Ref	Approach Min. Loudness
dBA threshold 1 55 dBA area	50.4	35.28	67.2	61.16
dBA threshold 2 75 dBA area	2.28	2.04	2.76	1.84
EPNL threshold 1 65 EPNdB area	79.56	41.04	93.2	62.96
EPNL threshold 2 85 EPNdB area	6.48	4.28	6.56	2.96
Loudness threshold 1 65 phons area	84.92	58.84	102.24	94.68
Loudness threshold 2 85 phons area	4.64	3.36	7.8	6.2
Tonality threshold 1 0.075 t.u. area	1.84	12.56	172.24	142.4
Tonality threshold 3 0.10 t.u. area	0	0.52	127.84	112.2
Sharpness threshold 1 0.75 acum area	51.12	38.24	94.84	83.2
Sharpness threshold 2 1.0 acum area	17.28	14.2	27.28	21.32

3. Optimized SR design for minimum 0.1 t.u. community impacted area –minimum tonality SR design:

Table 8.7 shows the relevant values for the SR aircraft design variant which produced the minimum cumulative 0.1 t.u. tonality impact on the ground. It can be noticed that the minimum tonality design is significantly different from the minimum EPNL and minimum loudness designs, with the optimizer selecting a smaller engine via a T/W value of 0.275 and a larger wing via a W/S value of 556 kg/m² to minimize the 0.1 t.u. tonality impact on the ground. It can be seen that the tonality optimized design does not result in an increase in the MTOW and OWE values or on the block fuel and hence does not show, at least at a conceptual design phase, any clear negative effects on the aircraft weight and fuel consumption compared to the reference SR design. This situation may of course change as the design would progress to the more detailed design phases. With regards to the SR design requirements, because of the smaller engine and larger wing of the minimum tonality design, it narrowly fails to meet the required TOFL of 2200 m, requiring 2273 m to takeoff. The climb performance is also not as efficient as the reference SR design, but nonetheless still meets the SR requirements. As can be expected, the larger wing allows the minimum tonality design variant to have a lower approach speed and a smaller landing distance to come to a halt after touchdown.

Table 8.7: Comparison of reference SR aircraft and minimal tonality optimized designs

<i>Parameter Name</i>	<i>SR-Ref</i>	<i>SR-Min. Tonality</i>
<i>Engine geometry parameters</i>		
Fan inlet area, A_{fan} [m^2]	2.058	1.895
Fan rotor blades, B [-]	31	43
Fan stator vanes, V [-]	36	48
Fan tip des. Mach, $M_{t,d}$ [-]	1.43	1.41
Primary jet area, $A_{jet,1}$ [m^2]	0.201	0.172
Secondary jet area, $A_{jet,2}$ [m^2]	1.01	0.92
<i>Airframe geometry parameters</i>		
Wing area, S [m^2]	117.68	131.35
Wing span, b [m]	33.39	35.24
Flap area, S_f [m^2]	8.48	9.47
Flap span, b_f [m]	8.51	8.99
<i>Aircraft design and performance parameters</i>		
Wing-loading, W/S [kg/m^2]	629	556
Thrust-to-Weight ratio, T/W [-]	0.312	0.275
SLST [kN]	113.34	98.36
MTOW [kg]	74014	73046
OWE [kg]	40166	39731
Block fuel [kg]	13910	13548
TOFL [m]	1962.05	2273.4
Time to climb to ICA [min]	15.89	22.25
Approach speed, V_{app} [m/s]	138.05	130.48
LDN [m]	1517.45	1425.88
<i>Cumulative community impact areas</i>		
85 EPNdB EPNL area [km^2]	13.04	13.08
85 phon loudness area [km^2]	12.44	13.64
0.1 t.u. tonality area [km^2]	127.84	12.44

The noise impact of the minimum tonality SR design variant is considerably different to that of the EPNL and loudness optimized aircraft designs presented earlier. It can be seen in Table 8.8 for noise impact at the certification points that the changes in the dBA metric between the two designs are very minute, although a considerable reduction in the EPNL value at flyover point of close to 5 EPNdB and an increase at approach point of 1.5 EPNdB are observed. The dBA metric is thus unable to capture the difference in the sounds of the reference and tonality optimized designs. It can be seen that in terms of the sound quality metrics, the loudness at the flyover point is only slightly reduced but a large reduction in tonality of the optimized aircraft of 42% is produced at the flyover point. At the approach point, the minimum tonality design produces a considerable increase in loudness of close to 9 sone but reduces the tonality by

35%. The sharpness of the aircraft noise remains more or less unchanged at the flyover point, with a very slight increase observed at the approach point.

The community noise impact of the minimum tonality SR design variant is presented in Table 8.9. The changes in the dBA impacted area are again minimal between both designs, with a slight increase in the 55 dBA threshold area observed during departure due to the less steep climb over the later departure phase of the minimum tonality SR variant due to its larger wing size (cf. Fig. 7.9 (right)). Although noticeable changes at the certification points for the EPNL metric were observed, the changes in the EPNdB impacted areas for both departure and approach are much lower. The minimum tonality variant produces a 14% larger loudness impacted area on the ground during departure and produces a very slight increase in the loudness impacted area during approach, although a larger increase in loudness of 9 sone was observed at the approach certification point. These differences in the noise impact at certification points and community noise indicate once again that considering the noise impact solely at the certification points may not always be representative of the noise impact felt by residents living over larger distances from the airport.

Table 8.8: Certification noise impact comparison of reference SR aircraft and minimum tonality optimized design

<i>Certification noise impact</i>	<i>Flyover SR-Ref</i>	<i>Flyover Min. Tonality</i>	<i>Approach SR-Ref</i>	<i>Approach Min. Tonality</i>
SPL [dBA]	73.50	74.31	89.0	90.69
EPNL [EPNdB]	89.15	84.11	99.07	100.56
Loudness [sone]	24.28	23.69	80.03	88.98
Tonality [t.u.]	0.064	0.037	0.106	0.069
Sharpness [acum]	1.17	1.16	1.74	1.87

Table 8.9: Community noise impact comparison of reference SR aircraft and minimum tonality optimized design

<i>Community noise impact</i> [km ²]	<i>Departure SR-Ref</i>	<i>Departure Min. Tonality</i>	<i>Approach SR-Ref</i>	<i>Approach Min. Tonality</i>
dBA threshold 1 55 dBA area	50.4	60.84	67.2	65.6
dBA threshold 2 75 dBA area	2.28	2.28	2.76	2.6
EPNL threshold 1 65 EPNdB area	79.56	75.2	93.2	88.0
EPNL threshold 2 85 EPNdB area	6.48	5.76	6.56	7.32
Loudness threshold 1 65 phons area	84.92	97.0	102.24	103.32
Loudness threshold 2 85 phons area	4.64	5.4	7.8	8.24
Tonality threshold 1 0.075 t.u. area	1.84	0	172.24	68.24
Tonality threshold 3 0.10 t.u. area	0	0	127.84	12.44
Sharpness threshold 1 0.75 acum area	51.12	50.88	94.84	90.4
Sharpness threshold 2 1.0 acum area	17.28	19.4	27.28	28.8

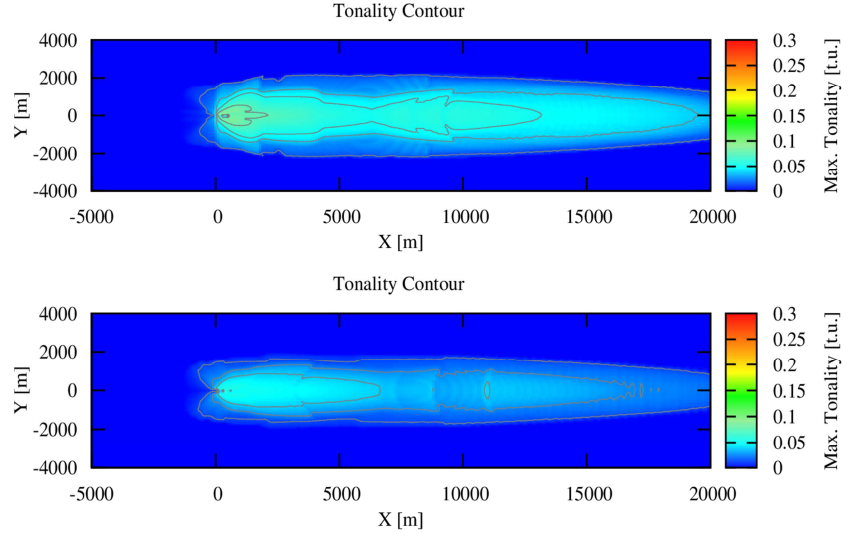


Figure 8.3: Standard departure tonality contours for the reference SR aircraft (top) and minimal tonality SR aircraft design variant (bottom)

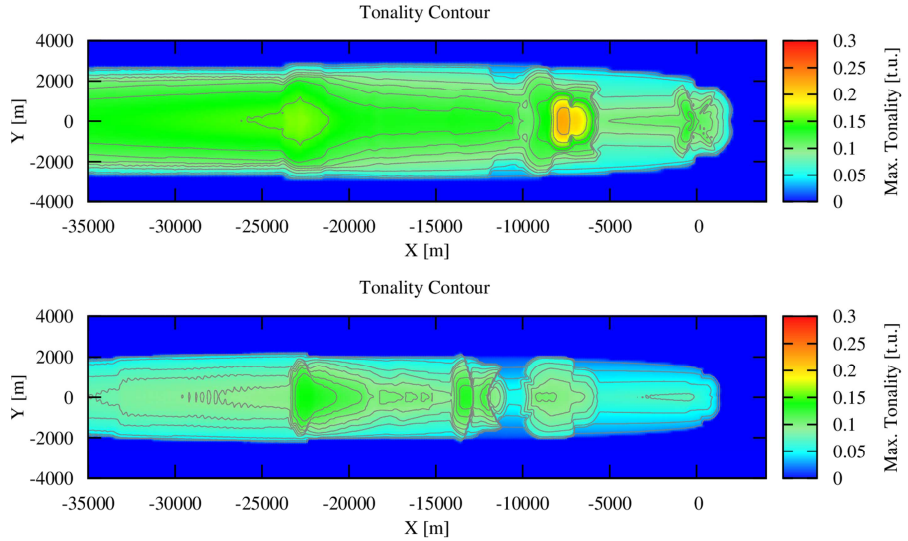


Figure 8.4: Standard approach tonality contours for the reference SR aircraft (top) and minimal tonality SR aircraft design variant (bottom)

The community noise impact in the tonality metric, in contrast to the other metrics, shows very significant reductions for the minimum tonality SR design when compared to the reference SR design. It can be seen that the tonality during departure is completely reduced to values below 0.075 t.u. and large reductions of 60% for the 0.075 t.u. impacted area and 90% for the 0.1 t.u. impacted area are observed during approach. This reduction in tonality is shown visually using the tonality contours for the minimum tonality design, which are compared to the reference SR tonality contours (shown again for a direct comparison) in Fig. 8.3 and Fig. 8.4. It can be seen that for departure the tones have been reduced to very low intensities both laterally and directly below the flight path, and for approach the tonality exceeds the higher threshold of

0.1 t.u. only for some limited regions, as was shown numerically in Table 8.9. Besides the numerical and visual representation of the changes in the tonal content or other changes in aircraft noise sound quality, the changes in the actual *sound* produced are analyzed in the next subsection.

8.1.1 Correlation of optimized designs with sound

The ultimate goal of a metric that is used to assess aircraft noise should be an as close as possible approximation to the actual sound that is produced. This sound is after all what is actually heard by the residents and any metric that can better capture the sound characteristics of aircraft noise than the currently used metrics in the aerospace industry would allow a better correlation to what the residents find annoying in the aircraft sounds that they are exposed to. It is for this reason that the research presented in this dissertation employed the use of the sound quality metrics, which may help in indicating if the current metrics are sufficient to judge the sounds of current as well as future aircraft or more information is obtained by using the alternate sound quality metrics. The optimized designs for various metrics presented in this chapter were optimized in order to minimize the community noise impact they cause numerically and various changes in both the level and quality of aircraft noise were observed, which could be understood visually via the spectra, by following the time-dependent noise variation and on a more overall level via the maximum value noise contours in the various metrics. Since the goal of the noise metrics is ultimately an estimation of the sound and its correlation to the experienced annoyance, synthetic sounds of the optimized SR aircraft design variants were created using the auralization infrastructure of RWTH Aachen University and compared with the sounds of the reference SR aircraft.

Fig. 8.5 shows the spectrograms for the SR standard approach at a ground location of $(X, Y) = (-25 \text{ km}, 0 \text{ km})$ for the reference SR design in Fig. 8.5 a), for the minimum tonality variant in Fig. 8.5 b), for the minimum EPNL variant in Fig. 8.5 c) and for the minimum loudness variant in Fig. 8.5 d). The standard approach procedure is compared for sound first, as it involves less deviations in the flight paths of the various optimized designs and also since the tonal content is more prominent during approach than during departure. The comparison of Fig. 8.5 a) and Fig. 8.5 b) shows that overall the reference and minimum tonality SR designs have spectrograms that deviate hardly at all in terms of the broadband content, but differ quite clearly in terms of tonal content. The highlighted area of the spectrograms in Fig. 8.5 a) and Fig. 8.5 b) show that the fundamental tone has been shifted to a slightly higher frequency but its intensity has been reduced considerably for the minimum tonality design, by close to 10 dB. Furthermore, the reference SR aircraft spectrogram has three noticeable tones with two having a significant intensity for large durations of the procedure whereas the minimum tonality version has two tones noticeable, with only the fundamental fan tone having a reasonable, albeit much reduced intensity. The difference in broadband content is very subtle but the overall sound which is produced, due to the lower tonality, has a gained a perceptibly different character. Knowing that the tonal content is a significant contributor to the perceived annoyance as outlined in Chapter 3, the minimum tonality SR design may have lowered the experienced annoyance due to the SR aircraft primarily by a redistribution of the spectral energy without drastic changes to the aircraft design. More certainty as to whether a clear reduction in annoyance based on the altered sound is achieved will require feedback from psychoacoustic surveys with test audiences, an aspect which as mentioned earlier, was beyond the scope of the current research work.

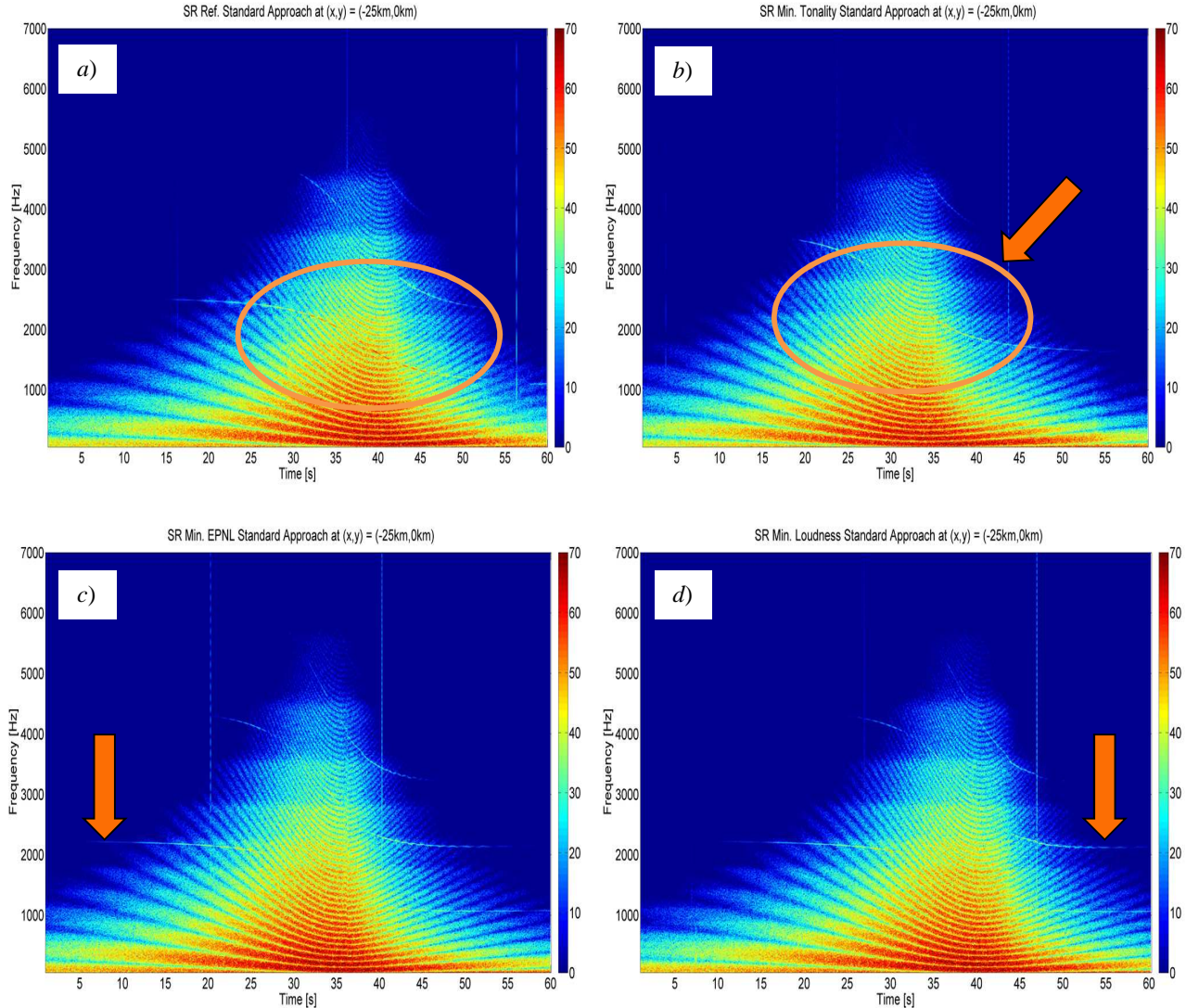


Figure 8.5: Spectrograms of synthetic audio created at $(X, Y) = (-25 \text{ km}, 0 \text{ km})$ for a standard approach procedure – a) reference SR aircraft, b) minimum tonality variant, c) minimum EPNL variant and d) minimum loudness variant

Fig. 8.5 c) and Fig. 8.5 d) show the sounds produced at the same ground location if the minimum EPNL and minimum loudness designs are flown virtually over a standard approach procedure. It can be seen that both design variants produce very similar sounds at the same ground location. The broadband content is slightly increased for both designs compared to the reference SR aircraft at the mentioned ground location and for both variants it can be noticed that the tones also have slightly reduced intensities, implying that they became slightly less prominent compared to the reference SR design. It can also be noticed for both the minimum EPNL and minimum loudness designs that the tones occur at slightly lower frequencies and are absorbed less efficiently by the atmosphere, thereby making them audible over longer durations of the procedure than what is seen in the reference SR spectrogram.

Fig. 8.6 shows the differences in the sounds produced between the reference SR aircraft in Fig. 8.6 (left) and the minimum loudness SR variant in Fig. 8.6 (right) for a standard departure at a ground location of $(X, Y) = (12.5 \text{ km}, 0 \text{ km})$. At this ground location, the minimum loudness design shows a clearly reduced overall spectral energy compared to the reference SR aircraft due to the aircraft being higher at the same location and the larger engine being quieter for the minimum loudness (and the very similar minimum EPNL) design. The fan tone that is slightly noticeable in Fig. 8.6 (left) has also been removed in the minimum loudness design departure spectrogram in Fig. 8.6 (right), again due to the aircraft being at higher altitudes and the high frequency fan tone being absorbed more strongly by the atmosphere than during the SR aircraft departure.

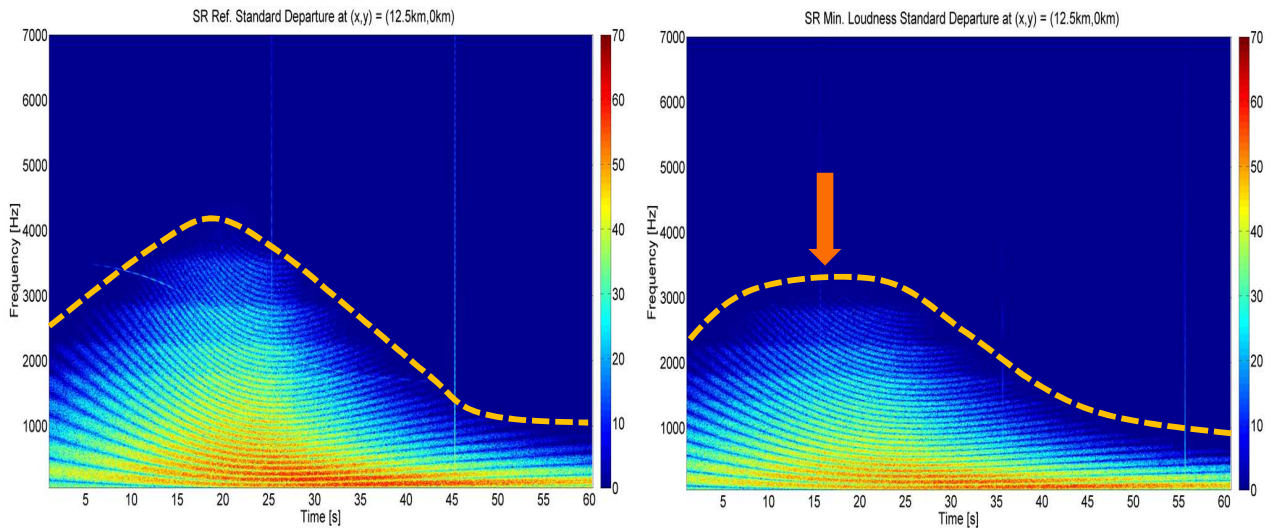


Figure 8.6: Spectrograms of synthetic audio created at $(X, Y) = (12.5 \text{ km}, 0 \text{ km})$ for a standard departure procedure - reference SR aircraft (left) and minimum loudness variant (right)

It can be seen that based on the sample spectrograms presented in this subsection, as well as based on the analysis presented in this section till now, the EPNL and loudness metrics capture the overall spectral energy of the SR design quite well. The tonal content is however not sufficiently captured by the EPNL metric as the minimum EPNL design attempted to minimize both the broadband and tonal content of the aircraft noise simultaneously and resulted in a sound that ended up being closer to the minimum loudness design rather than to the minimum tonality design for the SR aircraft. This can be attributed to the lower tonality of the SR aircraft, which for most cases does not result in high enough tonal penalties during the EPNL metric calculation. The tonality metric however captures the tonal content of aircraft noise very well, producing clear changes in the tonality experienced by residents on the ground, with only slight changes to the other sound characteristics caused in parallel. The analysis presented thus far would indicate that a combination of the loudness and tonality metrics, such as that proposed by the modified psychoacoustic annoyance metric mentioned in Section 3.1 may provide a different means of assessing both the broadband and tonal content of aircraft noise simultaneously than the EPNL metric. Such a metric would also reflect the advances in psychoacoustics over the previous many decades and would reflect the annoyance aspect of aircraft noise in a possibly superior way to the currently used EPNL metric.

A preliminary optimization for the modified PA metric was performed over the course of this dissertation as well. The metric was implemented in the assessment component of INSTANT according to Eq. 3.1 to Eq. 3.5, although the sharpness weighting term had to be reduced from $S = 1.75$ acum to $S = 1.0$ acum as aircraft noise for commercial aircraft for the most cases rarely reaches such high sharpness values, which may be common on other machinery or household appliances for which the PA metric was originally developed. The roughness metric was not implemented in INSTANT as mentioned earlier due to the insufficient temporal resolution of the flight paths and also due to the roughness of commercial turbofan engine aircraft being of lower relevance than for propeller based engines. For this reason, the roughness weightage term was given a value of zero in the metric's current application. As such, the implementation and subsequent optimization of the SR aircraft for the modified PA metric should only be seen as a possible method of combining the effects of loudness and tonality in one metric, in an alternate way to the EPNL metric, rather than as a definite superior solution. The modified PA metric would have to be more generally validated and adapted more broadly for aircraft noise in all flight phases before it would be suitable for a more general application in the aerospace industry. The optimized design for minimum modified PA community noise impact turned out to lie closer to the minimum tonality SR variant than to the minimum EPNL variant. The optimizer of the parameter study manager module also selected a T/W value of 0.275 for the minimum modified PA design but selected a smaller wing size with a slightly higher W/S of 646 kg/m^2 rather than a larger wing size which was selected for the minimum tonality design. This is because the optimizer attempted to minimize both the tonality (by selecting a smaller engine) as well as the loudness (by reducing the broadband airframe noise) of the SR aircraft noise.

8.1.2 Comparison with current aircraft having acoustic liner technology

It was shown in Section 5.2 that acoustic liner technology plays a very crucial role in the certification for noise of current commercial aircraft. It was shown that significant cumulative EPNdB reductions of 9.3 EPNdB are achieved for the SR aircraft when the effect of modern acoustic liners is activated. The influence of acoustic liner technology is aimed predominantly to damp and reduce fan noise intensity, especially the intensity of the fan tones emanated from both the fan inlet and exhaust. One of the goals of this dissertation has been to develop a capability with which a trade-off could be performed between the use of acoustic liners, which add weight to the aircraft and are also costly, to inherent aircraft noise and annoyance reduction by design via a readjustment of the spectral energy between the broadband and tonal components.

Table 8.10 and Table 8.11 show the comparison of the certification and community noise impact of the reference SR aircraft with and without acoustic liner technology for both conventional and sound quality metrics. For certification noise, it can be seen in Table 8.10 that the use of acoustic liner technology in this case can reduce the cumulative EPNdB value by a slightly higher amount of 10.2 EPNdB due to the SR aircraft used in the optimizations having a slightly different overall weight and hence slightly different flight paths. The use of acoustic liner material also results in favorable reductions in the sound quality metrics, with large reductions in loudness at the certification points observed and slight reductions in tonality and sharpness values.

It can be seen that the acoustic liner material reduces the EPNL impact particularly effectively with significant reductions seen at the certification points and also for community noise impacted area in Table 8.11, when compared to the reference SR design without acoustic liner material. For community noise

impact, the 65 EPNdB area is for instance reduced by 23% due to acoustic liner material and the 85 EPNdB impacted area is reduced by 39% during takeoff, with comparable EPNdB reductions seen during the approach phase. The significant reductions in loudness seen at the certification points are however not seen to the same extent via the community impacted loudness areas, with lower reductions of between 5% and 6% observed for the 65 phon loudness impacted area for departure and approach. As can be expected, the use of acoustic liner material results in a favorable reduction of the tonal impact on the community, by producing reductions in tonality impacted areas during the approach phase of 22% for the 0.075 t.u. tonality impacted area and 36% for the 0.1 t.u. tonality impacted area. As such, the use of acoustic liner material on current aircraft engines does produce a clear reduction in the noise impact for residents both in terms of level and quality of aircraft noise.

Comparing with the optimized aircraft designs however, it can be observed that the acoustic liner material still does not reduce the tonal content by the very large amounts shown by the minimum tonality design, both at certification as well as for community noise impact. It appears from the preliminary analysis carried out in this dissertation that the use of the acoustic liner material has been specialized to result in EPNdB reductions and it does this quite effectively when compared to the reference design without acoustic liner technology. Nonetheless, the use of acoustic liner technology still does not reduce the EPNdB impacted areas either during departure or approach to the extent of the minimum EPNL optimized design. The same can be said about the reduction in loudness, which is also not reduced by using acoustic liner technology as effectively as by a design optimized for minimal loudness (cf. Table 8.6). It can be said that based on the analysis carried out in this chapter, significantly higher reductions in both level as well as quality of aircraft noise could be obtained if either the level or quality is considered from an early design phase, rather than by using acoustic liner material at a later stage as is the convention today.

One factor not considered in the analysis for acoustic liner material is the actual added weight to the reference SR aircraft design due to use of the acoustic liner material on the engines. The slightly increased weight of the minimum EPNL or minimum loudness design for instance is in the range of the weight that is added on current aircraft by use of acoustic liner material. As the minimum tonality design showed no clear increase in weight and the minimum EPNL and minimum loudness designs showed only a slight increase in aircraft weight, it may on an aircraft level be more advantageous in terms of aircraft weight (besides being more effective at reducing noise impact) to design aircraft for inherently acceptable sounds rather than solely using acoustic liner technology. The capability presented in this dissertation can be used to perform this trade-off, aiding aircraft and engine designers to assess what design options could ultimately result in the optimal solution for both optimal performance and optimal sound.

Table 8.10: SR aircraft reference with liner and minimum tonality optimized designs comparison

<i>Certification noise impact</i>	<i>Flyover SR-Ref</i>	<i>Flyover SR-Ref-with liner</i>	<i>Approach SR-Ref</i>	<i>Approach SR-Ref-with liner</i>
SPL [dBA]	73.50	73.79	89.0	88.0
EPNL [EPNdB]	89.15	81.71	99.07	96.29
Loudness [sone]	24.28	20.73	80.03	68.55
Tonality [t.u.]	0.064	0.048	0.106	0.098
Sharpness [acum]	1.17	0.93	1.74	1.50

Table 8.11: SR aircraft reference with liner and minimum tonality optimized designs comparison

<i>Community noise impact [km²]</i>	<i>Departure SR-Ref</i>	<i>Departure SR-Ref-with liner</i>	<i>Approach SR-Ref</i>	<i>Approach SR-Ref-with liner</i>
dBA threshold 1 55 dBA area	50.4	49.44	67.2	61.88
dBA threshold 2 75 dBA area	2.28	1.72	2.76	1.6
EPNL threshold 1 65 EPNdB area	79.56	60.96	93.2	73.0
EPNL threshold 2 85 EPNdB area	6.48	3.96	6.56	2.8
Loudness threshold 1 65 phons area	84.92	80.92	102.24	95.8
Loudness threshold 2 85 phons area	4.64	3.56	7.8	6.0
Tonality threshold 1 0.075 t.u. area	1.84	0.52	172.24	134.68
Tonality threshold 3 0.10 t.u. area	0	0	127.84	81.44
Sharpness threshold 1 0.75 acum area	51.12	38.56	94.84	61.88
Sharpness threshold 2 1.0 acum area	17.28	12.0	27.28	16.32

9 Conclusions and outlook

9.1 Conclusions

This dissertation was written with the goal of highlighting the need for an alternate assessment of aircraft noise and providing a means of incorporating the alternate assessment approach in the aircraft design process. Using this approach aircraft could be designed in the future that produce sounds which are perceived as less annoying and therefore more acceptable by residents living in airport communities. The reason for adopting an alternate approach to aircraft noise assessment using metrics that capture the different sound characteristics of aircraft noise in a superior way was the different sound produced by current aircraft compared to aircraft that flew when the conventional metrics for aircraft noise assessment were developed. Noise components that were not prominent in the early stages of jet aviation have gained prominence today, and the currently used metrics have been found to be deficient in capturing the detailed aircraft noise sound characteristics. Particularly the tonal content was seen to be an aspect that would need improvement in the way it is assessed currently using the EPNL metric, keeping in mind future propulsion concepts such as CROR engines which are projected to enter the aerospace market in the coming decades.

The best approach in improving on the currently used metrics in the aerospace industry was reasoned to be the approach followed by other product industries such as automotive and industrial design, which make use of the sound quality metrics to perform sound engineering of products i.e. predicting any adverse sound effects and removing them by modifying the product's design. Such an approach had only been applied to aircraft sounds in a very preliminary way by other organizations, and no attempt had been made till now to assess the annoyance of aircraft noise during the design phase using the sound quality metrics of loudness, tonality and sharpness. This dissertation made a first attempt to not only assess current aircraft for their annoyance using the sound quality metrics, but also use it as an optimization target during the design process such that aircraft designs that produce minimal annoyance could be produced by design. This approach can not only produce more acceptable aircraft sounds but also reduce the need to use late noise reduction measures such as acoustic liner technology, used currently on all modern turbofan engines.

In order to be able to assess aircraft noise during the aircraft design process, a means was needed to predict the aircraft noise firstly at the source and subsequently on the ground, where it would reach the residents. For this purpose, parametric semi-empirical and semi-analytical models were judged to be the most suitable as they offer the computational efficiency required for aircraft design purposes and also reflect the physics that is behind the generated noise at the source. Some of these models are more of an empirical nature, such as Heidmann's model for fan noise prediction due to the numerous complex fan noise generation mechanisms involved in its prediction which are more difficult to predict analytically. Other models incorporate aspects of aeroacoustic theory such as the jet velocity correlation with Lighthill's acoustic power law in Stone's jet noise prediction model and the aircraft airspeed correlation in Fink's model for trailing edge and gear noise prediction. Fink's model is more analytical in nature as it approximates the directivities of the airframe components for instance using cosine and sine relations identified in aeroacoustic theory by Ffowcs-Williams and Hall as well as by Curle. The parametric source

noise models were seen to predict aircraft noise with a reasonable accuracy both at the source as well as on the ground, although modest to large differences could be observed for certain polar angles and frequencies. It was important for the purposes of this dissertation's research work that the models predict trends in tonal and broadband noise variation correctly for different aircraft and different designs, even if they do not provide an exact match to measured data. This requirement was seen to be fulfilled quite well by the implemented parametric models.

The noise from the source has to be assessed on the ground, for which the propagation effects of geometric spreading, atmospheric absorption, ground reflection and lateral attenuation were applied to the source noise, taking into account the specific aircraft-observer geometry. The source noise models as well as the propagation methods were combined to develop an overall aircraft noise simulation and assessment module – INSTANT. For performing aircraft noise assessment during aircraft design, INSTANT was integrated in the aircraft design and optimization environment MICADO, which provided the necessary source noise inputs over the entire flight path for both departure and approach procedures. In this way, a noise assessment capability was developed for this dissertation which could assess aircraft noise for both noise certification of aircraft designs, as well as for the noise impact caused on communities living in airport vicinities. Besides being able to assess aircraft noise in the conventional metrics of dBA and EPNL, the assessment capability of INSTANT was extended to include assessments in the sound quality metrics. The methods of Zwicker, von Bismarck and Aures were implemented for this purpose to predict the loudness, sharpness and tonality of the simulated aircraft noise spectra on the ground. As these metrics, particularly loudness and tonality were known to be primary contributors to the perceived annoyance due to aircraft noise, assessment in the sound quality metrics allowed a means of assessing the annoyance caused by aircraft noise.

The use of the aircraft noise assessment during aircraft design capability was then used to perform parametric design sensitivities by firstly varying noise relevant engine geometry parameters and following their effect on both the noise level and sound quality of aircraft noise. Some important results of this engine geometry variation were that a larger engine is quieter but more tonal, decreasing the fan rotor blade number can increase the tonality, increasing the primary and secondary jet areas can increase the loudness and decrease simultaneously the tonality and reducing the blade tip design Mach number or increasing the rotor-stator spacing can reduce the noise impact in both conventional and sound quality metrics. These results can be seen as design guidelines for aircraft and engine designers when performing aircraft and engine design and considering noise or annoyance impact in parallel.

Secondly, the overall aircraft design parameters of thrust to weight ratio and wing-loading were varied as individual geometry variations are not always feasible during the design process and their effect on the noise and annoyance impact was also quantified. The major results of the overall aircraft design variations were that a larger wing can increase the loudness of aircraft noise and at the same time reduce the tonality (due to tonal prominence and masking effects) and a smaller wing has the opposite effect of reducing loudness and increasing tonality. It was also seen that a larger engine can be significantly quieter than a smaller engine, although with a much higher tonality. This observation corresponds to the current trends where as high as possible bypass ratios are pursued, which lower jet noise due to lower jet velocities but at the same time have an increased fan noise intensity. For these very high bypass ratio engines, the use of acoustic liner technology to reduce fan noise becomes essential. This use could be reduced if the tonal

content is considered from an early design phase and the entire spectral signature of the aircraft is regarded as a whole, as has been done in this dissertation.

The parametric design variations were then performed simultaneously to explore the optimization possibilities for producing aircraft designs that minimize the annoyance impact by having considered the annoyance impact as an optimization target. For this purpose, optimized designs for the EPNL metric, loudness metric and tonality metric were produced using the MICADO environment by using the cumulative community noise impacted area for each metric as a minimization target. It was found that the minimum EPNL design and minimum loudness design were very similar to each other, having an as large as possible engine and a smaller wing than the reference aircraft to minimize the EPNdB and loudness impacted areas. The similarity of the minimum EPNL and minimum loudness designs indicated that the EPNL metric captured the loudness aspect of aircraft noise for the reference short-range aircraft design but not the tonal content, which for the short-range aircraft was relatively low. The tone penalties used in the EPNL metric calculation were in this case not high enough to be captured by the EPNL metric. The minimum tonality design minimized the tonality impacted area by reducing the engine size and increasing the wing size. In terms of impact on aircraft performance and weight, a slight increase in weight was seen for the minimum EPNL and minimum loudness designs, but no weight penalty was observed for the tonality optimized design, at a conceptual design phase.

A conversion to sound of the optimized aircraft design noise impact showed that the minimum EPNL and minimum loudness designs reduced the overall spectral energy of aircraft noise, whereas the minimum tonality design altered solely the fan tonal noise intensity, without significantly affecting the broadband aircraft noise components. The reductions in tonal intensity of the minimum tonality design compared to the reference design could be perceived audibly and the fundamental tone was seen in the spectrograms to have a reduced intensity of approximately 10 dB at a sample ground location for a standard approach procedure. The changes in sound due to the minimum EPNL and minimum loudness designs could only mildly be observed during the approach phase, although a large overall reduction of overall spectral energy was observed during the departure phase for both designs. Based on these results, it was concluded that depending on the metric chosen as a target for reducing noise or annoyance impact, considerably different sounding aircraft designs could be obtained. Whether the optimized aircraft sounds are indeed judged to be less annoying to the reference aircraft sounds will have to be confirmed via psychoacoustic surveys using test audiences, a task which could not be performed within the scope of this dissertation's research work.

A comparison of the optimized designs with current aircraft having acoustic liner technology was also performed and indicated that although acoustic liner technology produces favorable reductions in all the conventional as well as sound quality metrics, much more significant reductions can be obtained via the optimized aircraft designs, which consider aircraft noise or annoyance early during the design phase. An aircraft designed to minimize the tonality impact on the community can reduce the tonal impact much more effectively than the use of acoustic liner technology.

The overall results of the research work carried out in this dissertation indicate that it is indeed possible to influence the sounds of current aircraft towards less annoying or more acceptable sounds, by knowing beforehand which design change or parameter variation can result in an improvement or deterioration of

the sound. The conventional metrics currently used in the aerospace industry can be improved upon as they fail in capturing many characteristics of aircraft sounds which directly cause the perception of annoyance to residents. The more detailed psychoacoustic knowledge incorporated in the sound quality metrics allows both the broadband and tonal components of aircraft noise to be captured in a superior way to the dBA or EPNL metrics. The dBA metric doesn't account for many different spectral characteristics and the EPNL metric can prove deficient in capturing the tonal content, an aspect which was considered during its development but may require an improvement for aircraft sounds of modern aircraft of today as well as advanced aircraft of the future.

The aim ultimately is the use of a possible metric that considers aircraft noise characteristics in more detail than the current EPNL metric and would be able to capture differences in sound in a more complete and comprehensive manner. This would make it suitable not just for the assessment of sounds of current high bypass ratio engine and geared turbofan engine aircraft, but also for the assessment of future concepts such as aircraft powered with CROR engines. Based on the analysis carried out in this dissertation, a metric that combines the effects of loudness and tonality, such as the modified psychoacoustic annoyance metric of More et al. could provide a possible improvement over the EPNL metric. Such a metric would however require further validation via psychoacoustic testing for several aircraft during various flight phases before it could be used more universally for aircraft noise annoyance assessment.

The overall aim of reducing the annoyance caused by aircraft noise to residents is lowering the resistance to expansion of air-traffic infrastructure projected for the coming decades. Mere reduction in dBA or EPNdB values without actually considering the sound that reaches the residents may not suffice in achieving this goal. As such, alternate noise assessment which results in aircraft that sound less annoying or more acceptable to the residents becomes increasingly important. One way of achieving the goal of lowering resistance to aircraft noise is using noise reduction technologies such as acoustic liner material or chevron nozzles; another way of achieving this goal is to design aircraft that may inherently sound more acceptable, as has been attempted to be shown in the research work of this dissertation.

9.2 Outlook

A number of simplifications had to be made for the research work in this dissertation in order to successfully integrate aircraft noise annoyance assessment during the aircraft design process. Furthermore, a number of interesting research directions could not be pursued within the scope of the current research work. The following improvements and further research possibilities for the future can be suggested:

- The parametric semi-empirical models used for the source noise modeling provide only a limited accuracy and more accurate source noise models would be desirable to be able to predict the detailed effects that typically occur at the source and affect the quality of the sound produced at the ground. These detailed effects had to be neglected in this dissertation's research work.
- A 1/3 octave spectral analysis was performed, which is only suited for the fan or LP rotor-stator interaction tones but not for the buzzsaw tones for instance. A narrowband analysis approach would be

necessary if the more closely spaced buzzsaw tones or the numerous propeller tones produced by turboprop or CROR engines are to be considered in the sound quality analysis.

- Further research and analysis with a metric combining the effects of loudness and tonality and its comparison to the EPNL metric would be a necessary next step, in order to definitively suggest improvements that would result in a better capturing of aircraft noise sound characteristics and any changes in the spectral content. Such a metric would have to be suitable not just for assessing current turbofan powered aircraft but also any advanced turboprop or distributed propeller propulsion concepts.
- Variations of the airframe geometry components such as the wing sweep, aspect ratio, or the landing gear components may also be fruitful in order to further quantify the design sensitivities on noise and annoyance impact.
- A more detailed analysis of the optimization possibilities for long-range aircraft with high to very high bypass ratio engines would also be desirable, to append the limited and preliminary analysis performed so far for long-range aircraft designs.
- A detailed validation of the predicted sound quality with measured aircraft noise audio for several short-range and long-range aircraft would also be important in order to compare the predicted annoyance results with the annoyance caused by actual aircraft.
- An extension of the current analysis to unconventional aircraft concepts that are expected to enter the aerospace market in the future such as CROR engines and Distributed Electric Propulsion would help in seeing if the drastically different sounds produced by these concepts could also be favorably altered via design changes. Noise reducing technologies such as acoustic liner material cannot be used for the ‘open’ rotor blades and will therefore require other means such as noise shielding or improved blade aerodynamics to counter their increased annoyance. A similar approach of optimizing the open rotor sounds at an early design phase may yield additional benefits in their sound quality improvement and annoyance reduction.

References

- [1] J. Leahy, "Flying on Demand Global Market Forecast 2014-2033," Airbus, 2014.
 - [2] R. Tinseth, "Boeing Current Market Outlook 2014," Boeing, 2014.
 - [3] Fraport, "Ready for the future Annual Report 2011," Fraport, 2011.
 - [4] Heathrow Airport, "Airports Commission: Long-term hub capacity options - Heathrow airport limited response," Heathrow, London, 2013.
 - [5] Munich Airport, "Annual Traffic Report 2013 - Air traffic statistics," Munich Airport, Munich, 2013.
 - [6] M. J. Smith, Aircraft Noise, Cambridge: Cambridge University Press, 2004.
 - [7] ICAO, "Annex 16 to the Convention on International Civil Aviation: Environmental Protection Volume 1 - Aircraft Noise," ICAO, Montreal, 2011.
 - [8] C. Hughes, "The promise and challenges of Ultra High Bypass ratio engine technology and integration," in *AIAA Aero Sciences Meeting*, Orlando, Florida, 2011.
 - [9] R. P. Hellman and E. Zwicker, "Why can a decrease in dB(A) produce an increase in loudness?," *Journal of the Acoustical Society of America*, vol. 82, no. 5, pp. 1700-1705, 1987.
 - [10] R. P. Hellmann, "Contribution of tonal components to the overall loudness, annoyance and noisiness of noise: Relation between single tones and noise spectral shape," NASA CR-3892, 1985.
 - [11] A. Kjellberg, M. Goldstein and F. Gamberale, "An assessment of dB(A) for predicting loudness and annoyance of noise containing low frequency components," *Journal of low frequency noise and vibration*, vol. 3, no. 3, pp. 10-16, 1984.
 - [12] D. A. McCurdy, "Annoyance caused by advanced turboprop aircraft flyover noise," NASA TP-2782, 1988.
 - [13] T. Mavris, J. Tai, R. Young and B. Havrilesko, "Open rotor noise impact on airport communities," PARTNER Project 35 Final Report, 2011.
 - [14] B. Scharf and R. P. Hellman, "Comparison of various methods for predicting the loudness and acceptability of noise, Part II: Effects of spectral pattern and tonal components," U.S. Environmental Protection Agency, Report 550/9-79-102, 1977.
 - [15] K. P. Shepherd, J. D. Leatherwood and S. A. Clevenson, "Effect of low frequency tones and turbulent-boundary-layer noise on annoyance," NASA TP-2202, 1983.
 - [16] B. Berglund, U. Berglund and T. Lindvall, "Scaling loudness, annoyance and noisiness of aircraft noise," *Journal of the Acoustical Society of America*, vol. 57, no. 4, pp. 930-934, 1975.
 - [17] K. Berckmans, K. Janssens, P. Sas and W. Desmet, "Model based synthesis of aircraft noise to quantify the subjective human perception," *Journal of Sound and Vibration*, vol. 311, no. 3-5, pp. 1175-1195, 2008.
 - [18] A. K. Sahai, E. Anton, E. Stumpf, F. Wefers and M. Vorlaender, "Interdisciplinary auralization of takeoff and landing procedures for subjective assessment in Virtual Reality environments," in *18th AIAA/CEAS Aeroacoustics Conference*, Colorado Springs, CO, 2012.
 - [19] A. K. Sahai, E. Anton and E. Stumpf, "An interdisciplinary approach for a virtual air-traffic system simulation for subjective assessment in VR environments," in *28th International Congress of the Aeronautical Sciences (ICAS)*, Brisbane, Australia, 2012.
 - [20] M. J. Lighthill, "On sound generated aerodynamically I. General theory," *Proceedings of the Royal Society of London, Series A, Mathematical and Physical Sciences*, vol. 211, no. 1107, pp. 564-587, 1952.
-

-
- [21] M. J. Lighthill, "On sound generated aerodynamically II. Turbulence as a source of sound," *Proceedings of the Royal Society of London, Series A, Mathematical and Physical Sciences*, vol. 222, no. 1148, pp. 1-32, 1954.
 - [22] T. R. Meerburg, R. J. Boucherie and M. J. van Kraaij, "Noise load management at Amsterdam Airport Schiphol," NLR, LVNL and University of Twente, 2007.
 - [23] Aerodynamics and design group, "Noise," Stanford University , [Online]. Available: <http://adg.stanford.edu/aa241/noise/noise.html>. [Accessed 26 03 2015].
 - [24] P. R. Gliebe, "The GE90: Quieter by design - Quieter aircraft engines through leveraging new technologies," Berkley Airport Noise Symposium - Doing the Wright stuff:100 years of aviation and the environment, Berkley, 2003.
 - [25] S. Bartosch, "Impact of system capacities on air traffic forecasts," DLR, ILR of RWTH Aachen University, Hamburg, 2014.
 - [26] J. Schultz, Community Noise Rating, Applied Science Publishers, 1982.
 - [27] E. Sengpiel, "Sound measuring (Noise measuring)," Tontechnik Rechner - Sengpielaudio, [Online]. Available: <http://www.sengpielaudio.com/calculator-dba-spl.htm>. [Accessed 26 03 2015].
 - [28] Harris Miller Miller Hanson , "Study of low frequency aircraft takeoff noise at Baltimore-Washington international airport," HMMH, 1998.
 - [29] B. H. Sharp, Y. A. Gurovich and W. W. Albee, "Study of low-frequency aircraft noise research and mitigation," Wyle Report WR 01-21, Wyle Acoustics Group, 2001.
 - [30] K. D. Kryter, "Concepts of perceived noisiness, their implementation and application," *Journal of the Acoustical Society of America*, vol. 43, no. 2, pp. 344-361, 1967.
 - [31] Federal Aviation Administration (FAA), "Noise standards: Aircraft type and airworthiness certification, calculation of effective perceived noise level from measured data," Federal Aviation Regulations Part 36, Appendix A2 to Part 36 - Section A36.4, 2002.
 - [32] W. C. Sperry, "Aircraft noise evaluation," FAA Technical Report 550-003-03H, 1968.
 - [33] G. J. Ruijgrok, Elements of aviation acoustics, VSSD, Delft University Press, 1999.
 - [34] K. D. Kryter and K. S. Persons, "Judges noisiness of a band of random noise containing an audible pure tone," *Journal of the Acoustical Society of America*, vol. 38, no. 1, pp. 106-112, 1965.
 - [35] K. S. Persons, "The effects of duration and background noise level on perceived noisiness," FAA-ADS-78, 1966.
 - [36] A. C. McKennel, "Aircraft noise annoyance around London (Heathrow) airport: The Social Survey," Central Office of Information (COI), London, 1963.
 - [37] S. Fidell, "The Schultz curve 25 years later: A research perspective," *Journal of the Acoustical Society of America*, vol. 114, no. 6, pp. 3007-3015, 2003.
 - [38] H. M. Miedema and H. Vos, "Exposure-response relationships for transportation noise," *Journal of the Acoustical Society of America*, vol. 104, no. 6, pp. 3423-3445, 1998.
 - [39] K. Genuit, "Fluglaerm und psychoakustische Bewertungen," in DEGA, 2012.
 - [40] G. Warwick, "Airbus, Snecma tackle open-rotor integration," *Aviation Week and Space Technology*, 31 March 2014.
 - [41] J. W. Little and J. E. Mabry, "Development and validity of the noise unit called Effective Perceived Noise Level," The Boeing Company, 1968.
 - [42] J. B. Ollerhead, "Subjective evaluation of general aviation aircraft noise," FAA-NO-68-35, 1968.
 - [43] S. More, "Aircraft noise metrics and characteristics," PhD thesis Purdue University, 2010.
 - [44] E. Zwicker and H. Fastl, Psychoacoustics -Facts and models, Berlin, Heidelberg, New York: Springer Verlag, 1990.
-

References

- [45] A. V. Oppenheim and R. W. Schafer, Discrete-time Signal Processing, Prentice Hall Signal Processing Series, Prentice Hall, 1989.
 - [46] H. Fastl, Communication Acoustics: Psychoacoustics and sound quality, Berlin, Heidelberg: Springer-Verlag, 2005.
 - [47] R. Rylander, S. Soerensen and K. Berglund, "Re-analysis of aircraft noise annoyance data against the dB(A) peak concept," *Journal of Sound and Vibration*, vol. 36, pp. 399-406, 1974.
 - [48] J. R. Angerer, R. A. Erickson and D. A. McCurdy, "Development of an annoyance model based upon elementary auditory sensations for steady-state aircraft interior noise containing tonal components," NASA TM-104147, 1991.
 - [49] W. Aures, "Procedure for calculating the sensory euphony of arbitrary sound signals," *Acustica*, vol. 59, pp. 130-141, 1985.
 - [50] E. Zwicker, "On the dependence of unbiased annoyance on loudness," in *International Conference on Noise Control Engineering; Newport Beach, CA, USA*, 1989.
 - [51] E. Zwicker and B. Scharf, "A model of loudness summation," *Psychological Review*, vol. 72, pp. 3-26, 1965.
 - [52] G. von Bismarck, "Sharpness as an attribute of the timbre of sounds," *Acustica*, vol. 30, pp. 159-172, 1974.
 - [53] B. Scharf, R. P. Hellman and J. Bauer, "Comparison of various methods for predicting the loudness and acceptability of noise," US Environmental Protection Agency, Report 550/9-77-101, 1977.
 - [54] R. P. Hellman, "Loudness, annoyance and noisiness produced by single tone noise complexes," *Journal of the Acoustical Society of America*, vol. 72, no. 1, pp. 62-73, 1982.
 - [55] H. Fastl, "Trading numer of operations versus loudness of aircraft," in *Internoise 90*, 1990.
 - [56] T. Cox, "Sharpness and booming," University of Salford Manchester, [Online]. Available: <http://www.salford.ac.uk/computing-science-engineering/research/acoustics/psychoacoustics/sound-quality-making-products-sound-better/sound-quality-testing/sharpness-booming>. [Accessed 27 03 2015].
 - [57] D. Västfjäll and M. Kleiner, "Emotion in product sound design," in *Journe'es Design Sonor*, Paris, France, 2002.
 - [58] M. Vorländer, Auralization: Fundamentals of acoustics, modeling, simulation, algorithms and acoustic Virtual Reality, Berlin: Springer, 2008.
 - [59] K. Janssens, A. Vecchio, P. v.d. Ponseele and H. v.d. Auweraer, "Synthesis of aircraft flyover noise for target sound design," *Forum Acusticum*, 2005.
 - [60] S. A. Rizzi, A. R. Aumann, L. V. Lopes and C. L. Burley, "Auralization of Hybrid Wing-Body aircraft flyover noise from system noise predictions," *Journal of Aircraft*, vol. 51, no. 6, pp. 1914-1926, 2014.
 - [61] S. A. Rizzi, D. B. Stephens , J. J. Berton, D. E. Van Zante, J. P. Wojno and T. W. Goerig, "Auralization of flyover noise from open rotor engines using model scale test data," in *20th AIAA/CEAS Aeroacoustics Conference*, Atlanta, GA, USA, 2014.
 - [62] D. L. Palumbo, D. M. Nark, C. L. Burley and S. A. Rizzi, "Aural effects of Distributed Propulsion," in *14th AIAA Aviation Technology, Integration and Operations Conference*, Atlanta, GA, USA, 2014.
 - [63] J. R. Hardwick, "Synthesis of rotorcraft noise from flyover data," Master thesis, Virginia Polytechnic Institute and State University, 2014.
 - [64] K. White, M. Arntzen, A. Bronkhorst and M. Meeter, "Continuous Descent Approach (CDA) compared to regular descent procedures: Less annoying?," in *Internoise 2014*, Melbourne, Australia, 2014.
-

-
- [65] M. Arntzen and D. Simons, "Modeling and sysnthesis of aircraft flyover noise," *Applied Acoustics*, vol. 84, pp. 99-106, 2014.
 - [66] R. E. Caves, L. R. Jenkinson and D. P. Rhodes, "Development of an integrated conceptual aircraft design and noise model for civil transport aircraft," in *ICAS Congress*, Melbourne, Australia, 1998.
 - [67] A. Manneville, D. Pilczer and Z. S. Spakovszky, "Noise reduction assessment and preliminary design implications for a functionally silent aircraft," in *10th AIAA/CEAS Aeroacoustics Conference*, 2004.
 - [68] N. E. Antoine, "Aircraft optimization for minimal environmental impact," PhD dissertation, Stanford University, 2004.
 - [69] L. T. Leifsson, "Multidisciplinary design optimization of low-noise transport aircraft," PhD dissertation Virginia Polytechnic Institute and State University, 2005.
 - [70] L. E. Bertsch, "Noise prediction within conceptual aircraft design," PhD thesis, TU Braunschweig, 2013.
 - [71] M. Schütte, U. Müller and R. Drobietz, "An European Project - Sound Engineering For Aircraft (SEFA)," in *World Congress of Ergonomics*, Maastricht, The Netherlands, 2006.
 - [72] M. Bauer, D. Collin, U. Iemma, K. Janssens, F. Marki and U. Müller, "COSMA - A European approach on aircraft noise annoyance research," in *Internoise 2014*, Melbourne, Australia, 2014.
 - [73] F. Marki, K. Gulyas, F. Augusztinovicz, R. Bisping, M. Bauer, M. Bellmann, H. Remmers, D. Sabbatini, H. van der Auweraer and K. Janssens, "Sound synthesizer tool for on-line sound quality analysis and target sound design of aircraft flyovers," in *Internoise 2011*, Osaka, Japan, 2011.
 - [74] U. Müller, "Community Oriented Solutions to Minimise aircraft noise Annoyance," in *Aviation Noise Impacts Roadmap Annual Meeting*, Washington, USA, 2011.
 - [75] M. Diez and U. Iemma, "Multidisciplinary conceptual design optimization of aircraft using a sound-matching-based objective function," *Engineering Optimization*, vol. 44, no. 5, pp. 591-612, 2012.
 - [76] M. S. Howe, "A review of the theory of trailing edge noise," NASA CR 3021, 1978.
 - [77] S. W. Rienstra and A. Hirschberg, An introduction to aeroacoustics, Eindhoven University of Technology, 2004.
 - [78] J. Delfs, Grundlagen der Aeroakustik: Basics of Aeroacoustics, TU Braunschweig, 2011.
 - [79] N. Curle, "The influence of solid boundaries upon aerodynamic sound," *Proceedings of the Royal Society of London A*, vol. 231, pp. 505-514, 1955.
 - [80] J. E. Ffowcs-Williams and L. H. Hall, "Aerodynamic sound generation by turbulent flow in the vicinity of a scattering half plane," *Journal of Fluid Mechanics*, vol. 40, no. 4, pp. 657-670, 1970.
 - [81] J. E. Ffowcs-Williams and D. L. Hawkings, "Sound generation by turbulence and surfaces in arbitrary motion," *Philosophical transactions of the Royal Society of London*, vol. 264, pp. 321-342, 1969.
 - [82] M. E. Goldstein, Aeroacoustics, New York: McGraw-Hill Book Company, 1976.
 - [83] W. E. Zorumski, "Aircraft noise prediction program theoretical manual," NASA TM 83199, 1982.
 - [84] M. F. Heidmann, "Interim prediction method for fan and compressor source noise," NASA TM-X-71763, 1979.
 - [85] J. J. Emmerling, S. B. Kazin and R. K. Matta, "Core engine noise control program, Vol III: Supplement 1 - Prediction methods," FAA-RD-74-125, III-1, 1976.
 - [86] R. K. Matta, G. T. Sandusky and V. L. Doyle, "GE core engine noise investigation - Low emission engines," FAA-RD-77-4, 1977.
 - [87] J. R. Stone, "An improved prediction method for the noise generated in flight by circular jets,"
-

References

- NASA TM 81470, 1980.
- [88] M. R. Fink, "Airframe noise prediction method," FAA-RD-77-29, 1977.
 - [89] L. V. Lopes and C. L. Burley, "Design of the next generation aircraft noise prediction program: ANOPP 2," in *17th AIAA/CEAS Aeroacoustics Conference*, Portland, OR, USA, 2011.
 - [90] K. B. Kontos, B. A. Janardan and P. R. Griebe, "Improved NASA ANOPP noise prediction computer code for advanced subsonic propulsion system. Volume I: ANOPP evaluation and fan noise model improvement," NASA CR-195480, 1996.
 - [91] K. B. Kontos, R. E. Kraft and P. R. Griebe, "Improved NASA ANOPP noise prediction computer code for advanced subsonic propulsion systems. Volume 2: Fan suppression model development," NASA CR-202309, 1996.
 - [92] J. Kurzke, "Gasturb 11 Users Manual - A program to calculate design and off-design performance of gas turbines," GasTurb GmbH, Institute of Jet Propulsion and Turbomachinery of RWTH Aachen University, 2007.
 - [93] J. H. Miles, "Separating direct and indirect turbofan engine combustion noise using the correlation function," in *48th AIAA Aerospace Sciences Meeting*, Orlando, FL, USA, 2010.
 - [94] Advisory Council for Aviation Research and Innovation in Europe - Report of the group of personalities, "Meeting society's needs and winning global leadership," European Aeronautics: A vision for 2020, 2001.
 - [95] R. Wahls, "N+3 Technologies and Concepts," in *Green Aviation Summit - Integrated solutions for fuel, noise and emission reduction NASA Ames Research Center*, 2010.
 - [96] E. L. Bertsch, S. Guerin, G. Looye and M. Pott-Polenske, "The parametric aircraft noise analysis module - status overview and recent applications," in *17th AIAA/CEAS Aeroacoustics Conference*, Portland, OR, USA, 2011.
 - [97] N. van Oosten, "SOPRANO," in *SOPRANO Workshop*, Madrid, Spain, 2007.
 - [98] S. Hosder, "Clean wing airframe noise modeling for multidisciplinary design and optimization," PhD dissertation Virginia Polytechnic Institute and State University, 2004.
 - [99] C. Y. Kapper, "Validation of Aircraft Noise Prediction Program," NASA CR-159047, 1979.
 - [100] K. Risse, E. Anton, T. Lammering, K. Franz and E. Stumpf, "An integrated environment for preliminary aircraft design and optimization," in *53rd AIAA ASME Conference*, Honolulu, Hawaii, 2012.
 - [101] A. K. Sahai and E. Stumpf, "A comparative analysis of the subjective assessment of standard and noise abatement flight procedures," in *NoiseCon 2013 - Proceedings of NoiseCon and InterNoise 2013, INCE*, Denver, CO, USA, 2013.
 - [102] A. K. Sahai and E. Stumpf, "Incorporating and minimizing aircraft noise annoyance during conceptual aircraft design," in *20th AIAA/CEAS Aeroacoustics Conference - Part of AVIATION forum*, Atlanta, GA, USA, 2014.
 - [103] A. K. Sahai, F. Wefers, S. Pick, E. Stumpf, M. Vorländer and T. Kuhlen, "Interactive simulation of aircraft noise in aural and visual virtual environments," *Applied Acoustics*, vol. 101, pp. 24-38, 2016.
 - [104] K. H. Horstmann, "Ein Mehrfach-Traglinienverfahren uns seine Verwendung für Entwurf und Nachrechnung nichtplanarer Flügelordnungen," DLR Report DFVLR-FB 87-51, 1987.
 - [105] J. Roskam, *Airplane Design*, Ottawa, Kansas: Roskam Aviation and Engineering Corp., 1985.
 - [106] D. Raymer, *Aircraft Design: A Conceptual Approach*, Washington D.C.: American Institute of Aeronautics and Astronautics, 1989.
 - [107] B. Malone and W. H. Mason, "Multidisciplinary optimization in aircraft design using analytic technology models," *Journal of Aircraft*, vol. 32, no. 2, pp. 431-438, 1995.
-

-
- [108] W. H. Mason, Analytic models for technology integration in aircraft design, AIAA Paper No. 90-3262, 1990.
 - [109] T. Lammering, E. Anton and R. Henke, "Validation of a method for fast estimation of transonic aircraft polars and its application in preliminary design," in *Applied Aerodynamics: Capabilities and future requirements*, Bristol, UK, 2010.
 - [110] D. Y. Tan, "Design trade studies and assessment for advanced quiet aircraft concepts," MS Thesis MIT, 2005.
 - [111] IHS - Mark Daly (Editor), Jane's Aero-Engines, Jane's Information Group, 2007.
 - [112] N. Meier, "Civil Turbojet/Turbofan Specification," Jet-engine.net, 2005. [Online]. Available: <http://www.jet-engine.net/civtfspec.html>. [Accessed 28 03 2015].
 - [113] E. Torenbeek, Synthesis of subsonic airplane design, Springer, 1982.
 - [114] E. Anton, T. Lammering and R. Henke, "Fast estimation of top-level requirement impact on conceptual aircraft designs," in *10th AIAA ATIO Conference*, Fort Worth, TX, USA, 2010.
 - [115] G. C. Oates, Aircraft propulsion systems technology and design, AIAA Education Series, 1989.
 - [116] J. Allison, B. Roth, M. Kokkolaras, I. Kroo and P. Papalambros, "Aircraft family design using decomposition based methods," in *11th AIAA Multidisciplinary Analysis and Optimization Conference*, 2006.
 - [117] K. Franz, K. Risse, T. Lammering, E. Anton and R. Hörschemeyer, "Economics of laminar aircraft considering off-design performance," in *8th AIAA Multidisciplinary Design Optimization Specialist Conference*, Honolulu, Hawaii, 2012.
 - [118] F. Wefers, A. K. Sahai and M. Vorländer, "VATSS - Ein System zur interaktiven Simulation von Fluglärm," in *Fortschritte der Akustik: DAGA 2012 38. Deutsche Jahrestagung für Akustik*, Darmstadt, Germany, 2012.
 - [119] T. Finken, "Vergleich von Methoden zur Lärmuntersuchungen an Open-Rotor und Ultra-High-Bypass Triebwerken," Master Research Study, ILR of RWTH Aachen University, Aachen, Germany, 2014.
 - [120] M. Tekaat, "Implementierung und Bewertung eines semi-empirischen Verfahrens für die Prognose und Modellierung von Open-Rotor Triebwerkslärm," Master thesis, ILR of RWTH Aachen University, Aachen, Germany, 2014.
 - [121] S. L. Heath and G. L. McAninch, "Propagation effects of wind and temperature on acoustic ground contour levels," in *44th AIAA Aerospace Sciences Meeting and Exhibit*, Reno, Nevada, USA, 2006.
 - [122] M. Arntzen, "Aircraft noise calculation and synthesis in a non-standard atmosphere," PhD thesis, Faculty of Aerospace Engineering, TU Delft, Delft, The Netherlands, 2014.
 - [123] L. C. Sutherland, "Review of experimental data in support of a proposed new method for computing atmospheric absorption losses," DOT-TST-75-87, US Department of Transport, 1975.
 - [124] American National Standard Institute, "American national standard method for the calculation of the absorption of sound by the atmosphere," ANSI S1.26-1978, 1978.
 - [125] International Organization for Standardization (ISO), "Acoustics - Attenuation of sound during propagation outdoors - Part 1: Calculation of absorption of sound by the atmosphere," ISO-9613-1:1993(E), 1993.
 - [126] C. F. Chien and W. W. Soroka, "Sound propagation along an impedance plane," *Journal of Sound and Vibration*, vol. 43, no. 1, pp. 9-20, 1975.
 - [127] M. E. Delany and E. N. Bazley, "Acoustical properties of fibrous absorbent materials," *Applied Acoustics*, vol. 3, no. 2, pp. 105-116, 1970.
 - [128] W. L. Willshire, "Assessment of ground effects on the propagation of aircraft noise: The T-38A flight experiment," NASA TP-1747, 1980.
-

References

- [129] W. L. Willshire, "Lateral attenuation of high bypass ratio engined aircraft noise," NASA TM-81968, 1981.
 - [130] FAA Office of Environment and Energy, "Integrated Noise Model (INM) Version 7.0 Technical Manual," FAA-AEE-08-01, 2008.
 - [131] M. D. Guynn, J. J. Berton, M. M. Tong and W. J. Haller, "Advanced single-aisle transport propulsion design options revisited," in *AIAA Aviation Technology, Integration and Operations Conference*, USA, 2013.
 - [132] Society of Automotive Engineers (SAE), "Prediction method for lateral attenuation of airplane noise during takeoff and landing," SAE AIR-1751, Warrendale, Pennsylvania, USA, 1981.
 - [133] H. Yoshioka, "Evaluation and prediction of airport noise in Japan," *Journal of the Acoustic Society of Japan*, vol. 21, no. 6, pp. 314-344, 2000.
 - [134] I. L. Granoien, R. T. Randeberg and H. Olsen, "Corrective measures for the aircraft noise models NORTIM and GMTIM: Development of new algorithms for ground attenuation and engine installation effects," SINTEF Telecom and Informatics, Trondheim, Norway, 2002.
 - [135] J. de Luis, "A process for the quantification of aircraft noise and emissions interdependencies," PhD dissertation, Georgia Institute of Technology, 2008.
 - [136] E. Zwicker, "Procedure for calculating loudness of temporally variable sounds," *Journal of the Acoustical Society of America*, vol. 62, no. 3, pp. 675-682, 1977.
 - [137] National Institute of Advanced Industrial Science and Technology (AIST), "Full revision of international standards for equal-loudness level contours (ISO 226)," Latest research archive AIST, 2003.
 - [138] S. S. Stevens, "The measurement of loudness," *Journal of the Acoustical Society of America*, vol. 27, pp. 815-829, 1955.
 - [139] Z. Zhang and M. Shreshta, "Sound quality user-defined cursor reading control - Tonality Metric," IMM. Technical University of Denmark, Brüel & Kjaer, 2003.
 - [140] R. Fridrich, "Estimation of loudness by Zwicker's method," [Online]. Available: <http://fridrichacoustical.com/media/5aab44bbc747b14ffff963cfffe417.pdf>. [Accessed 29 03 2015].
 - [141] E. Zwicker, H. Fastl and C. Dallamayr, "Basic program for calculating the loudness of sounds from their 1/3-oct band spectra according to ISO 532B," *Acustica*, vol. 55, pp. 63-67, 1982.
 - [142] S. Kerber, "Loudness - Calculation according to DIN 45631," Institute of Human Machine Interaction, TU Munich, [Online]. Available: <http://www.mmk.ei.tum.de/~kes/LoudnessMeter/index.html>. [Accessed 05 09 2014].
 - [143] American National Standards Institute (ANSI), "Measurement of sound pressure levels in air," ANSI S1.13, 2005.
 - [144] G. R. Bienvenue, M. A. Nobile, M. J. Corkery and S. M. Miscedra, "Quantifying subjective responses to discrete tones in noise from computer and business equipment," in *InterNoise 89*, USA, 1989.
 - [145] T. Pedersen, M. Sondergaard and B. Andersen, "Objective method for assessing the audibility of tones in noise," Joint Nordic Method version -2, DELTA Acoustics and Vibration, 2000.
 - [146] E. Terhardt, G. Stoll and M. Seewan, "Algorithm for extraction of pitch and pitch salience from complex tonal signals," *Journal of the Acoustical Society of America*, vol. 71, no. 3, pp. 679-688, 1982.
 - [147] A. Hastings, K. Lee, P. Davies and A. Surprenant, "Measurement of the attributes of complex tonal components commonly found in product sound," *Noise Control Engineering Journal*, vol. 51, no. 4, pp. 195-209, 2003.
-

Appendix A: Noise relevant engine geometry parameter estimation

This appendix shows the empirical equations used to approximate the noise relevant engine geometry parameters mentioned in Chapter 4 for the various engine components. The figures show the various geometry values that were collected for current civil turbofan engines having low (e.g. the JT9D variants) to high bypass ratios (e.g. the GE90 variants). The horizontal axis is the Sea-level Static Thrust in kN in all the figures shown, and the vertical axis shows the relevant engine geometry parameter values. The figures also show the best-fit curve for each parameter and the empirical equation that describes the best-fit curve is shown above each figure. All equations have been integrated in INSTANT and have been seen to provide realistic and reasonable values for currently used commercial turbofan engine geometry parameters, within the maximum and minimum limits for each parameter shown in the corresponding figure.

i. Fan inlet area:

$$A_e(x) = -1.257 \cdot 10^{-7}x^3 + 9.835 \cdot 10^{-5}x^2 - 0.005703x + 1.624$$

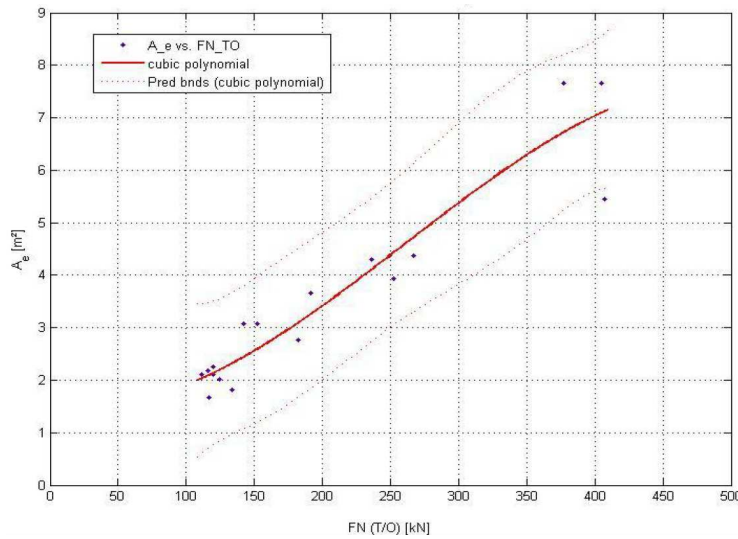


Figure A.1: Best-fit curve and corresponding empirical equation for estimating the fan inlet area based on the engine's SLST

ii. Fan rotor blade number:

$$B(x) = -6.025 \cdot 10^{-10}x^5 + 8.44 \cdot 10^{-7}x^4 - 0.0004494x^3 + 0.1123x^2 - 13.03x + 592$$

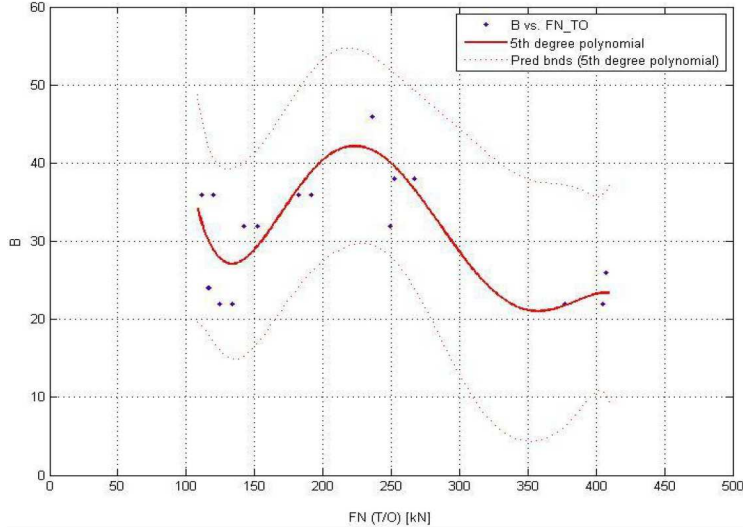


Figure A.2: Best-fit curve and corresponding empirical equation for estimating the fan rotor blade number based on the engine's SLST

iii. Fan rotor tip design Mach number:

$$M_{t,d}(x) = -5.745 \cdot 10^{-6}x^2 + 0.002379x + 1.231$$

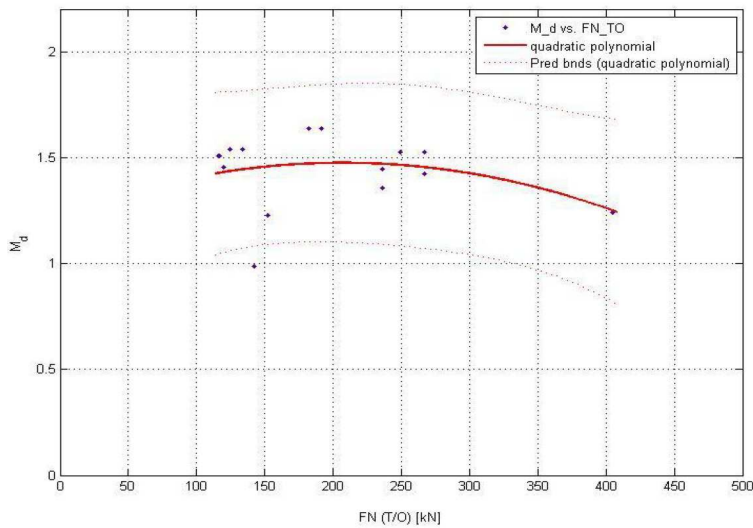


Figure A.3: Best-fit curve and corresponding empirical equation for estimating the fan rotor tip design Mach number based on the engine's SLST

iv. Combustor entrance area:

$$A_{combustor}(x) = 1.602 \cdot 10^{-9}x^4 - 1.611 \cdot 10^{-6}x^3 + 0.0005721x^2 - 0.08258x + 4.439$$

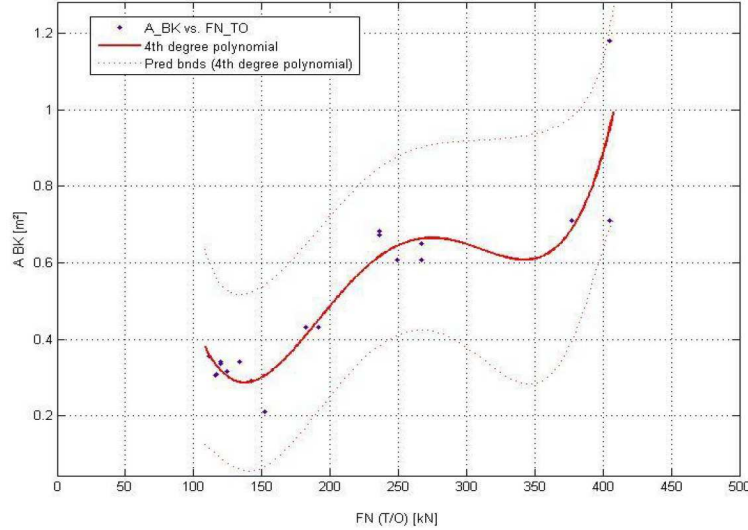


Figure A.4: Best-fit curve and corresponding empirical equation for estimating the combustor entrance area based on the engine's SLST

v. LP Turbine entrance area:

$$A_{turbine}(x) = 1.473 \cdot 10^{-5}x^2 - 0.0003554x + 0.4768$$

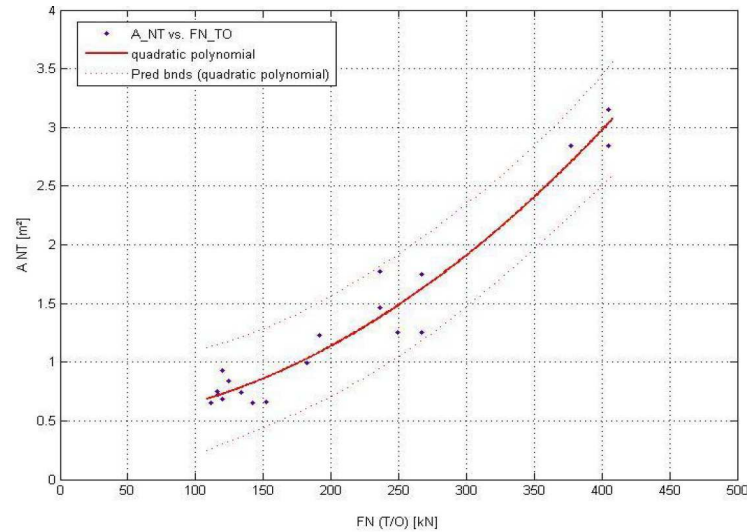


Figure A.5: Best-fit curve and corresponding empirical equation for estimating the LP turbine entrance area based on the engine's SLST

vi. LP Turbine rotor blade number:

$$B_{turbine}(x) = -0.001156x^2 + 1.409x - 138.9$$

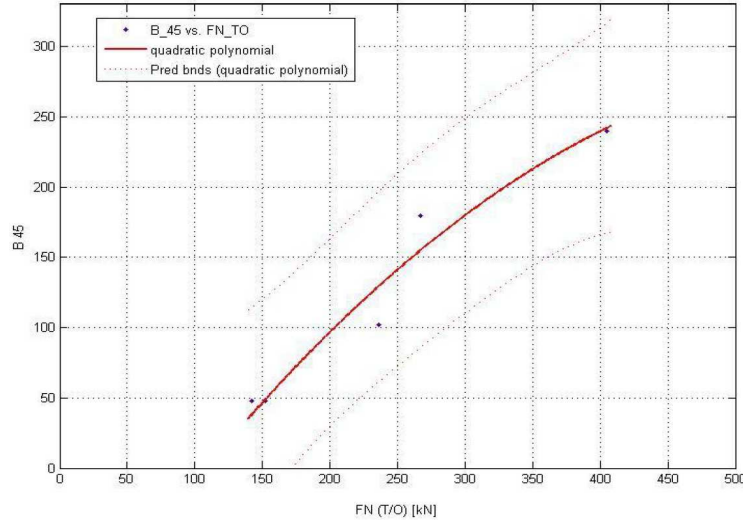


Figure A.6: Best-fit curve and corresponding empirical equation for estimating the LP turbine rotor blade number based on the engine's SLST

vii. Primary jet area:

$$A_{j,1}(x) = -5.951 \cdot 10^{-6}x^2 + 0.001019x + 0.044$$

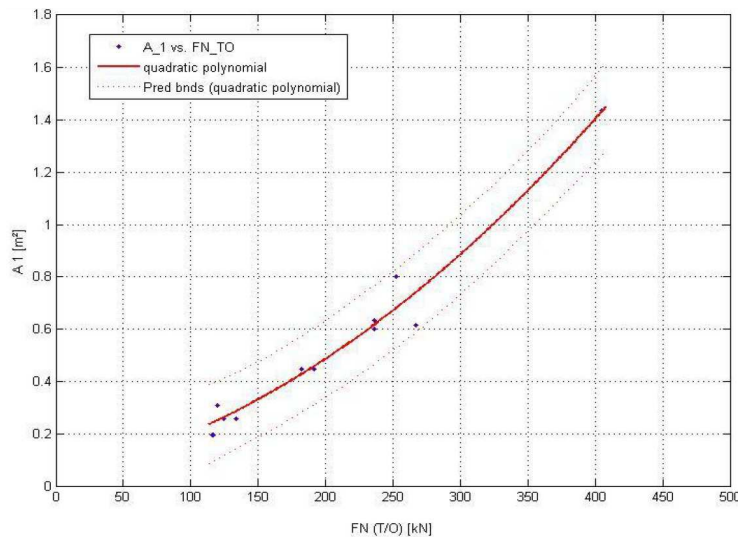


Figure A.7: Best-fit curve and corresponding empirical equation for estimating the primary jet area based on the engine's SLST

viii. Secondary jet area:

$$A_{j,2}(x) = 1.254 \cdot 10^{-5}x^2 + 0.002358x + 0.4487$$

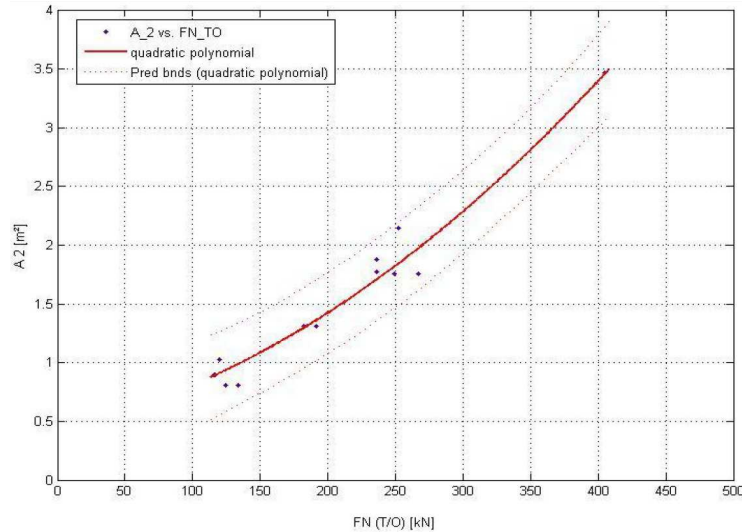


Figure A.8: Best-fit curve and corresponding empirical equation for estimating the secondary jet area based on the engine's SLST

Appendix B: Annoyance assessment of noise abatement flight procedures

This appendix aims to give an impression of the community noise impact changes due to changes to aircraft's flightpath. This done by presenting the noise contours in both conventional and sound quality metrics analogous to the analysis presented in Section 5.2.2 and Section 6.2. The contours are presented for both the SR aircraft as well as for the LR aircraft for a Continuous Descent Approach with a 4° glideslope angle. The flight paths have been modeled using the Mission Analysis tool of the MICADO software and the noise contours have been created using the noise prediction software INSTANT.

1. SR aircraft Continuous Descent Approach (CDA)

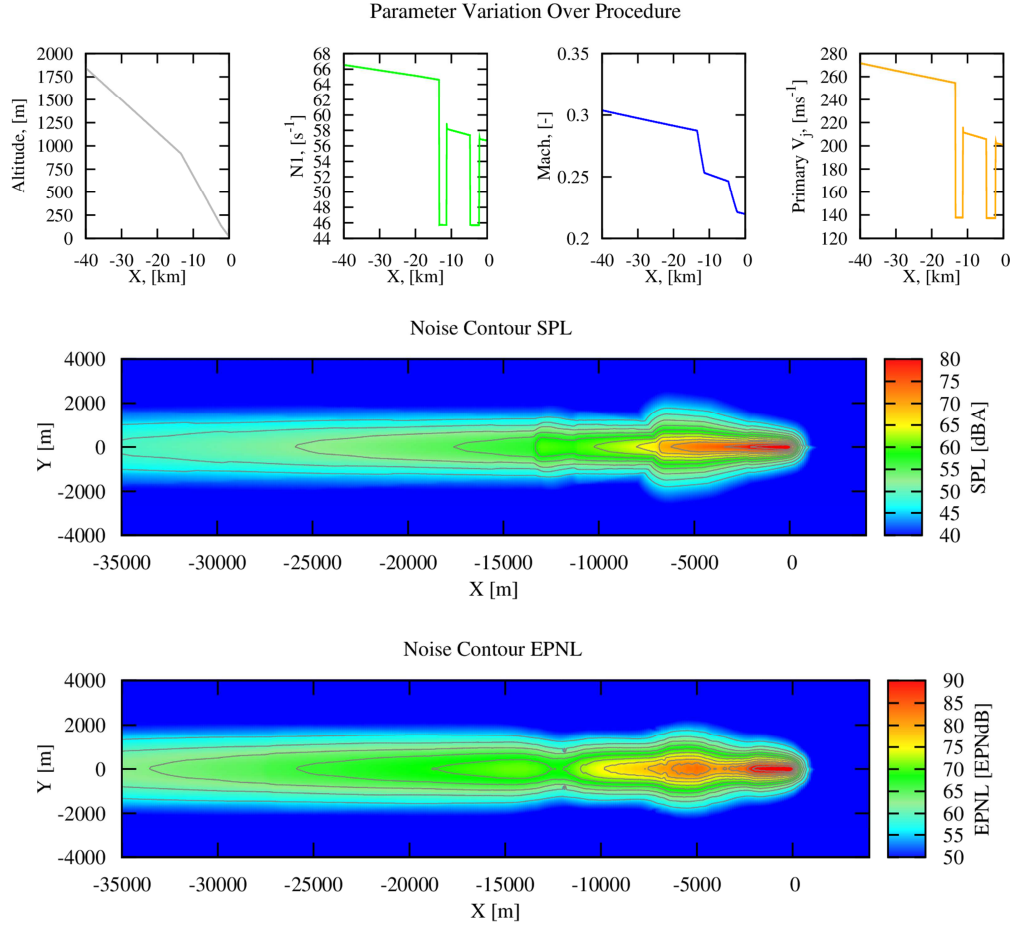


Figure B.1: Flight parameter variation and noise contours in the conventional metrics of dBA and EPNL for the SR aircraft CDA with 4° glideslope

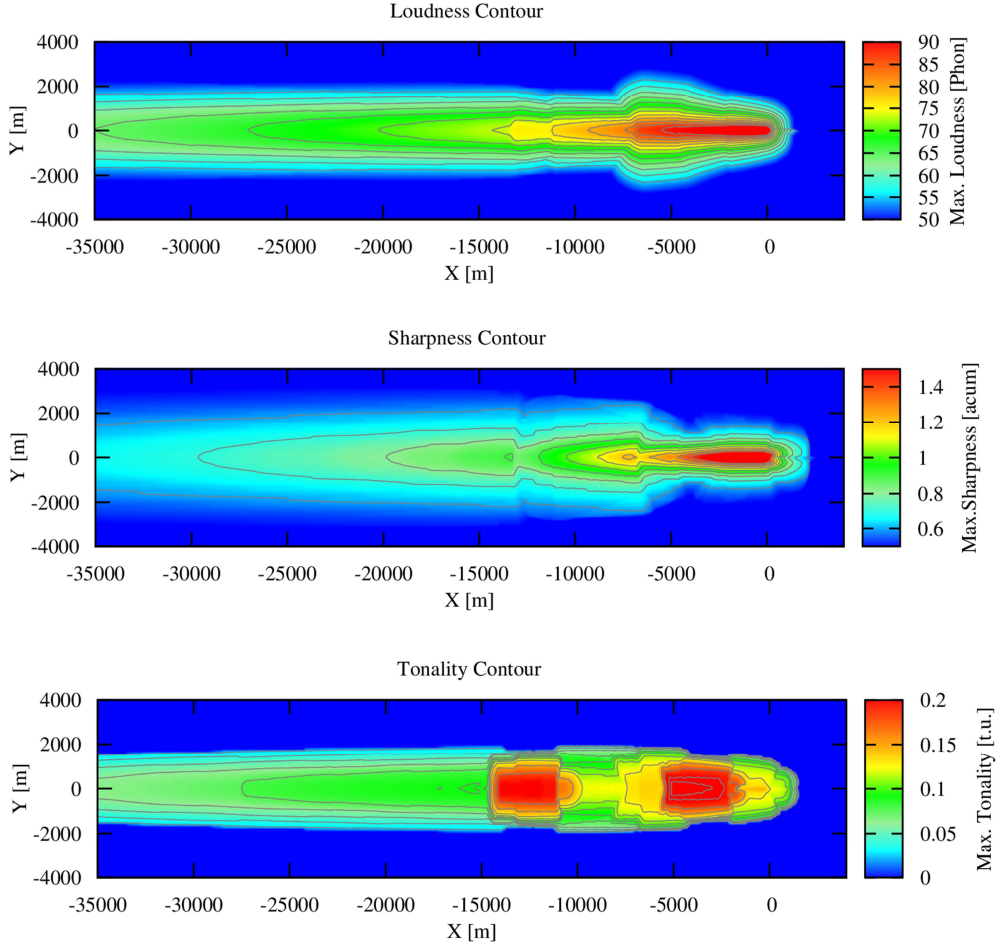


Figure B.2: Noise contours in the sound quality metrics of loudness (top), sharpness (middle) and tonality (bottom) for the SR aircraft CDA with 4° glideslope

Comparing the noise contours presented in Fig. B.1 and Fig. B.2 to the noise contours of the SR aircraft standard approach in Fig. 5.20 and Fig. 6.10, it can be observed that the CDA procedure with 4° glideslope results in a clear reduction in community noise impact in terms of both the level as well as quality of noise. The reductions are primarily due to the aircraft being on the whole higher to the ground than during the conventional approach and the aircraft not flying the horizontal segment that is common in a conventional step descent. The large reduction in thrust setting (shown via lower NI and jet velocity values) at $X = -13$ km however results in a very large increase in tonality from $X = -14$ km to $X = -12$ km, which may be perceived as more annoying than a standard approach at those ground locations. This increase in tonality is not captured by any of the metrics other than the tonality metric.

2. LR aircraft Continuous Descent Approach (CDA)

Fig. B.3 and Fig. B.4 show the conventional and sound quality contours for the long-range LR aircraft flying a CDA with 4° glideslope. Comparing Fig. B.4 with Fig. 6.12, similar reduction in the noise

metrics to the SR CDA procedure can be observed for the LR CDA for the loudness and sharpness metrics. The main difference to SR reductions is in the tonality contour for the LR CDA procedure. It can be seen that on the whole, the LR aircraft flying a CDA with 4° glideslope will have a slightly higher tonality impact on the community compared to the standard approach procedure. The main benefit in terms of tonality is due to the elimination of the horizontal step segment in the CDA procedure, which resulted in a large increase in the tonality impact on the ground from $X = -33$ km to $X = -26$ km in Fig. 6.12 (bottom). Fig. B.4 shows a more uniform (albeit slightly increased) tonality impact for the LR CDA procedure. The large increase in tonality seen when the thrust setting is reduced during the final approach is also observed for the LR aircraft, although since it has a much higher tonality than the SR aircraft (due to the GE90 engine having more dominant fan noise than the V2500 engine), the increase in tonality is not as pronounced as it was observed for the SR CDA in Fig. B.2 (bottom). The overall increase in tonality impact seen in the tonality contour for the LR CDA procedure is again not seen in the other metrics.

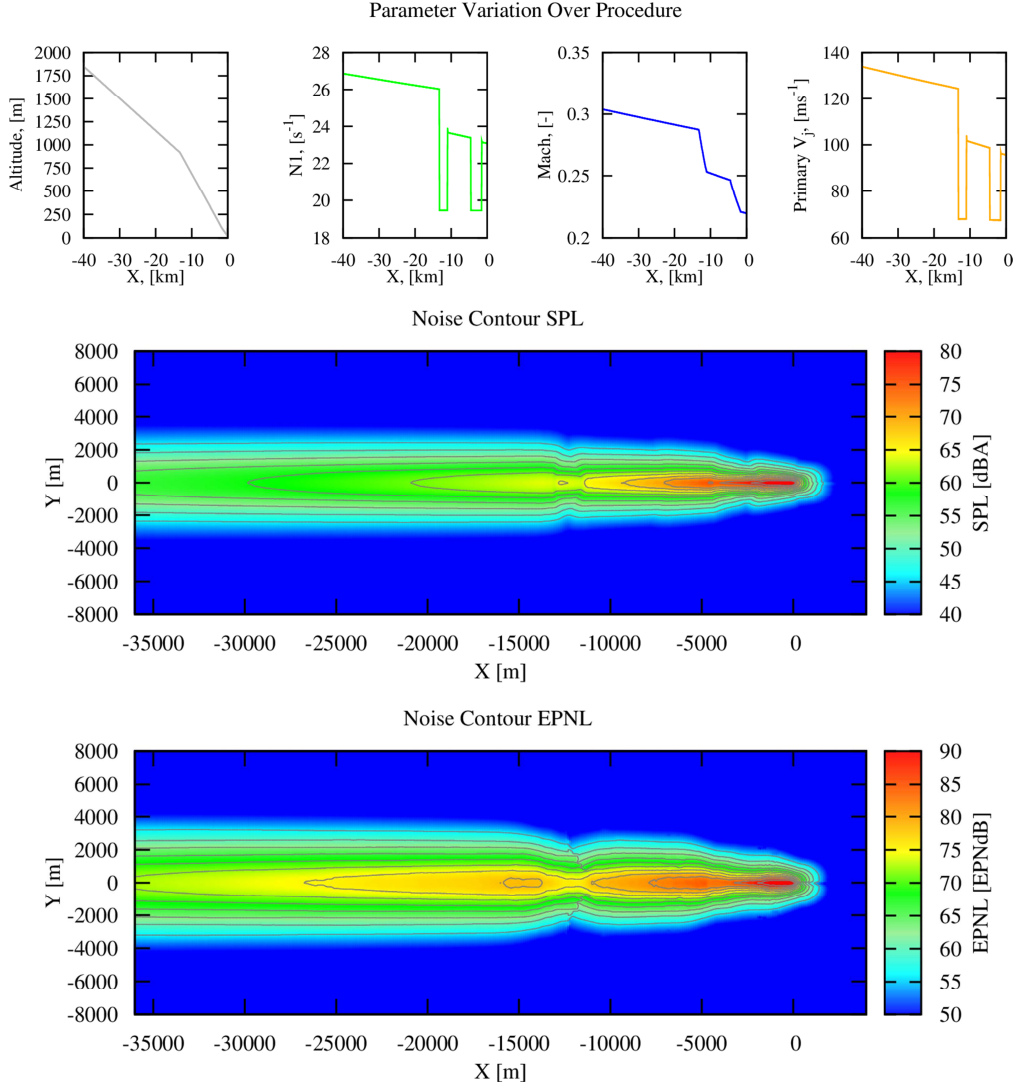


Figure B.3: Flight parameter variation and noise contours in the conventional metrics of dBA and EPNL for the LR aircraft CDA with 4° glideslope

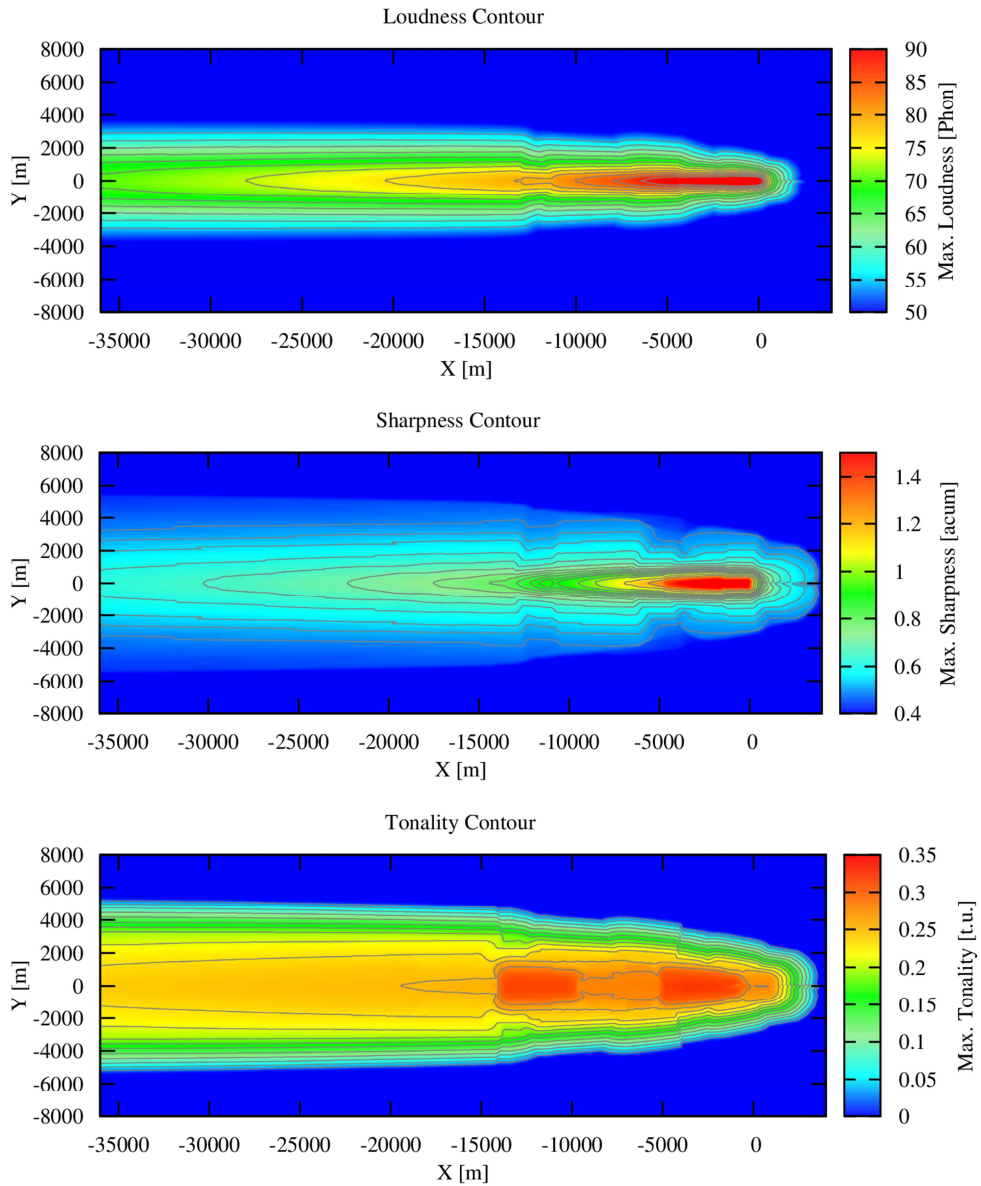


Figure B.4: Noise contours in the sound quality metrics of loudness (top), sharpness (middle) and tonality (bottom) for the LR aircraft CDA with 4° glideslope

